



**University of  
Nottingham**

UK | CHINA | MALAYSIA

*Title:*

**Peripheral contributions to the development and maintenance  
of inflammation and pain in arthritis**

**Dimitrios Amanitis**

**A thesis submitted to the University of Nottingham for the  
degree of Doctor of Philosophy (PhD.)**

**May 2022**

## **Abstract**

Vascular endothelial growth factor A (VEGF-A) is a key regulator of vascular growth, permeability, and neuronal function. During articular inflammation in osteoarthritis (OA) and rheumatoid arthritis (RA), there is increased synovial angiogenesis and upregulation of angiogenic growth factors such as VEGF-A. VEGF-A comprises of two splice variant families, VEGF-A<sub>xxx</sub>a and VEGF-A<sub>xxx</sub>b (xxx represents the number of amino acids, from 121 to 206), resulting from alternative splice site selection in exon 8. Distal site selection and VEGF-A<sub>xxx</sub>a expression is controlled by Serine/Arginine Rich Splicing Factor Kinase 1 (SRPK1), which phosphorylates Serine/Arginine Rich Splicing Factor 1 (SRSF1), inducing its translocation to the nucleus. In most normal tissues, VEGF-A<sub>xxx</sub>b isoforms predominate, with anti-nociceptive and anti-angiogenic functions. In contrast, in pathological conditions such as inflammation and solid tumours SRPK1/SRSF1 activation causes VEGF-A<sub>xxx</sub>a isoforms to predominate, exerting pro-nociceptive and pro-angiogenic actions. VEGF-A has been proposed as a therapeutic target in OA. To date, a relation between VEGF-A and pain in OA has been reported, but there are no published data on the functionally distinct VEGF-A splice variants inflammation and pain in human OA and RA.

This thesis examines the relationships between the expression of VEGF-A splicing isoforms and the components of the VEGF-A splicing axis, inflammation and pain in human sex, and macroscopic chondropathy-matched OA and RA synovial samples from total knee replacement and post-mortem donors. The expression and regulation of the VEGF-A splicing axis was examined by immunohistochemical staining for activated splicing factor SRSF1, splicing kinase SRPK1, total VEGF-A and the two families of VEGF-A splicing isoforms VEGF-A<sub>xxx</sub>a and VEGF-A<sub>xxx</sub>b. Protein expression was measured as the fractional area of staining (VEGF-A and isoforms, SRSF1, SRPK1 and Dyrk1A). SRSF1 activation was measured by the degree of nuclear localisation of SRSF1 compared to the total cell numbers in superficial synovium.

According to principal component analysis structural abnormalities such as synovial thickening significantly contribute to the VEGF-A<sub>xxx</sub>b. Similarly, synovitis was positively correlated with the levels of SRSF1 and VEGF-A, but no alterations were documented regarding the two isoforms in relation to the synovitis. Expression of the related splicing kinase Dyrk1A, implicated in RA, was also positively related to the degree of inflammation. Nuclear SRSF1 was significantly correlated with inflammation score ( $r = 0.52$ ,  $p < 0.05$ ). Total VEGF-A expression was significantly increased

in RA compared to PM and OA (H (2) =23.3,  $p<0.001$  RA cf. OA,PM; ;RA median=0.4, IQR(0.37,0.59); OA median=0.24, IQR(0.19,0.33);PM median=0.18, IQR(0.15,0.2) and was also correlated with the severity of inflammation ( $r=0.47$   $p<0.05$ ). VEGF-A<sub>xxx</sub>b showed no change in expression in OA or RA, although VEGF-A<sub>xxx</sub>b staining intensity was significantly higher in RA samples, compared to controls (H (2) =7.2  $p=0.02$ ; RA median=2.3(1, 4); PM median=0.9 (0.7, 1.4)).

Similarly, symptomatic OA was associated with significantly increased SRPK1, SRSF1 and VEGF-A expression, while the VEGF-A<sub>xxx</sub>b isoform was significantly reduced. SRPK1 expression was similar across all conditions. SRSF1 showed significantly higher expression in the OA tissue compared to PM (H(2)= 11.29,  $p=0.002$ ; OA median=0.2, IQR(0.15, 0.28); PM median=0.09, IQR(0.07, 0.16)), and significantly higher nuclear localisation (indicating activation) in RA vs. OA, and in both RA and OA vs PM (H(2)=37.65,  $p<0.0001$  RA cf. PM;  $p=0,007$  OA cf. PM; RA median=89, IQR(83, 93); OA median=36.1, IQR(29, 42); PM median=19.8, IQR(14,21)). Nuclear SRSF1 was significantly correlated with inflammation score ( $r= 0.52$ ,  $p<0.05$ ). Total VEGF-A expression was significantly increased in RA compared to PM and OA (H (2) =23.3,  $p<0.001$  RA cf. OA,PM; ;RA median=0.4, IQR(0.37,0.59); OA median=0.24, IQR(0.19,0.33);PM median=0.18, IQR(0.15,0.2)) and was also correlated with the severity of inflammation ( $r=0.47$   $p<0.05$ ). VEGF-A<sub>xxx</sub>b showed no change in expression in OA or RA, although VEGF-A<sub>xxx</sub>b staining intensity was significantly higher in RA samples, compared to controls (H (2) =7.2  $p=0.02$ ; RA median=2.3(1, 4); PM median=0.9 (0.7, 1.4)).

Cultures of human primary fibroblast-like synoviocytes (FLS) were stimulated with tumour necrosis factor- $\alpha$ , and the effects on SRPK1, SRSF1 and VEGF-A expression were determined. An in vitro model of synovial inflammation, using fluorescently labelled THP1 monocytes and was used to determine the effect of VEGF-A, VEGF receptor tyrosine kinase inhibitors, and SRPK1 inhibition on monocyte adherence to an FLS monolayer.

Alteration of splicing kinases CLK1-4 and DYRK1a with T-025 was able to significantly increase SRSF1 mRNA expression, and I also confirmed the presence of VEGF-A mRNA in HFLS, however, no splice variants could be detected.

These results indicate that the VEGF-A expression and splicing axis is altered in relation to both inflammation and pain, but in distinct ways. I present evidence that inhibition of VEGF-A splicing controls could affect both inflammation, such as in OA flares, and pain in OA.

## **Publications Abstracts and Awards**

OARSI Connect '21 Virtual World Congress – Oral presentation: Changes in the vascular endothelial growth factor a splicing axis in human synovium are related to arthritis pain.

SoLS PGR conference 2020 – Oral presentation: Changes in the vascular endothelial growth factor (VEGF-A) splicing axis in human synovium are related to inflammation in Arthritis. Awarded best oral presentation.

EULAR 2020 E-Congress – Abstract publication and Poster presentation: Changes in the vascular endothelial growth factor A (VEGFA) splicing axis in human synovium are related to inflammation in arthritis. Awarded with an E-bursary.

6th UK RNA Splicing Workshop 2019 +SoLS PGR conference 2019 – Poster Presentation: Changes in SRSF1 splicing factor expression in human synovium are related to inflammation in arthritis. Awarded for best poster presentation

## **Acknowledgements:**

This thesis would not have been possible without the help, advice, and encouragement of a lot of amazing people. To begin with I would like to offer my deepest thank you and gratitude to my supervisors Professor Lucy Donaldson and Professor David Walsh. Over the course of my PhD, I learned a great deal from both of you. How to ask the big questions and how to identify what my data actually mean, how to persist when everything seems to go wrong and how to move forward and adapt to the ever-changing world of research.

To all my colleagues that I worked alongside in the past 4 years, thank you! To Nick Beazley Long, who was there whenever I needed him at the start of this journey, to answer and explain any crazy question I may have had, from experimental procedures to speculations of research questions. To Daniel McWilliams and Seyed Shahtaheri, you have been a great help from the start with their guidance and support, making the task of working on two different campuses a wonder. To Caroline Howells, a big thank you. You only came to the lab close to me finishing my experimental work, but your presence made these last few months a bit easier to navigate. Your support and our conversations were an amazing boost to cross the finish line. I owe you a lot. To the rest of our research group, Matt, Roaa, Roheena, Zoe and James; thank you all for being part of this journey in your own way. You are all amazing people, and I can only wish you all the best. Thanks to my friends from the E floor in QMC, Luke, Sarah, Ged, and Anya; this PhD would not have been as enjoyable if it was not for our coffee and lunch breaks.

My final thanks should go towards these individuals who without them I would not have finished this journey. Firstly, to my family; Mum, Dad, and my sister. Even though not physically close, I knew I could always rely on you to support me in any way possible. You have given me your support without a second thought, and you have encouraged me to keep going. You were there on the good days, and on the days when everything seemed hopeless. This thesis is evidence of the support care and love I had the luck to receive for as long as I remember. And to the “unsung heroes”, friends I met these past years, friends that would always be around to help me blow some steam off and relax. Whether it was a walk around Nottingham or inviting me for dinner after a full day of work in the lab. Friends that would listen to me explaining complex molecular work for hours. You made this journey so much easier.

Last, but not least I want to thank my supervisor Professor Lucy Donaldson one more time. I could not imagine having a better supervisor for my PhD. Your guidance and support defined this journey. I cannot thank you enough.

**Author's Declaration**

I, Dimitrios Amanitis, confirm that the work presented in this thesis was carried out in accordance with the requirements of the University's Regulations and Code of Practice for Research Degree Programs and that it has not been submitted for any other academic award. I confirm that the work and views demonstrated in this thesis are my own. Where information has been derived from other sources, I confirm this has been indicated in the thesis.

SIGNED.....Amanitis Dimitrios ..... DATE.....31/05/2022.....

Σὰ βγεῖς στὸν πηγαῖμὸ γιὰ τὴν Ἴθάκη,  
νὰ εὐχέσαι ν᾿ἴναι μακρὺς ὁ δρόμος,  
γεμάτος περιπέτειες, γεμάτος γνώσεις.

**Κ. Π. Καβάφης**

As you set out for Ithaka  
hope your road is a long one,  
full of adventure, full of discovery.

**C. P. CAVAFY**

## Table of Contents

1. Introduction .....	22
1.1 Arthritis .....	22
1.2 Anatomy of the normal human knee joint .....	23
1.2.1 Healthy articular cartilage.....	25
1.2.2 Normal subchondral bone .....	26
1.2.3 Normal synovium .....	26
1.3 Rheumatoid arthritis.....	27
1.3.1 Aetiology and pathophysiology of rheumatoid arthritis .....	27
1.3.2 Classification and diagnosis of rheumatoid arthritis .....	28
1.3.3 Treatment and management of rheumatoid arthritis .....	29
1.4 Osteoarthritis .....	31
1.4.1 Aetiology and pathophysiology of OA .....	31
1.4.2 Classification and diagnosis of osteoarthritis .....	32
1.4.3 Articular cartilage changes in osteoarthritis.....	33
1.4.4 Synovial inflammation in osteoarthritis.....	35
1.4.5 Inflammatory mediators in osteoarthritis .....	36
1.4.5.1 Cytokines.....	36
1.4.5.2 Chemokines.....	37
1.4.5.3 Matrix metalloproteases (MMPs).....	37
1.4.5.4 Growth factors .....	38
1.4.5.5 Nerve growth factor.....	38
1.4.5.6 Transforming growth factor (TGF)- $\beta$ .....	38
1.4.5.7 Vascular endothelial growth factor .....	39
1.4.6 Management and treatment of osteoarthritis .....	40
1.4.6.1 Non-pharmacological management of OA .....	42
1.4.6.2 Pharmacological management of OA .....	42
1.4.6.3 Total-knee replacement surgery.....	43
1.5 Osteoarthritis and pain .....	44
1.5.1 Innervation of the knee joint .....	44
1.5.2 Pain.....	47
1.5.3 Pain and peripheral nociception in OA .....	48
1.5.4 Joint tissue remodelling and destabilisation.....	48

1.5.5	Inflammatory pain mechanisms. ....	49
1.5.6	Synovitis and pain .....	50
1.5.7	Neuropathic pain. ....	50
1.6	Vascular endothelial growth factors .....	51
1.6.1	Alternative splicing and vascular endothelial growth factor-A.....	53
1.6.2	Splicing mechanisms – constitutive and alternative splicing.....	53
1.6.3	The spliceosome .....	55
1.6.4	Splicing kinases and arthritis.....	57
1.6.5	Control of SR proteins.....	58
1.6.6	Control of VEGF-A alternative splicing.....	59
1.6.7	The VEGF-A families of alternatively spliced isoforms.....	60
1.6.8	VEGF-A isoform interaction with VEGF receptors .....	62
1.6.9	Vascular endothelial growth factor and pain .....	63
1.7	Hypothesis.....	64
2.	Methods.....	65
2.1	Introduction .....	65
2.2	Case Selection .....	65
2.3	Tissue collection and processing.....	66
2.4	Histological Staining .....	66
2.4.1	Haematoxylin and eosin.....	66
2.5	Immunohistochemistry.....	67
2.5.1	Indirect Immunohistochemistry .....	68
2.5.2	Indirect Immunohistochemistry protocol .....	70
2.5.3	Optimisation of the indirect IHC method .....	71
2.5.4	Controls for indirect IHC. ....	74
2.6	Immunofluorescence .....	75
2.7	Synovial Histological Scoring.....	78
2.8	Image analysis and quantification .....	80
2.9	General cell culture methods.....	84
2.9.1	Preparation and storage of cell stocks.....	84
2.10	Protein isolation and quantification .....	85
2.11	Western blotting .....	86
2.12	RNA extraction .....	88

2.13 cDNA synthesis.....	89
2.13.1 Polymerase Chain Reaction Primers .....	90
2.13.2 Polymerase chain reaction (PCR) .....	91
2.14 Statistical Analysis.....	92
3. VEGF-A splicing events and inflammation in the synovium of OA and RA knee joints. ....	96
3.1 Introduction .....	96
3.1.1 Alternative splicing and inflammation in arthritis. ....	97
3.2 Materials and Methods.....	100
3.2.1 Human tissue collection and preparation.....	100
3.2.2 Cases for the pilot study and the optimisation of experimental methods.....	100
3.2.3 Cases for the investigation of the VEGF-A splicing axis in synovial inflammation.....	100
3.2.4 Immunohistochemistry - optimisation and analysis.....	102
3.2.5 Image capture, data extraction and analysis .....	108
3.3 Results.....	110
3.3.1 Pilot study: determination of sampling frequency for minimal staining, through the coefficient of variation analysis .....	110
3.3.2 Optimisation of immunofluorescence in human knee synovium.....	111
3.3.3 Case information – summary table and illustrations of the histology.....	113
3.3.4 Splicing axis changes in inflamed synovium .....	116
3.3.5 Expression of SRPK1 is increased in inflamed knee synovium from patients with RA or OA compared to controls, and expression is related to the severity of histological inflammation	119
3.3.6 Expression of SRSF1 is increased in inflamed knee synovium from patients with RA or OA compared to controls and is related to the severity of histological inflammation .....	121
3.3.7 SRSF1 activation is increased in inflamed knee synovium from patients with RA or OA compared to controls and is related to the severity of histological inflammation .....	122
3.3.8 Expression of total (pan)VEGF-A is increased during inflammation between patients with RA and OA compared to controls in knee synovial tissue and expression is positively related to the severity of histological inflammation .....	123
3.3.9 Expression of the VEGF-A <sub>xxx</sub> b isoforms is significantly decreased in inflamed knee synovium between patients with RA and OA compared to controls as well as having no relationship to the severity of inflammation .....	126
3.3.10 Ratios of VEGF-A <sub>xxx</sub> b / VEGF-A <sub>xxx</sub> a expression.....	130
3.3.11 Expression of the splicing kinase Dyrk1A is related to the severity of histological inflammation, particularly in RA. ....	131
3.4 Summary of the Results .....	133

3.5 Discussion.....	134
3.5.1 Principal component regression analysis - Predictors of VEGF-A <sub>xxx</sub> b expression in inflammation in OA and RA synovium .....	134
3.5.2 Changes in the VEGF-A splicing axis and relationship to inflammation in OA and RA synovium	135
3.5.3 The expression of the splicing kinase SRPK1 showed no significant differences between OA and RA and was not related to the level of synovitis. ....	136
3.5.4 Expression and activation of SRSF1 were significantly increased in both OA and RA, and activation correlated with the level of synovitis.....	137
3.5.5 Expression of total VEGF-A by both fractional area and integrated density increased in OA, further increased in RA, and correlated with inflammation. ....	139
3.5.6 Expression of anti-angiogenic VEGF-A <sub>xxx</sub> b by fractional area not changed in the OA and RA groups, and not correlated with inflammation, but integrated density was higher in RA and correlated with inflammation. VEGF-A <sub>xxx</sub> a not altered.....	140
3.5.7 Expression of the related splicing kinase Dyrk1A is related to the severity of histological inflamma,in particularly in RA. ....	142
3.6 Optimisation and limitations .....	143
3.7 Concluding remarks .....	144
4. VEGF-A splicing events and pain in knee joint synovium from people with OA.....	146
4.1 Introduction .....	146
4.2 Materials and Methods.....	150
4.3 Results.....	155
4.3.1 Case information – summary table and illustrations of the histology.....	155
4.3.2 Splicing axis changes in symptomatic painful chondropathy .....	156
4.3.3 Alterations in the splicing axis SRPK1, SRSF1, panVEGF-A and VEGF-A <sub>xxx</sub> b in synovial tissue during synovitis.....	158
4.3.4 Expression of SRPK1 is increased in the synovium from patients with painful symptomatic OA compared to controls showcasing asymptomatic chondropathy.....	159
4.3.5 Expression and activation of SRSF1 is increased in the synovium from patients with symptomatic painful OA compared to controls.....	160
4.3.6 Expression of panVEGF-A is increased during painful OA compared to controls in knee synovial tissue .....	162
4.3.7 Expression of the VEGF-A <sub>xxx</sub> b and VEGF-A <sub>xxx</sub> a isoforms in human knee synovium is significantly associated to painful OA in comparison to non-painful controls. ....	163
4.3.8 Expression of the splicing kinase Dyrk1A is related to the increased levels of pain encountered in symptomatic chondropathy cases compared to asymptomatic chondropathy	166

4.4 Summary of the results.....	168
4.5 Discussion.....	168
4.5.1 Expression of SRPK1 is increased in the synovium from patients with painful symptomatic OA compared to controls with asymptomatic chondropathy .....	169
4.5.2 Expression and activation of SRSF1 is increased in the synovium from patients with symptomatic painful OA compared to controls.....	170
4.5.3 Expression of panVEGF-A is increased during painful symptomatic chondropathy in OA compared to controls in knee synovial tissue.....	170
4.5.4 The relative expression of the VEGF-A <sub>xxx</sub> b and VEGF-A <sub>xxx</sub> a splice isoforms in human knee synovium is significantly altered in painful OA. ....	172
4.5.5 Expression of the splicing kinase Dyrk1A is related to pain in symptomatic chondropathy OA cases compared to asymptomatic chondropathy .....	174
4.6 Concluding remarks and limitations .....	175
5. The control of VEGF-A splicing in, and the effect of VEGF-A isoforms and splicing kinases on monocyte adherence to, human fibroblast like synoviocytes <i>in vitro</i> .....	178
5.1 Introduction .....	178
5.1.1 Development of small molecule splicing kinase inhibitors.....	181
5.1.2 SRPIN340.....	183
5.1.3 SPHINX31 .....	184
5.1.4 T-025 .....	185
5.1.5 SM04690 (Lorecivint) .....	185
5.1.6 Griffin6 .....	185
5.1.7 Preliminary data.....	186
5.2 Materials and Methods.....	187
5.2.1 Splicing kinase inhibitors.....	187
5.2.2 Workflow for effects of HFLS treatment with SRPK1 and Clk1/2 inhibitors in culture	188
5.2.3 Expression of VEGF-A, SRPK1, SRSF1 and I-CAM-1 in HFLS .....	189
5.2.4 Monocyte adherence to fibroblast-like synoviocytes – <i>in vitro</i> inflammation assay.	195
5.2.5 Cell culture for protein quantification .....	196
5.2.6 Data extraction and analysis.....	199
5.3 Results.....	200
5.3.1 SRPK1, SRSF1 and VEGF-A are expressed in HFLS in culture and expression of SRSF1 is altered splicing kinase inhibition. ....	200
5.3.2 Expression of SRPK1 in human fibroblast like synoviocytes .....	200

5.3.3	Expression of SRSF1 mRNA in HFLS and effect of splicing kinase inhibitors.....	200
5.3.4	Expression of VEGF-A mRNA in HFLS and effect of TNF- $\alpha$ and splicing kinase inhibitors.....	202
5.3.5	Mechanisms underpinning monocyte adhesion to human fibroblast-like synoviocytes <i>in vitro</i>	205
5.3.6	VEGF-A splice variants alter I-CAM-1 expression in human fibroblast-like synoviocytes.....	205
5.3.7	THP-monocyte adherence to HFLS is mediated through an I-CAM-1/ VEGF-A/SRPK1-dependent mechanism and is reduced by inhibition of ICAM-1, SRPK1 and/or VEGF receptors <i>in vitro</i> .	210
5.4	Summary of results .....	214
5.5	Discussion.....	215
5.5.1	SRPK1, and SRSF1 expression in HFLS in culture and alteration by TNF- $\alpha$ , and splicing kinase inhibition.....	215
5.5.2	VEGF-A isoform and ICAM-1 expression in HFLS.....	216
5.5.3	THP-monocyte adherence to HFLS <i>in vitro</i> is mediated by VEGF-A receptor 2 and I-CAM-1.	218
5.5.4	THP-monocyte adherence to HFLS is mediated through an SRPK-1-dependent mechanism <i>in vitro</i> .....	220
5.5.5	Splicing kinase inhibitors.....	221
5.6	Concluding remarks .....	222
6.	Discussion.....	223
7.	Proposed future work.....	229
8.	Appendix 1 .....	230
9.	References .....	232

## Table of Figures

<b>Figure 1</b> Anterior view of the anatomy of the knee joint, the anatomy of the cartilage of a synovial joint as well as of the synovium .....	24
<b>Figure 2</b> Pre mRNA transcript that showcasing different splicing mechanisms. Different colours denote different exons, with black lines expressing introns, and the dotted lines showing splicing events. ....	54
<b>Figure 3</b> The human serine/arginine splicing proteins.. .....	56
<b>Figure 4</b> Schematic of the two potential pathways through which SRSF1 is phosphorylated by the complex of CLK-1 and SRPK1 .....	59
<b>Figure 5</b> Illustration of a Y-shaped structure of an IgG antibody. ....	68
<b>Figure 6</b> Representation of the Peroxidase/Anti-Peroxidase (PAP) detection method. ....	69
<b>Figure 7</b> Schematic representation of the Avidin- Biotin detection method.. .....	70
<b>Figure 8</b> Schematic representation of the IHC protocol used throughout the experimental work of the thesis. ....	74
<b>Figure 9</b> Schematic demonstration of a fluorescent microscope. ....	76
<b>Figure 10</b> Schematic representation of the IHC protocol using the Alkaline phosphatase – fast red substrate kit. ....	78
<b>Figure 11</b> Demonstration of synovial inflammation scoring based on the Haywood et al criteria. ....	80
<b>Figure 12</b> Analysis of Fractional area using a custom-made macro implemented in KEIS imaging software.....	82
<b>Figure 13</b> “Sandwich” transfer block cassette. The block comprises of 2 sponges, 4 blot papers, 1 nitrocellulose membrane and the gel of interest .....	87
<b>Figure 14</b> Visual representation of the parallel analysis process to determine PCs and eigenvalues from the initial dataset .....	94
<b>Figure 15</b> Schematic representation of the general IHC protocol used throughout the experimental work in this chapter.....	106

<b>Figure 16</b> Schematic representation of the IHC protocol used throughout the experimental work of the thesis using the Alkaline phosphatase – fast red substrate kit. ....	107
<b>Figure 17</b> Determination of the required number of fields to minimise the variance of data collected using sequential sampling of the synovial lining.....	110
<b>Figure 18</b> Determination of the required number of fields to minimise the variance of data collected using hotspot sampling of the synovial lining. ....	111
<b>Figure 19</b> expression of SRSF1 in the human synovia lining.....	112
<b>Figure 20</b> Human synovial tissue under fluorescent light with SRSF1 being in red and Dapi in blue. ....	113
<b>Figure 21</b> Loadings plot of the PCA analysis for the dataset of the VEGF-A splicing axis and indicators of OA and RA disease. ....	117
<b>Figure 22</b> SRPK1 expression in synovium from human tissue. A-C typical images SRPK1 immunoreactivity .....	120
<b>Figure 23</b> Representative images of the 3 groups that were used to quantify the fractional area .....	121
<b>Figure 24</b> SRSF1 is expressed in the cytosol in postmortem control and osteoarthritic synovium (red arrows) and in synoviocytes nuclei in both OA and RA synovium.....	123
<b>Figure 25</b> Photomicrographs of representative samples of human synovium, showing the expression pattern of panVEGF-A in different groups. ....	124
<b>Figure 26</b> panVEGF-A expression expressed as Integrated density.....	125
<b>Figure 27</b> Photomicrographs of representative samples from human knee synovium showing the expression pattern of VEGF-A <sub>xxx</sub> a in the three different groups.....	127
<b>Figure 28</b> VEGF-A <sub>xxx</sub> a expression as quantified by integrated density. ....	128
<b>Figure 29</b> Photomicrographs of representative samples from human knee synovium showing the expression pattern of VEGF-A <sub>xxx</sub> b.....	129
<b>Figure 30</b> VEGF-A <sub>xxx</sub> b expression (integrated density). ....	130
<b>Figure 31</b> VEGF-A <sub>xxx</sub> b/ VEGF-A <sub>xxx</sub> a expression ratio for each individual group.....	131

<b>Figure 32</b> Photomicrographs of representative samples from human knee synovium showing the expression pattern of the splicing kinase DYRK1a .....	132
<b>Figure 33</b> Schematic representation of the IHC protocol used throughout the experimental work of the thesis. ....	153
<b>Figure 34</b> Loading plot of the PCA for the dataset of the VEGF-A splicing axis and indicators of OA disease.....	157
<b>Figure 35</b> SRPK1 expression in synovium from human tissue. A-C typical images SRPK1 immunoreactivity.....	159
<b>Figure 36</b> SRSF1 expression in synovium from human tissue. A-C typical images SRSF1 immunoreactivity.....	161
<b>Figure 37</b> SRSF1 is expressed in the cytosol in normal physiological conditions, and it is translocated in the nuclei during disorders such as OA. ....	162
<b>Figure 38</b> Photomicrographs of representative samples of human synovium, showing the expression pattern of panVEGF-A in the two distinct groups. ....	163
<b>Figure 39</b> Photomicrographs of representative samples from human knee synovium showing the expression pattern of VEGF-A <sub>xxx</sub> b between the symptomatic and non-symptomatic groups. ....	164
<b>Figure 40</b> Photomicrographs of representative samples from human knee synovium showing the expression pattern of VEGF-A <sub>xxx</sub> a in the two different groups.....	165
<b>Figure 41</b> VEGF-A <sub>xxx</sub> b/ VEGF-A <sub>xxx</sub> a expression ratio for the two groups.....	166
<b>Figure 42</b> Photomicrographs of representative samples from human knee synovium showing the expression pattern of the splicing kinase DYRK1a .....	167
<b>Figure 43</b> PanVEGF-A and ICAM-1 are increased in a dose-dependent manner by TNF- $\alpha$ in cultured HFLS. ....	180
<b>Figure 44</b> Representations of the individual structures for the splicing kinase inhibitors used in this study. ....	183
<b>Figure 45</b> Illustration of the structure of the 24 well plate and the treatments used for the RNA- extraction work.....	188

<b>Figure 46</b> Simple flow chart illustrating the experimental procedure from RNA extraction to visualisation of the PCR results .....	190
<b>Figure 47</b> Representative simulation of the primer binding sites on the exons of VEGF-A sequencing .....	197
<b>Figure 49</b> PCR gel for the SRPK1 gene expression in HFLS. ....	200
<b>Figure 50</b> Reverse transcription PCR for SRSF1 mRNA expression in Human fibroblast like synoviocytes (HFLS) after TNF- $\alpha$ and SPHINX31/Griffin 6/T-025 inhibitor treatment .....	201
<b>Figure 51</b> PCR gel used to detect mRNA expression of VEGF-A in HFLS cells.....	202
<b>Figure 52</b> Representative image of a PCR gel demonstrating the mRNA expression of VEGF-A in HFLS cells using the VEGF-A primer set 1. ....	203
<b>Figure 53</b> Image of the PCR gel demonstrating the mRNA expression of VEGF-A after re-amplification, in order to sequence each band individually.....	204
<b>Figure 54</b> HFLS derived from both normal and RA joints were treated with VEGF-A <sub>165a</sub> or VEGF-A <sub>165b</sub> , to identify any potential alterations to the ICAM-1 gene expression levels.....	206
<b>Figure 55</b> HFLS derived from both normal and RA joints were treated with ascending concentrations of VEGF-A <sub>165a</sub> or VEGF-A <sub>165b</sub> , to determine effect on ICAM-1 mRNA expression levels. ....	208
<b>Figure 56</b> Western blot for ICAM-1 and GAPDH in human fibroblast like synoviocytes after TNF- $\alpha$ and anti-VEGFR2 treatment. A. ....	209
<b>Figure 57</b> THP-1 cells were plated over HFLS to measure fluorescent levels of adherent monocytes.....	211
<b>Figure 58</b> Treating RA HFLS with SPHINX after treatment with TNF- $\alpha$ reduces the overall levels of ICAM-1 fluorescence as induced by THP adherence ( .....	213
<b>Figure 59</b> Summary of the hypotheses, findings, and their interpretation in the thesis. Upward arrow denotes an increase, downward arrow a decrease. VEGFR: VEGF receptor, NGF: nerve growth factor. A full explanation of the diagram is in the text. ....	223

## Table of Abbreviations

ABC	Avidin-Biotin complex
AC	Asymptomatic chondropathy
ACR	American College of Rheumatology
AKT	Protein kinase B
ALK5	Activin-like kinase 5
ALP	Alkaline phosphatase
ARA	American rheumatism association
ASF/SF2	Serine/arginine-rich splicing factor 1
ATCC	American type culture collection
ATP	Adenosine 5'-triphosphate
BCL	B-cell lymphoma 2
BML	Bone marrow lesions
BMP	Bone morphogenetic proteins
BSA	Bovine serum albumin
CCL2	Chemokine ligand 2
CCP	A cluster
CD31	A cluster of differentiation 31
CDC	Centre for Disease Control and Prevention
CDKPRR	Cysteine, aspartate, lysine, proline, arginine
CLK	Cdc like kinase
CNV	Choroidal neovascularisation
COX	Cyclooxygenase
CV	Coefficient of variation
CXC	Chemokine group
DAB	Diaminobenzidine
DAPI	4',6-diamidino-2-phenylindole
DC101	Anti-VEGFR2 antibody
DEPC	Disease-modifying
DMARD	Disease modifying anti-rheumatic drugs
DMEM	Disease-modifying

DMOAD	Disease modifying osteoarthritis drugs
DMSO	Dimethyl-sulfoxide
DNA	Deoxyribonucleic acid
dNTPs	Deoxyribonucleotides
DTT	Dithiothreitol
DYRK	Dual-specificity tyrosine phosphorylation-regulated kinases
ECM	Extracellular matrix
EDTA	Ethylenediaminetetraacetic acid
EGTA	Ethylene glycol-bis ( $\beta$ -aminoethyl ether)-N,N,N',N'-tetraacetic acid
ERK	Extracellular regulated kinase
ESR	Erythrocyte sedimentation rate
FA	Fractional area
FBS	Fetal bovine serum
FGF	Fibroblast growth factor-2
FH2	Dihydrofolic acid
FH4	Folinic acid
FITC	Fluorescein isothiocyanate
FLS	Fibroblast like synoviocyte
FR	Fast red
G6	Griffin 6
GAPDH	Glyceraldehyde 3-phosphate dehydrogenase
GSK3B	Glycogen synthase kinase-3 beta
HA	Hyaluronic acid
HFLS	Human fibroblast like synoviocytes
HIER	Heat induced antigen retrieval
HIF	Hypoxia inducible factor
HIPK	Homeodomain-interacting protein kinase
HRP	Horseradish peroxidase
HTM	High threshold mechanoreceptors
HUVEC	Human umbilical vein endothelial cells
IASP	The concentration
IC <sub>50</sub>	Concentration required for 50% Inhibition

ICAM-1	Intracellular adhesion molecule-1
IEG	Immediate-early genes
IFN- $\gamma$	Interferon gamma
IHC	Immunohistochemistry
IL-1 $\beta$	Interleukin
KCl	Potassium chloride
LN	Liquid nitrogen
MAPK	Mitogen-activated protein kinases
MCP	Monocyte chemotactic protein
MGC	Multinucleated giant cells
MIP	Macrophage inflammatory protein
MKNK2	Serine/threonine kinase
MMLV	Molony murine leukaemia virus
MMP	Matrix metalloproteases
MRI	Magnetic resonance imaging
MTX	Methotrexate
NFAT	Nuclear factor of activated T cells
NGF	Neuronal growth factor
NICE	National Institute for Health and Care Excellence
NMD	Nonsense-mediated decay
NRP	Neuropilins
NSAID	Non-steroidal anti-inflammatory drugs
OA	Osteoarthritis
OARSI	Osteoarthritis research society international
PAP	Peroxidase/anti-peroxidase
PBS	Phosphate buffered saline
PC	Principal component
PCA	Principal component analysis
PCR	Polymerase chain reaction
PCR	Principal component regression
PECAM-1	Platelet and Endothelial Cell Adhesion Molecule-1
PFA	Paraformaldehyde

PI3	Phosphoinositide 3-kinase
PIGF	Placental growth factor
PIER	Proteolytic-induced epitope retrieval
PLC $\gamma$	Phospholipase $\gamma$
PMSF	Phenylmethanesulphonyl fluoride
PVDF	Polyvinylidene difluoride
QST	Quantitative sensory testing
RA	Rheumatoid arthritis
RF	Rheumatoid factor
RNP	Nuclear ribonucleoprotein
ROI	Region of interest
RPE	Retinal pigmented epithelium
RRM	Rna recognition motif
RRMH	RRNA Recognition Motif homology
SDS	Sodium dodecyl sulfate
SLE	Systemic lupus erythematosus
SRPK1	Serine/arginine protein kinase
SRSF1	Serine/arginine rich splicing factor 1
TAE	Tris acetate EDTA
TBS	Tris-buffered saline
TGF- $\beta$	Transforming growth factor - $\beta$
THP1	Human Monocyte-like Cells
TKR	Total knee replacement surgery
TNF	Tumour necrosis factor
TRITC	Tetramethyl rhodamine isothiocyanate
TRPA1	Transient Receptor Potential cation channel subfamily A member 1
TRPV1	Transient Receptor Potential cation channel subfamily V member 1
VAS	Visual analogue scale to measure pain
VEGFA	Vascular endothelial growth factor A
VEGFB	Vascular endothelial growth factor B
VEGFR	Vascular endothelial growth factor Receptor
WOMAC	Western Ontario and McMaster Universities Osteoarthritis index

# 1. Introduction

## 1.1 Arthritis

Arthritis is a common chronic condition with at least 1 in 5 adults in the UK suffering from knee arthritis. The term “arthritis” is used as an umbrella term to reference joint pain and/or disease. More than 100 types of arthritis are prominent, in people of all races, genders and ages, such as osteoporosis, osteoarthritis, autoimmune and inflammatory arthritis or rheumatoid arthritis, axial spondylarthritis, or juvenile idiopathic arthritis ([versusarthritis.org](http://versusarthritis.org)). A true estimate of people affected by arthritis cannot be calculated, as many patients do not seek medical help until they show severe symptoms. A rough estimate suggests that at least 54 million people in the US are suffering from arthritis with 10 million people in the UK suggested to have arthritis. According to the CDC (Centre for Disease Control and Prevention), in the period between 2013 and 2015, 7.1% of people aged 18-44 years, 30% of people aged 45 to 64 years old and 50% of people aged above 65 have reported doctor-diagnosed arthritis. In the same period, 26% of women and 19% of men have been reported with doctor diagnosed arthritis. 16% of normal weight adults and 31% of obese adults have been diagnosed with arthritis respectively.

These numbers suggest that the disease places a heavy burden on society (Bitton 2009) due to the cost of treatments and the increased life expectancy. Currently, more than 100,000 total knee replacement (TKR) operations are performed yearly by the NHS (NHS Digital Feb 2022). The disease seems to be more prevalent among women, not to mention that the number of people with arthritis increases yearly. Current estimates support that by 2040 26% of US adults aged over 18 years old will have doctor-diagnosed arthritis (CDC.com).

Some of the more common arthritis symptoms include pain, decreased range of motion, stiffness and swelling. There is a variance in how the symptoms present themselves; for example, they can be mild or severe and they can progressively get worse over time, or stay the same through the years. Arthritis may also result in chronic pain, rendering daily tasks such as walking or climbing stairs impossible. Joint damage and changes are also evident in severe arthritis.

Osteoarthritis (OA) and rheumatoid arthritis (RA) are two of the most common forms of arthritis affecting many synovial joints, with OA affecting nearly 9 million people in the UK and RA affecting nearly 500 000 people in the UK in NHS ([www.nhs.uk](http://www.nhs.uk)). A variety of joints throughout the human body can be affected by either of these conditions, but they occur most often in the

knees, hips, lower back and neck, small joints of the fingers and the bases of the thumb and big toe for OA and the hands, feet, wrists, elbows, knees, and ankles for RA.

The knee joint is a common target in arthritis research. Knee arthritis (either OA or RA) is highly prevalent when compared to the other joints (e.g., hip OA), and it also often presents in younger age groups (Heidari 2011). The occurrence of knee OA for example is positively related to age and further increases with the higher expectancy of life as well as the higher average weight of the population (Heidari 2011).

Alteration in the knee joint, evident through radiographic imaging as well as the presence of pain, are the two primary clinical manifestations of arthritis. However full understanding of the contribution of joint pathology in the development and maintenance of inflammation and pain is still poorly understood. The pathological alterations in joint tissues in early onset OA/RA are difficult to characterise since they can develop in absence of symptoms such as pain or stiffness, so investigation of mechanisms in preclinical knee OA and RA is challenging.

## **1.2 Anatomy of the normal human knee joint**

The synovial joint connecting the upper and lower bones of the leg, namely the knee, is the largest synovial joint in the human body. The joint is formed by the articulation of the medial and lateral condyles of the femur with the medial and lateral plateaux of the tibia (tibia and femur are respectively the lower and the upper bones of the leg (Figure 1). The articulation of the bones is stabilised by ligaments and surrounded by the joint capsule. The main knee joint ligament is the posterior and anterior cruciate ligament, the medial ligament and lateral collateral ligaments (Figure 1, (Claes, Vereecke et al. 2013). Ligaments are identified as intra-articular (positioned within the joint), or extracapsular (outside the capsule). The menisci are fibrocartilage structures that also stabilise the joint and additionally distribute the load on the joint and reduce the shock of load bearing.

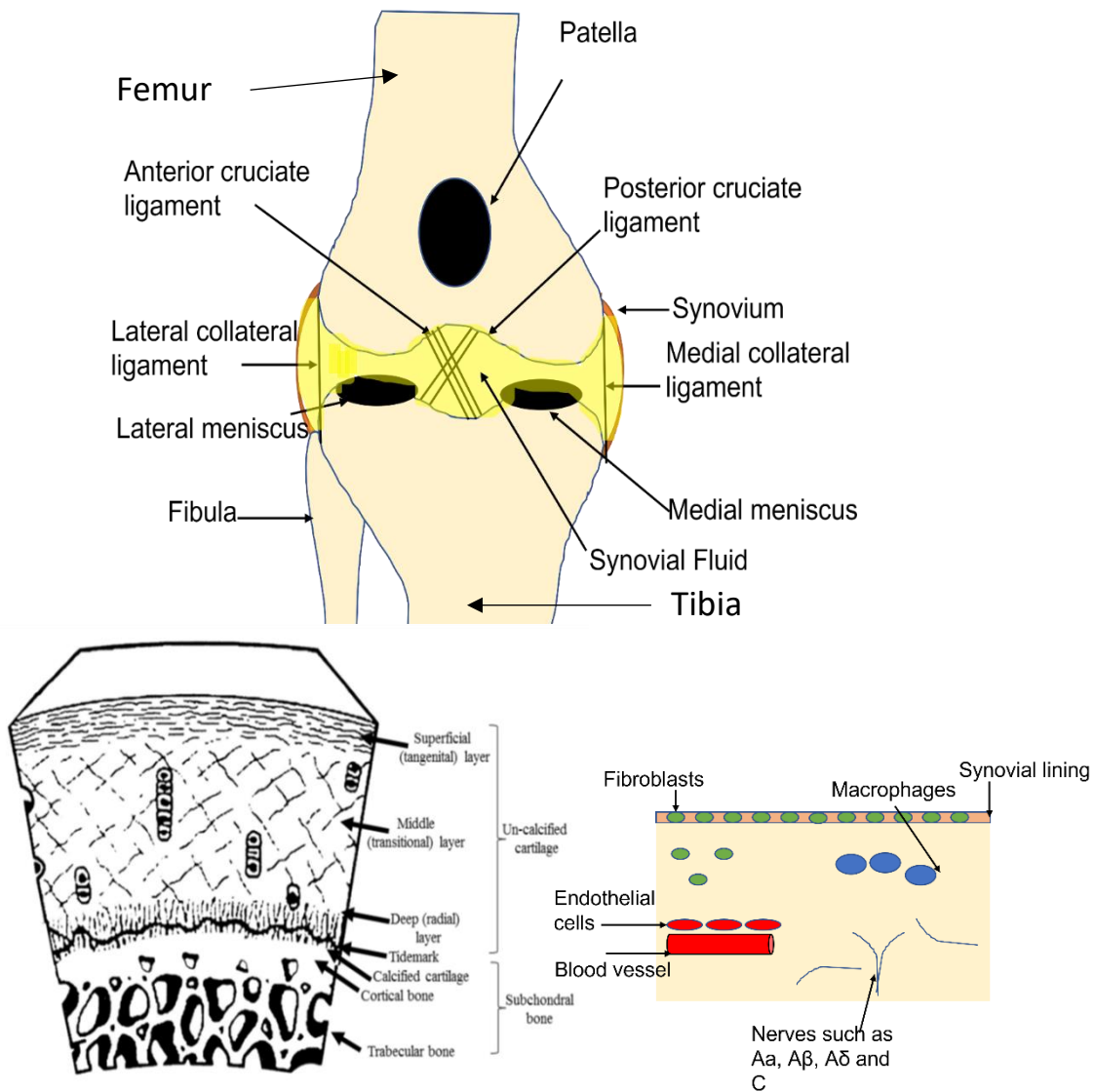


**Figure 1** Anterior view of the anatomy of the knee joint, the anatomy of the cartilage of a synovial joint as well as of the synovium. The knee joint is made up of three bones the tibia, femur, and patella. Four ligaments, thick bands of tissue stabilise the knee joint. These are the Medial Collateral Ligament (MCL), the Lateral Collateral Ligament (LCL), the Anterior Cruciate Ligament (ACL) and the Posterior Cruciate Ligament (PCL). Cartilage is separated into calcified and non-calcified. In the synovium, fibroblasts, endothelial and macrophages can be encountered alongside nerves such as the A $\alpha$ , A $\beta$ , A $\delta$  and C fibers. Figure adapted from (Mandelbaum et al., 1998).

### 1.2.1 Healthy articular cartilage

The bony ends of the knee joint are covered with articular cartilage. Articular cartilage has unique properties which act to protect the joint from weight bearing and dissipate tensile loads. In conjunction with the synovial fluid present in the synovial capsule, cartilage plays a major role in the generation of a low-friction joint surface. Chondrocytes in cartilage are responsible for the production and maintenance of a highly organized extracellular matrix (ECM) comprising of collagen type II, proteoglycans, glycoproteins as well as non-collagenous proteins. This ECM matrix provides the compressive resistance properties of the articular cartilage (Goldring and Marcu 2009, Heijink, Gomoll et al. 2012).

Cartilage has four distinct layers; at the top is the superficial or tangential layer (Figure 1). This area is adjacent to the synovial cavity and represents between 10-20% of the cartilage in the knee joint. Elongated chondrocytes are evident in the superficial layer (Pearle, Warren et al. 2005). Moreover, it lacks proteoglycan components, with collagen 1,2 and 3 being present (Fujioka, Aoyama et al. 2013). After the aforementioned layer, there is the middle or intermediate layer representing approximately half of the cartilage. Chondrocytes are more round in this area, with thick collagen fibres diagonally oriented (Martel-Pelletier and Pelletier 2010). The deep layer or radial zone, rich in proteoglycans, contains chondrocytes aligned distinctly in columns (Pearle, Warren, & Rodeo, 2005). Below this is the calcified layer which is adjacent to the subchondral bone (Madry, van Dijk et al. 2010). The point at which the deep cartilage layer changes to the calcified layer is referred to as the tidemark and is a mineralized area approximately 3-5  $\mu\text{m}$  thick.

Chondrocytes in the different layers of the cartilage have different structures as well as they have the ability to produce different growth factors and specific ECM proteins (Akkiraju and Nohe 2015). Chondrocytes in the superficial zone are flat and elongated producing collagen II, IX and XI and aggrecans, while when in the middle zone they are still elongated but produce procollagen II, collagen IX and XI, biglycan and decorin (Akkiraju and Nohe 2015). Chondrocytes on both layers express growth factors such as IGF-1, FGF-2 -9 -18, TGF- $\beta$ 1 and Wnt -5a, -7a. Of course, the corresponding receptors of these growth factors can be found in the chondrocytes such as FGFR-2, IGF1R, TGFBR1, TGFBR2 (Witt, Salamon et al. 2017). In the deep zone of the cartilage, chondrocytes are big cells with larger nuclei producing procollagen II, collagen type X,

biglycan, decorin, aggrecans and MMP13, with different growth factors compared to the other layers such as BMP2, VEGF, FGF-2, TGF- $\beta$ 1 (Akkiraju & Nohe, 2015).

Articular cartilage is both avascular and aneural (see section on nerve supply below). Normal articular cartilage is hypoxic, and since no blood vessels exist oxygen and nutrients are supplied by diffusion from the synovial environment or from the subchondral bone (Walsh and Haywood 2001, Sophia Fox, Bedi et al. 2009). Chondrocytes in articular cartilage are specifically adapted to a low oxygen environment (Lafont 2010) and mechanical compression.

### **1.2.2 Normal subchondral bone**

The role of the subchondral bone is to support the cartilage by absorbing the mechanical pressure extruded to the joints (Radin and Rose 1986). The subchondral bone consists of the subchondral bone plate which is mineralised (Milz and Putz 1994), the subchondral trabecular evident due to its porous appearance, and subchondral bone marrow which contains fatty marrow (Milgram 1983, Walsh, McWilliams et al. 2010).

Evidence exists of channels that originate in the subchondral bone and breach the tidemark extending into the decalcified cartilage in human OA and animal models (Clark 1990, Suri, Gill et al. 2007, Walsh, McWilliams et al. 2010). These channels are indicative of subchondral bone remodelling, and it has been shown that blood vessels and fine unmyelinated sensory nerves are localized in these channels potentially contributing to pain and inflammation in arthritis (Duncan 1983, Burr and Schaffler 1997, Suri, Gill et al. 2007). The subchondral bone contains, in normal tissue, both sensory and sympathetic nerves, potentially demonstrating the role of the bone in tibiofemoral pain. Substance P-immunoreactive sensory nerve fibres have been described in the subchondral bone of patellae and lumbar facet joints from patients with OA, however it is unclear if these sensory nerves display enhanced sensitivity in OA joints.

### **1.2.3 Normal synovium**

The synovial capsule which encases the knee joint is comprised of two parts: the synovium and the external fibrous connective tissue (Ralphs and Benjamin 1994). The synovium also consists of two layers, the intimal lining, also referred to as synovial membrane, which is a discontinuous layer normally 1-4 cells thick (Haywood, McWilliams et al. 2003, Smith 2011). The intimal layer is responsible for the production of synovial fluid, absorption from the joint cavity

as well as exchanges between blood and the fluid. Fibroblast like cells in the synovium are present in the intimal layer, synthesizing and secreting extracellular proteins such as hyaluronic acid, and also possessing stem cell-like properties being able to differentiate into cells for cartilage repair (Iwanaga, Shikichi et al. 2000).

The subintimal layer has sparse cellularity, contains loose and dense collagenous and adipose tissue, blood and lymphatic vessels, and few inflammatory cells (e.g., macrophages) (Haywood et al., 2003; Smith, 2011). The subintimal layer consists of loose connective tissue with the ability to prevent damage and collision between the bursae, tendons, and joints by re-shaping itself. The subintimal layer is highly vascularized, serving as a transport mediator of nutrients, immune modulation, and inflammation responses in the joint (D. A. Walsh & Haywood, 2001).

While the work presented in this thesis concentrates on synovial mechanisms contributing to inflammation and pain, primarily in human OA, I also include a brief overview of RA.

## **1.3 Rheumatoid arthritis**

### **1.3.1 Aetiology and pathophysiology of rheumatoid arthritis**

Rheumatoid arthritis is one of the most common forms of inflammatory arthritis affecting approximately 1% of the UK population according to the National Institute for Health and Care Excellence (NICE). It affects 1.5 men and 3.6 women per 10 000 people in UK ranging from ages between 30-50 years. Inflammatory arthritides form a group of chronic diseases many of which are triggered by an autoimmune response directed against the joints and multiple other tissues, resulting in joint inflammation and damage (Karmakar, Kay et al. 2010). Joint pain and stiffness on movement are the primary symptoms, however, connective tissue may also be affected such as heart, lungs and other organs leading to cardiovascular diseases (atherosclerosis), lymphomas, pleural effusion, interstitial lung disease, Felty's syndrome (enlarged spleen and low white blood cells) etc, ([cks.nice.org.uk/topics/rheumatoid-arthritis](https://cks.nice.org.uk/topics/rheumatoid-arthritis), (Adams, Walsh et al. 2010). The joint inflammation caused by the autoimmune "attack" results in inflammation, swelling and pain in the synovial joints. A cardinal feature of RA is the proliferation, migration, and invasion of fibroblast-like synoviocytes into other tissues. Pannus is a type of extra growth in your joints specifically in the synovium, that can cause pain, swelling, and damage to your bones, cartilage, and other tissue encountered in RA. Due to the aggressive nature of pannus invasion, it has been

likened to a tumour (Charbonneau, Lavoie et al. 2016), and fibroblast-like synoviocytes are active contributors to joint destruction in RA (Müller-Ladner, Ospelt et al. 2007). Hands, particularly finger joints, feet, wrists, elbows, ankles, and knees are most commonly affected (<https://www.ncbi.nlm.nih.gov/books/NBK384455/>). As the disease progresses the articular cartilage and subchondral bone are progressively damaged, and eventually the cartilage can be completely degraded, and due to extensive remodelling joints can become fused, leading to reduced mobility and increased pain (Guo, Wang et al. 2018). RA is typically a symmetrical disease, a feature that is usually part of the diagnosis of the disease, along with the presence of active inflammation, which can result in pain at rest (Guo et al., 2018).

### **1.3.2 Classification and diagnosis of rheumatoid arthritis**

The American College of Rheumatology alongside the European Alliance Association for Rheumatology proposed criteria in 2010 to enable consistent classification of RA in the early stages of the disease, in order to begin effective early treatment to prevent bone destruction and radiological progression (Finckh, Liang et al. 2006, van der Kooij, le Cessie et al. 2009). Specifically, polyarthralgia with symmetrical joint involvement in the joints of hands and feet was considered the most typical presentation for RA. Morning stiffness accompanied by symmetrical inflammation was also considered as a baseline common symptom for RA. To confirm the diagnosis of RA joint erosion must be present. This is shown as bone erosion, a peri-inflammatory destructive bone lesion that radiologically refers to a break in cortical bone with destruction of the natural barrier between the extra skeletal tissue and the bone marrow compartment. The criteria set out by ACR, and EULAR only accepts clinical examination with the presence of definitive synovitis for diagnosis of RA. MRI and radiographic practices are used in the prediction of the progression of RA and to aid in the distinction between RA and undifferentiated arthritis (Colebatch, Edwards et al. 2013). The classification scoring criteria for RA as described by ACR/EULAR 2010 are described in Table 1.

**Table 1 Classification criteria of the ACR/EULAR 2010 for diagnosis of RA (Kay and Upchurch 2012)**

<b>Joint involvement (clinical synovitis)</b>	<b>Grading</b>	<b>Serology</b>	<b>Grading</b>	<b>Acute phase reactants</b>	<b>Grading</b>	<b>Duration of symptoms</b>	<b>Grading</b>
1 large joint	0	RF and anti-CCP	0	Normal C reactive protein and ESR	0	<6 weeks	0
2-10 large joints	1	RF or anti-CCP <3	2	Abnormal C reactive protein and ESR	1	>6 weeks	1
1-3 small joints	2	RF or anti-CCP > 3	3				
4-10 small joints	3						
>10 joints	5						

***\*RF=rheumatoid factor, anti-CCP= anti-cyclic citrullinated peptide, ESR=erythrocyte sedimentation rate. Depending on the grading on each individual category (joint involvement, serology, acute phase reactants and duration of symptoms) an overall score is produced. If the sum of the grades is equal or higher than 6 then the patient can be diagnosed with definitive RA.***

### **1.3.3 Treatment and management of rheumatoid arthritis**

In the UK, the strategy for RA treatment is one of ‘treat-to-target’ and aims to achieve disease remission or low activity. First line management for patients suffering from RA is therefore administration of conventional disease modifying anti-rheumatic drugs (cDMARDs) such as methotrexate alone or in combination with other cDMARDs (e.g., leflunomide, sulfasalazine or

hydroxychloroquine). The most common traditional DMARD is methotrexate (MTX), an analogue to folic acid that inhibits dihydrofolic acid (FH<sub>2</sub>) conversion to folinic acid (FH<sub>4</sub>). MTX is an effective DMARD working through immunosuppression, but that has potentially dangerous side effects such as liver problems, cirrhosis, and bone marrow deterioration. However, when compared to other DMARDs the incidence of these side effects is relatively low (Tian and Cronstein 2007). Hydroxychloroquine (Plaquenil) is one alternative to MTX; an antimalarial drug that decreases the expression of pro-inflammatory cytokines from monocytes (Silva, Mariz et al. 2013).

If this treatment does not achieve remission or low disease activity, then the biological/synthetic DMARDs that primarily target TNF- $\alpha$  are prescribed. One of the main targets of the biological DMARDs is TNF- $\alpha$ , an inflammatory cytokine elevated in the joints of people with RA. Etanercept (TNF- $\alpha$  inhibitor protein), infliximab (chimeric anti- TNF- $\alpha$  antibody) and adalimumab (monoclonal antibody against TNF- $\alpha$ ) promote alleviation of symptoms by blocking the migration of inflammatory cells in the joints. It is common for these drugs to be used in conjunction with other DMARDs such as MTX, and their efficacy in reducing disease activity and halting the progression of joint destruction in RA is great (Gay, Clarke et al. 2010, Lis, Kuzawińska et al. 2014, Perpétuo, Caetano-Lopes et al. 2017). Adverse effects associated with the biologic DMARDs can be serious, particularly in people with cardiac conditions, and also include neurological effects and increased risk of infection (Tovey and Lallemand 2011, Rein and Mueller 2017, den Broeder, van Herwaarden et al. 2018). Previously DMARDs have been considered to cause lymphomas as an adverse effect, however, after a study in 2021, namely on (Hellgren, Di Giuseppe et al. 2020), they showed that bDMARDs do not further heighten the risk of lymphoma but rather reduce the lymphoma risk in RA.

Even when the disease is well controlled by DMARDs a significant proportion (~30%) of people with RA still experience pain (Altawil, Saevarsdottir et al. 2016). In these circumstances, RA pain is controlled by non-steroidal anti-inflammatory drugs (NSAIDs), either traditional drugs such as acetylsalicylate (aspirin) or ibuprofen or selective Cox-2 inhibitors. As effective as these NSAIDs can be, for instance, aspirin one of the longest NSAIDs used against RA due to inhibition of prostaglandins, adverse effects such as tinnitus, hearing loss, renal damage, and gastric ulceration are major concerns. Selective COX-2 inhibitors (e.g., Celebrex) have also been used as a potential drug depending on the risk of adverse events with traditional NSAIDs (Ong, Lirk et al. 2007). They are only used when the risk of the traditional NSAIDs is high, for example when there

is an existing kidney disease. If prescribed with proton pump inhibitors, the adverse effects are not high for the traditional treatments, and the adverse effects with Cox-2 selective inhibitors are not significantly lower in most people (Ong, Lirk et al. 2007). Some opioid analgesics have been used and played a role in an effective but short management of RA pain however the adverse effects far outweigh the benefits. UK recommendations are that the evidence does not support the use of opioids for the treatment of RA pain (<https://www.nice.org.uk/guidance/ng100/evidence/evidence-review-g-analgesics-pdf-4903172324>). Weak opioids could be considered such as codeine, dextropropoxyphene, and tramadol, however, great care must be exercised by practitioners and patients a practice however that is not as common in UK (Richards, Whittle et al. 2012, Whittle, Colebatch et al. 2012).

Systemic, intramuscular, and intraarticular corticosteroids have been used with success to combat local symptoms of inflammation (Combe, Landewe et al. 2017). The underlying mechanism includes the inhibition of phospholipid release, decreasing the activity of eosinophils and thus decreasing the levels of inflammation. Due to adverse effects such as suppression of the hypothalamic-pituitary-adrenal axis (HPA) great care is advised when corticosteroids are being prescribed (Liu, Ahmet et al. 2013), and they are only recommended in the UK for the management of short-term flares, or where other drug treatments have been discussed and not taken up, and/or failed.

Finally, surgery is also used in the treatment of RA, particularly in the case of persistent pain and synovitis, loss of joint function, and joint deformity. Total joint replacement is however often only available to people with “end-stage” RA pathology with severe pain, joint destruction and deformity and compromised function, although this is not always the case.

## **1.4 Osteoarthritis**

### **1.4.1 Aetiology and pathophysiology of OA**

According to OARSI, OA is a disorder that involves joints, and it is associated with cell stress as well as extracellular matrix degradation. These changes are initiated by injury which in turn initiate repair responses and pro-inflammatory pathways of innate immunity. Manifestation and progression of the disease includes abnormal joint tissue metabolism, anatomic and physiologic

alterations such as cartilage degradation and bone remodelling, and joint inflammation (<https://oarsi.org/research/standardization-osteoarthritis-definitions>).

Osteoarthritis (OA), the most common form of arthritis is a disease of the aged population. It is a chronic condition that can affect any joint, but it occurs most often in the knees, hips, lower back and neck, small joints of the fingers and the bases of the thumb and big toe (Heidari, 2011). Development of OA is linked to previous trauma and can affect athletes, members of the military and people who work physically demanding jobs. Age, weight, and trauma to the joint due to repeating movements, in particular, squatting and kneeling are common risk factors of OA, but the precise aetiology of the disease is not completely understood. Knee OA has been thoroughly researched since it is highly prevalent when compared to the other types (e.g., hip OA), but also since it can be presented at younger age groups. The occurrence of knee OA is positively related to age and further increases with the higher expectancy of life as well as the higher average weight of the population (Heidari 2011). OA is characterised by stiffness and pain on movement, particularly after periods of immobility. There may also be 'flares' when joints become inflamed, and these are usually painful.

Although OA has long been regarded as a degenerative disease of the cartilage, recent studies have shown that the pathophysiology of OA is more complex than initially thought, with all the tissues in the synovial joint being involved in the pathogenesis (Loeser, Goldring et al. 2012, Aspden and Saunders 2019) re-examined the idea of OA being characterised as a joint disorder than a cartilage disorder suggesting that changes encountered in the bone and soft tissue of the joint alongside cartilage changes promote a more balanced approach for characterizing OA as a joint failure disease.

Current estimates suggest that cases of OA will increase in the future, due to longer life expectancy, increased levels of obesity in the population and sports injury. There are no existing disease-modifying osteoarthritic drugs (DMOADs) (see also section 1.4.6 treatments for OA), and thus OA represents a significant clinical unmet need.

### **1.4.2 Classification and diagnosis of osteoarthritis**

Two distinct classification grades exist for OA; idiopathic OA (or primary) where no obvious cause of the disease can be identified, or secondary OA where joint trauma or medical conditions such as inflammatory arthritis can be identified as a precipitating factor (Altman, Asch et al. 1986,

Gelber, Hochberg et al. 2000). While OA can affect single joints (monoarticular OA), it can also affect more joints in the human body and in this case, it is classified as generalized OA.

The different clinical and pathological OA classification criteria were defined in 1986 by the American College of Rheumatology (Altman et al., 1986), as illustrated in Table 2. Joint pain is the main clinical criteria present in all the diagnosis for knee joint OA alongside a combination of clinical radiographic and pathological features. The European League Against Rheumatism (EULAR), have defined a standard procedure to identify and diagnose knee OA which includes high importance clinical signs such as (knee) pain, morning stiffness, reduced function, and bone growths/ enlargement (osteophytes) (Zhang, Nuki et al. 2010).

**Table 2 The ACR criteria to identify idiopathic osteoarthritis of the synovial knee joint table (adapted from Altman et al., 1986)**

**\*Synovial fluid signs of OA include viscous or clear and white blood cells below 2000.mm<sup>-3</sup>**

Clinical and laboratory	Clinical and radiographic	Clinical
Knee pain	Knee pain	Knee pain
<i>At least 5 of:</i>	Osteophytes	<i>At least 3 of:</i>
Age>50	<i>At least 1 of:</i>	Age>50
Stiffness	Age>50	Stiffness
Crepitus	Stiffness	Crepitus
Bone tenderness		Bone tenderness
Bone enlargement		Bone enlargement
No palpable warmth		No palpable warmth
Synovial fluid signs of OA		

### 1.4.3 Articular cartilage changes in osteoarthritis

Articular cartilage damage is a key pathology in OA, but given its aneural nature, and the lack of correlation between radiographic joint changes, and pain (Felson 2005, Hill, Hunter et al. 2007), destruction and loss of cartilage itself is unlikely to be the direct cause of pain (Swales, Athanasou et al. 2014).

Degradation of cartilage is a major pathological feature of OA and can be measured histologically with a grading system developed by Mankin (Mankin, Dorfman et al. 1971), using a scale from 0 (normal) to 6 (complete degradation). Currently, OARSI grades are more commonly used for the evaluation of cartilage damage as described in Li et al., 2021 (Li, Liem et al. 2021).

**Early OA** – (normal cartilage, or beginnings of surface fibrillation, loss to surface, normal chondrocytes, or slight hypercellularity, normal matrix, or slight loss of constituents and structure).

Characteristic evidence of OA progression in the cartilage includes surface fibrillation and loss of cartilage surface (Pesesse, Sanchez et al. 2011). In early OA, overexpression of collagen type 2 and aggrecan synthesis by chondrocytes is evident (Swales, Athanasou, & Knowles, 2014).

Molecular changes in the structure of cartilage proteoglycans are also evident in OA or inflammatory arthritis without OA (Malfait and Schnitzer 2013). In healthy joints aggregated proteoglycans are present, which disaggregate following cartilage damage, resulting in increased hydraulic permeability, and chondromalacia and loss of cartilage stiffness (Franz, Hasler et al. 2001). This cartilage softening is a key early pathological feature of OA and is also evident at macroscopic inspection of the knee joint.

**Moderate OA** - (clefts, chondrocyte clusters, loss of matrix, changes in tide mark)

As the disease progresses, release of proteolytic enzymes and matrix metalloproteases (MMPs) from chondrocytes, results in further degradation of the cartilage (Reboul, Pelletier et al. 1996). Signalling through receptors such as the Fibroblast growth factor-2 (FGF-2) (Nummenmaa, Hämäläinen et al. 2015), or the activin-like kinase 5 receptor ALK5 affect the levels of MMP13 (Blaney Davidson, Remst et al. 2009). More specifically, as OA progresses, chondrocytes become hypertrophic and cluster, which is associated with increased levels of MMP13 and expression of collagen type X (Aigner, Reichenberger et al. 1993, Sandell and Aigner 2001, James, Appleton et al. 2005). As a result of these changes, clefts perpendicular to the cartilage surface develop, which can penetrate as deep as the calcified layer in advanced OA. The loss of integrity in the collagen network and ECM, as well as reduced adhesion of chondrocytes, results in increased water content in the cartilage (Berberat, Nissi et al. 2009).

**Advanced OA** – (cartilage disorganisation, hypocellularity, loss of matrix, calcification, loss of tidemark, loss of cartilage). Calcification of the cartilage and duplication of the tidemark. In end stage OA, complete loss of articular cartilage can be observed.

Vascular and neuronal invasion into clefts in the cartilage (Aso, Shahtaheri et al. 2020) can be identified as a potential mechanism of OA pain. Cartilage tidemark breaching was evident in 43% of TKR cases compared to only 11% of non-OA control cases (Suri, Gill et al. 2007). Phenotypic modification of chondrocytes to express angiogenic factors, such as vascular endothelial growth factor (VEGF) may play a crucial role in vascular invasion (Murata, Yudoh et al. 2008). NGF production has been identified as a mediator for innervation of the damaged cartilage alongside the blood vessel invasion in late-stage OA.

#### **1.4.4 Synovial inflammation in osteoarthritis**

Inflammation in the synovium, synovitis, is now a well-recognised feature of OA in both early and late stages (Smith, Triantafillou et al. 1997). Synovitis in OA can present with varying levels of inflammation and can be either episodic or persistent.

Synovitis can be observed from the stages of early OA. During OA synovitis, synovial histology is altered, characterised by an increase in the thickness of the synovial lining, now comprising by more than 7 cells deep, accompanied by cellular hypertrophy and hyperplasia, and characterised by the presence of CD4 positive lymphocytes or T helper cells and CD68 positive macrophages, increased angiogenesis and vascularisation associated with increased expression of angiogenic factors such as VEGF-A, and synovial tissue expansion (Benito, Veale et al. 2005). Infiltrating macrophages form multinucleated giant cells (MGCs), that are present in increased numbers in OA and RA. Macrophages and MGCs produce many of the pro-inflammatory cytokines important in OA progression (Mathiessen and Conaghan 2017). In severe cases, lymphoid aggregates may also be observed (Haywood, McWilliams et al. 2003). Synovial inflammation in end-stage OA has a positive relationship with the degree of synovial angiogenesis and VEGF-A expression in macrophages and synoviocyte-like fibroblasts. Synovial tissue for histological examination can be obtained during arthroplasty in patients with symptomatic OA (Myers, Brandt et al. 1990, Haywood, McWilliams et al. 2003). Synovitis can often be present before evidence of cartilage damage in OA (Mathiessen and Conaghan 2017), and products of cartilage damage cause synovial inflammatory responses, showing complex interactions of changes in different parts of the joint in OA.

### **1.4.5 Inflammatory mediators in osteoarthritis**

There are many important pro-inflammatory mediators released in osteoarthritic joints, such as cytokines, chemokines, matrix metalloproteases (MMPs) and growth factors that contribute to the propagation and maintenance of inflammation and joint damage in OA, leading to a complex OA pathogenesis. This thesis cannot give a fully comprehensive list of all mediators potentially involved, so I concentrate on the major cytokines, chemokines, and growth factors here.

#### **1.4.5.1 Cytokines**

Cytokines are glycoprotein molecules secreted from inflammatory cells inducing inflammation, that can have both pro-inflammatory and anti-inflammatory profiles, and that are strongly associated with the maintenance and progression of OA (Zhang and An 2007, Kapoor, Martel-Pelletier et al. 2011).

Two of the most studied pro-inflammatory cytokines in the context of OA pathogenesis are tumour necrosis factor-alpha (TNF- $\alpha$ ) and interleukin-1 beta (IL-1 $\beta$ ), both of which are also targets for bDMARDs treatment in RA. Synovial, and inflammatory cells and chondrocytes can all secrete these cytokines (Sellam and Berenbaum 2010). IL-1 $\beta$  and TNF- $\alpha$  can also trigger the release of other cytokines such as IL-6 or IL-8, leukocyte inhibitory factor and COX-2 (Fernandes, Martel-Pelletier et al. 2002, Fehrenbacher, Burkey et al. 2005, Goldring and Otero 2011). MMP gene expression and growth factor expression, such as NGF and VEGF-A, have also been proved to be related to the actions of TNF- $\alpha$  and IL-1 $\beta$  (Fernandes, Martel-Pelletier et al. 2002, Honorati, Cattini et al. 2004).

IL-1 $\beta$  and TNF- $\alpha$  activate downstream signalling pathways such as the nuclear factor kappa-b and the p38 mitogen-activated kinase pathway (Albert S. Baldwin 1996, Kapoor, Martel-Pelletier et al. 2011). The role of these pathways in inflammation is facilitated through activation of different pro-inflammatory cytokines including IL-2, IL-6, IL-8, IL-12, and interferon gamma IFN- $\gamma$ ) (Albert S. Baldwin 1996, Roman-Blas and Jimenez 2006). Cytokines, e.g., IL-6, are positively related to heightened pain sensitivity in people with inflammatory OA (Wojdasiewicz, Poniatowski ł et al. 2014), and can act directly on nociceptive neurons (Schaible 2014). Other cytokines, such as IL-17 can induce the production of chemokines e.g., IL-8, from cells including chondrocytes and synovial fibroblasts, implying a catabolic role for some chemokines in OA pathogenesis (Honorati, Bovara et al. 2002).

### 1.4.5.2 Chemokines

Chemokines are cytokines with distinct chemotactic properties, that can induce movement of immune cells such as macrophage, monocytes, and lymphocytes, to and from inflammatory tissue (Haringman, Gerlag et al. 2006, Zhang and An 2007, Wojdasiewicz, Poniatowski Ł et al. 2014). There are four chemokine groups in the chemokine family; C-C chemokine group, including the monocyte chemotactic protein (MCP) and the macrophage inflammatory protein (MIP); the C-X-C group, which includes example members such as the chemokine ligand 1/2/5/10 (CXCL1, CXCL2, CXCL5, CXCL10); the C group including lymphotactin; and finally, the CXXXC chemokine group with fractalkine being an example member (Zhang and An 2007). Some chemokines are associated with increased pain states in OA, for example, MCP and CCL2 (monocyte chemoattractant protein 1/chemokine ligand 2) are associated with increased pain scores in patients (Cuellar, Scuderi et al. 2009). Fractalkine, the only member of CX3C, is detected in the synovial fluid of people with OA, and fractalkine levels are positively related to the severity of OA (Zou, Li et al. 2013, Wojdasiewicz, Poniatowski Ł et al. 2014)

### 1.4.5.3 Matrix metalloproteases (MMPs)

Matrix metalloproteases (MMPs) are part of a larger family of zinc dependent endopeptidases, classified into 5 groups described in Table 3 (Murphy, Knäuper et al. 2002, Park, Lee et al. 2004). During inflammatory OA, MMPs have been identified as enhancers of joint destruction through proteolytic matrix degradation (Park et al., 2004), while inducing inflammation through upregulation of other cytokines and chemokines (McQuibban, Butler et al. 2001, McQuibban, Gong et al. 2002).

**Table 3 Classification of the different groups of matrix metalloproteases with their individual family members**

Matrix metalloprotease group	Family members
Collagenases	MMP1, MMP8, MMP13
Gelatinases	MMP2, MMP9
Stromelysins	MMP3, MMP10, MMP11
Membrane type	MMP14/15/16/17, MMP24
Other	MMP7/11/12/20/23/28

#### **1.4.5.4 Growth factors**

Several different growth factors are involved in the development and maintenance of OA, with prime examples including NGF (nerve growth factor), transforming growth factor (TGF)- $\beta$  and vascular endothelial growth factor (VEGF)-A (for detailed overview, see section 1.6) (Ferrara and Henzel 1989, Tsuchida, Beekhuizen et al. 2014).

#### **1.4.5.5 Nerve growth factor**

NGF is a member of the neurotrophin family and is essential in the development of the sympathetic and parasympathetic neuronal growth as well as the survival of the nervous system (Levi-Montalcini 1987). Previously published data support the role of NGF as the origin and maintenance of hyperalgesia particularly in inflammatory conditions (Woolf, Ma et al. 1996). During arthritis, the NGF levels are elevated in the synovial fluid of patients with symptomatic OA (symptoms include joint pain, aching, and stiffness) (Halliday, Zettler et al. 1998, Barthel, Yeremenko et al. 2009, Raychaudhuri, Raychaudhuri et al. 2011). Evidence suggests that NGF increases nociceptor excitability and pain behaviour in OA, thus mediating inflammatory pain through this pathway (Ashraf, Mapp et al. 2014). Clinical trials that blocked NGF using specific antibodies against the growth factor have shown successful reduction of pain in patients with severe OA, also suggesting a link between NGF and symptomatic OA. Inflammatory mediators that are upregulated in inflammation and damaged tissue (IL-1 $\beta$  and TNF- $\alpha$  for example) promote the expression of NGF in surrounding cell types such as macrophages and synoviocytes (Barthel, Yeremenko et al. 2009, Takano, Uchida et al. 2019) (which in turn binds to TrkA receptors (tyrosine kinase receptors) (Kras, Weisshaar et al. 2015, Nwosu, Mapp et al. 2016) inducing further release of other inflammatory molecules and NGF (Bruno and Cuello 2006, Sellam and Berenbaum 2010). This interaction induces pain transmission through NGF, which further induces peripheral sensitization of nociceptors leading to hyperalgesia.

#### **1.4.5.6 Transforming growth factor (TGF)- $\beta$**

TGF- $\beta$  regulates functions in healthy and disease states such as cell proliferation, formation and repair of tissues and inflammation. Three distinct peptides are recognised namely TGF- $\beta$ 1, TGF- $\beta$ 2, and TGF- $\beta$ 3 (Newfeld, Wisotzkey et al. 1999). Deficiencies of these peptides leads to developmental issues in mice, for instance TGF- $\beta$ 1 deficiency results in lethal knock outs due to defective endothelial differentiation (Dickson, Martin et al. 1995). TGF- $\beta$ 2 knockout mice show

developmental defects of the heart, spinal column, eye, and inner ear while being lethal shortly after birth (Sanford, Ormsby et al. 1997). TGF- $\beta$ 3 knockout mice exhibit defectiveness in lung development, with a cleft palate, and are lethal shortly after birth (Proetzel, Pawlowski et al. 1995).

Healthy synovial joints and more specifically articular cartilage contain large quantities of TGF- $\beta$ , with TGF- $\beta$ 1 representing 60%-85% (Albro, Nims et al. 2013). When sufficient mechanical force is applied in the joint TGF- $\beta$  is released from its latency binding peptide (LAP), however as soon as 2 hours after the mechanical stimuli the active TGF- $\beta$  signalling is reduced to the initial levels (Zielinski, Bartels et al. 2000, Hinz 2009, Hinz 2015).

In OA joints, TGF- $\beta$  is upregulated in synovial fluid by proteolytic activation and has been found to be overexpressed (Aida, Maeno et al. 2006). Overexpression of the growth factor activates cells that are not normally exposed to high levels of TGF- $\beta$ , leading to altered cell differentiation and leading to hypertrophic cells. This event occurs through the Smad1/5/8 pathway, leading to the growth factor losing its protective effect on the cartilage. Such events promote the inflammatory profile and destruction of the joint leading to extended inflammation (Retting, Song et al. 2009, Finsson, Parker et al. 2010, Hellingman, Davidson et al. 2011).

#### **1.4.5.7 Vascular endothelial growth factor**

Multiple studies have shown that VEGF-A is involved in the pathogenesis of arthritis, mainly because the principal function of VEGF-A is the ability to promote the growth of vascular endothelial cells (ECs) (Ferrara and Davis-Smyth 1997) in angiogenesis in inflammation. However, the functions of VEGF-A are not limited to angiogenesis and vascular permeability (Senger 2010), for example it can also affect the function of immune cells and consequently affect the host response to inflammation or tumours (Goel and Mercurio 2013). VEGF-A is expressed by many cell types in addition to endothelial cells, such as fibroblasts, platelets, neutrophils, macrophages, (Peach, Mignone et al. 2018) neurons (Beazley-Long, Hua et al. 2013), and astrocytes (Ijichi, Sakuma et al. 1995). VEGF-A is best known for its actions on endothelial cells and blood vessels, through which it promotes physiological and pathological angiogenesis. These actions are important in physiological angiogenesis, such as in wound healing and in the reproductive systems (Shibuya 2013), and pathological angiogenesis promoting tumour growth (Florea, Mottaghy et al. 2021), neovascularisation in retinal diseases such as diabetic retinopathy

and age-related macular degeneration (Sadda, Guymer et al. 2020), in diabetic renal disease (Cai, Chatziantoniou et al. 2021), and in RA and OA (Le and Kwon 2021).

VEGF-A is increased in the serum of RA patients (Nakahara, Song et al. 2003), and VEGF-A levels in synovial fluid and serum correlate well with arthritic disease activity in both late-stage OA and RA and are strongly associated with the number of swollen joints (Sokolove and Lepus 2013). VEGF-A expression is induced in synoviocytes by hypoxia, and inflammatory mediators (Jackson, Minton et al. 1997). Synovial tissues of people with arthritis show increase numbers of macrophages, as well as fibroblasts and macrophages show increased expression of VEGF-A (Hamilton, Nagao et al. 2016). In more advanced OA, VEGF-A contributes to articular cartilage degeneration, and neurovascular invasion, increased migration, and activity of macrophages in synovium, and activation of fibroblasts and neutrophils that contribute to a feed-forward loop that increases the levels of cytokines and VEGF-A, amplifying the inflammatory response (Hamilton, Nagao et al. 2016, Nagao, Hamilton et al. 2017). VEGF-A has multiple splice variants of varying amino acid length, with different potential functions and tissue distributions. Vascular endothelial growth factor isoforms VEGF<sub>121</sub> and VEGF<sub>165</sub> are expressed in RA synovium (the number denotes the number of amino acids in the variant) (Pufe, Petersen et al. 2001), and different isoforms like VEGF<sub>121</sub> and VEGF<sub>189</sub> are found in osteoarthritic cartilage (Pufe, Petersen et al. 2001).

As vascular endothelial growth factor, its splice variants and their contribution to inflammation and pain in arthritis is the main focus of this thesis, greater detail on the complete VEGF family, its splice variants and the function of the family members is given in sections 1.6 below.

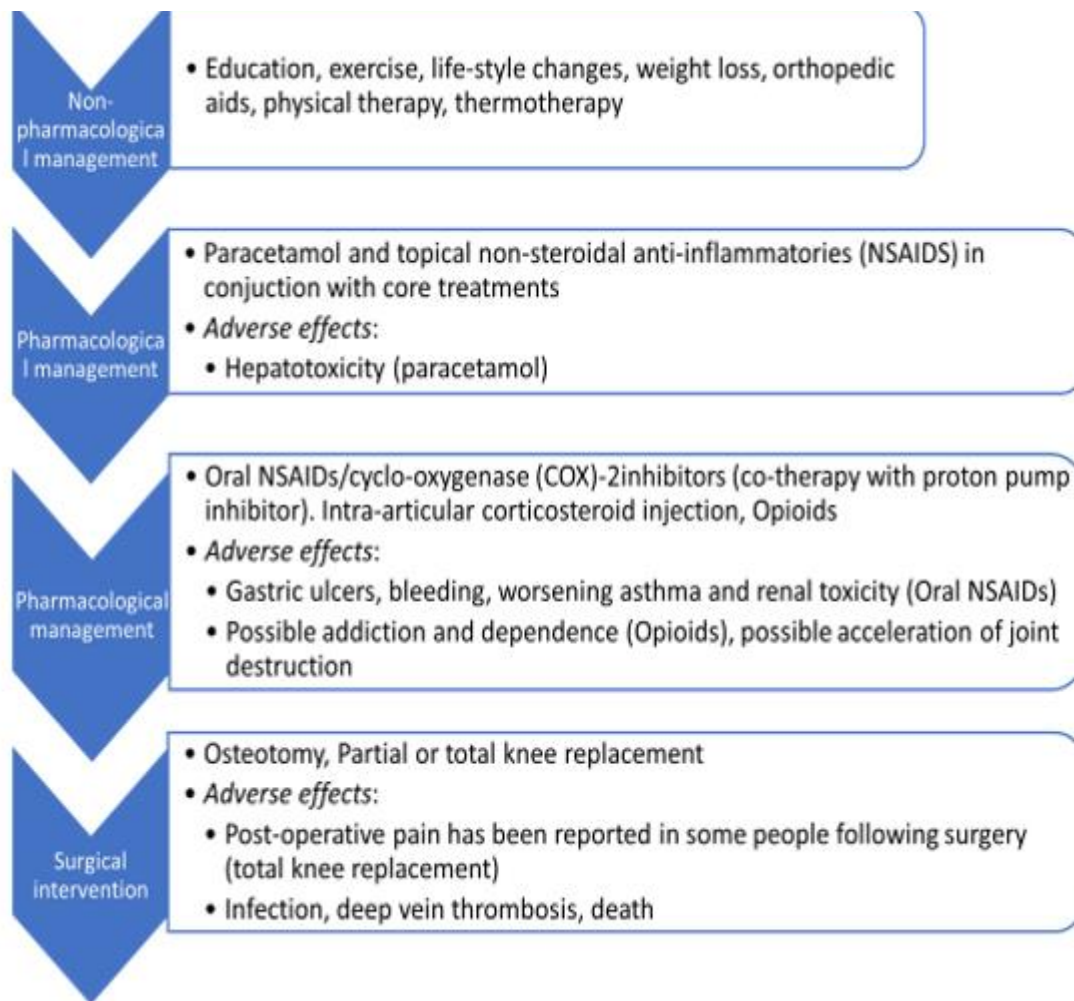
#### **1.4.6 Management and treatment of osteoarthritis**

Even though several different treatments for OA exist, given its complex disease process no cure has yet been developed. Management of the symptoms requires a holistic approach, with a combination of pharmacological and non-pharmacological treatments to alleviate symptoms, inflammation, pain and increase joint mobility as well as quality of life. Table 3 shows a schematic analysis for the roadmap of treatments currently available and recommended for patients with OA in the USA. Similarly, in UK patients diagnosed with OA are offered first non-pharmacological treatment (exercise, weight loss, electrotherapy, acupuncture), before being offered pharmacological management such as oral analgesics (NSAIDs, Cox-2 inhibitors), topical

treatments or intra-articular injections. Following this the patients may be referred for consideration for joint surgery.

Initially people with OA are provided with the core treatment strategy, consisting of non-pharmacological modalities. In the case of no remission of symptoms and pain, pharmacological options may be prescribed, and in the severe cases of OA, when the pain is assessed as an 8/10 in a pain questionnaire from the patients, surgical treatment may be offered. Of course, each of these treatments have adverse effects which are described in Table 4.

**Table 4 Flow chart for the diagnosis of OA based on the classification criteria used by the American College of Rheumatology**



### **1.4.6.1 Non-pharmacological management of OA**

The first step of the core treatment for non-pharmacological management of OA is life-style changes. Moderate exercise is encouraged, to maintain joint motility, range of movement, and muscle strength to stabilise joints. Weight loss is also recommended where obesity is a major co-morbidity factor for OA (Christensen, Astrup et al. 2005). In most cases these two approaches have shown good results, reduced pain and improving function of knee OA (Messier, Loeser et al. 2004). Finally, combination with physiotherapy also reduces symptoms through increased muscle strength and stability.

### **1.4.6.2 Pharmacological management of OA**

The first option for pharmacological treatment alongside non-pharmacological management is paracetamol, which is effective against mild to moderate OA pain. Of course, the adverse effects of long-term paracetamol use can be dangerous providing its toxicity effects, thus OARSI guidelines advice caution in the prescription of it (McAlindon, Bannuru et al. 2014). Of course, this is not the only issue with paracetamol use; there is a narrow therapeutic window and the potential for overdose, particularly in the forgetful elderly. However, at the correct dose paracetamol is safer than NSAIDs. Similarly, NICE guidance recommends paracetamol as the first line of treatment, alongside topical NSAIDs, before intra-articular steroid injections and opioids. Non-steroidal anti-inflammatory drugs (NSAIDs) are primary candidates for prescription to alleviate inflammation in the affected joints. All NSAIDs including ibuprofen and naproxen, two core examples, inhibit the cyclo-oxygenase enzymes (COX-1 and COX-2) to reduce the synthesis of prostaglandins, which induce inflammation and pain (Zarghi and Arfaei 2011). However, prostaglandins are also part of the gastric mucosal defence, and integral to kidney function, thus long-term use of NSAIDs have the potential of adverse effects in the gastrointestinal tract and renal systems (Ofman, MacLean et al. 2002, Harirforoosh and Jamali 2009).

In more severe OA, paracetamol and topical NSAIDs may not be effective to alleviate inflammation and pain. In these cases, either oral NSAIDs or COX-2 inhibitors are considered alongside therapies to avoid the adverse effects of NSAIDs, such as proton pumps inhibitors (Scheiman 2013).

Cortico-steroid injections are recommended as adjunct treatment alongside NSAIDs in patients with severe pain and can alleviate symptoms in patients that were not responding in the previous

treatments (Raynauld, Buckland-Wright et al. 2003). However, due to the nature of the corticosteroids, the injections should be offered up to four times a year.

Injections with hyaluronic acid (a natural protein component of cartilage and synovial fluid) have similar efficacy to NSAIDs, while reducing the potential adverse effects (Ishijima, Nakamura et al. 2014), however, there are studies suggesting that hyaluronic acid is not effective (McAlindon, Bannuru et al. 2014), with OARSI suggesting caution when prescribed and not recommending it for use. Contrary to that, recent publications such as (Bucci, Chen et al. 2022), suggest that HA injections are effective in delaying TKR, like glucocorticoid.

All the OA treatments used and described primarily target pain control, and none are capable of affecting OA disease progression. There are therefore many treatment strategies in active development for both alleviation of pain and modification of disease.

Anti-nerve growth factor (NGF) however, has been reported to alleviate pain in patients suffering from rapidly progressing OA (Lane, Schnitzer et al. 2010, Sanga, Katz et al. 2013), however, it carries the risk of aggravating the structural progression of OA (Miller, Block et al. 2017).

### **1.4.6.3 Total-knee replacement surgery**

In end stage OA, and when pharmacological treatments are not effective in alleviating the symptoms (severe pain, stiffness, disability, loss of function) surgical treatments are indicated. These can include osteotomy, which attempts to shift the weight borne from the diseased area to a healthy compartment of the knee joint, and joint replacement surgery to replace either part or the whole diseased knee joint (uni-compartmental knee replacement for the former, and TKR for the latter). Of course, it is important to note that the treatments suggested here are not necessarily sequential; not every patient is treated with osteotomy before knee replacement). However, patients experience post-surgical pain 3 years after the replacement surgery. A study by Wylde et al. (Wylde, Rooker et al. 2011) showed that 44% of patients experienced pain 4 years after arthroplasty with 6% experiencing severe neuropathic pain. In a re-examination of the same concept in 2018, (Wylde, Beswick et al. 2018) approximately 20% of patients experience chronic pain after TKR.

## 1.5 Osteoarthritis and pain

### 1.5.1 Innervation of the knee joint

Both sensory and sympathetic nerves innervate the knee joint (Gardner 1948). The majority of the synovial joint is innervated by low (touch/pressure sensitive) and high threshold (nociceptive) sensory neurons (Dye, Vaupel et al. 1998), including but not limited to the synovium, fat pad, the subchondral bone, and the joint capsule (Lehner, Koeck et al. 2008). The articular cartilage is however aneural (Amin, Guerhazi et al. 2008, Ashraf, Mapp et al. 2011, Ashraf, Wibberley et al. 2011). There is very little known about why cartilage remains aneural unless damaged, but proteoglycans seem to maintain the non-innervation of the cartilage, as loss of proteoglycan from cartilage is associated with increased vessel and nerve growth in intervertebral discs (Binch, Cole et al. 2014, Pecchi, Priam et al. 2014). Moreover, NGF is expressed in deep normal chondrocytes in the knee joints however it is not clear why its expression does not translate to innervation (Gigante, Bevilacqua et al. 2003).

Sensory nerves have cell bodies in the dorsal root ganglia, and long fibres (in humans > 1m in length innervating distal areas) which function to convey sensory information from the peripheral innervated areas to the central nervous system.

Table 5 and 6, show the classification and properties of sensory neurons (Eitner, Hofmann et al. 2017).

Large, myelinated A $\alpha$  and A $\beta$  fibre neurons (also known as group I and II afferents) are rapidly conducting (>30m.s<sup>-1</sup> in larger animals) and are predominantly low threshold mechanoreceptors, primarily supplying proprioceptive information from joints (Julius and Basbaum 2001). A $\alpha$  fibres innervate muscle spindles rather than joint tissues. In joints, A $\beta$  fibres innervate the capsule and subcapsular tissues, and are activated by low intensity stimulation such as joint movement in the normal range. Although nociceptive A $\beta$  fibres can represent up to 30% of the nociceptive innervation in some tissues such as skin (Djoughri and Lawson 2004), there are very few reports of A $\beta$  nociceptors innervating joints or contributing to arthritic pain. It is unclear whether /how they contribute to joint pain as the small number of available studies reports are contradictory (Schaible and Schmidt 1988, Dorn, Schaible et al. 1991, Wu and Henry 2010).

Joint A $\delta$  fibre neurons (also known as group III neurons) are characterised by a fast conduction speed of 12-30m.s<sup>-1</sup>, and can have low threshold or nociceptive properties, i.e., they are activated by actual, or potential tissue damaging stimuli. Cutaneous A $\delta$  fibres are classified as Types I and II, both of which are mechanosensitive but with different thresholds (Table 5). Type I A $\delta$  fibres are thought to mediate 'first pain', rapidly perceived, well localised sharp pain, and contribute to acute noxious spinally-mediated withdrawal reflexes (Ploner, Gross et al. 2002). A $\delta$  fibres respond to both normal joint movement, and noxious movements outside the normal range, and can also become sensitised at rest and to movement and direct stimulation in arthritis (Coggeshall, Hong et al. 1983, Schaible and Schmidt 1985, Schaible and Schmidt 1988, Okun, Liu et al. 2012).

C fibre neurons (or group IV neurons) have unmyelinated fibres with slower conduction velocities <1.4 -2 m.s<sup>-1</sup> depending on species. There are several groups of identified C fibre sensory neurons that respond to different modalities of stimuli, both noxious (high threshold, tissue damaging) and innocuous (Table 5-6). C fibre nociceptors mediate 'second pain', slower, longer lasting poorly localised burning aching pain that can often result in incapacity. C-fibre high threshold mechanoreceptors (HTM), C-polymodal, and C-unresponsive, also known as 'silent' nociceptors are all important in arthritis pain (Coggeshall, Hong et al. 1983, Schaible and Schmidt 1985, Schaible and Schmidt 1988, Okun, Liu et al. 2012, Neogi, Guermazi et al. 2016).

Both A $\delta$  fibres and C fibres, can be activated by either mechanical or thermal stimuli, with a main difference being the higher threshold for activation evident in the C fibres (Voscopoulos and Lema 2010).

**Table 5 Classification and properties of sensory neurons (Julius and Basbaum 2001)**

## Response properties of primary afferent neurons

Modified from Julius and Basbaum, Nature 2001

	Thermal threshold	Mechanical threshold
 <b>Aa and Ab fibres (non-nociceptive)</b> Myelinated Large diameter Proprioception, light touch	None (NR not responsive)	Low
 <b>Ab and Ad fibres (nociceptive)</b> Myelinated (thick – thin) Large – medium diameter “First pain”	Type I (AMH/polymodal)(Ab& Ad) High >53°C  Type II (AMH) (all Ad) ~46°C (‘First pain’)	Low (‘First pain’)  V. High (?‘silent’ or ‘unresponsive’)
 <b>C fibres</b> Unmyelinated Small diameter Nociception Innocuous temperature, itch ‘stroking’	C-HTM C-heat C-cold C-polymodal C-‘unresponsive’ C-cool/warm C-pruriceptive C-LTM	High~43°C High Low ~6°C High NR Low NR NR Low

“Second pain”

**Table 6 Classification and properties of sensory neurons**

Neuron type	Function	Myelinated	Diameter	Innervation target
Aβ	Proprioception	Yes	Thick	Capsule, fat pads, ligaments, menisci
Aδ	Nociception	Yes	<5μm	Capsule ligaments, menisci bone
C	Nociception	No	<2μm	Capsule ligaments, menisci bone

## 1.5.2 Pain

Pain as defined by Merksey and Bogduk in 1994 is “an unpleasant sensory and emotional experience associated with actual or potential tissue damage or described in terms of such damage”; it is an evolutionary need to prompt us to avoid harmful stimuli from our environment. According to IASP (International Association for the Study of Pain) (<https://www.iasp-pain.org/publications/iasp-news/iasp-announces-revised-definition-of-pain/>), the definition of pain has been expanded including 6 key notes:

- Pain is a personal experience, affected by biological, psychological, and social factors.
- Pain and nociception are not the same event, since pain cannot be inferred only on activity of sensory neurons
- The concept of pain is learnt by individuals through their life experiences
- Report of pain differs based on individuals and should always be respected
- Pain has an adaptive role, but it affects function, social and psychological well-being
- Pain can be described verbally, however inability to communicate does not translate to inability to communicate pain

Distinct forms of pain, defined by mechanisms or clinical presentation are nociceptive, nociplastic, inflammatory or neuropathic, which can be acute or chronic, and mediated by peripheral and/or central mechanisms.

Pain can be characterised as brief, acute, driven by minor tissue damage exciting sensory nociceptors before it recedes; or chronic, when the pain persists over a longer period becoming debilitating.

Under normal conditions nociceptor terminals located in the periphery only respond to, and are activated by high intensity mechanical, physical, or chemical potentially harmful stimuli. These stimuli are transduced into action potentials by receptors and channels in the nerve terminals in peripheral tissues. These mechanisms are not in the scope of this thesis, but key channels are TRPV1 and TRPA1 in C fibre nociceptors and their involvement in heat nociception and mechanical and chemical sensitisation respectively (Delmas, Hao et al. 2011, Khan, Khan et al. 2019), and TRPV4 and Piezo channels in mechanonociception (Tsunozaki and Bautista 2009) (Giniatullin 2020). Signals are transmitted to the dorsal horn of the spinal cord where nociceptive endings terminate on projection and interneurons in laminae I (C and A $\delta$ -fibres), II (C-fibres), IV (A $\beta$  fibres) and V (A $\beta$ -fibres) (Cohen and Mao 2014, Garcia-Ramirez, Ha et al. 2021). Incoming

signals are processed and integrated in the spinal cord, and transmitted through ascending pain pathways (the spinothalamic, spinoreticular and spinomesencephalic tracts) to the thalamus and then somatosensory and insular cortexes where sensation is perceived. Descending pathways from cortex, periaqueductal grey, and rostroventral medulla can also inhibit or facilitate processing of signals at spinal cord and higher levels (Hassan and Walsh 2013, Ossipov, Morimura et al. 2014).

Repeat and intense stimulation of the peripheral or central nociceptive pathways marks the remodelling of the neuronal architecture transforming the pain from an acute brief sensation to chronic. When the nociceptor threshold is reduced resulting in altered pain processing, both the dorsal horn and the brain centres where pain is being perceived are subject to phenotypic alterations. Nerve damage could potentially induce neuropathic pain; chemicals secreted from damaged tissue can sensitise the sensory endings of afferent nerves leading to development of neuropathic pain, which in turn may lead to excitability changes within the nerves (Dickenson 2002). In OA, symptoms of neuropathic pain may be evident (lower pain thresholds) in patients, while also pertaining a connection with joint damage from previous knee injuries (Valdes, Suokas et al. 2014).

### **1.5.3 Pain and peripheral nociception in OA**

The synovial joint and all its tissues, except the articular cartilage, are innervated by nociceptive fibres (McDougall 2006, Hunter, Guermazi et al. 2013). Theories of pain generation in OA include:

#### **1.5.3.1 Joint tissue remodelling and destabilisation.**

Bone changes, such as osteophytes, sclerosis and cysts are some of the main alterations in the remodelling of the articular joint happening in OA (Sofat, Ejindu et al. 2011). Loss of articular cartilage results in joint space narrowing alongside subchondral bone defects, osteophyte formation and synovitis (Woldin B. Pain in osteoarthritis: can prolotherapy help? *Pain* 2014; 24:17). Studies show that pain has a strong association with bone marrow lesions, synovitis, and joint effusion, but a weaker association with cartilage damage (Felson, Chaisson et al. 2001, Hill, Gale et al. 2001, Kornaat, Bloem et al. 2006, Baker, Grainger et al. 2010).

### 1.5.3.2 Inflammatory pain mechanisms.

During inflammation pro-inflammatory mediators are released from local damaged cells and tissues, and from infiltrating immune cells and local nerve terminals. Tissue injury and immune cell infiltration and activation results in release of multiple mediators including the prostaglandins, ATP, bradykinin, serotonin, and NGF, into synovial joints (Rang, Bevan et al. 1991). Activation of local nerve terminals stimulates neurogenic inflammatory responses and release of neuropeptides such as substance P and calcitonin-gene-related peptide from nerve terminals. Substance P is also released from the inflammatory cells and causes blood vessel dilation and increased permeability, promoting inflammation.

These inflammatory mediators are induced by inflammatory cytokines and chemokines such as TNF- $\alpha$  and IL-1 $\beta$  which not only perpetuate the inflammatory process, but also act directly on nociceptors (Schaible et al., 2014) changing their responses, and lead to pain. Pro-inflammatory cytokines and their association to pain has been well explored. One important example in both inflammatory and OA is TNF- $\alpha$  (a mediator that is successfully targeted in treatment of RA disease (Ma and Xu 2013)). Synovial TNF- $\alpha$  levels are positively associated with OA knee pain (Stannus, Jones et al. 2013) and synovial thickening in early OA in humans (Youssef, Haynes et al. 1997), and increased nociception in arthritis in rats (Orita, Koshi et al. 2011). TNF- $\alpha$  and IL-6, another pro-inflammatory cytokine important in the pathogenesis of arthritis, strongly correlate with pain measured on the Western Ontario and McMaster Universities Osteoarthritis index (WOMAC) questionnaire, and joint stiffness and radiographic grading based on the Kellgren-Lawrence scale (Orita, Koshi et al. 2011) respectively. Chemokines are also associated with pain, with monocyte chemoattractant protein 1 (MCP-1)/CCL2 and macrophage inflammatory protein-1 $\beta$  (MIP-1 $\beta$ /CCL4) being significantly associated with acute knee pain (Cuellar, Scuderi et al. 2009). MCP-1 has been previously linked to pain behaviour in the destabilisation of the medial meniscus model in mice (Miller Rachel, Tran Phuong et al. 2012), in active RA (Meehan, Regan et al. 2021) and OA (Kanyama, Kuboki et al. 2000), and in the generation of neuropathic pain (Ji, Xu et al. 2009). Finally, recent data show that autoantibodies may also be involved in peripheral mechanisms of pain in RA (Goebel, Andersson et al. 2022).

Many inflammatory mediators, chemokines and cytokines are known to act directly on peripheral nerve terminals to sensitise and activate them by changing their excitability (Yam, Loh et al. 2018). Sensitisation of nerve terminals in joints causes them to fire more easily, in response

to low threshold stimuli that could be in the normal physiological range, such as normal joint movement (Schaible and Schmidt 1985, Schaible and Schmidt 1988, Schaible 2014). Activation causes them to fire action potentials, which may result in the perception of pain under normal conditions if the signals are strong enough to activate cortical perceptual areas. In addition to nociceptors becoming more excitable, a class of neurons known as silent nociceptors that cannot be activated by physiological stimulation can become sensitised and active. Together these changes increase the action potential barrage and nociceptive input in the spinal cord (Schaible and Grubb 1993).

#### **1.5.4 Synovitis and pain**

Synovitis in both RA and OA is recognised as an important feature for the pathologies of both diseases (Smith, Triantafillou et al. 1997, Haywood, McWilliams et al. 2003, Bondeson, Wainwright et al. 2006). The synovial tissue is richly innervated with sensory nerves and is believed to play a major role in the pathogenesis of both arthritic disease and pain, due to the increase in inflammatory mediators described above (de Lange-Brokaar, Ioan-Facsinay et al. 2012), and synovial hyperplasia and invasion in RA (Müller-Ladner, Ospelt et al. 2007). The fluctuations in pain levels experienced by patients with arthritis are correlated to the levels of synovitis evident in their synovial joints (Zhang, Nevitt et al. 2011). Moreover, intra-articular anti-inflammatory drugs such as glucocorticoids (Raynauld, Buckland-Wright et al. 2003) and NSAIDs (Pincus 2001, Boureau, Schneid et al. 2004) can reduce inflammation in arthritis, showing the importance of synovial inflammation in OA pathophysiology. The relationship between synovitis degree and pain is sometimes not as clear as the association between synovitis and functional impairment (Liu et al., 2010). In late-stage OA, matrix fragments from the damaged articular cartilage as well as loose osteophytes, may be incorporated into the synovium through phagocytosis (Sellam and Berenbaum 2010, Swales and Athanasou 2010). This drives an inflammatory response against the “foreign” bodies in the synovium, with pro-inflammatory mediators diffusing into the cartilage promoting cartilage degradation (Sellam and Berenbaum 2010), resulting in release of more inflammatory molecules, and potentially increased pain.

#### **1.5.5 Neuropathic pain.**

OA pain has been considered to be part neuropathic (Soni, Batra et al. 2013). Based on definition, a lesion affecting the somatosensory system with a plausible distribution of the pain

corresponding to peripheral innervation, is called neuropathic pain (Treede, Jensen et al. 2008, Thakur, Dickenson et al. 2014). Thus, a neuropathic component would imply that the neurons innervating the joint undergo some damage, and such a condition may cause pain by itself, independently of the pathological changes in the joint.

Questionnaires such as PainDETECT alongside description of pain by OA patients, lead to the conclusion that approximately 34% of the individuals diagnosed with OA suffer from neuropathic pain like symptoms such as burning pain, tingling, numbness, more referred pain, and high pain intensity (Hochman, French et al. 2010). However, no information is available for nerve damage in human OA. Stimuli of the QST (quantitative sensory testing) are focused on cutaneous sensation, making assessment of sensory changes not easily diagnosable (Treede et al., 2008).

## **1.6 Vascular endothelial growth factors**

The mammalian VEGF family includes VEGFs-A, B, C, and D, and placental growth factor (PlGF) (Ferrara 2005, Chung and Ferrara 2011). Each of the VEGFs have distinct functions and act through three distinct receptor tyrosine kinases, VEGF receptors (VEGFR) - 1 (a.k.a. Flt-1), VEGFR2 (a.k.a. Flk-1/KDR) and VEGFR3 (a.k.a. Flt-4), and their co-receptors neuropilins (NRP)-1 and 2. Members of the VEGF family and its receptors are implicated in a large number of physiological and pathological processes including both RA and OA, and solid tumours, principally due to their actions on angio- and lymphangiogenesis, and on cellular proliferation (Shaik, Cuthbert et al. 2020, Le and Kwon 2021).

Vascular endothelial growth factor-A (VEGF-A) is the prototypical member of the VEGF family and was first identified and named as Vascular Permeability Factor (Senger, Galli et al. 1983), denoting its profound effects on extravascular fluid accumulation. VEGF-A is a key regulator in promoting endothelial cell survival, migration, proliferation and permeability and of course physiological and pathological angiogenesis (Ourradi, Blythe et al. 2017). Knockout of VEGF-A is embryonically lethal, even in heterozygotes, because of its major role in the embryonic development of blood vessels (Hiratsuka, Kataoka et al. 2005). VEGF-A is best known for its actions on endothelial cells and blood vessels, through which it promotes physiological and pathological angiogenesis. These actions are important in physiological angiogenesis, such as in wound healing and in the reproductive systems (Shibuya 2013, Pang, Bates et al. 2017, Pang, Bates et al. 2017), and pathological angiogenesis promoting tumour growth (Florea, Mottaghy et al. 2021), neovascularisation in retinal diseases such as diabetic retinopathy and age-related

macular degeneration (Rebhun, Moreira-Neto et al. 2020), in diabetic renal disease (Cai, Chatziantoniou et al. 2021), and in RA and OA (Le and Kwon 2021). The functions of VEGF-A are however not limited to angiogenesis and vascular permeability, for example it can also affect the function of immune cells and consequently affect the host response to inflammation or tumours (Goel and Mercurio 2013). VEGF-A is expressed by many cell types in addition to endothelial cells, such as fibroblasts, platelets, neutrophils, macrophages, (Peach, Mignone et al. 2018) neurones (Beazley-Long, Hua et al. 2013), and astrocytes (Ijichi, Sakuma et al. 1995).

The functions of VEGF-A have been principally thought to be mediated through binding to the vascular endothelial growth factor 2 (VEGFR2), but VEGF-A also binds to VEGFR1, thought to act as a decoy receptor, with a 10-fold higher affinity (Lal, Puri et al. 2018). VEGFR1 is expressed in the same cells as VEGF-A and when activated is known to exert effects such as resistance to synoviocyte apoptosis, cell survival and proliferation, monocyte/macrophage activation and migration (Shibuya 2001, Shibuya 2015), promotion of pathological rather than physiological angiogenesis (Lohela, Bry et al. 2009), and of inflammation and vascular permeability (Gavard and Gutkind 2006, Uemura, Fruttiger et al. 2021), all recognised features of OA and RA.

VEGF-B is highly expressed in the heart and skeletal muscles, and it is not necessary and sufficient for normal development since genetic VEGF-B knockout mice had no change in mortality rates. Interestingly VEGF-B does not promote angiogenesis, however recent studies have identified the prominent role of VEGF-B in sensitizing endothelial cells to VEGF-A angiogenesis (Kivelä, Bry et al. 2014, Robciuc, Kivelä et al. 2016). Moreover, treating cells like cardiomyocytes with VEGF-B (which also plays a role in the nervous and the cardiovascular system) after hypoxia significantly reduces the percentage of apoptotic cells (Zentilin, Puligadda et al. 2010).

Both VEGF-C and VEGF-D promote angiogenesis while acting on permeability through VEGFR2 and lymph-angiogenesis through VEGFR3, suggesting a critical role in neuronal and cardiovascular development. Treatment with VEGF-C VEGF-D induces lymphatic EC angiogenesis. Knockout of VEGF-D has no obvious phenotype, and deletion of VEGF-C is embryonically lethal due to non-complete lymphatic vessel development (Lal, Puri et al. 2018). Finally, PlGF, is a pro-angiogenic growth factor that binds only to VEGFR1. PlGF knockout shows that this factor is not required for angiogenesis during embryogenesis, as knockouts show no obvious phenotype. Interestingly, knockout of PlGF results in impaired pathological angiogenesis

in conditions such as ischemia, (Lal et al., 2018), and evidence suggests that this results from a loss of the synergy between PlGF and VEGF-A under such conditions (Shibuya 2011).

Activation of all the VEGF receptors is associated with events key to arthritis, particularly the associated inflammation, including angiogenesis (VEGFR2), lymphangiogenesis (VEGFR3), and monocyte/macrophage activation in both inflammatory and non-inflammatory conditions (VEGFR1) (Shibuya 2015).

### **1.6.1 Alternative splicing and vascular endothelial growth factor-A**

As mentioned in section 1.4.5.7 (growth factors in OA - vascular endothelial growth factor) above, multiple VEGF-A splice variants have been described with different features and potentially different functions. These are generated by alternative pre-mRNA splicing. Before I describe the complex alternative splicing of VEGF-A and the implications of this for function, I will first explain the relevant mechanisms of alternative splicing.

### **1.6.2 Splicing mechanisms – constitutive and alternative splicing**

For the majority of genes in eukaryotic organisms, RNA is transcribed from DNA as pre-mRNA and during transcription, is processed to become mature messenger RNA (mRNA). RNA splicing is an important step of this processing, involving the removal of introns. The coding sequences in exons are spliced together in this process to form mRNA. Currently two types of splicing are recognised; constitutive and alternative (or regulated) splicing. The former is the process of removing introns and recombining the exons in the order they appear in the gene to generate a mature mRNA. Constitutive splicing is a key process in the formation of many mRNAs/proteins necessary for normal function and often cell survival and if inhibited can result in cell death. Inhibition of constitutive splicing is being actively explored as cancer treatment (Salton and Misteli 2016).

Alternative splicing is a process where different exons from the same gene are combined in mRNAs to produce diverse mature mRNAs. Exons may be skipped, only alternative /exclusive exons included, introns can be retained, and alternative start and stop sites used to generate different mature mRNAs from the same gene (Wang, Liu et al. 2015). These alterations in gene transcription increases the size of the proteome in comparison to the genes of an organism. Current estimates suggest that the human genome contains approximately 20 - 25 000 genes, while the number of identified proteins surpass 100 000. It is currently estimated that over 95%

of the human genome is alternative spliced, effects that can be inhibited by developmental stage or tissue relative factors (Chen and Manley 2009). Analysis of expression sequence tags have revealed 6 main mechanisms of alternative splicing (Blencowe 2006). Figure 2 shows a visual representation of these mechanisms (Donaldson and Beazley-Long 2016).

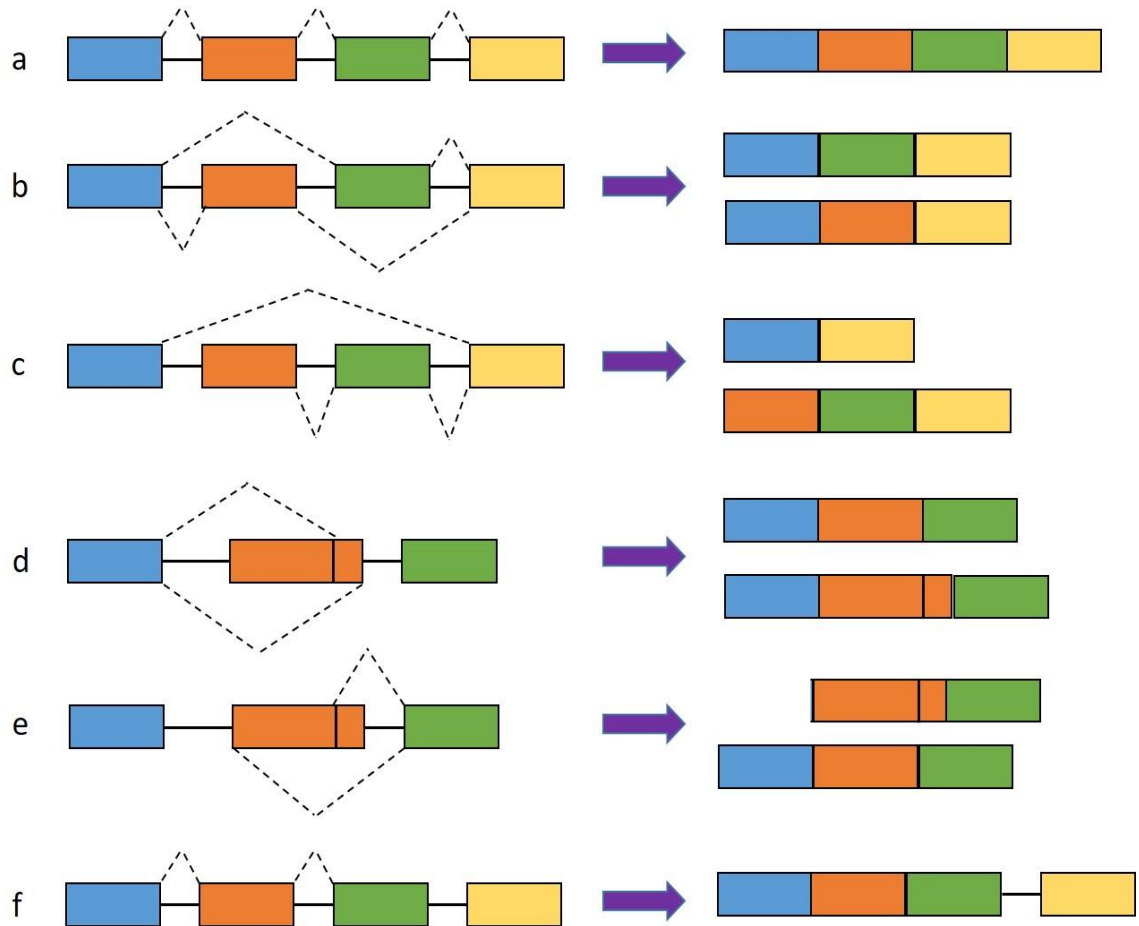


**Figure 2** Pre mRNA transcript that showcasing different splicing mechanisms. Different colours denote different exons, with black lines expressing introns, and the dotted lines showing splicing events. **A)** Constitutive splicing, with intron exclusion and exons connected. **B)** Mutually exclusive exons. The result of the alternative splicing here that the same exons can be used for different splicing results and that exons can be omitted from splicing selection. **C)** Exon skipping with exon 1 or 2 being omitted from the final mRNA transcript. **D,** **E)** alternative splice site selection; 3' for D and 5' for E, resulting in different 3' or 5' sequences. **F)** Intron retention, where the intron between the last two exons is retained.

Alternative splicing plays a major role in the production and function of multiple proteins, and any potential dysregulation in the process can contribute to pathological conditions such as cancer, dementia, and arterial disease (Ward and Cooper 2010, Zhang, Qian et al. 2021). Altered or un-regulated splicing in pathological conditions may lead to non-functional proteins, or

nonsense-mediated decay of mRNAs with loss of function, and changes in alternative splicing may lead increased resistance to drugs (e.g. chemotherapy), contributing to tumour survival (Eblen 2012). Alternative splicing can affect both normal tissues, and pathological changes, therefore control of the splicing events is pivotal to counter dangerous pathologies.

### **1.6.3 The spliceosome**

The process by which introns are removed, and exons may be skipped, is mediated by a dynamic and flexible macromolecular mechanism, namely the spliceosome. It is composed of the U1, U2, U4, U5 and U6 small nuclear ribonucleic proteins, snRNPs (Wilkinson, Charenton et al. 2020), configured to identify the 5' splice site. This is a branch point sequence near the 3' end of an intron in the nuclear pre-mRNA that contains adenosine and is responsible for combining two exons after the intron release (Zhang, Tolzmann et al. 2011, Hoskins and Moore 2012). The U1 and U2 regions form a complex (namely the "A complex") which can identify the intron by the 5' splicing site. The complex then attaches to the pre-mRNA using interactions with other 3 snRNPs (U4/5/6) (which form the "B complex"). Initially the U4 snRNP detaches from the complex to begin the process of intron exclusion, before being remodelled to the "C complex" to catalytically enable the connection of the exons in the mature mRNA (Will and Lührmann 2011). The excised intron decays and the components of the dismantled spliceosome are recycled (Lee and Rio 2015).

The process described above is constitutive splicing. For alternative splicing, the spliceosome is modified by differential motifs on the pre-mRNA sequence, which alter the behaviour of the complex. For example, the branch point sequence is an example of such a motif, where the adenosine on the 3'-end of splice site of an intron accepts the guanosine residue at the 5' splice site end of the next exon, creating an intron-exon AG boundary motif at the 3' splice site. Upstream or downstream of these motifs, the nucleotide sequence determines whether the splice site is weak or strong. It is interesting to note that when the spliceosome encounters a weaker splice site, it leads to removal of the intron and the exon together (Dvinge 2018).

Several key regulators exist that can control alternative splicing and could "guide" the spliceosome. RNA Binding Proteins (RBPs), also known as splicing factors, could regulate alternative splicing (Fu and Ares 2014). Two of the most common RBPs encountered are the hnRNPs (heterogeneous nuclear ribonucleoproteins) and the serine/arginine rich splicing factors

(SR proteins). These splicing factors could bind to pre-mRNA and regulate the mRNA splicing and thus the resulting protein (Zhou and Fu 2013).

The human SR protein family has some distinct structural features as shown in figure 3.

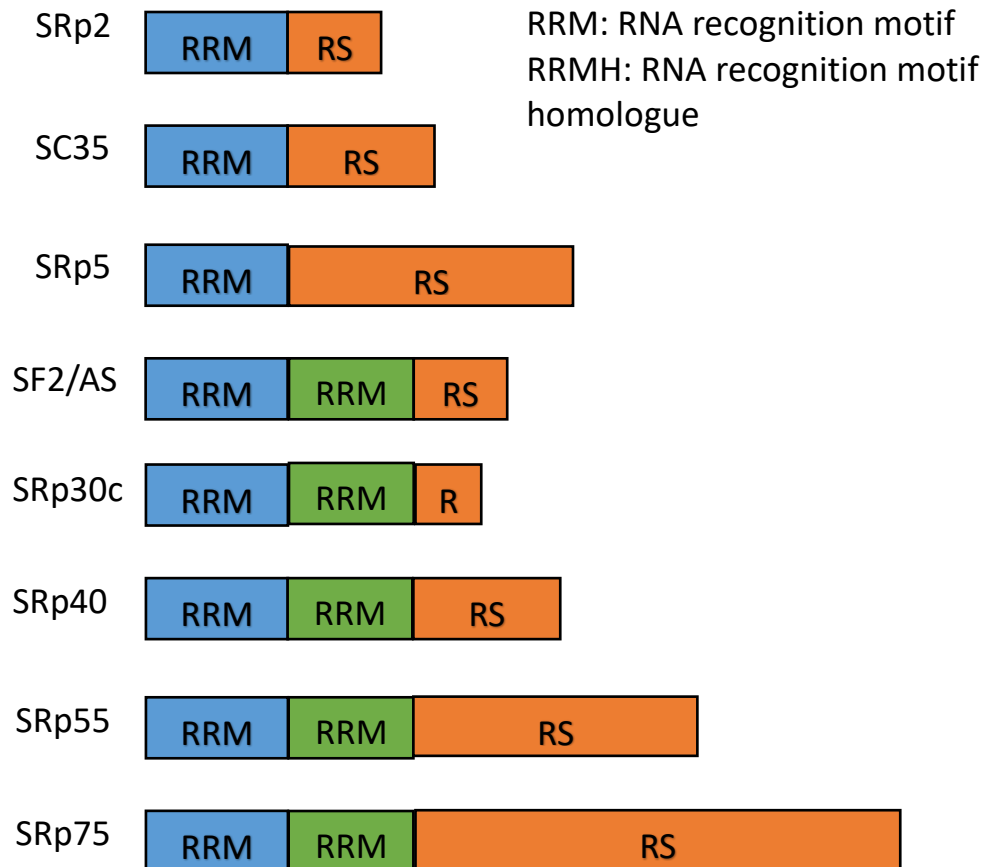


**Figure 3** The human serine/arginine splicing proteins. 9 human SR proteins are described here, with their distinct morphological features. The RRM domain which is a RNA recognition motif, the RRMH domain, with H standing for homology, the RS domain an arginine/serine rich domain in the proteins and the Zn domain, a Zinc knuckle (Shepard and Hertel 2009).

All SR proteins contain a serine/arginine rich RS domain at the C terminus, which is responsible for enhancing splicing. Furthermore, one of the functions of the SR domain is to facilitate nuclear translocation of the SR protein, acting as a signal, mediating interactions between the SR protein and the nuclear receptor transportin-SR (first paper to show this (Shepard and Hertel 2009)). The RNA Recognition Motif (RRM) domain facilitates the recognition of small RNA sequences namely the SREs (splicing regulatory elements) which can be enhancers of exon or intron splicing (Shen and Green 2006, Wang and Burge 2008, Ghosh and Adams 2011).

The hnRNPs have a competitive relationship with the SR proteins. An example of this is the relationship between SRSF1 (also known as ASF/SF2), an SR protein that shuttles between the nucleus and the cytoplasm depending on the phosphorylation state, and the hnRPA1 protein. When hnRPA1 concentration is higher than SRSF1, it antagonises SRSF1 leading to selection of the distal splicing sites. However, when SRSF1 is upregulated, the opposite occurs with splice site selection preferentially at proximal splice sites. The balance between such functions of splicing factors dictates the levels, the nature, and the results of the alternative splicing within the human body (Ladomery, Harper et al. 2007, Golan-Gerstl, Cohen et al. 2011, Gonçalves, Henriques et al. 2014).

#### **1.6.4 Splicing kinases and arthritis**

There is a large family of splicing kinases, which are involved in the assembly of the spliceosome largely through their actions on the phosphorylation of splicing factors, such as the SR proteins. This family includes the cyclin-dependent-like (cdc-like) kinases CLKs 1-4, the serine/arginine-rich protein kinases (SRPKs), and the dual-specificity tyrosine phosphorylation-regulated kinases (DYRKs) (Qin, Qin et al. 2021).

To date, DYRK1A and CLKs 1 and 2 splicing kinases have been directly implicated in arthritis. In humans DYRK1A is expressed in both adults and embryos, (Guimerá, Casas et al. 1996) and is implicated in both Down's syndrome and Alzheimer's disease (Liu, Wang et al. 2022). Recent evidence also suggests it is involved in tumorigenesis (Rammohan, Harris et al. 2022). DYRK1A is increased in human fibroblast like synoviocytes (HFLS) in RA, and inhibition of DYRK1A prevents the migration, invasion, and proliferation of HFLSs (Guo, Zhang et al. 2018), as seen in pannus formation in RA joints. It also regulates the differentiation of T-helper and T-regulatory cells (Khor, Gagnon et al. 2015).

CLK2 and DYRK1A affect Wnt signalling (Granno, Nixon-Abell et al. 2019), which when dysregulated causes disease in most tissues, and is implicated in cartilage and synovial changes in OA (Qin, Qin et al. 2021). A novel Wnt inhibitor, Lorecivint, in successful clinical trial as a DMOAD due to its positive effects on pain, and potentially also on cartilage damage and synovial inflammation, is thought to exert its actions through CLK and DYRK inhibition (Deshmukh, O'Green et al. 2019, Yazici, McAlindon et al. 2020).

### 1.6.5 Control of SR proteins

The function of SR proteins is tightly regulated, denoting their essential role in health and disease. The SR proteins themselves can also be alternative spliced, with transcripts that are functional, or transcripts that are targeted for NMD (nonsense-mediated decay) (Ladomery 2013), which downregulates or autoregulates the functions of SRs depending on the state and needs of the organism (more details on the autoregulation of SR proteins can be found in Results chapter 5. In many cases, upstream mediators such as the splicing kinases influence the expression or the active state of SR proteins, a prime example being SRSF1 which translocates to the nucleus after phosphorylation by the serine/arginine protein kinase, SRPK1. Modifications such as phosphorylation take place in the RS domain of the SR proteins. It is important to note that even after phosphorylation, SRSF1 may still not be functional in the nucleus as it may be held in nuclear speckles (Spector and Lamond 2011). CLK-1 can act to release SRSF1 from speckles, through additional phosphorylation (Aubol, Wu et al. 2016). Briefly, the complex of the two kinases CLK-1 and SRPK1 release SRSF1 in two distinct ways:

1. Rapid phosphorylation pathway (Figure 4). CLK-1 phosphorylates the Ser-Pro residues of the RS domain of SRSF1, while in a complex with SRPK1, to circumvent its slow turnover number (the number of chemical conversions at a given concentration), before releasing the splicing factor to facilitate the spliceosome (Nowak, Woolard et al. 2008, Aubol, Wu et al. 2016).
2. Slow phosphorylation pathway. CLK-1 binds to SRSF1 at its N-terminus where it phosphorylates the RS domain stochastically (Aubol, Plocinik et al. 2013). SRPK1 then removes the attached CLK-1 from the N terminus, releasing the phosphorylated protein (figure 4). The mechanisms involved in this control of alternative splicing demonstrate its complexity and illustrate the potential number of splicing targets that could be identified and controlled.

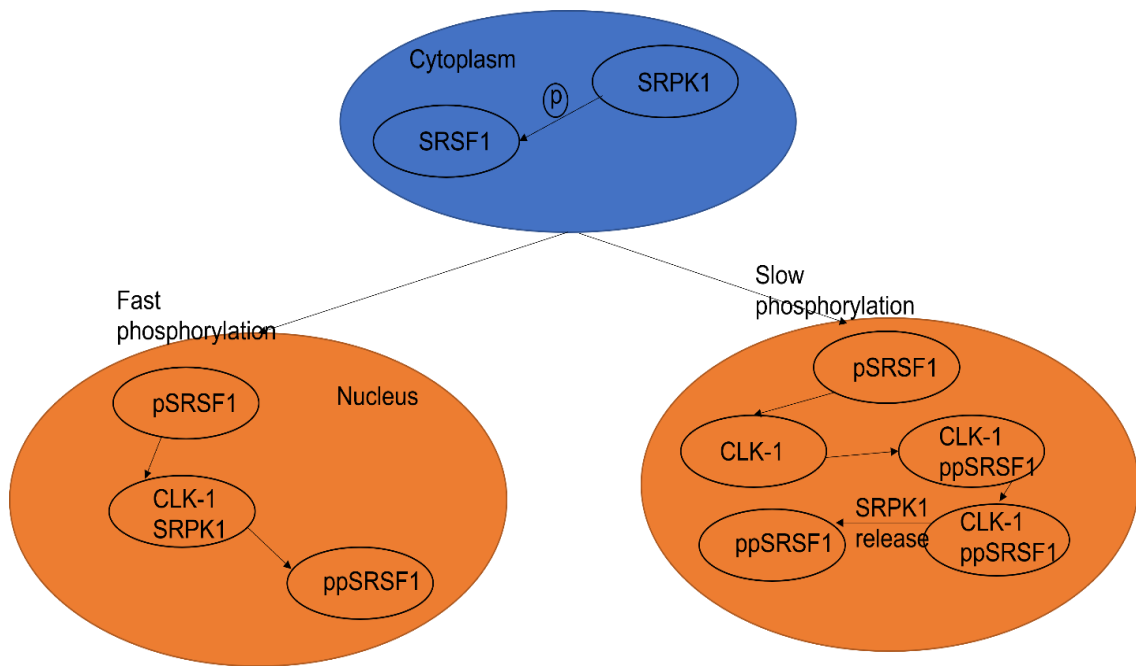


**Figure 4 Schematic of the two potential pathways through which SRSF1 is phosphorylated by the complex of CLK-1 and SRPK1. SRPK1 phosphorylates SRSF1 in the cytoplasm, resulting in SRSF1 translocation into the nucleus, usually into nuclear speckles. On the left, the fast phosphorylation pathway is shown, where a CLK-1/SRPK1 complex rapidly further phosphorylates the SRSF1 RS domain leading to release from speckles. On the right, while in the right is the slow phosphorylation pathway, where phosphorylated SRSF1 is hyper phosphorylated by CLK1, and then released from the complex with CLK1 by SRPK1, allowing release from speckles and interaction with the spliceosome. Figure adapted from (Aubol Brandon, Wozniak Jacob et al. 2021).**

There is also evidence supporting interactions between DYRK1A and SRSF1. DYRK1A phosphorylates SRSF1 at Serines-227, 234 and 238 (Shi, Zhang et al. 2008), promoting movement into nuclear speckles. This increases alternative splicing of 3R-tau, increasing this compared to 4R tau, which can promote neurofibrillary degeneration (Shi, Zhang et al. 2008), which is related to Alzheimer’s disease and other neurodegenerative diseases, and suggests potential therapeutic value of DYRK1A inhibition.

### 1.6.6 Control of VEGF-A alternative splicing

While there is considerable understanding of splicing kinase, and SR protein contributions to spliceosome function and alternative splicing mechanisms, there are relatively few identified downstream targets of specific splicing kinases. Fewer than 20 SRPK1 targets are currently known, all of which are implicated in tumorigenesis/neoplasia (Hulse, Beazley-Long et al. 2014).

One prominent target of SRPK1-mediated alternative splicing is VEGF-A, which is also a key factor in RA and OA pathology. In addition to the alternative splicing that produces the different isoform variants, SRPK1 drives the production of has two distinct splicing isoform families. Splicing due to the actions of SRSF1, results in the VEGF-A<sub>xxx</sub>a and the VEGF-A<sub>xxx</sub>b isoforms, with pro-angiogenic and nociceptive functions for the former, and anti-angiogenic, anti-nociceptive functions for the latter, denoting that control of the VEGF-A splicing events could potentially lead to new therapeutic targets for analgesia in general and new potential therapeutic targets against inflammation in arthritis.

### **1.6.7 The VEGF-A families of alternatively spliced isoforms**

The human VEGF-A gene has 8 exons (Figure 5) and complex alternative splicing results in two distinct VEGF-A families. Currently, nine VEGF-A transcripts of various lengths exist in humans; VEGF-A<sub>206</sub>, VEGF-A<sub>189</sub>, VEGF-A<sub>183</sub>, VEGF-A<sub>165</sub>, VEGF-A<sub>162</sub>, VEGF-A<sub>148</sub>, VEGF-A<sub>145</sub>, VEGF-A<sub>121</sub> and VEGF-A<sub>111</sub>, the 6 most studied of these are shown in Figure 5 (Woolard, Bevan et al. 2009, Guyot and Pagès 2015) .

The VEGF-A<sub>xxx</sub>a family (Figure 5), where xxx denotes the number of amino acids, is the best characterised family, the archetypal and predominant form being VEGF-A<sub>165</sub>a. This is the isoform best characterised for its actions on angiogenesis, lymphangiogenesis and vascular permeability as described in section 1.6.

Alternative splicing affects the function of the members of the VEGF-A<sub>xxx</sub>a family - exons 1-5 are key for cellular location (exon 1), ligand dimerization, VEGF receptor 1 binding and glycosylation (exon 3), VEGF receptor 2 binding (exon 4) and plasmin cleavage. Isoforms containing exons 6 and 7 (isoforms 206, 189, 145, 143) can bind heparin, which affects whether the isoform can easily diffuse, and binding to the co-receptor NRP-1 is facilitated by exon 7 (isoforms 206, 189,183, 165, 148) which affects the strength of VEGFR2 signalling, as engagement with NRP on ligand binding results in full receptor activation (Woolard, Bevan et al. 2009, Guyot and Pagès 2015). VEGF-A<sub>xxx</sub>a isoforms are the pro-angiogenic variants and perform key roles in vascular development during embryogenesis (Harris, Craze et al. 2012) to the extent that heterozygote knockout of VEGF-A is embryonically lethal (Carmeliet, Ferreira et al. 1996, Ferrara, Carver-Moore et al. 1996). VEGF-A<sub>xxx</sub>a upregulation and splicing is controlled by hypoxia through hypoxia inducible factor HIF-1alpha (Levy, Levy et al. 1995). Very little is known about the control of splicing of the different VEGF-A<sub>xxx</sub>a isoforms, but there are significant variations in the

expression of isoforms in healthy tissues (Whittle, Gillespie et al. 1999), as well as in disease, as mentioned above (section 1.4.5.7 VEGF-A and arthritis). The most commonly studied variants are VEGF-A<sub>121a</sub>, VEGF-A<sub>145a</sub>, VEGF-A<sub>165a</sub>, VEGF-A<sub>183a</sub> and VEGF-A<sub>189a</sub>.

VEGF-A is also alternative spliced to produce a second isoform family, which are known to be anti-angiogenic (VEGF-A<sub>xxx</sub>b isoform), and to antagonise binding of VEGF-A<sub>xxx</sub>a isoforms at VEGFRs. The two families result from alternative splicing in exon 8, with use of either the proximal (VEGF-A<sub>xxx</sub>a) or distal (VEGF-A<sub>xxx</sub>b) splice sites in exon 8 (Bates, Cui et al. 2002, Lodomery, Harper et al. 2007, Gammons, Lucas et al. 2014). In theory all transcripts can be present in each family, except for VEGF-A<sub>148a</sub> since it lacks exon 8 (Whittle, Gillespie et al. 1999). The function of VEGF-A<sub>148a</sub> remains unclear (Woolard, Bevan et al. 2009). The most commonly studied variants above are also the only variants for which a VEGF-A<sub>xxx</sub>b variant has been identified (Nowak, Woolard et al. 2008).

In most healthy tissue, under normal physiological conditions the VEGF-A<sub>xxx</sub>b isoforms predominate in accordance with their core functions of maintaining tissue integrity and function in non-angiogenic tissue (DRG, skin and colon) (Pritchard-Jones, Dunn et al. 2007, Varey, Rennel et al. 2008, Hulse, Beazley-Long et al. 2014).

The only difference between VEGF-A<sub>xxx</sub>a and VEGF-A<sub>xxx</sub>b isoforms are the 6 C-terminal amino acids, which are CDKPRR (cysteine, aspartate, lysine, proline, arginine arginine) in VEGF-A<sub>xxx</sub>a and SLTRKD for VEGF-A<sub>xxx</sub>b (serine, leucine, threonine, arginine, lysine, aspartate) (Bates, Cui et al. 2002). These six amino acids are sufficient to confer the functional differences between the isoform families, i.e., the pro- and anti-angiogenic properties.

The selection of either the proximal or distal splice site in exon 8 depends on the activation of splicing kinases and splicing factors. Hypoxia, IL-1 $\beta$  or TNF-alpha (TNF- $\alpha$ ) activate the splicing kinase SRPK1, which leads to the selection of the proximal splice site and alternative splicing to produce VEGF-A<sub>xxx</sub>a mRNAs (Nowak, Woolard et al. 2008, Nowak, Amin et al. 2010, Carter, Cherry et al. 2011, Biselli-Chicote, Biselli et al. 2017, Lin, Lee et al. 2017). This splicing event introduces a stop codon in exon 8a (Figure 5) and results in a C terminal sequence of CDKPRR. Under physiological conditions, controlled by Wnt signalling (Amin, Oltean et al. 2011), or in response to transforming growth factor beta, CLK and SRSF6/SrP55 activation (Nowak, Woolard

et al. 2008) lead to distal splice site selection, a frame shift and introduction of an alternative stop codon in exon 8b, resulting in the C terminal sequence SLTRKD and VEGF-A<sub>xxx</sub>b isoforms (figure 5 (Donaldson and Beazley-Long 2016)).

### **1.6.8 VEGF-A isoform interaction with VEGF receptors**

Both isoform families could bind and exert effects through the tyrosine kinase receptors/vascular endothelial growth factor receptors 1 and 2, VEGFR2 (Ferrara, Gerber et al. 2003). However, it is important to note that even though they can bind to the same receptors, they do not facilitate the same downstream signalling pathways (Kawamura, Li et al. 2008, Peach, Mignone et al. 2018), and this is a consequence of the difference in the C terminal 6 amino acids (Delcombel, Janssen et al. 2013).

On binding to VEGF-A<sub>xxx</sub>a forms dimers and stabilises the interaction between the VEGFR2 dimer and the co-receptor NRP-1 (Ballmer-Hofer, Andersson et al. 2011). The creation of the complex of the VEGFR2, NRP-1 and VEGF-A<sub>xxx</sub>a is then followed full receptor phosphorylation especially at key residues such as the Y1175, which controls the activation of signalling from the receptor (Hulse, Drake et al. 2016, Peach, Kilpatrick et al. 2018, Peach, Mignone et al. 2018, Peach, Kilpatrick et al. 2019) , and downstream signalling leading to angiogenesis and changes in vascular permeability (Carmeliet, Ferreira et al. 1996, Fu and Shen 2004, Beazley-Long, Hua et al. 2013). Signalling through activation of phospholipase C, protein kinase C, phosphoinositide 3-Kinase (PI3 kinase) and protein kinase B (Harper and Bates 2008, Kerbel 2008) leads to downstream events such endothelial proliferation and migration occur, as well as vasodilatation and angiogenesis (Benton and Whittmore 2003, Qiu, Hoareau-Aveilla et al. 2009). VEGF-A<sub>165a</sub> is a full agonist of VEGFR2 whereas VEGF-A<sub>165b</sub> is a partial agonist but has the same affinity for VEGFR2 (Woolard, Wang et al. 2004, Peach, Kilpatrick et al. 2019). When VEGF-A<sub>165b</sub> binds to VEGFR2, NRP-1 is not stabilised in its interaction with VEGFR2 dimers (Harper and Bates 2008, Ballmer-Hofer, Andersson et al. 2011, Peach, Kilpatrick et al. 2018, Peach, Mignone et al. 2018, Peach, Kilpatrick et al. 2019), there is a different tyrosine phosphorylation pattern, and partial receptor activation, which is theorised to be a result of incomplete rotation of the kinase domain (Kawamura, Li et al. 2008). This may be because there is incomplete phosphorylation of Y1175 by VEGF-A<sub>165b</sub> binding. As NRP-1 binds to exon 7, however there is evidence that exon 8 is also involved in NRP-1 binding. Therefore, since both isoform families can bind to VEGFR2, it is

theorised that both exon 7 and 8 are required for full activation of the receptor through NRP-1 (Kawamura, Li et al. 2008, Peach, Kilpatrick et al. 2019).

We know that in the absence of the other family there is less effective receptor binding by VEGF- $A_{xxx}b$  isoforms. The competition for binding is a different thing, which also affects the activation of the receptor and the downstream effects of course- VEGF- $A_{165}b$  isoform binds VEGFR2 with approximately equal affinity as VEGF- $A_{165}a$ , and VEGFR1 with much higher affinity and can therefore also act as a competitive antagonist to VEGF- $A_{165}a$  at the receptors (Ladomery, Harper et al. 2007). VEGF- $A_{165}b$  may exert its anti-angiogenic effects by either blocking or competing for binding at VEGFR2, and/or by stimulating different downstream signalling pathways that do not stimulate angiogenesis. The full signalling cascade evoked in response to VEGF- $A_{165}b$  acting at VEGFR2 is not yet fully known but may be similar in the same cell type. For example, VEGF- $A_{165}a$  signals through PLC, diacyl-glycerol, and calcium release in endothelial cells (Pocock et al 2002 Moss et al 2015) but not in primary sensory neurons where neither isoform stimulates increased intracellular calcium (Moss et al 2015). In HUVECs (Human umbilical vein endothelial cells) VEGF- $A_{165}a$  and VEGF- $A_{165}b$  activate similar signalling pathways, despite less activation of VEGFR2 by VEGF- $A_{165}b$  (Magnussen, Rennel et al. 2010).

### **1.6.9 Vascular endothelial growth factor and pain**

The two VEGF-A splice variant families exert opposite effects on angiogenesis (Harper and Bates 2008). Both VEGF- $A_{165}a$  and VEGF- $A_{165}b$  are cytoprotective *in vitro* and *in vivo* (Sondell, Lundborg et al. 1999, Beazley-Long, Hua et al. 2013, Hulse, Beazley-Long et al. 2014). We were the first to show that VEGF- $A_{xxx}a$  and VEGF- $A_{xxx}b$  have distinct and opposite effects on nociception (Hulse, Beazley-Long et al. 2014), and that this, like angiogenesis, is attributable to the C-terminal 6 amino acid differences in the sequences. VEGF- $A_{165}a$  directly activated and sensitised nociceptive neurons *in vivo* (Hulse, Beazley-Long et al. 2014, Selvaraj, Gangadharan et al. 2015), and sensitised primary sensory neurons *in vitro*, actions that could be blocked with VEGF- $A_{165}b$  (Hulse, Beazley-Long et al. 2014). VEGF-A has been reported to contribute to pain in multiple models of musculoskeletal (Das, Kc et al. 2018, Micheli, Parisio et al. 2021), visceral (Xie, Iguchi et al. 2022), and neuropathic pain (Kiguchi, Kobayashi et al. 2014, Micheli, Parisio et al. 2021). Both VEGFR1 and VEGFR2 have been described as contributing to both peripheral (Hulse, Beazley-Long et al. 2014, Lopez-Bellido, Puig et al. 2019, Micheli, Parisio et al. 2021) and central nociception (Hulse, Drake et al. 2016, Hu, Yang et al. 2019, Lee, Son et al. 2019, Lopez-Bellido,

Puig et al. 2019) in various animal models, while others suggest that the nociceptive actions of VEGF-A appear to be mediated through VEGFR1 (Selvaraj, Gangadharan et al. 2015). While VEGFR1 has higher affinity for VEGF-A than that of VEGFR2, the induced tyrosine kinase activity is 10-fold weaker (Sawano, Takahashi et al. 1996). It is possible that VEGF-A isoforms can act on nociception through both receptors as both receptors are expressed on nociceptors (Hulse, Beazley-Long et al. 2014, Selvaraj, Gangadharan et al. 2015) and both possess tyrosine residues in the carboxy terminal region which are believed to be crucial for downstream signalling through PLC $\gamma$  (Shibuya 2013). The receptor(s) involved may also be dependent on site (peripheral versus central) or the condition studied.

## **1.7 Hypothesis**

### **Overall hypothesis**

Alternative splicing and control of vascular endothelial growth factor isoform expression is associated with pain and disease in osteoarthritis

### **Subsidiary hypotheses**

- Changes in VEGF-A splicing and splicing control are positively associated with inflammation in OA and RA synovium.
- Changes in VEGF-A splicing and splicing control mechanisms are positively associated with pain in OA.
- Control of alternative splicing of VEGF-A in the synovial joint of arthritic patients is facilitated by the presence of inflammation and pain, an effect that is inhibited in human synovial fibroblasts via inhibition of splicing kinases.

### **Thesis Aims**

- To identify the relationship between the splicing axis of VEGF-A and inflammation in the synovium of the joint from patients with OA and RA
- Investigate the relationship of VEGF-A and its splicing axis with the pain developed in symptomatic OA versus non-symptomatic OA
- Assess the results of splicing kinase inhibition in human fibroblast like synoviocytes, in relation to the VEGF-A splicing axis

## **2. Methods**

### **2.1 Introduction**

The general methodology used within the research project outlined in the thesis will be presented here. Human tissue was obtained with consent from either patients of symptomatic OA and/or RA patients who underwent total knee replacement surgery (TKR) or the next of kin (closest living relative or relatives including spouses, siblings etc) of post-mortem (PM) cases. All procedures involving human tissue were approved by the United Kingdom National Research Ethics Service (Nottingham Research Ethics Committee 1 (05/Q2403/24) and Derby Research Ethics Committee 1 (11/H0405/2)).

### **2.2 Case Selection**

The Arthritis Research UK Pain Centre's joint tissue repository, containing samples from > 3000 cases was screened to select cases according to each study criterion. All arthroplasty samples were collected from patients based on the classification criteria from the American College of Rheumatology (ACR) (Altman, Asch et al. 1986) at the time of their surgery, with their consent. In the case of post-mortem tissue samples informed consent was also obtained from next of kin. Arthroplasty samples with primary features including pain, stiffness, decreased range of motion, bone enlargement, presence of osteophytes, sclerosis of the joints, and cysts were collected from patients. Post-mortem tissue samples were carefully selected, for which no pain had been reported by the donor in the last year of life. Clinical data available to us rely on case notes and from interviews with relatives. Clinical data are limited regarding the PM cases, but include presence of knee pain, and any previous diagnosis of OA, presence of osteophytes or joint stiffness. To validate that the PM knees had no evidence of OA, radiographic and macroscopic evaluation of the knees was performed by the clinical technician Roger Hill. Exclusion criteria for non-OA controls consisted of a history of OA, Heberden's nodes identified on clinical examination, macroscopic chondropathy lesions of grade 3 or 4 in the medial tibiofemoral compartment, or osteophytes on direct visualization of the dissected knee.

For the PM cases both left and right knees were available, and for all studies tissue from the left knees were collected unless otherwise stated. For the arthroplasty cases tissue samples were selected based on availability of the tissue but focusing on left knee tissue samples when

applicable. I focussed on the left knees to as a general guideline through the study to minimise potential variance.

Even though the basis for the selection criteria was that cases were age and sex matched, specific selection criteria for the individual studies will be described in later chapters since case selection was in accordance with the individual hypotheses.

## **2.3 Tissue collection and processing**

After collection, all tissue samples were processed at King's Mill Hospital by Roger Hill (research technician).

Synovium from the medial joint line from PM and TKR cases was collected from the surgeons and the technician (Roger Hill). The samples were fixed in formalin for 3-5 days and embedded in paraffin wax blocks. For the embedding procedure, metal moulds were placed onto a hot plate. Paraffin wax was dispensed into the metal moulds using a Tissue Tek® embedding centre (model TEC5 EME2; Sakura Finetek Europe, The Netherlands). The samples were orientated parallel to the block surface and pressed down with forceps, before transferring to a cold plate to allow the wax to set. For labelling purposes, a cassette was placed on top of the mould and filled with wax. After the wax had completely solidified, by placing the mould on to a cold plate, excess wax was shaved off, and the cassette was stored in room temperature.

Thin paraffin tissue sections (8 µm) were cut with a Bright 8000 sliding microtome with the help of Dr. Seyed Shahtaheri in the Rheumatology lab in the Clinical Sciences building in the City Hospital Nottingham. The individual sections were placed in a water bath at 40°C for 3 minutes to help the sections to flatten before collecting the samples, on electrostatically charged poly-l-lysine glass slides. Sections were left to dry at room temperature before being heated to 59°C in an oven for 2 hours to allow the embedded tissue to dry and adhere on the slides. Samples were then stored in sealed slide boxes and kept at room temperature.

## **2.4 Histological Staining**

### **2.4.1 Haematoxylin and eosin**

Haematoxylin and eosin (H&E) co-staining is one of the most common staining procedures used in histology to examine tissue morphology and structural detail. In this procedure, haematoxylin is chemically oxidised, producing haematein, which when combined with aluminium ions

produces haemalum (King and King 1986). The latter is the active staining agent and can bind and stain nuclear basophilic or acidic structures (such as DNA or RNA) to a blue/purple colour when rinsed with a weak base such as alkaline tap water. Eosin on the other hand is an acidic dye, used as a counterstain to haematoxylin, which binds to acidophilic structures such as proteins, cytoplasmic filaments, and intracellular membranes. These structures are stained in varying degrees of pink and red (Downie 1990).

### **Haematoxylin and eosin staining protocol.**

Haematoxylin and eosin staining was used for synovial histological scoring (section 2.7). 8µm paraffin tissue sections were immersed in xylene for 5 minutes, which acts as a paraffin solvent to remove the wax. The sections were then re-hydrated in descending ethanol concentrations (100%, 90%, 70%) for 5 minutes respectively, followed by a 5-minute wash with distilled water. The sections were then immersed in Mayer's haematoxylin for 15 minutes, followed by rinsing in tap water. After a brief immersion in acid alcohol for (1% HCl in 70% ethanol for 20seconds) to remove excess stain, sections were washed with tap water for 3 mins, before being placed in a 1% eosin solution for 1 minute and then washed again for 1 minute in tap water. Sections were then dehydrated in ascending concentrations ethanol (70%, 90%, 100%) and xylene for 5 minutes each respectively before being mounted with DPX and a glass coverslip.

## **2.5 Immunohistochemistry**

Immunohistochemistry (IHC) uses immunological, histological, and biochemical methods to determine the presence and localisation of specific cellular components (antigens). Labelled antibodies are used to bind to the antigens, either in tissue samples or cell preparations. Proteins, lipids, or carbohydrates can be some of the antigens that are generally targeted. The antibody binding site is what we refer to as epitope of an antigen. To visualise the binding of the primary antibody to the epitope a step of enzyme or fluorescent conjugation to the antibody is required. Currently IHC plays a central role in clinical diagnosis.

Antibodies are immunoglobulins formed in the humoral immune system by plasma cells after recognition of specific foreign antigens. IgG is the most common type of antibody used; it has a Y-shaped structure with two light and two heavy polypeptide chains (Figure 6). Three distinct regions can be identified on an antibody, one Fc section (which interacts with cell surface receptors) and two F(ab) regions (the antigen binding regions). The Fc fragment binds to Fc receptors on the immune cells and enables activation of immune responses. The antigen-

antibody binding requires specificity which is achieved by variations in the Fc regions of the antibody, which are specific to particular antigenic epitopes.

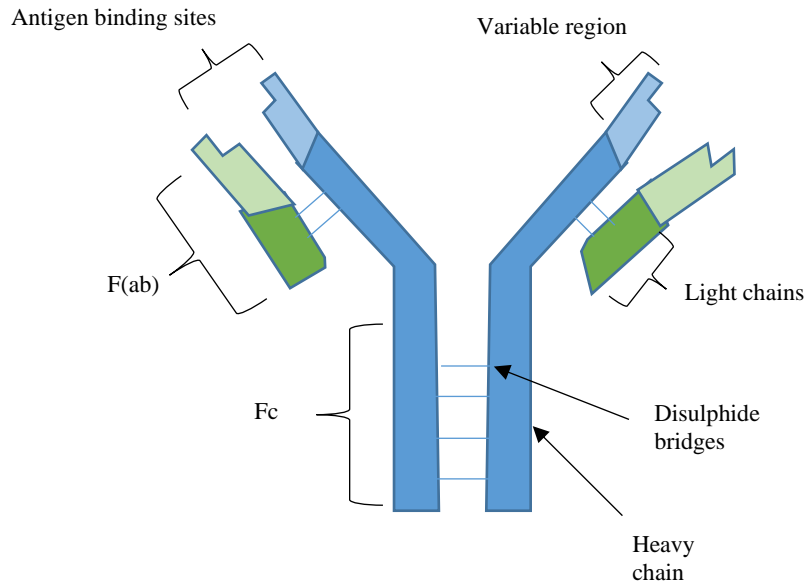


**Figure 5 Illustration of a Y-shaped structure of an IgG antibody. The heavy and the light chains are joined by disulphide bonds. Specificity of antigen-antibody binding is achieved by the variation in amino acid sequences of the variable region of the antibody. The antibody is comprised of two regions: Fc and F(ab) regions.**

### 2.5.1 Indirect Immunohistochemistry

Currently two different IHC methods are most widely used - direct and indirect immunohistochemistry. In direct IHC the primary antibody is directly labelled for detection of binding. Direct IHC is most useful for detection of highly expressed antigens as it has lower sensitivity than indirect IHC.

Indirect IHC methods use primary antibodies that are not labelled or conjugated with other molecules and secondary antibodies which are conjugated or labelled instead. In indirect IHC the primary antibody binds the antigen, and then a secondary antibody, raised against the host species of the primary antibody is bound to the primary antibody. The secondary antibody is labelled either with a fluorescent agent, an enzyme that generates a chromogen, or bound directly to a chromogen.

The most common methods to enhance the signal from antibodies is the peroxidase/anti-peroxidase (PAP) or the Avidin-Biotin complex (ABC) detection methods. The PAP method depends on the formation of the PAP complex as shown in Figure 7.

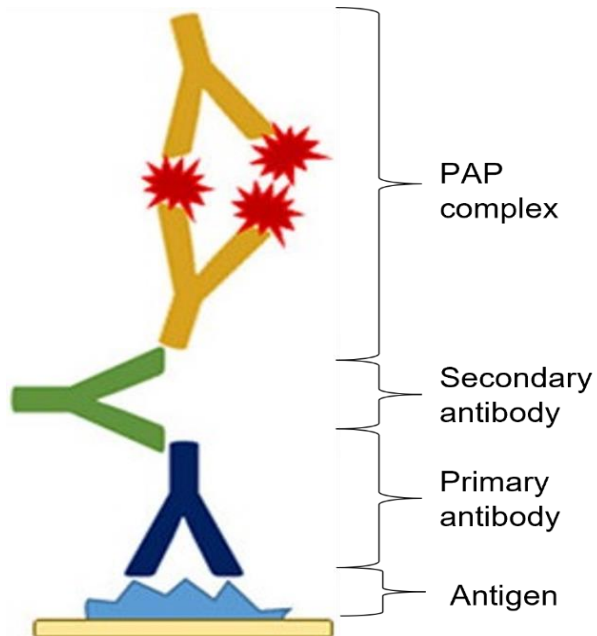


**Figure 6 Representation of the Peroxidase/Anti-Peroxidase (PAP) detection method adapted from Enzo life sciences (Enzo Life Sciences, Plymouth Meeting, PA, USA) where the PAP complex will bind to the secondary antibody after the latter was bound to the primary antibody and the antigen.**

The ABC method also uses a secondary antibody to bridge between the primary antibody and an avidin-biotin complex, based on the non-covalent interaction between these molecules.

The ABC method comprises of a three-step detection procedure as shown in Figure 8.

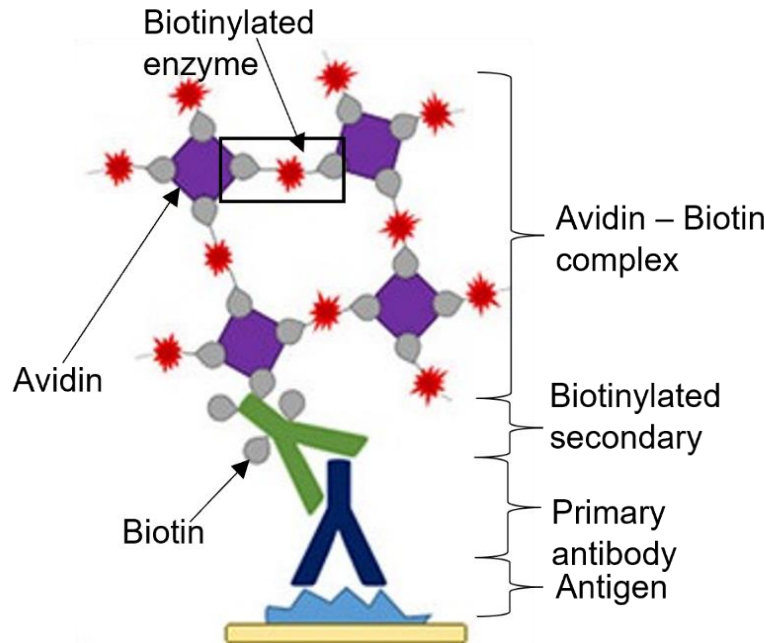


**Figure 7 Schematic representation of the Avidin- Biotin detection method. An un-labelled primary antibody (dark blue) binds specifically to an antigen of interest on the cell surface (light blue on yellow matrix). A biotinylated secondary antibody (green) binds to the primary antibody. Incubation of the tissue section with avidin (purple) and biotinylated-peroxidase enzyme (grey/orange) which forms macromolecular complexes through avidin-biotin interactions. These can then be visualised by a variety of chromogens labels such as DAB. (Enzo Life Sciences, Plymouth Meeting, PA, USA).**

The main advantage of the ABC procedure is that the formation of the complex increases the enzyme-antibody ratio, resulting in higher signal. There are a few drawbacks that also need to be considered. For example, due to the size of the AB complex, the structures may be difficult to be diffused from the tissue. Moreover, there is endogenous biotin which is a source of background because of avidin binding. However, due to the benefits described, the avidin biotin complex is the most widely used procedure in both research and the diagnostic field.

### **2.5.2 Indirect Immunohistochemistry protocol**

Indirect ABC IHC was used to visualise VEGF-A (isoforms and panVEGF-A), SRSF1, SRPK1, and DYRK1a immunoreactivity as it demonstrates distinct advantages over direct IHC.

The finalised general IHC protocol can be seen in Figure 9 below. Information on how different steps in the protocol were optimised for each primary antibody and to minimise non-specific staining are detailed in sections below.

Initially the samples were rehydrated in xylene for 5 mins to remove the paraffin wax. Sections were rehydrated in sequential descending concentrations of ethanol (100%, 90%, and 70%) for 5 minutes each, followed by tap water and phosphate buffered saline (PBS) washes for 5 minutes respectively. Antigen retrieval was then performed by incubation of sections in Tris-EDTA-Tween20 solution for 30 minutes in a water bath at 65 °C. The samples were cooled for 10 minutes using running tap water, before a wash with PBS for 5 minutes. Endogenous peroxidases were blocked by immersion in 3% H<sub>2</sub>O<sub>2</sub> for 30 minutes, and following a further 5-minute PBS wash, blocking was performed with freshly made 5% BSA in PBS for 1 hour at room temperature in a humid environment. Primary antibody concentration was antibody specific (Table 9).

Sections were incubated in primary antibody in blocking solution overnight at 4 °C in a humid environment. The following day, sections were washed twice for 5 minutes in PBS before application of the secondary antibody in the appropriate concentration in PBS for 2 hours in room temperature in a humid environment. Sections were then washed twice in PBS for 5 minutes, before applying the ABC kit for 15 minutes, followed by another 5-minute PBS wash, application of diaminobenzidine (DAB) for 5 minutes, and then two quick washes in distilled H<sub>2</sub>O, to remove excess DAB product. Sections were then counterstained with haematoxylin as in section 2.4.1. with the change that after the tap water wash, instead of eosin staining, the sections were dehydrated in ascending ethanol concentrations (70%, 90%, 100%) for 5 minutes each, and dehydrated in xylene for 5 minutes. Finally, the sections were coverslipped with glass coverslips and DPX.

### **2.5.3 Optimisation of the indirect IHC method**

#### Primary and secondary antibodies

Several different primary and secondary antibodies were used throughout the experiments described in the thesis. Specific information regarding the primary antibodies and secondary antibodies used is detailed in Table 9, and any differences between the information in this Table and in results chapters are highlighted in those chapters.

**Table 7 List of antibodies used in the different IHC studies presented**

<i>Antibodies</i>	<i>Active Concentration</i>	<i>Catalogue</i>	<i>Details</i>	<i>Manufacturer</i>
anti-SRSF1 antibody	0.005mg/ml	No. 32-4500	Mouse monoclonal anti-SRSF1 (96)	Thermofisher Scientific, UK
anti-SRPK1 antibody	0.002mg/ml	No. SAB4502857	Rabbit polyclonal Anti-SRPK1	Sigma Aldrich, UK
VEGF C-1	0.002mg/ml	No. sc-7269	Mouse monoclonal anti-VEGF	Santa Cruz, UK
VEGF-A <sub>165</sub> b	0.005mg/ml	No. MAB3045-SP	Monoclonal Mouse IgG1 Clone # 56-1	R&D systems, UK
VEGF-A <sub>xxx</sub> a	-	-		
Anti-DYRK1A	0.001mg/ml	No. HPA015323	Rabbit polyclonal Anti-DYRK1A	Sigma Aldrich, UK
Secondary Goat a-Rabbit	0.012mg/ml	No. 65-6140	Goat anti-Rabbit Secondary Ab	Thermofisher Scientific, UK
Secondary Goat a-Mouse	0.13mg/ml	No. 31800	Goat anti-Mouse Secondary ab	Thermofisher Scientific, UK

**Nonspecific staining.** This can occur due to antibody binding to antigens other than the desired target. Consequently, non-specific binding of the primary antibody can induce high background staining masking the signal from the antigen of interest. Non-specific staining can be reduced by blocking steps that reduce primary antibody binding to non-specific sites before incubation with the primary antibody. Serum is usually used for this purpose as this will prevent binding of the primary antibodies to the Fc receptors on the cell surfaces. The serum used can be derived from any species, except the species in which the primary antibody was raised, as in this situation the secondary antibodies will bind to the serum in the blocking solution and generate significant non-specific signal. Best results are usually achieved when using blocking serum from the species in which the secondary antibody was developed, i.e. if the secondary antibody is an anti-mouse antibody raised in goat, goat serum should be used.

By using a protein blocking reagent, non-specific binding of antibodies to tissue or to Fc receptors can be prevented. Blocking is essential in IHC since, despite the specificity of the primary antibody, intermolecular forces can promote non-specific binding. In theory, any protein with no affinity to the target antigen can be utilised for blocking, however certain proteins are more efficient to bind in non-specific sites. One of the most common blocking agents is serum, since it contains antibodies that bind non-specifically to sites. As a standardised procedure the serum should match the species where the secondary antibody was raised. Bovine serum albumin is also a commonly preferred blocking agent, with the benefit that no matching to the species of the secondary antibody is needed. Endogenous peroxidases, enzymes that catalyse oxidation by hydrogen peroxide, are also a source of background staining, by reacting to the chromogens producing non-specific staining. Following standardised protocols, I used a 5% BSA blocking solution to block non-specific binding of the two antibodies, as well as 3% H<sub>2</sub>O<sub>2</sub>, to block any activity of the endogenous peroxidases (Figure 3). This resulted in consistently low background /non-specific staining. Further information on optimisation of blocking protocols for specific investigations are detailed in later chapters.

Following the incubation of the samples with both antibodies, two major steps of IHC protocols were employed, namely the amplification step using the Avidin-biotin complex (ABC) as well as the visualisation step using either alkaline phosphatase (AP) or 3,3'-Diaminobenzidine (DAB).

Both reactions can result in non-specific staining. When using DAB staining, the conjugated horseradish peroxidase oxidises DAB, forming a brown precipitate, which can be visualised using light microscopy. The longer the DAB is allowed to precipitate the lower the signal to noise ratio can become, due to exacerbation of background staining with non-specific precipitation in tissues. I maintained the length of DAB incubation at 5 minutes, a time frame that was long enough for the immunoreactivity to be enhanced and allow for further analysis, without exacerbating the non-specific staining. Optimisation steps for protocols using alkaline phosphatase are detailed below.

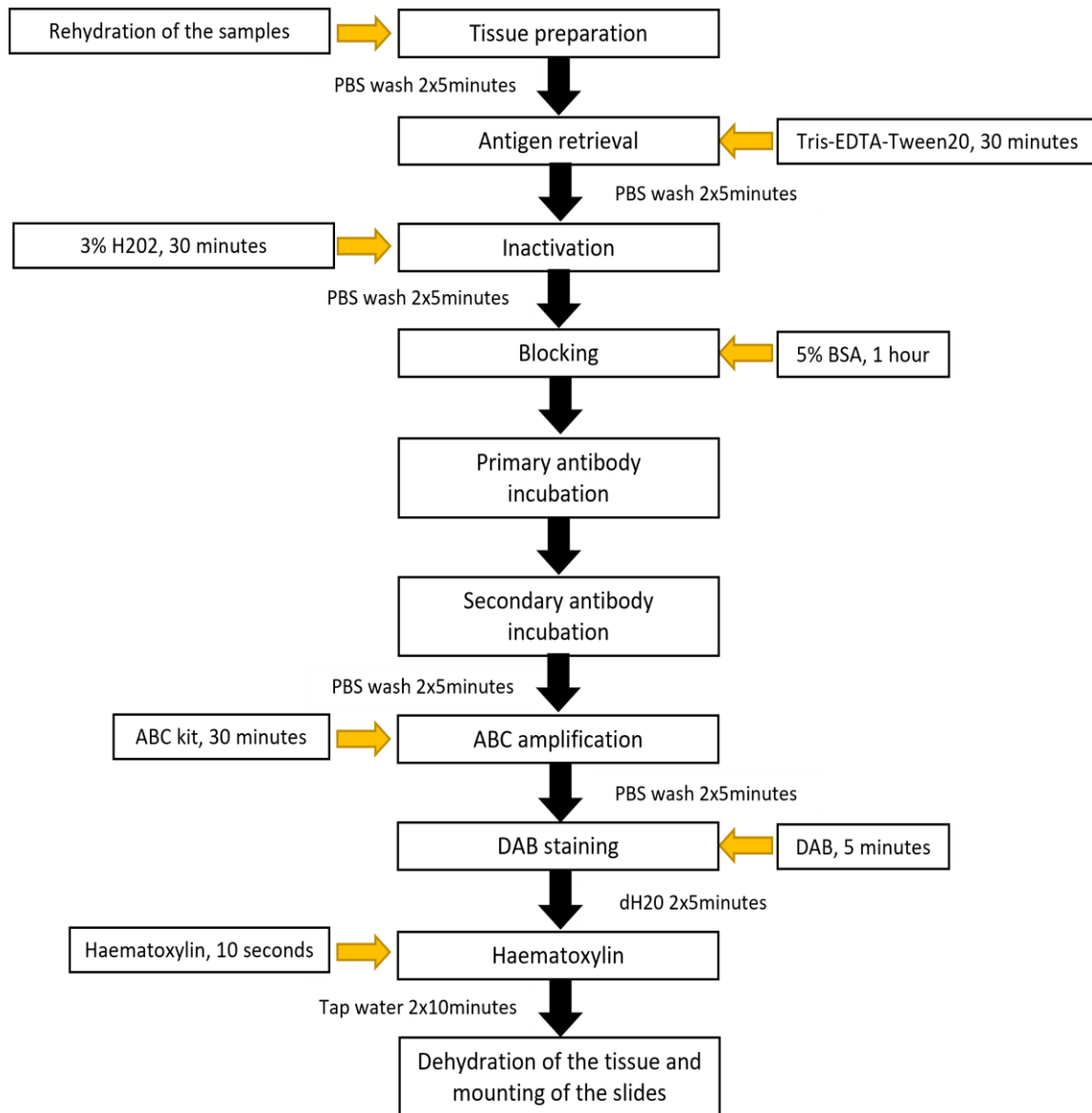


**Figure 8 Schematic representation of the IHC protocol used throughout the experimental work of the thesis.**

#### **2.5.4 Controls for indirect IHC.**

Finally, the last step in optimising the IHC experiments was the inclusion of controls to confirm and validate the IHC staining results. Negative controls are used to determine whether the immunoreactivity detected is due to the epitope of the target correctly interacting with the paratope of the antibody. Two negative controls were used: first, omission of the primary antibody and replacing it with blocking solution. This control is used to show whether there is

non-specific binding of the secondary antibody. To verify that the primary antibody binds an antigen in the tissue, additional tissue sections were incubated with an IgG from the same species in which the primary antibody of interest, i.e., either mouse or rabbit IgG. This controls for non-specific binding of the primary antibodies and this isotype-matched control was used for all the primary antibodies.

## 2.6 Immunofluorescence

Immunofluorescence (IF) is a common technique used to detect the location of the antigen of interest using fluorescence. One of the main benefits of IF is the ability to investigate the relationship of two antigens of interest by double labelling with two different fluorescent labels, as this is possible but less straightforward using IHC. Primary or secondary antibodies are conjugated to a fluorophore label (like the direct and indirect IHC protocols) for direct and indirect IF (Odell and Cook 2013).

The absorbance of excitation light by fluorophores and the consequent emission of light is the main method of detection in immunofluorescence. The detected fluorescent emission is attributed to a conformational change in the structure of the fluorophore. When electrons, which are normally based on an orbital around the nucleus are excited by absorption of photons, they are rapidly move to a less stable energy position further away from the nucleus. The excitation of the electrons is rapid, and the light emitted is due to the electron dropping back to its initial energy state (Lichtman and Conchello 2005).

Figure 10 shows an overview of the process for the visualisation of an immunofluorescent specimen. A light source illuminates the subject through an excitation filter specific for the fluorophore. Three commonly used fluorescent molecules are DAPI (4',6-diamidino-2-phenylindole) (359nm excitation peak, 457nm emission peak), FITC (Fluorescein isothiocyanate) (496nm excitation peak, 519nm emission peak) and TRITC (tetramethyl rhodamine isothiocyanate) (561nm excitation peak, 570nm emission peak).

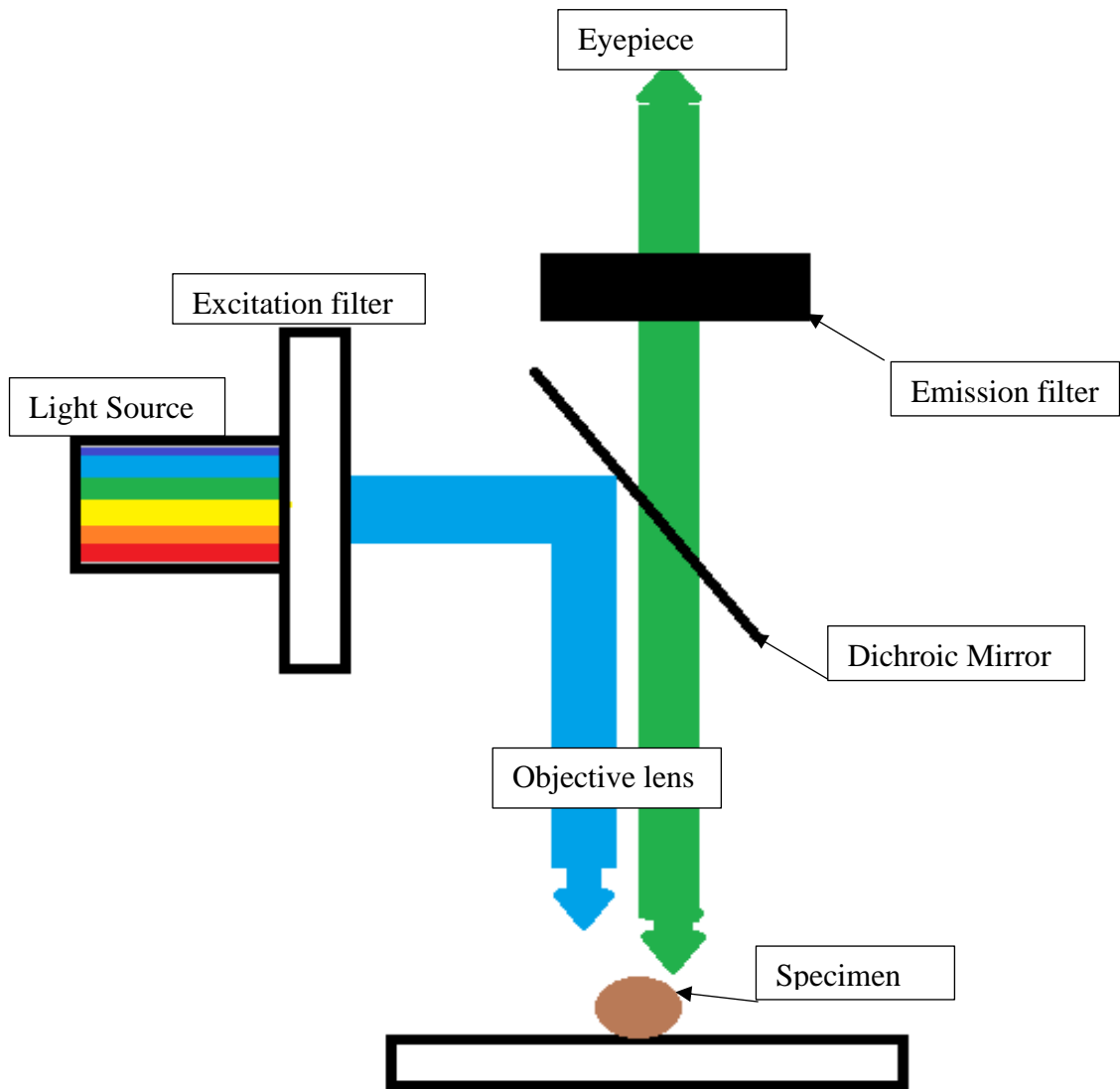


**Figure 9 Schematic demonstration of a fluorescent microscope. The excitation filter permits only the desired wavelength of light to pass through. The light is reflected off the dichroic mirror to illuminate the fluorophore bound to the specimen. Emitted light from the fluorophore passes through the dichroic mirror and emission filter to the eyepiece.**

Immunofluorescence was trialled as a technique to enable us to take advantage of double labelling in the tissue, to enable more precise cellular identification in addition to localisation of the targets. However, due to the processing of the tissue from collection to experimental use, which included formalin fixing steps, de-calcification and paraffin embedding, very high levels of auto-fluorescence were evident. Previous work suggested that standard immunofluorescent protocols can rarely be used effectively in similarly processed archived tissue due to the nature

of formaldehyde to produce high volumes of autofluorescence (Baschong, Suetterlin et al. 2001). Some studies have used alkaline phosphatase-Fast Red (ALP-FR) substrate in IHC, combined with the nuclear stain 4',6-diamidino-2-phenylindole (DAPI) for colocalization of signal, using a combination of light and fluorescent microscopy to visualise the fluorescent immunostaining with ALP-FR and the fluorescent nuclear DAPI signal (Walsh, Wade et al. 1998) with some success.

DAPI is a blue-fluorescent DNA stain that exhibits ~20-fold enhancement of fluorescence upon binding to AT regions of double stranded DNA. It is excited at 405 nm and is commonly used as a nuclear counterstain in fluorescence microscopy, flow cytometry, and chromosome staining. Alkaline phosphatase (AP) is a substrate commonly used in IHC visualisation; fast red (FR) is the chromogenic substrate that in reaction with AP produces an insoluble red fluorescent precipitate at the reaction site (Speel, Schutte et al. 1992). This precipitate results from hydrolysis of naphthol phosphate esters, included in the reaction, to phenols and phosphates, followed by coupling to colourless diazonium salts to produce the insoluble dye. The aim of the optimisation of ALP-FR IHC was to provide us with the ability to both automate the counting for the localisation of activated/phosphorylated SRSF1 by detection of nuclear SRSF1 signal by colocalization with DAPI.

I therefore developed an immunofluorescence labelling protocol for SRSF1 in archived formalin-fixed human synovial samples, to take advantage of the property of alkaline phosphatase to fluoresce under illumination at the 560nm wavelength.

The protocol developed used the same protocol as that for the general IHC experiments (as in Figure 10) with a few minor differences (Figure 11). Firstly, HIER was reduced to 20 minutes instead of 30 minutes but was done at the same temperature. Another difference during this procedure, is that instead of incubating the slides using the ABC kit for the HRP enzyme, I used the VECTASTAIN® ABC-AP Kit with AP-Fast red, (AK-5000, Vectorlab UK) for 30 minutes as per the instructions of the manufacturer. After secondary antibody incubation and two 5-minute washes in PBS, the AP substrate was applied to visualise the immunoreactivity signal (Vector® Red Substrate Kit, Alkaline Phosphatase, SK-5100 Vectorlab, UK) as indicated in Figure 11. The 5-minute incubation took place in the dark to prevent bleaching of fluorescent signal and was followed by four 5-minute washes in PBS, before the slides were mounted using a DAPI fluoromount (cat. number: 00-4958-02 - ThermoFisher Scientific, UK). After mounting, the slides

were kept in the dark at 4 °C, to avoid bleaching of the fluorescent properties of both AP-FR, and DAPI. It is important to note that the number of washes between every step were also increased compared to the previous protocol, to reduce the background staining.

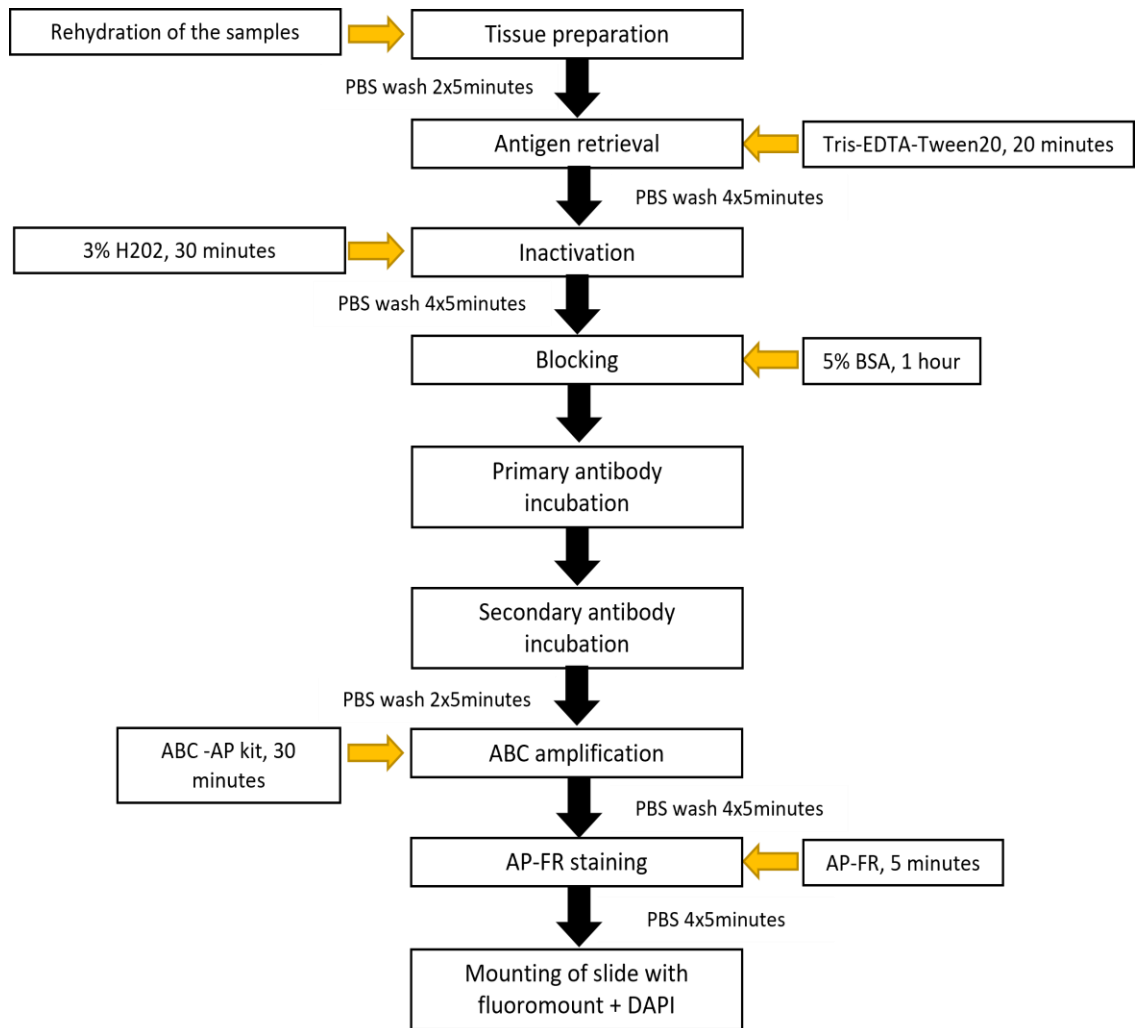


**Figure 10 Schematic representation of the IHC protocol using the Alkaline phosphatase – fast red substrate kit.**

## 2.7 Synovial Histological Scoring

Haywood et al developed a 4-point scaling system (Haywood, McWilliams et al. 2003) which is the one used throughout the studies presented here (Figure 12). In contrast to the Krenn score which was used previously, the Haywood scale examines the three criteria, as shown in Table 10.

Grade 0: the tissue was normal with a synovial lining of <4 cells thick, sparse cellular distribution, with few or no inflammatory cells).

Grade 1: mild inflammation with synovial lining of 4 or 5 cells thick, increased synovial cellularity as well as some presence of inflammatory cells.

Grade 2: moderate inflammation with synovial lining of 6 to 7 cells thick, dense cellularity with a high percentage of inflammatory cells present, no lymphoid aggregates.

Grade 3: severe inflammation with a synovial lining >7 cells thick, dense cellularity, inflammatory cell infiltration, as well as evidence of perivascular lymphoid aggregates (Haywood, McWilliams et al. 2003).

PM samples were used as controls and as such, cases from that group should not have synovitis score  $\geq 2$  as a synovitis score of 0 or 1 would be considered normal/healthy tissue. PM samples with high synovitis score, as determined post-hoc, were thus excluded unless otherwise indicated.

**Table 8 Scoring system for the histological accession of the synovial tissue inflammation developed by Haywood et al. 2003**

Grade	Synovial lining thickness	Cellularity	Inflammatory cells
0: Normal	<4 cells	Sparse	None or Few
1: Mild Inflammation	4-5 cells	Increased	Some
2: Moderate inflammation	6-7 cells	Dense	Many, with no lymphoid aggregates
3: Severe inflammation	>7 cells	Dense	Many, with lymphoid aggregates

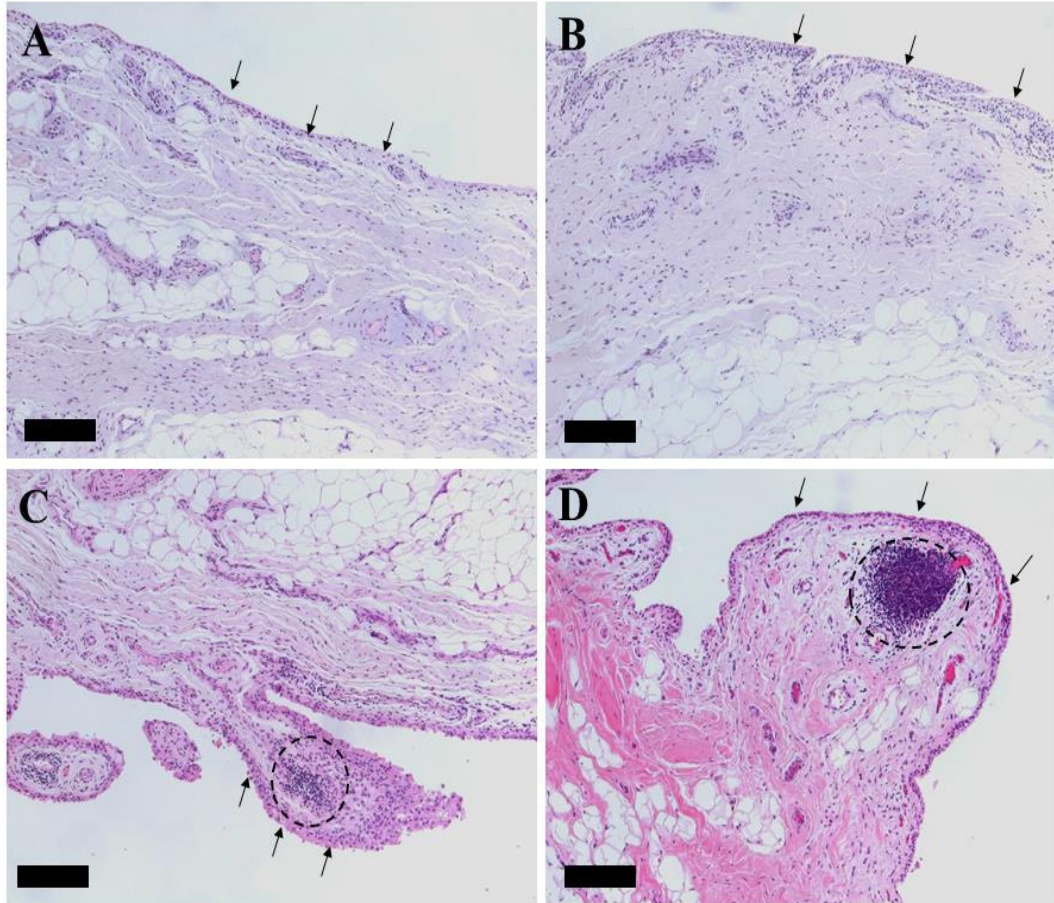


**Figure 11 Demonstration of synovial inflammation scoring based on the Haywood et al criteria. A. Normal synovium (grade 0), B. low inflammation synovium (grade 1), C. Moderately inflamed synovium (grade 2) with the dotted circles showcasing a cluster of inflammatory cells, D. Severely inflamed synovium (grade 3) with the circle indicating a lymphoid aggregate. Arrows indicate the lining surface. Image captured at 4x magnification. Haematoxylin and eosin were used to visualize the tissue.**

## 2.8 Image analysis and quantification

Histological scoring for the studies described in this work was completed by a single observer (Dimitrios Amanitis) blinded to classification criteria and the details of the samples using a Zeiss Axioscop-50 microscope (Carl Zeiss, Welwyn Garden City, UK). Prior to the scoring the observer was trained and his ability to score the samples was evaluated based on a comparison to a secondary observer (more details can be found in chapter 3.2). The blinding process was completed with the help of Seyed Shahtaheri after the IHC protocol had been completed. The samples were given a provisional code number before being assessed to reduce bias. Synovial

inflammation was graded by examining haematoxylin and eosin-stained sections using both 20x and 40x magnification depending on the stain and the method of quantification used (see chapters 3 and 4).

Fibroblast-like synoviocytes fractional area of IHC staining was quantified using a 3-CCD camera and KS300 image software (Zeiss). Immunoreactivity areas were identified by an individual observer, an image was captured, and the ROI (region of interest) was highlighted which included synovial lining and approximately 100um of sub-lining tissue. Background staining was removed from the positive staining after thresholding the image based on the negative control to create a mask as seen in Figure 13. The total area of the tissue captured, as well as the area of the positive staining was also measured. Fractional area was calculated as the quotient of the positive area divided by the total area.

Data was collected using a 20x objective lens with 3 different fields of view per sample. This was determined as the minimum number of fields of view that could be collected that would result in the lowest variation in fractional area measurement in a pilot study (see Chapter 3). More detailed explanation on the validation of the most appropriate approaches to the analysis of synovial staining is in Chapter 3, section 3.3.1 Results. If no synovial lining was detected in the sample, then the sample was excluded.

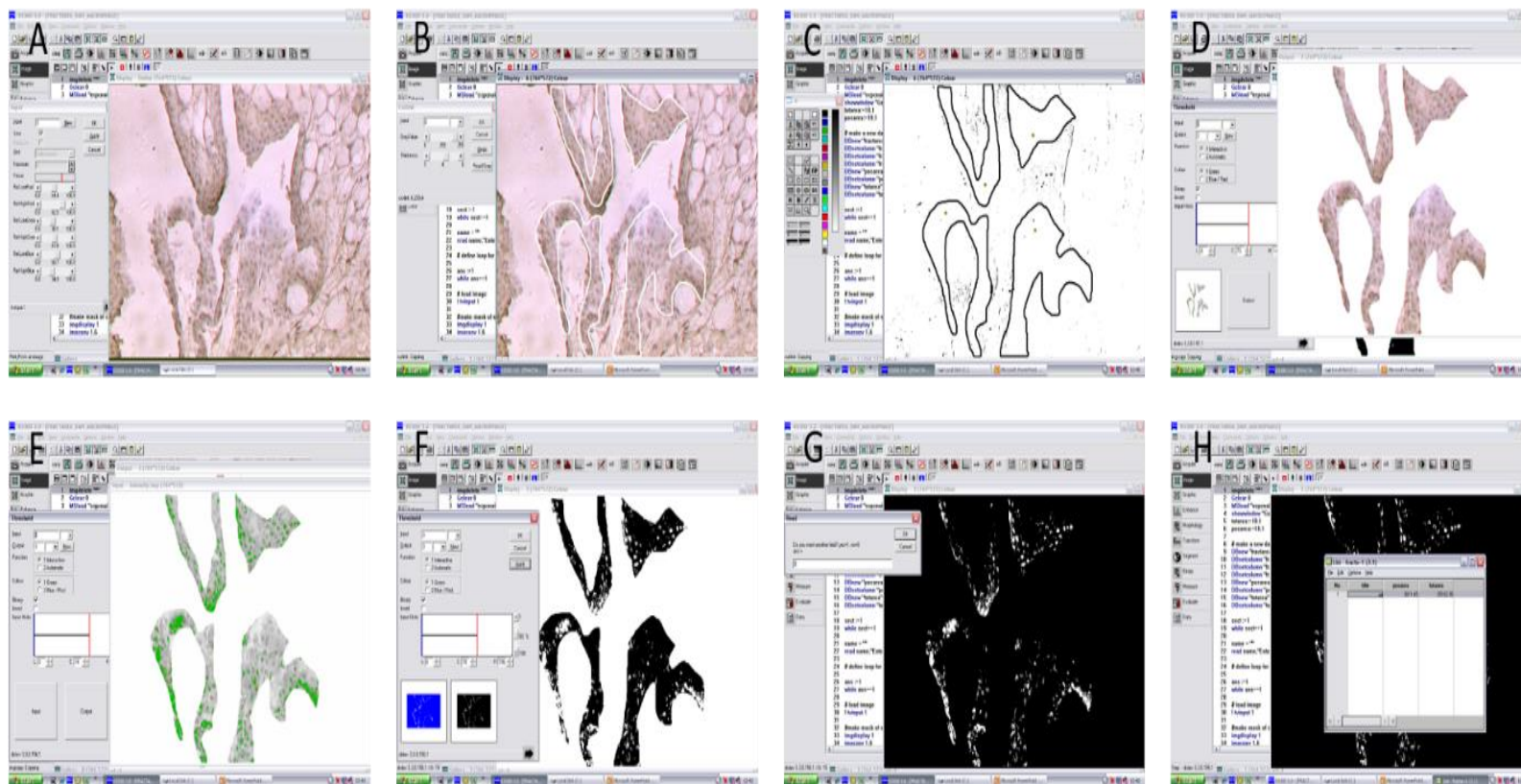


**Figure 12 Analysis of Fractional area using a custom-made macro implemented in KEIS imaging software. A-B) First an image of the desired field of view is acquired and saved locally within the macro. C) The tissue of interest is selected by outlining it with the selection tool of the software used. D-E) By previously setting the background staining levels using the negative controls, the thresholding excludes any background staining. It is important for these values to remain equivalent throughout the data extraction. F-H) Results are saved and transferred to an Excel file for further analysis.**

Following the fractional area analysis cells with SRSF1 nuclear localisation were counted manually by using the cell counter plugin in Fiji (Rueden, Schindelin et al. 2017). The plugin the cells counted can be separated with several different “pointers” (depending on how many distinct cell groups there are) and provides the final numbers of the cells marked. Using the plugin and counting the cells on a captured image enabled high quality digital image enlargement and ensured high precision throughout the process of cell counting. To avoid potential bias, the observer was completely blinded to the details of the image analyses. This was achieved by using a custom-made macro, which saved all the images with a random coding number. The initial identification for the images was automatically saved by the macro in an excel file which was only accessed by the observer after the analysis was concluded. For SRSF1 nuclear localization, the number of cells with strong nuclear staining were first counted (strong nuclear staining would be considered if more than 70% of the nuclei was stained) and then divided by the total number of positive cells in the same area, to provide a ratio representing the percentage of SRSF1 nuclear translocation.

Quantification of staining intensity was measured as per integrated density using a custom written macro in Fiji (Rueden, Schindelin et al. 2017) (Dimitrios Amanitis see Appendix 1). The macro automated the process of selecting the images from a specified folder and scaled /re-calibrated the images from pixels to micrometres using the embedded scale bars. The macro then de-convoluted the images to three channels: one containing the stain of interest, one containing only the haematoxylin staining, and one with no staining. The channel with the stain of interest was then thresholded to a specific value previously set using the negative control as a basis and finally the macro automatically set the region of interests (ROI) and measured the integrated density of the stain in the ROI. To confirm consistency in the output of the macro, for example if there were artifacts in the tissue, pause steps were included in the macro to allow the researcher to validate that no errors occurred. The results were then exported directly to Excel using a commercially available plugin Read and Write Excel (Anthony Sinadinos, Brenden Kromhout) for further analysis. The sum of each of these values was calculated and then, the average area, mean, and density was calculated. In certain samples due to the condition of the tissue post-experiment, the target of 3 images acquired could not be reached, because the lining had been destroyed during tissue processing. In these cases, by necessity, fewer technical replicates were used.

## **2.9 General cell culture methods**

To investigate fibroblast-like synoviocytes (FLS) activation and differentiate normal FLS activity from inflammation derived activity, human fibroblast like synoviocytes (HFLS) were used (Cell Applications Inc, US). The inflammatory profile of HFLS was investigated after treatment of the cells with TNF- $\alpha$  to trigger an inflammatory response. All cell lines were grown in T25 flasks (Corning) following thawing and then passaged to T75 flasks (Corning) following expansion. Incubation of the cells was at 37°C at 5% CO<sub>2</sub> unless otherwise stated (Sanyo MCO-18AC).

Normal HFLS and HFLS from people with RA were acquired through Cell Application Inc US or the European Collection of Cell Cultures (ECACC) at passage 1 and cultured and expanded in high-glucose Dulbecco's Modified Eagle Medium (DMEM, GIBCO 13345364-500ml), containing 20% fetal bovine serum (FBS, SIGMA F2442- 500ml) and 2mM L-Glutamine (SIGMA G7513-100ml). Cells were grown until they reached a maximum of 80% confluence, after which they were passaged. For passage, culture medium was aspirated, and cells washed with phosphate buffered saline (PBS, D8537-500ml). PBS was consequently aspirated and replaced by 3ml of 1x Trypsin-EDTA (Trypsin=0.05%w/v, EDTA = 0.5mM – T4049, 100ml) in a T75 flask. Cells were then placed in the incubator at 37°C in 5% CO<sub>2</sub> /95% O<sub>2</sub> for no longer than 2 minutes. Using no less than three times the trypsin volume, the Trypsin-EDTA solution was quenched using the HFLS growth medium and following centrifugation at 150G for 5 minutes the cells were counted using a Haemocytometer (catalogue number:5610, Vetlab supplies UK). HFLS were split and plated at 1:2 ratio due to the low expansion rates of the cell line.

### **2.9.1 Preparation and storage of cell stocks**

Cell stocks were prepared by following the protocol above for general culture, but after trypsinisation and centrifugation, cells were collected in a 50ml Falcon tube. Cells were then re-suspended in freezing medium consisting of basal growth medium (DMEM + 20%FBS + 2mM L-glutamine) and 10% dimethyl-sulfoxide as cryo-preserved (DMSO, ThermoFisher 20688) at a cellular density of 5x10<sup>5</sup>/ml. Cryo-vials (Nunc V7384) were used to aliquot the cells and were placed in an isopropanol chamber (Mr Frosty, SIGMA C1562), for freezing overnight at -80°C before storage in liquid nitrogen (LN).

When thawing cell stocks, aliquots were rapidly removed from LN and mixed with pre-warmed growth media (heated to 37°C) to a final volume of 5ml. Immediately after, the cells were

centrifuged for 5 minutes at 150G to remove any excess DMSO content, then resuspended and transferred to a T75 flask with 7ml of medium.

## **2.10 Protein isolation and quantification**

Following culture under experimental conditions as above (2.9.1), FLS were washed three times in ice cold PBS, followed by a 5-minute incubation with lysis buffer to dissociate the cells. Lysis buffer contained RIPA buffer containing (30mM HEPES, pH 7.4, 150mM NaCl, 1% Nonidet P-40, 0.5% sodium deoxycholate, 0.1% sodium dodecyl sulphate, 5mM EDTA, 1mM NaVO<sub>4</sub>, 50mM NaF, 1mM PMSF, 10% pepstatin A, 10 µg/ml leupepsin, and 10 µg/ml aprotinin - SIGMA R0278), with added phenylmethylsulphonyl Fluoride (PMSF) protease inhibitor (1mM SIGMA P7626), protease inhibitor cocktail (blocking serine proteases e.g., trypsin, aminopeptidases, cysteine proteases and acid proteases - SIGMA P8340), 1mM Na<sub>3</sub>VO<sub>4</sub> and 10mM NaF. All procedures were performed on ice throughout the procedure.

Cells were detached from the wells with a cell scraper and collected in cold Eppendorf tubes after thorough pipetting to break up clumps of cells. Centrifugation of the samples at 13000G for 15 minutes at 4°C, was followed by isolation of the supernatant which was stored -80°C until use. Protein quantification was performed on a plate reader (Victrox4, PerkinElmer) using the Bradford Assay (Bradford reagent, SIGMA B6916).

The principle of the Bradford assay to detect and quantitate proteins is based on the binding of protein molecules to Coomassie dye under acidic conditions, resulting in a colour change from brown to blue in proportion to the amount of protein present in a sample. The presence of lysine, arginine and basic amino acids contribute to the formation of a protein dye complex which is detected in the assay. Protein standards are used alongside the assay to subtract background as well as to create a standard curve to quantify the amount of protein in the experimental samples. The protein standards include concentrations to cover the potential range of protein concentrations in the samples, and the range covered by the sensitivity of the assay. At high concentrations the assay colour intensity plateaus as at high protein concentrations the colimetric change saturates. Thus, at high protein concentrations, sample dilution may be needed to ensure that the protein is measurable within the assay limits. Bovine serum albumin (BSA) is the most used standard protein for the Bradford assay. Specifically, the standard curve usually consists of ten serial concentrations between 4000 µg/ml to 0 µg/ml. Alongside the standards, samples are assessed in 2 or 3 technical replicas. For each sample, 300 µl of the

Bradford assay reagent is added, before completing the assay in a suitable plate reader. From the assay results the protein concentration of the samples is calculated and used for calculation of gel loading and further analysis.

## **2.11 Western blotting**

Western blotting, or protein immunoblotting, is a commonly used analytical technique to detect and quantify specific proteins either in homogenized tissues or cell extracts. Western blotting was first introduced by Towbin (Towbin, Staehelin, & Gordon, 1979) for qualitative and semi-quantitative protein analysis. The technique is based on the technique of separation of a mixture of proteins based on their molecular weight, usually measured in kiloDaltons (kDa). In a typical Western blot protocol, the samples are denatured and separated by PAGE (polyacrylamide gel) electrophoresis. Proteins are then transferred to a membrane, usually either nitrocellulose or polyvinylidene difluoride (PVDF) by wet or dry electrophoretic transfer. Both types of membrane have merits, for example PVDF is often preferred as it has a higher protein binding capacity than nitrocellulose, thus allowing higher sensitivity. In contrast, nitrocellulose membranes produce lower background noise and are ideal for detecting lower molecular weight proteins. For all the experiments here, nitrocellulose membranes were used. Following transfer to the membrane of choice, protein is detected by a method like that described for indirect immunochemistry/immunofluorescence in sections 2.5 and 2.6.

Western blotting was attempted to identify expression of the adhesion factor ICAM-1 in response to incubation with tumour necrosis factor alpha (TNF- $\alpha$ ) to determine the contribution of inflammatory mediator stimulation to the adhesion of monocytes to FLS.

After calculating the concentration of protein in the samples of interest, samples were separated using SDS-PAGE gel. A volume of each protein sample containing 20ug of protein was mixed with 2x Laemmli buffer (Sigma S3401- 62.5mM Tris-HCl, 2% SDS, 20% glycerol, 0.01% bromophenol blue, 5%  $\beta$ -mercaptoethanol, pH 6.8) to give a final protein concentration of 1 $\mu$ g/ $\mu$ L in 1x Laemmli buffer. Proteins are denatured for 5 minutes at 95 C, centrifuged for 5 minutes at 12000g, and loaded on a 4-15% gradient SDS-PAGE gel (BIORAD Mini-PROTEAN® TGX™ Precast Protein Gels, 4561084) along with a protein size marker (LI-COR Biosciences™ Chameleon Duo Pre-stained Protein Ladder – 15521165 FischerScientific). Proteins were subject to electrophoresis in chilled running buffer (0.25M Tris, 1.92M glycine, 1% SDS Ph8.6) for 70 minutes at 120V, or until the loading buffer dye reached the end of the gel. The gel was then

removed from the plates and equilibrated in chilled transfer buffer (25mM Trizma, 192mM glycine, 20% methanol) on a shaker for 10 minutes.

Samples were then transferred to nitrocellulose membranes by wet sandwich transfer (BioRad) in transfer buffer. Initially a “sandwich” transfer block is made (as shown in the figure 14).

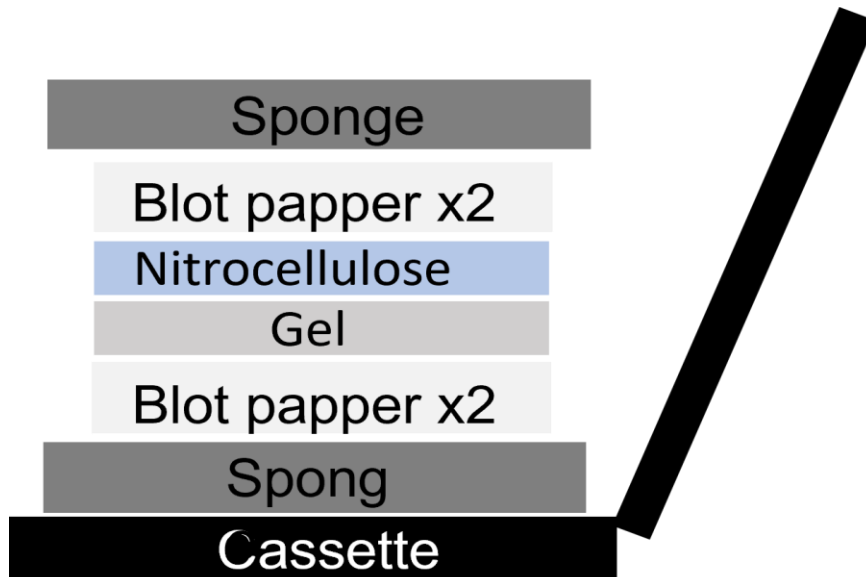


**Figure 13** “Sandwich” transfer block cassette. The block comprises of 2 sponges, 4 blot papers, 1 nitrocellulose membrane and the gel of interest

The block comprises of 2 sponges, 4 blot papers, 1 nitrocellulose membrane and the gel of interest. After soaking the individual parts in the TB buffer, the cassette was assembled as following: 1 sponge- 2 blot papers-gel-nitrocellulose membrane-2 blot pappers-1 sponge. The cassette was closed firmly and was placed in the gel tank completely submerged in TB. Electrophoretic protein transfer to the membrane took place at 80V for 2 hours, then the membrane was removed and transferred for 5 minutes to a buffer solution of 0.01% TBS-Tween 20 on a shaker.

Any incubation or wash step from this point forward was performed with gentle agitation either on a shaker or a roller. Membranes were blocked for non-specific binding using 2% BSA in 0.01% TBS-Tween solution for 1 hour in room temperature. Incubation with the primary antibody was performed overnight in a cold room (anti- ICAM-1, Thermofisher Scientific MA5407) with gentle agitation. Membranes were also incubated with anti-GAPDH (Glyceraldehyde 3-phosphate dehydrogenase) secondary antibody (0.5 µg/ml) as a loading control. Fluorescent secondary antibodies specific to the primaries were applied for 1 hour in room temperature after three 10-

minute washes in 1x TBS-T. Two secondaries were used exclusively: a donkey anti-rabbit IgG IRDye 680RD (ab216779, Abcam) and a Goat anti-Mouse IgG H&L IRDye® 800CW (ab216772 Abcam). Membranes were washed three times with 0.01% TBS-Tween for 5 minutes respectively, and secondary antibody binding visualized on the Licor Odyssey imaging system (Licor, UK).

## 2.12 RNA extraction

Total ribonucleic acid (RNA) was extracted from cultured HFLS to investigate differences in the splicing pathway of VEGF-A. After treating the cells with the appropriate compounds/drugs (Chapter 5), the cells were washed with PBS. Following removal of PBS, 250µl of Tri-reagent (ThermoFisher, AM 9738) was added to each well (for cells cultured in 24well plates). Cells were scraped repeatedly until the mixture became homogenized with no cellular clumps. The cell lysates were then transferred to sterile Eppendorf tubes and incubated for 5 minutes in room temperature to promote the release of RNA from the breakdown of the nucleoproteins. Chloroform (SIGMA, C2432) was then added to each of the mixtures (50 µl), and after thorough mixing tubes were incubated at room temperature for 15mins. Centrifugation for 15 minutes at 12000G and 4°C resulted in three distinct layers; the top clear, aqueous solution containing RNA, a milky interface white layer containing DNA and a lower organic solvent pink layer containing proteins. Aspiration of the upper layer yielded approximately 150ul of the solution containing RNA which was then transferred to fresh sterile Eppendorf tubes. RNA was precipitated by addition of 125µl of isopropanol (Thermo-Fischer, 9500-1) followed by thorough mixing, incubation at room temperature for 10 minutes and centrifugation at 12000G for 10 minutes at 4°C. After centrifugation, the supernatant was discarded, and the RNA pellet washed with 250µl of RNase free 75% Ethanol (SIGMA 459836-1L) to remove residual salts. Following final centrifugation at 10000G for 5 minutes at 4°C, removal of the supernatant and drying with mild heat for 10 minutes, pellets were dissolved in 20µl of DEPC treated water (Invitrogen, 10289104), and either stored at -20°C if they were to be used the next day, or immediately quantified and purity tested using a Nanodrop 2000 spectrophotometer (Thermo-Fisher). For quantification, absorbance ratios at 260/280nm (absorbance wavelength of RNA/ absorbance wavelength of DNA) and 260/230nm (absorbance wavelength of RNA/ absorbance wavelength of proteins) were determined for 1µl samples of each RNA sample. RNA concentration was also determined (ng/ml).

### 2.13 cDNA synthesis

1µg of RNA solution acquired as described in section 2.12 was made up to 8µl in nuclease free water in a 200µl PCR tube (Starlab, I1402-8100), to synthesise complementary DNA (cDNA). When the concentration of RNA in the initial samples was significantly higher than 1µg/µl, final concentration was adjusted by addition of nuclease free water to ensure that the same input of RNA was used for each sample. Subsequently, when the total RNA derived from the cell lines was less than 1µg/ml, the total RNA used was dictated by the lowest yield sample. Avoiding genomic DNA contamination was critical in the samples, consequently they were treated with 1µl of RQ1 DNase (in 10mM HEPES, 50% v/v glycerol, 10mM CaCl<sub>2</sub> and 10mM MgCl<sub>2</sub>), per 1µg of RNA and 1µl of RQ1 DNase buffer (400mM Tris-HCl, 100mM MgSO<sub>4</sub> and 10mM CaCl<sub>2</sub>) for a total reaction mixture of 10µl (1µg of RNA in 8µl of water, 1µl of DNase and 1µl DNase reaction buffer). Tubes were incubated at 37°C for 30 minutes in a PTC-200 Thermocycler. The DNase activity was halted by addition of DNase stop solution (1µl of the stop solution – 20mM EGTA) to a final sample volume of 11µl and incubation at 65°C for 10mins, and the reaction was placed on ice.

Reverse transcription was performed by addition of 0.5µg of Oligo-dT primer (Promega C110A), which hybridizes to the mRNA polyA tails, plus 250ng of random hexamer primers, to prime the reverse transcription reaction, and the single-stranded DNA or RNA for extension. The reaction was incubated at 70°C for 10minutes and samples then placed on ice to stop the RNA from entering secondary conformation structures. 0.5mM dNTPS (deoxyribonucleotides), 4µl of 5x Molony Murine Leukaemia Virus (MMLV) reverse transcriptase (RT) buffer (250mM Tris-HCl, 375mM KCl, 15mM MgCl<sub>2</sub> and 50mM DTT) were added, along with 1.5µl nuclease free water to make the reaction volume up to 19µl, and finally 1µl of MMLV-RT enzyme was added to a final reaction volume of 20µl. MMLV-RT is an RNA-dependent DNA polymerase enzyme that can be used to generate cDNA from long messenger RNA templates (>5kb). It has lower RNase H activity, compared to other transcriptases, which helps to ensure the integrity of the RNA template. The enzyme is a product of the pol gene of MMLV and consists of a single subunit with a molecular weight of 71kDa. The final reaction volume was made up to 20µl by addition of 1µl of MMLV-RT enzyme to all samples. To generate cDNA, following addition of MMLV-RT, samples were incubated at 37°C for 60 minutes for cDNA extension, 42°C for 30 minutes for DNA polymerisation and 70°C for 10 minutes to inactivate the MMLV-RT. A 'no-RT' negative control, where the reaction mixture was exactly the same and went through the same incubations, but

did not include the MMLV-RT enzyme, was included for all the experiments to control for genomic DNA contamination. Following reverse transcription, samples were kept at -20°C until further use. All products used in this protocol were from the Promega Reverse Transcription System. (Promega A3500)

### **2.13.1 Polymerase Chain Reaction Primers**

Investigating physiological changes in gene expression via detection of molecular markers required the identification of primers and optimisation of protocols for the identification of key targets using polymerase chain reaction (RT-PCR) amplification of the reverse transcribed cDNAs from treated synoviocytes. The primers shown in Table 10 (listed in 5' to 3' format), derived from previous literature investigating these targets in human tissues. The human pan-VEGF-A primers were those described and used by Bates and colleagues (Bates, Cui et al. 2002) , the human VEGF-A<sub>165a</sub> and VEGF-A<sub>165b</sub> competitive primers used by the same group (Woolard, Wang et al. 2004), the human SRSF1 primers were those used by Zhou and colleagues (Zhou, Wang et al. 2019), and the human SRPK1 primers were those used by Wang and colleagues (Wang, Zhou et al. 2020).

All the primers shown in table 11 (sourced from Sigma-Aldrich) were checked for specificity for the targets using the NCBI primer blast, and to identify exon-intron junctions using Ensembl. The primers were lyophilised and reconstituted in RNase-free water to give 100 µM stock solutions that were stored at -20 C freezer. Prior to usage, the forward and reverse primers were combined in Eppendorf tubes from the aforementioned stock with 10 µl of the forward and 10 µl of the reverse primer alongside 80 µl of RNase free H<sub>2</sub>O, providing working stock solution of 10 µM, to avoid constant thawing cycles on our initial stocks.

**Table 9 Primers and accompanying product sizes**

Primer Target	Forward Primer	Reverse Primer	Product Size (bp)
Human VEGF-A isoforms pair 1	5'-GTAAGCTTGTACAAGATCCGCAGA CG	ATGGATCCGTATCAGTCTTTCCT	130b p and 64bp
Human VEGF-A <sub>165a</sub> and VEGF-A <sub>165b</sub> pair 2	GAGATGAGCTTCTACAGCAC	TTAAGCTTTCAGTCTTTCCTGGTGAGAGATCTGC A	220b p
Human SRSF1	GCCGCATCTACGTGGGTAAC	GAGGTCGATGTCGCGGATAG	95
Human SRPK1	GTGTGCCAGTCTTCTCAACTG	GGTCAGCAATCTTCACCTTGAG	217

### 2.13.2 Polymerase chain reaction (PCR)

The PCR method described here is the general protocol used, and more specific information on precise conditions are in Chapter 5, section 5.2.

A reaction mixture containing 50ng of cDNA (produced as described before in chapter 2.13), 0.5µM of each forward and reverse primer (1µl primer mix), 10µl of PCR Master Mix (Promega) (the master mix contains: 50 units/ml of Taq DNA polymerase supplied in a proprietary reaction buffer (pH 8.5), 400µM dATP, 400µM dGTP, 400µM dCTP, 400µM dTTP, 3mM MgCl<sub>2</sub>) and nuclease free water to a final volume of 20µl was prepared for each cDNA sample. Controls for DNA contamination of reagents were included with water replacing the cDNA sample in the same reaction mixture, the 'no-RT' control samples were included to determine whether genomic contamination was present even after DNase treatment. PCR reactions were carried out in 200µl thin-walled tubes in a PTC-200 thermocycler, using a denaturation step at 95 °C for

5 minutes, annealing and extension temperatures and times as detailed in Chapter 5, section 5.2, a final extension step of 72°C for 10 minutes, and cooling to 4°C. Reactions were stored at 4°C overnight or visualized by gel electrophoresis immediately.

For gel electrophoresis, 3% agarose gels were made by dissolving 6g of agarose (Sigma, A9535) in 200ml of TAE buffer (40mM Tris base, 1mM EDTA, 0.1042% v/v glacial acetic acid), dissolved by heating in a microwave at maximum power for 30seconds. Once dissolved the agarose solution was allowed to cool until it could be held, before adding ethidium bromide (5µl per 100mL Sigma, E1510) for DNA visualization on a GelDoc system (BioRad, UK). The gel was formed in the gel running plate with loading wells created with a plastic 'comb'. Once the gel had solidified, After the comb was removed and the gel on the plate submerged in fresh TAE buffer in a gel tank (BioRad), 4µl of 6x loading buffer (Thermo, R061, Orange G Dye + Xylene cyanole FF in Glycerol) was added to each sample for a total volume of 24 µl. Up to 20µl of each sample reaction, was then loaded onto the gel, alongside with 5µl of DNA markers (Bio-Line 50BP Hyperladder) also included in at least one lane for amplicon size comparison. The DNA was electrophoresed at 90V for 90minutes, and then DNA was visualised on a UV transilluminator to check separation and imaged with a GelDoc UV visualisation plate system and software (BioRad UK). Images were exported in TIFF format.

## **2.14 Statistical Analysis**

All statistical analyses were performed using GraphPad Prism software (GraphPad Prism version 8.0.0 for Windows, GraphPad Software, San Diego, California USA, [www.graphpad.com](http://www.graphpad.com)).

Specific information on statistical tests used for the individual studies are given in the respective chapters in figure legends. Significance was accepted when  $p < 0.05$  as per convention. All figures shown are mean  $\pm$  standard deviation unless otherwise stated.

I also utilized another statistical analysis technique namely Principal Component Analysis or PCA. PCA is a statistical technique to handle multiple variables, achieved by reducing the dimensions of the dataset, without losing major information that would characterize the data. Main principle resides in dimensionality reduction, meaning the number of variables describing the dataset. By retaining as much information vital for our dataset and investigating the relations of the individual variables through PCA we stand in a favourable position to analyse multi-variant raw data. PCA relies heavily on the concept of feature extraction, denoting a projection of data to smaller number of dimensions, through linear combinations. Feature extraction is the process

through the original variables are analysed in order to construct a “new” set of variables, either through linear or non-linear analysis (with PCA being the linear analysis). These new linear combinations of the original variables are what is called in PCA the principal components or PCs. As a general guideline, these new variables are meant to contain the most useful information from the entire dataset, to which the original data will then be projected, minimizing the loss of information. PCs, considering they are linear combinations of our initial data, can be represented in line graphs where the data can be projected onto. Of key interest for a PCA is the variance of the dataset, provided that variables with greater variance contain more information for PCA. Main goal of PCA is to retain as much variance (information) as possible, and to guarantee that the PCs (new variables) can characterize the original dataset to the best of their abilities. Minimising the dataset, and projecting into a reduced dimensional space, will result in losing some information, however by fitting the data to the first principal component appears to successfully counter both the aforementioned issues. It is important to note that the number of PCs in a PCA is equal to the number of the original variables.

As a general rule the principal components are calculated as below:

$$PC1= a_1x_1 + a_2x_2 + a_3x_3$$

$$PC2= b_1x_1 + b_2x_2 + b_3x_3$$

with X representing the variables or samples, while a, b etc representing a standardised coefficient or Eigenvector. Eigenvectors are values that represent the direction of a PC, similar to the slope I would encounter on a regression analysis indicating a positive or negative relationship. There is another value of interest during a PCA test, namely Eigenvalues. These values represent the variance explained by principal components. The larger the eigenvalues, the larger the variance of the principal component, denoting the ability of this PC to explain/include more of the original data.

If I were to identify however all the possible PCs for a study, that would entail creating a new dataset that has the same dimensions as the original, denoting a need to specify which PCs are best suited to be retained for the purpose of analysis. A variety of methods have been introduced regarding PC selection. Initially, one of the simplest techniques for PC selection is to select the first X amount of PCs based on their eigenvalues (important to note, there is no underlying reasoning behind the selection, beyond selecting the PC with the highest variance). Moving forward, there is the “Kaiser rule”, which entails the selection of PCs with eigenvalues greater than 1. The main issue with this approach is that even with random data or noise in the PCA,

eigenvalues greater than 1 will still be selected, even though they are not useful. Both techniques are considered faulty and are not preferred due to not being able to account for variance due to noise.

Parallel analysis is a method focusing on selecting PCs without losing power due to noise. In short during a parallel analysis is described on figure 15.

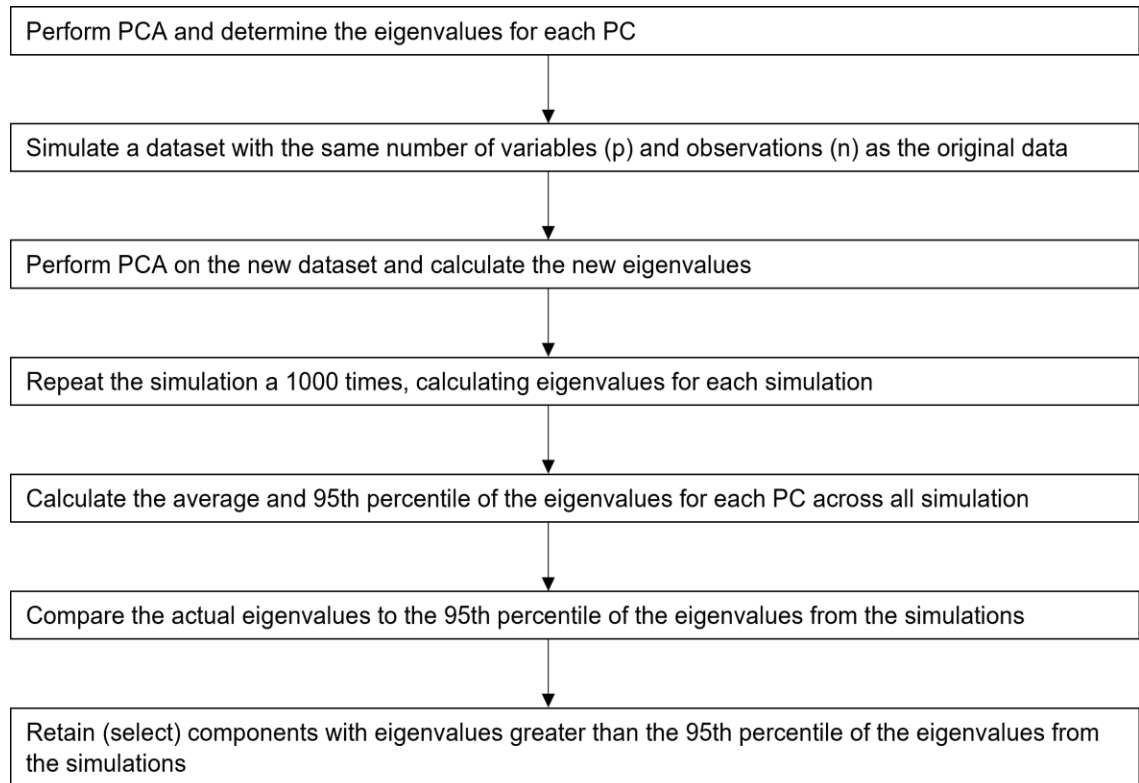


**Figure 14 Visual representation of the parallel analysis process to determine PCs and eigenvalues from the initial dataset**

PCA focuses on generating PCs with eigenvalues greater than 1, however the eigenvalues from the “noise” will decrease as the observations are increased. Retaining only eigenvalues greater than the 95th percentile I ensure that the variance of our PCs is variance not generated due to noise.

The data collected from PCA can be utilized for further analysis using a regression analysis. Specifically, principal component regression or PCR is a combination of multiple linear regression and principal component analysis. The logic behind PCR is similar to running a linear regression analysis, while focusing on reducing the number of predictors for future analysis. This is achievable by performing PCA and extracting the PCs desired, performing a multiple linear

regression using the principal components scores alongside a dependable variable and finally converting the coefficient estimates back to the original variables. Combining the two techniques offers great versatility in analysing the results, as well as it provides the opportunity to identify relationships between a large number of variables, without introducing variance in the analysis.

### **3. VEGF-A splicing events and inflammation in the synovium of OA and RA knee joints.**

#### **3.1 Introduction**

As introduced above VEGF-A has been extensively investigated in the context of arthritis, and is known to be an important driver for angiogenesis in inflammatory diseases like OA and RA. Tissue injury results in hypoxia, and upregulation of proinflammatory cytokines (such as IL-1 $\beta$  and TNF- $\alpha$  macrophage-migration inhibitory factor, prostaglandins), can act on surrounding cells such as keratinocytes (in skin) or synoviocytes to increase the expression of VEGF-A (Cho, Feng et al. 2006, Cho, Jung et al. 2006, Ryu, Lee et al. 2006, Kim, Park et al. 2007, Kim, Kim et al. 2015). Hypoxia induces HIF-1 $\alpha$ , which is a potent stimulator of VEGF-A expression and splicing to VEGF-A<sub>xxx</sub>a isoforms. Infiltrating neutrophils, monocytes, and macrophages, in addition to mast cells, also show increased VEGF-A expression. All these cell types contribute to the inflammatory process. VEGF-A is one of the most potent angiogenic factors recognised (Kim, Kim et al. 2015) in synovial inflammation (a major contributor to knee OA and RA). Early events of synovial proliferation lead to cartilage and bone destruction with angiogenesis promoting such events. VEGF-A is pertinent in the survival of synovial fibroblasts in RA, protecting the cells from apoptosis (Yoo, Kwok et al. 2008), and through this stimulation of synovial fibroblasts, VEGF-A can also indirectly induce osteoclastogenesis in RA (Kim, Kim et al. 2015).

In both RA and OA serum and synovial levels of VEGF-A concentrations are higher compared to controls, and where compared, are higher in RA than OA patients or controls (Mabey, Honsawek et al. 2014, Saetan, Honsawek et al. 2014, Kim, Kim et al. 2015) . VEGF-A levels also positively correlate to arthritic disease activity (Saetan, Honsawek et al. 2014, Clair, Kingery et al. 2019). In OA synovial fibroblasts or in serum of OA human patients VEGF levels are upregulated in relation to visfatin, a cytokine responsible for the stimulation and release of inflammatory cytokines in OA,(Tsai, Liu et al. 2020), moreover it is expressed in bone marrow and plays a role in the damage of synovial joint; a similar study suggests that apelin, which in synovial fluid is significantly and positively correlated with disease severity in OA(Hu, Tang et al. 2011), can also regulate angiogenesis progression driven by VEGF altering the OA progression (Wang, Kuo et al. 2020).

VEGF-A is important in the development of both articular cartilage and bone. While normal cartilage is hypoxic, in inflamed joints increased HIF-1 $\alpha$  causes upregulation of VEGF-A (Jackson, Minton et al. 1997), resulting in detrimental changes in chondrocyte metabolism (Murata, Yudoh et al. 2008). IL-1 $\beta$ /TNF- $\alpha$  upregulation under these conditions, also facilitate increased VEGF-A expression by superficial chondrocytes in OA (Walsh, McWilliams et al. 2010). VEGF-A and VEGFR expression is increased in OA cartilage (Qian, Xu et al. 2021). In addition to the changes in synovium and cartilage in OA, angiogenesis has been demonstrated in subchondral tissue in both RA and OA, facilitated by the same angiogenic cytokines, IL-1 $\alpha$ , IL-8 and IL-10 (Hulejová, Barešová et al. 2007).

VEGF-A neutralisation using bevacizumab (Avastin) (Nagai, Sato et al. 2014), an anti-VEGF-A<sub>121</sub> antibody (Sone, Kawakami et al. 2001), or knockdown with an intra-articular VEGF-A short hairpin RNA blocked disease progression in experimental OA, RA and OA in rabbit, mouse, and rat (Zhang, Crawford et al. 2016) respectively. Only one study showed data on synovitis, and this was unaffected by VEGF-A<sub>121</sub> neutralising antibody treatment, although joint structure was maintained by the treatment (Sone, Kawakami et al. 2001). Overall, there is therefore considerable evidence suggesting a strong relationship between VEGF-A, RA, and OA, particularly with respect to inflammation and joint damage.

### **3.1.1 Alternative splicing and inflammation in arthritis.**

Alternative splicing of fibronectin was first recognised to contribute to RA in 1996 (Hino, Maeda et al. 1996), when different fibronectin variants were reported to promote adherence and migration of synoviocytes (Hino, Maeda et al. 1996) and to be correlated with joint destruction (Shiozawa, Hino et al. 2001). Expression of specific variants of CD44 in synoviocytes, which is involved in cell-cell and cell matrix interactions, is higher in RA than OA synovium (Grisar, Munk et al. 2012), and these synoviocytes are invasive, but those from normal joints are not (Wibulswas, Croft et al. 2002).

Most of the studies to date either use or detect VEGF-A<sub>165a</sub> or panVEGF-A rather than multiple splice variants, unsurprising for the older literature as VEGF-A<sub>xxx</sub>b was only identified in 2002 (Harris, Craze et al. 2012, Kim, Lee et al. 2016). While there has been very little investigation of VEGF-A splice variant expression in arthritis to date, the alternatively spliced VEGF-A<sub>121</sub> and

VEGF-A<sub>165</sub> variants are expressed in RA synovium, as is VEGFR1 (Pufe, Petersen et al. 2001), whereas VEGF-A<sub>121</sub> and VEGF-A<sub>189</sub> are found in osteoarthritic cartilage (Pufe, Petersen et al. 2001). The splice variants within the VEGF-A<sub>xxx</sub>a/b families can be differentiated by RT-PCR, but the different families (VEGF-A<sub>xxx</sub>a/b) can only be identified with careful experimental design (Bates, Mavrou et al. 2013). Until recently there were no commercially available isoform-specific antibodies, all available VEGF-A antibodies were directed at the N terminus of the protein and therefore identified all splice variants, as they share a common N terminus. There is now a commercially available VEGF-A<sub>xxx</sub>b antibody (R&D) but no VEGF-A<sub>xxx</sub>a-specific antibody. None of the previous literature, therefore, has enabled any understanding of the changes in the expression of the different VEGF-A families and the relationship between inflammation and the control of splicing between the families.

In most normal tissues, VEGF-A<sub>xxx</sub>b is expressed at higher levels than VEGF-A<sub>xxx</sub>a (Harper and Bates 2008). An increased level of total VEGF-A in the inflammatory angiogenic conditions of RA/OA could result from an overall increase in expression of both families, and a greater increase in one family in comparison to the other, for example with the VEGF-A<sub>xxx</sub>a isoforms being expressed at a higher level than anti-angiogenic VEGF-A<sub>xxx</sub>b isoforms. The balance between the isoforms impacts the physiological events, and while it would be hypothesised that proangiogenic VEGF-A<sub>xxx</sub>a isoform expression level would be increased in inflammation, this has not yet been shown in human RA or OA.

This triggers the question about how the individual isoforms, how the splicing between the two families may be altered in inflammation in both RA and OA. It is unknown whether total VEGF-A changes with no shift in the balance of the isoform families, or if one of other splice variant family predominates under specific conditions. If splicing is shifted towards VEGF-A<sub>xxx</sub>a, then this pro-angiogenic isoform family would be increased in relation to the inflammatory profiles of either RA or OA while VEGF-A<sub>xxx</sub>b expression remains low.

While a strong relationship between VEGF-A and OA has been described, especially in HFLS or synovial fluid, there are no published data on the expression or actions of the distinct VEGF-A isoform families. Here I have investigated the relationship between synovial histological inflammation and the expression of the different VEGF-A isoform families, VEGF-A<sub>xxx</sub>a and VEGF-

A<sub>xxx</sub>b, as well as the expression and activation of the different components of the VEGF-A splicing axis.

VEGF-A<sub>xxx</sub>a could potentially be used as a predictor of inflammatory flares in arthritis, or potentially even earlier diagnosis. As serum levels in RA and OA are raised and reflect the intra-articular levels of total VEGF-A, this might enable blood screening for early disease. Such an approach could potentially pave the way for development of new drugs targeting specifically VEGF-A<sub>xxx</sub>a, reducing the potential risks involved with completely inhibiting total VEGF-A in elder populations. Alternatively, a relationship between inflammation and the splicing of the VEGF-A<sub>xxx</sub>a and VEGF-A<sub>xxx</sub>b families could lead to the control of alternative splicing as an alternative therapeutic strategy.

**Primary hypothesis:**

The activation of the SRPK1/SRSF1/VEGF-A splicing axis is greater in human OA and RA synovium with more severe inflammation.

Specific experimental hypotheses:

1. Expression of SRPK1 is increased in inflamed knee synovium from patients with RA or OA compared to controls, and expression is related to the severity of histological inflammation
2. Expression and activation of SRSF1 is increased in inflamed knee synovium from patients with RA or OA compared to controls and is related to severity of histological inflammation
3. Expression of total (pan)VEGF-A is increased during inflammation between patients with RA and OA compared to controls in knee synovial tissue and expression is positively related to the severity of histological inflammation
4. Expression of the VEGF-A<sub>xxx</sub>b isoform is significantly decreased while the VEGF-A<sub>xxx</sub>a isoform is increased in inflamed knee synovium between patients with RA and OA compared to controls as well as having a negative relation to the severity of inflammation
5. Expression of the related splicing kinase Dyrk1A is related to the severity of histological inflammation particularly in RA.

## **3.2 Materials and Methods**

### **3.2.1 Human tissue collection and preparation**

General methodology is given in chapter 2 (Methods), alongside the standardised protocol for tissue collection and sample processing. Details for histological grading are given in section 2.4.

Two distinct groups of cases were selected throughout this study. One group was used for optimisation experiments and a pilot study, whereas the second group was used for the main experiments described in this chapter.

### **3.2.2 Cases for the pilot study and the optimisation of experimental methods.**

The aim of the initial pilot study was to verify the feasibility and accuracy of our experimental methods, and to optimise methods, including data extraction and analysis methods, where necessary. Cases were selected on the required inflammation level as determined by scoring of haematoxylin and eosin-stained index slides from the repository of Arthritis Research UK Pain Centre (n=3, 3 patients with 1 sample per patient). For the pilot study and optimisation to provide the most consistent results, all cases were selected on the following criteria: a visible synovial lining and at least level 3 score of synovial inflammation. The levels of synovial inflammation were assessed using the Haywood scoring system, as explained in chapter 2 (Methods-Synovitis Histological Scoring section 2.7). As a brief reminder, this scaling system is based on a 4-grade scale; grade 0 = normal healthy synovium, with synovial lining <4 cells thick, grade 1 = mild inflammation with synovial lining 4-5 cells thick, grade 2 = moderate inflammation with a thick synovial lining of 6/7 cells, and finally grade 3 = severe inflammation with a synovial lining of more than 7 cells thick.

### **3.2.3 Cases for the investigation of the VEGF-A splicing axis in synovial inflammation**

Age and sex -matched cases were selected from the University of Nottingham biorepository. The tissue was supplied as fixed blocks ready for cutting. Sectioning was performed either by Dimitrios Amanitis or Seyed Sehatari; post-mortem samples of knee synovium (n=15) from

people with no recorded history of arthritis or knee pain obtained at autopsy, with no significant evidence of arthritis on inspection of articular surfaces or synovial microscopy in the 12 months prior to death, alongside arthroplasty-derived synovium samples from people with OA (n=36) and RA (n=14) comprised the two other groups.

The samples were selected based on qualitative inspection of the index slides from the repository of the pain centre, only if they showcased sufficient quantity and appropriate morphology of synovial lining. Specifically, post-mortem cases were selected only if the synovial inflammation evident in the index samples was of grade 1 or less based on the Haywood scaling system (Haywood, McWilliams et al. 2003).

Synovitis is identified histologically by markers such as thickening of the synovial lining in addition to inflammatory cell infiltration and increased cellularity. Krenn et al (Krenn, Morawietz et al. 2002, Krenn, Morawietz et al. 2006) developed a histopathological score examining three specific criteria; hyperplasia, cellularity and inflammatory infiltration are graded on a scale 0-3, with 0 being absent of feature and 3 severe features. The total synovitis score is being determined by the summation of each feature, with 0-1 score indicating no synovitis, 2-4 low synovitis and 5-9 high grade synovitis. A similar scoring system has also been developed by Haywood et al., 2003, in which the synovitis grades have been comprised in 3-point score system, encompassing the degree of synovial lining hyperplasia, cellularity and inflammatory infiltrate within each grade boundary. Score of 0 would indicate no synovitis; score of 1 mild synovitis; 2 moderate synovitis; 3 severe synovitis. The Haywood system offers a more concise method for synovitis scoring without losing any valuable information.

Selected RA cases were identified from consecutive RA synovial donations from joints removed for arthroplasty (total knee replacement, TKR). These cases have a variable degree of associated synovitis but tend to have higher synovitis scores than the OA cases, and in most cases of arthroplasty in RA, also have indications of secondary OA. OA cases were selected to include a range of different synovitis scores as a representative sample of the varied inflammation seen in OA for patients that have undergone TKR.

The same cases were used throughout the study for expression of all studied proteins. Information on each case included in the study was also obtained, and included at least sex, age,

diagnosis, race/ethnicity, age at TKR, whether the person reported pain at TKR, time since diagnosis, medications at the time of TKR, and any other clinical signs or symptoms.

Given that the index sample that was initially identified could have a different morphology compared to the final sample used in the study, as the sections used were from a deeper layer of the tissue, specific exclusion criteria were set for the post-mortem cases since they were the controls of this study. In the cases where a post-mortem sample was noted to have synovial inflammation of a grade 2 or 3 during the post-hoc analysis of the results, then the individual sample was excluded from the study, since the premise of these experiments was to compare arthritic samples to controls with no signs or symptoms of arthritis/inflammation.

### **3.2.4 Immunohistochemistry - optimisation and analysis**

General methodology on the HRP-ABC and ALP-ABC indirect immunohistochemical methods is described in chapter 2. The HRP-ABC method was chosen as the primary approach due to providing highly consistent results throughout the experiments

Indirect IHC was preferred to visualise VEGF-A (isoforms and panVEGF-A), SRSF1, SRPK1, and DYRK1a immunoreactivity. Wax embedded sections were pre-processed as described in Section 2.3 Tissue collection and processing. Tissue was dewaxed in xylene for 10 minutes, and rehydrated using descending concentrations of ethanol (100%, 90% and 70%) for 5 minutes respectively.

#### **Heat-induced antigen retrieval (HIER).**

Temperature grading and duration of treatments play a major role in the success of the epitope unmasking. The efficacy of the protocol relies heavily on the heating and the cooling of the samples following the HIER treatment. Most methods employ temperatures near 100°C, theoretically the optimal temperature to unmask the antigen epitopes. The consensus from literature suggests that with higher temperature and longer incubation times, the better the efficacy for HIER. However, there is an equilibrium to be reached after which no significant benefit can be achieved.

With this in mind a variety of temperatures and durations were investigated to identify the optimal conditions. Initially I investigated temperatures as high as 105 °C and as low as 50 °C, with incubation times varying from 5 minutes to 1 hour. The best and most reproduceable results were achieved at 65 °C with an incubation period at 20 minutes, after which the samples were cooled under running tap water for 10 minutes. This protocol provided good results regarding unmasking the epitopes as well as maintaining the integrity of the samples.

Finally, the chemical composition of the buffers plays a major role in HIER. Two distinct buffers exist that have both been used with success in the past. Citrate buffer (sodium citrate–citric acid) at pH 6.0 has been a staple when dealing with antigen retrieval. The low pH helps with maintaining the quality of the tissue during the experiment; however, it is not as potent in unmasking the epitopes as its higher pH counterparts. Tris-EDTA pH 9, a more basic buffer solution provides excellent antigen recovery, but as a downside, samples show enhanced tissue damage. Moreover, some type of detergent is usually added to the buffer as a step to improve performance and perforate cells. I investigated how both buffers work in different conditions. Tris-EDTA pH 9 seemed to have higher efficacy for our samples and antibodies, especially when paired with a lower temperature during the HIER protocol.

### **Blocking of non-specific antibody binding**

Moving forward the focus shifted towards optimising the blocking solutions as well as the concentration of the antibodies used. Based on previous publication, a number of different blocking solutions were trialled alongside different time windows. The buffer solution was based on the Bovine albumin serum, diluted in Phosphate buffer saline (PBS). Different concentrations of BSA were investigated ranging from 1% to 5%, alongside using different normal serums from either goat or horse (Normal horse serum or normal goat serum). I also tried blocking with different time intervals starting with 1 hour of blocking up to overnight blocking. The aim of these optimisation experiments was to identify a blocking solution that would provide the least amount of background possible in the most efficient way. Given that the work was performed on human tissue, the serums did not provide any significant changes in regard to blocking non-specific staining. The best results were identified after blocking the samples with a 5% BSA solution for 1 hour at room temperature in a humid environment. Similar to the BSA blocking, I investigated how endogenous peroxidases were affecting the non-specific background staining

in our samples. Different concentrations were tested ranging from 0.1% H<sub>2</sub>O<sub>2</sub> to 3% H<sub>2</sub>O<sub>2</sub>, for different time windows ranging from 10 minutes to 1 hour. Finally, the best results were evident when the samples were incubated with 3% H<sub>2</sub>O<sub>2</sub>, for 30 minutes.

In regard to the concentrations of antibodies a number of optimisations tries preceded the experiments. To validate optimal concentrations, parallel experiments were performed while changing single parameters. The aim of the optimising experiments was to achieve the best possible result as expressed per signal to noise ratio (a measure that compares the level of desired signal, in this case the antibody immunoreactivity, to background noise). Different final concentrations for the antibodies were tested, ranging from 0.001 mg/ml to 0.05mg/ml. To maximise the binding of primary antibodies to the antigens, the samples were left overnight in a humid environment at 4 °C.

A similar mindset was followed when investigating optimal conditions for the incubation with the secondary antibodies. The goal was to increase the signal to noise ratio, thus different dilutions were tested ranging from 0.01 mg/ml to 0.2 mg/ml alongside different incubation timings. Best results were obtained when the incubation times were 2 hours long. Final concentrations are denoted in the Methods Chapter 2.5, Table 9.

Following the incubation of the samples with both antibodies, two major steps of IHC protocols were optimised, namely the amplification step using the Avidin-biotin complex (ABC) as well as the visualisation step using either alkaline phosphatase (AP) or 3,3'-Diaminobenzidine (DAB). An ABC kit from Vector Laboratories UK was used (PK-6100), following the manufacturer's guidelines. Similarly, both the DAB and the AP kits were purchased from the same provider. In DAB staining, horseradish peroxidase can oxidise DAB, forming a brown precipitate, which can be visualised using light microscopy. The longer the DAB is allowed to precipitate the higher the signal to noise ratio would be due to exacerbation of background staining

The guidelines offered by the kits were first applied, however, after some optimisation experiments regarding time of application of the buffer solutions, I identified that shorter incubation times provided better results. I tested stopping the reaction at several different timepoints to identify the best signal to noise ratio I could achieve, with time frames ranging from 5 minutes to 30 minutes for both the ABC kit, as well as the DAB kit. Focusing on

reproducible results, I maintained the length of incubation at 5 minutes, a time frame that was long enough for the immunoreactivity to be enhanced and allow for further analysis, but not long enough to exacerbate the background staining.

Finally, when haematoxylin was applied to the samples to stain the nuclei of the cells, I identified that the strong distinct blue/purple staining was masking the immunoreactivity of the samples. I attempted diluting the haematoxylin using water in a 1:2 dilution however the results the blue distinct staining was still too prominent on the tissue. Consequently, I experimented with a rapid application of the stain, dipping the samples in haematoxylin for 5 seconds before removing them and instantly placing them in tap water, for washing the excess stain. This method provided the best results, thus I applied haematoxylin for 30 seconds on the samples, before washing them twice for 10 minutes in tap water. The finalised protocol for all the IHC experiments of this chapter can be seen in Figure 16.

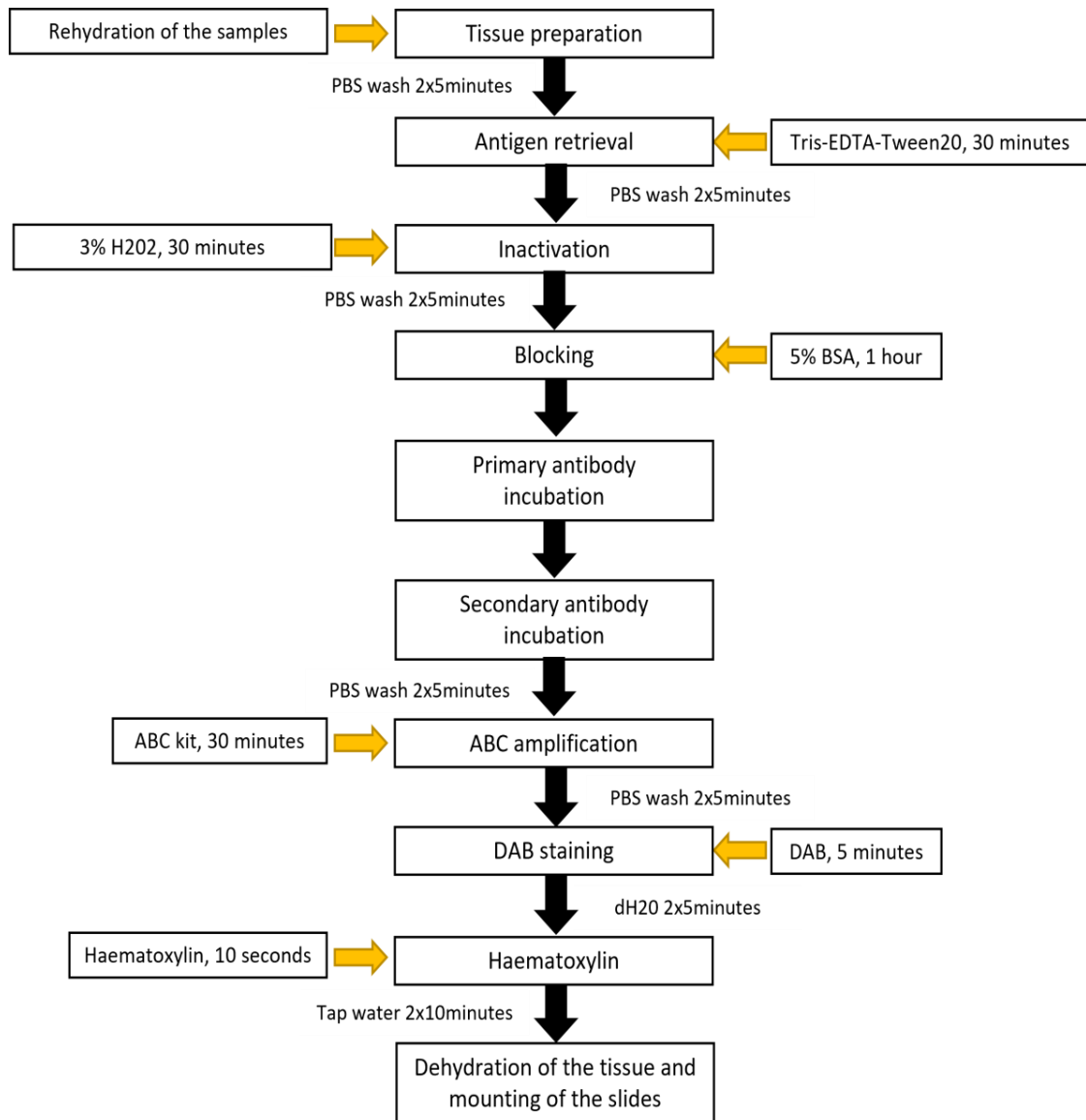


**Figure 15 Schematic representation of the general IHC protocol used throughout the experimental work in this chapter.**

### **Alkaline phosphatase-Fast Red (ALP-FR) immunohistochemistry**

ALP-ABC staining was optimised to use the Fast Red chromogen that fluoresces at 560nm, with the aim to use a double immunofluorescent technique in fixed tissue for cellular identification. Initially the same protocol as for the HRP-ABC method was used, however the signal to noise ratio was greatly increased, so further optimisation was needed. Initially I investigated altering the antigen retrieval temperature and timings. There is evidence, suggesting that higher temperatures showcase increased auto-fluorescence. I investigated how the immunoreactivity

would be enhanced if I lowered the temperature from 65 °C to 50°C. I also investigated different timings for the HIER protocol, ranging from 10 minutes to 60 minutes to accommodate for the difference in temperatures. The best results were noticed when I reduced the incubation time in the waterbath to 20 minutes instead of the previous 30 minutes, while keeping the temperature at 65°C. I also investigated different incubation times for the ABC-AP kit as well as the AP red substrate kit, ranging from 5 minutes to 30 minutes, with the signal to noise ratio being better when the incubation was 30 minutes long for the former and 5 minutes long for the latter. It is important to note that the number of washes was also increased to compensate for the increase in non-specific background staining. To that extent the final protocol of the fluorescent experiments can be seen in Figure 17.

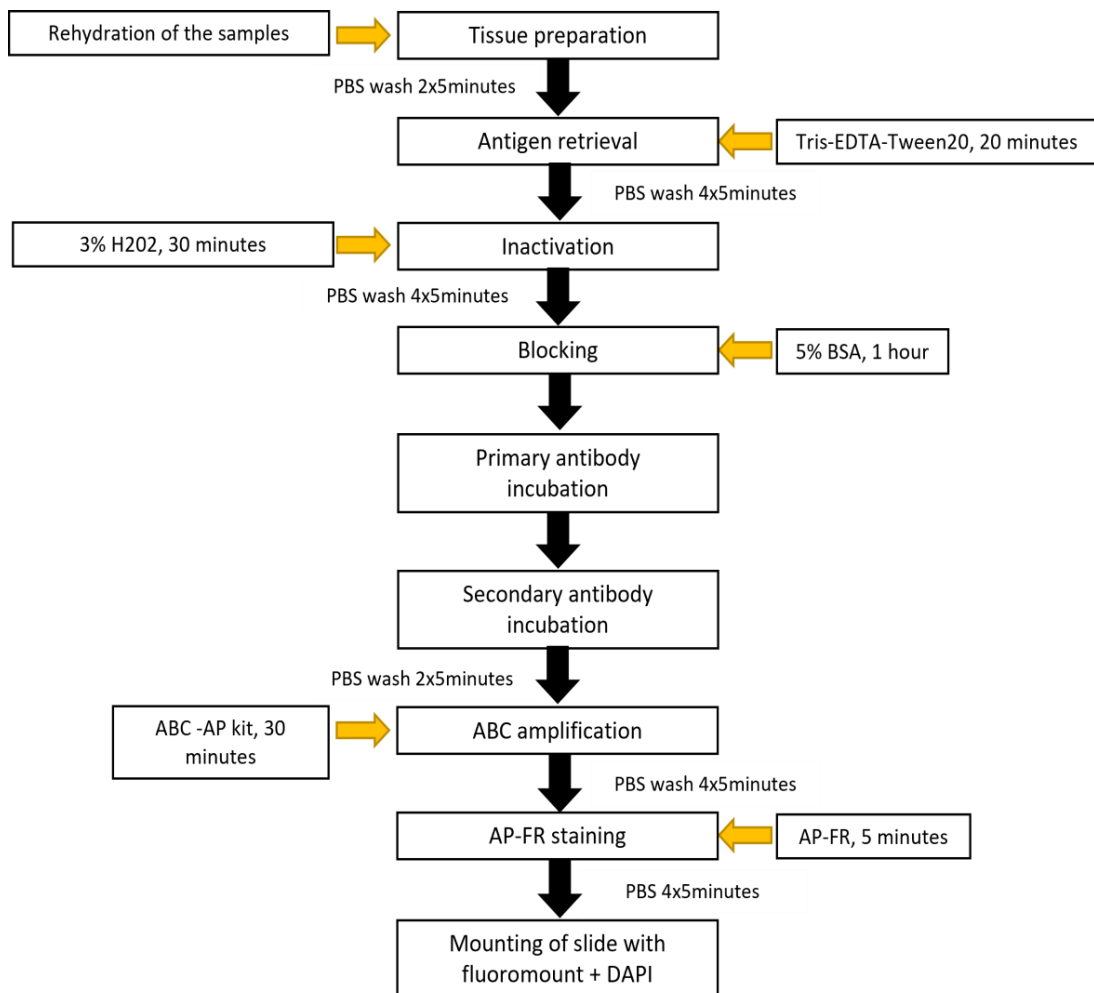


**Figure 16 Schematic representation of the IHC protocol used throughout the experimental work of the thesis using the Alkaline phosphatase – fast red substrate kit.**

### **Optimisation of HRP-DAB IHC analysis methods**

A pilot study was set up to determine the optimum method of analysis to maximise the power of the experiments while minimising the number of replicate fields analysed per section. Human synovium tissue was collected from three cases, ten slides from each case, stained for SRSF1 and the fractional area of the ten fields was measured (see *Image capture, data extraction and analysis* below).

A macro (developed by Dr. Daniel F McWilliams, City Hospital Nottingham, Haywood et. al 2003). This macro automatically thresholds the DAB staining in an image of a stained section and provides the positive area in the field of view as well as the total area, as described in detail in the methods chapter Figure 13. The fractional area is the result of the positive area divided by the total tissue area recorded. Two different methods were used when extracting data.

First, a sequential collection of fields of views were performed along the synovial lining, (analysed in Figure 2), and second, the fields of views concentrated on stained ‘hotspots’ along the synovial lining. The aim of the hotspot approach was to record those areas with the highest expression of SRSF1. Both methods were assessed to determine the optimal approach to be used in future. The “hotspots” were qualitative assessed by the observer who was blinded to the clinical details of the samples to avoid any potential bias.

The lining was chosen as the focus of our observations due to the role it plays in managing cellular and molecular translocation within the joint, alongside maintaining the health of the joint by regulating the synovial fluid.

The coefficient of variation (CV) of the fractional area was calculated as the standard deviation divided by the mean of fractional area multiplied by 100 to get the percentage of the variability between different fields. Mean values, standard deviation and CV were calculated for each of the fields identified for analysis, as described above, providing the variability per number of fields per subject (Figures 2 and 3). The CV’s per field per subject were used to calculate and plot the individual and mean CV of the 3 subjects per field

### **3.2.5 Image capture, data extraction and analysis**

All images and analysis were performed while blinded to the groups/samples to avoid any potential experimental bias. Histologic scoring and staining quantification were performed using a Zeiss Axioskop 50 microscope, by a single observer who was blinded regarding the details of the diagnostic group.

The expression of all the antigens was quantified as per fractional area as described above and in Chapter 2. For the SRSF1 localisation quantification manual cell counting was performed, using Fiji ImageJ as described in Chapter 2 (section Image analysis and quantification) at 40x magnification images. For both VEGFA and VEGFA<sub>165b</sub> expression the integrated density of the stain was also quantified using a custom-made macro made by (Dimitrios Amanitis see Appendix 1) as described in Chapter 2 (section 2.8).

I captured 3 fields per sample following the hot-spot technique, focussing on areas of the tissue that visually had more staining (Haywood et al 2003). Only areas within 100um deep of the synovial lining were captured and analysed. A custom-made macro allowed quantification of the DAB staining expressed as fractional area (area of positive stain/total area) per case quantified by computer assisted image analysis by thresholding the output of the stain against the haematoxylin staining (Haywood et al 2003).

Light microscope images were captured using a 3-CCD camera mounted on a Zeiss Axioscop-50 microscope (Carl Zeiss, Welwyn Garden City, UK) and analysed using a KS300 image analysis system (Imaging Associates Ltd., UK). Numerical data were exported and recorded and analysed using Excel and GraphPad Prism (v8.4.2 for Windows GraphPad Software, San Diego, California USA, [www.graphpad.com](http://www.graphpad.com)) (Figure 1). More detailed methods on the analysis procedures are in Chapter 2.4.5.

### **Data extraction and statistical analysis**

All statistical analyses were performed using GraphPad Prism software (v8.4.2 for Windows GraphPad Software, San Diego, California USA, [www.graphpad.com](http://www.graphpad.com)). Differences in fractional area of SRPK1 and SRSF1 expression were determined using either Kruskal Wallis one way-ANOVA followed by Dunn's multiple comparisons or by Mann-Whitney or Wilcoxon's tests depending on the numbers of groups and whether cases were paired. Specific statistical analyses are given in figure legends. For panVEGF-A and VEGF-A<sub>xxx</sub>b/a integrated density measurements were also performed after qualitative assessing the images to identify differences in staining intensity between groups. Correlations between inflammation scores and SRPK1, SRSF1 and VEGF expression, and SRSF1 activation were determined using two-tailed Spearman's rank correlation. Principal Component Regression (PCR) analysis was performed as explained in Methods chapter 2.14. VEGF-A<sub>xxx</sub>b expression (fractional area) was the dependent variable. For inclusion of clinical signs ARA criteria, effusion, synovial thickening, Heberden's nodes,

osteophytes, chondrocalcinosis and morning stiffness, these were transformed into binary values, where 0 is absence, and 1 is presence of effusion for example. Clinical details were collected characterised by clinical technician Roger Hill as described in previous publications (A, R et al. 2008), (Stoppiello, Mapp et al. 2014). Principal components were selected based on the two highest eigenvalues. Significance was denoted as  $p$  values of less than 0.05 as per convention.

### 3.3 Results

#### 3.3.1 Pilot study: determination of sampling frequency for minimal staining, through coefficient of variation analysis

For sequential field sampling, the lower the number of fields sampled, the higher the variability of the results, and as the number of analysed fields increased the variability reduced, reaching a plateau at ~20% variability when 4 fields were sampled (Figure 18A & B) (n=3; 3 patients one sample per patient).

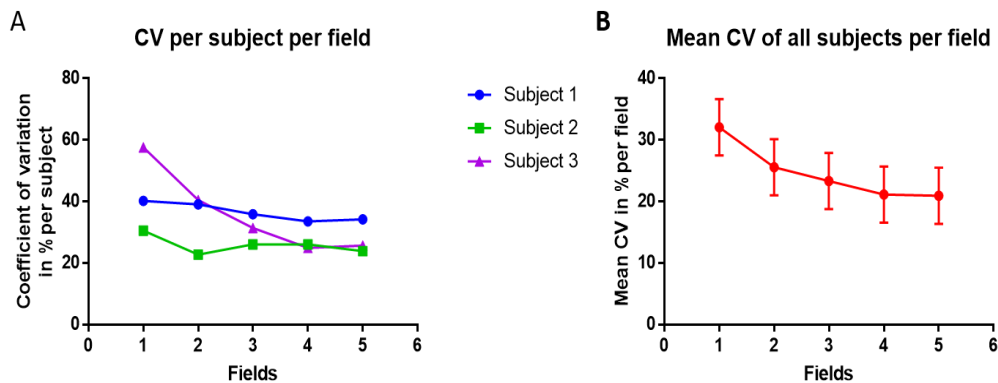


**Figure 17** Determination of the required number of fields to minimise the variance of data collected using sequential sampling of the synovial lining. Analysis of the first set of data from the collection of the sequential fields in the synovial lining. In figure 2A the individual Coefficient of variation (CV) values per subject per field can be seen, where all of them reached a plateau at around 4 fields of view. In B, the mean of the different CVs was calculated alongside the standard deviation. The Interquartile range (IQR) was calculated which was IQR=4.42 (Coefficient of variation analysis based on mean values and standard deviation, n=3)

For hotspot sampling, again, the lower the number of fields sampled, the higher the variability of the results, and as the number of analysed fields increased the variability reduced. This again reached a plateau at ~20% variability when 3-4 fields were sampled (Figure 19A & B).

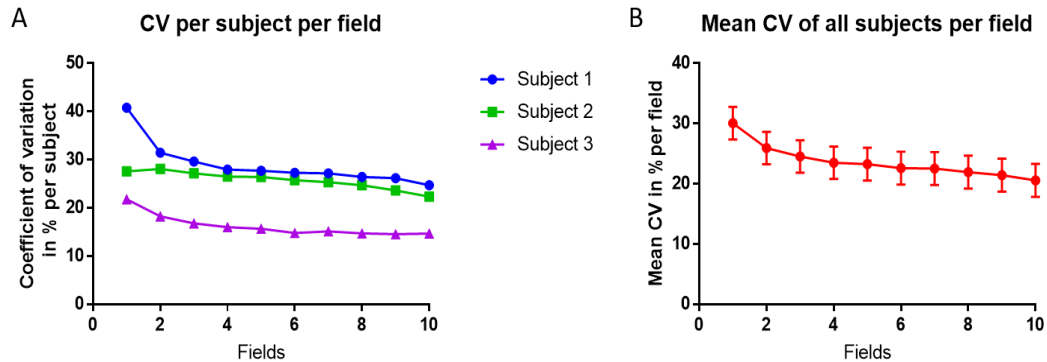


**Figure 18 Determination of the required number of fields to minimise the variance of data collected using hotspot sampling of the synovial lining. A) Individual CV values for each subject per field against the number of fields sampled. B) mean CV  $\pm$  SD (n=3) for the number of fields sampled. (Coefficient of variation analysis based on mean values and standard deviation, n=3)**

Based on these analyses, it was decided that further studies should include a single slide from each case with a minimum sampling of three fields per case recorded. Sequential and hotspot sampling did not show any major differences in the number of fields recorded before the coefficient of variation reached a plateau. I decided to move forward using the “hotspot” technique to eliminate the variation when selecting fields of view by always imaging the fields with the highest expression of SRSF1 after visual qualitative inspection of the tissue.

### 3.3.2 Optimisation of immunofluorescence in human knee synovium

The first successful attempt showed successful labelling of synovial fibroblasts for SRSF1 with the nuclear stain DAPI (Figure 20). Fig 6(A, B, C) shows the negative controls for the antibody used, showing minimum to no autofluorescence or non-specific binding. In Fig 6(I), the merged image of SRSF1 expression (in green) and DAPI (in purple) can be seen, with clear evidence of clean staining. There are also evident cells where SRSF1 and DAPI seem to be co-localised in the nucleus.

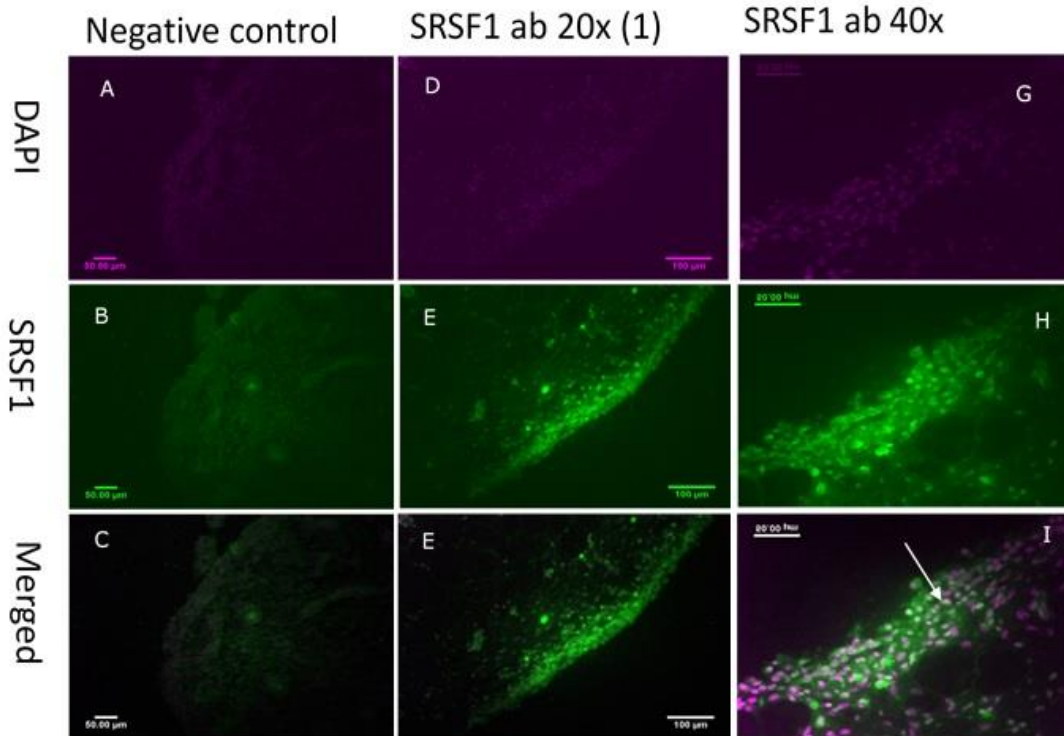


**Figure 19 A-C negative control showing no background staining or non-specific binding of our antibody on the tissue. D-E 20x magnification the expression of SRSF1 in the human synovia lining. G-I 40x magnification where evident localisation can be seen (arrows A clean negative control and clear signal from the SRSF1 staining can be seen in images B and E. The SRSF1 has been stained using the alkaline-phosphatase kit, while Dapi was used for identifying the nuclei of the cells. Dapi has been digitally changed to purple and SRSF1 to green so a better contrast would be provided to make localisation easier to notice. In image I the double staining can be seen (white arrow) in synovial fibroblasts. The colours in the images have been artificially added to enable better qualitative analysis**

Subsequent experiments, however, did not provide consistent staining across larger numbers of sections (Figure 21). Although negative controls had little autofluorescence or non-specific binding (Figure 20A-C), the positive staining did not show consistent immunofluorescence signal. Also, as it can be seen in Non-specific binding was also relatively high in the samples (Fig 21E & H). As decalcified paraffin embedded tissues present difficulties with IF (REF) and I could not achieve consistent results despite several attempts, the decision was made to continue with standard immunohistochemical techniques for further investigations.

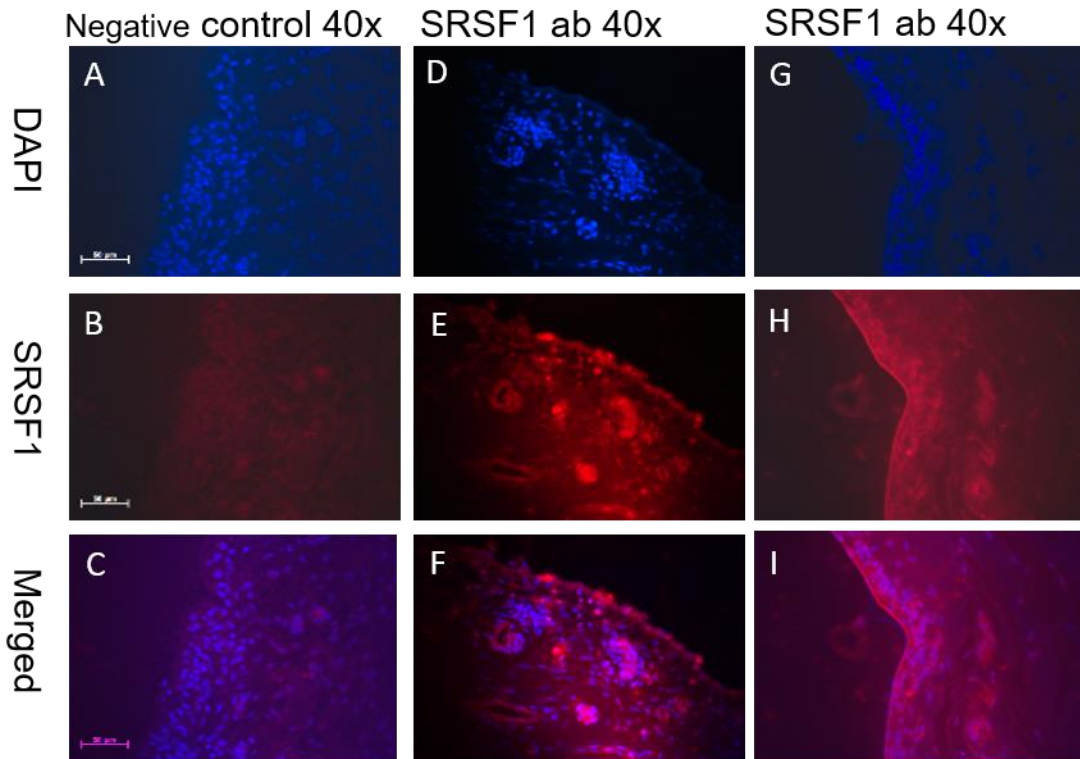


**Figure 20** Human synovial tissue under fluorescent light with SRSF1 being in red and Dapi in blue. A-C) The negative controls are clean showcasing no immunoreactivity of SRSF1. D-I) Representative images of the SRSF1 immunoreactivity with non- specific and high background staining. When compared to the previous images the staining pattern is different in as can be seen in image E. In image H the specific staining cannot be observed due to high background noise even after thresholding based on the negative controls. The result of the immunoreactivity is inconsistent among the samples, rendering analysis improbable compared to the clean signal to noise ration that was observed in previous experiments

### 3.3.3 Case information – summary table and illustrations of the histology

Patient demographics for this chapter’s samples are reported in table 11 and histopathological features based on which I scored the samples for synovitis are discussed in Methods chapter 2.9. All the tissues derived from white donors. The synovitis scores in the OA and RA groups were statistically different from the post-mortem control group. There were no other statistically significant differences between the three groups other than the incidence of morning stiffness > 2 hours, which affected a slightly higher proportion of the RA group. Also, below a table of the

cases used throughout this study can be found (table 11), and their specific N numbers per group per disease, per treatment.

**Table 11 Table of N numbers used throughout the study.**

Treatment		OA group	RA group	PM group
SRPK1		35	14	11
SRSF1		35	14	12
SRSF1 localisation		35	14	9
VEGF-A fractional area/int density		33	13	11
VEGF-A <sub>xxx</sub> a	Fractional area/int density	31	13	9
VEGF-A <sub>xxx</sub> b	fractional area/int density	34	13	11
DYRK1a		34	13	13

**Table 10 Clinical details and pathological characteristics of study groups <sup>1</sup>.**

Clinical or pathological characteristics	Osteoarthritis (n=36)	Rheumatoid arthritis (n=14)	Post-mortem (n=15)
Race / ethnicity (n)	White (34)	White (14)	White (15)
<sup>†</sup> Synovitis score (mean, SD)	2.4±0.8	2.6±0.7	0.5±0.5**
Age in years, mean (SD)	66±6.5	66.6±7.5	67±5.7
median (range, n)	64±25	66±24 (11/14)	66±15 (9/15)
Male: female	11:24	3:8	3:6
ARA criteria	Yes (35/36)	Yes (13/14)	No (8/15)
Arthritis Onset	>5years	>5 years (11/14)	N/A
Morning stiffness <30mins	Yes (26/35)	Yes (5/11)	N/A
Morning stiffness > 2 hrs	Yes (0/35)	Yes (3/11) **	N/A
<sup>††</sup> Mean (SD) time estimated morning stiffness (min)	37 ±13	72±48	
Effusion (n)	29/35	10/13	N/A
Synovial Thickening (n)	27/35	10/13	0/9
Heberden's nodes >2	7/33	1/11	1/9
Osteophytes	29/35	9/11	0/9
Chondrocalcinosis	4/35	0/13	N/A

1. Tissues were obtained at the time of total knee replacement for OA and RA or were obtained PM from cadaver donors. Some details were unavailable for some donors and so were not included in the values given above. The numbers on which data are based/calculated are shown in brackets where these are different from the overall group total shown in row 1. <sup>†</sup>Synovitis score using Haywood's (REF) 4-grade scale; grade 0 = normal healthy synovium, synovial lining <4 cells thick; grade 1 = mild inflammation with synovial lining 4-5cells thick; grade 2 = moderate inflammation with a thick synovial lining of 6/7 cells, and grade 3 = severe inflammation with a synovial lining > 7 cells thick. <sup>††</sup> <30 min estimated as 29min, <1 hour as 59min, 1-2hours as 119 min and >2 hours as 130 min. \*\*p<0.01 cf. other groups one way ANOVA & Tukey's test (synovitis): Chi squared test (morning stiffness >2 hours). N/A not applicable.

### 3.3.4 Splicing axis changes in inflamed synovium

To determine changes in splicing kinases and the VEGF-A splicing axis with synovial inflammation, knee synovium samples from 1. post-mortem knee synovium (n=15) from people with no history of arthritis or knee pain obtained at autopsy; 2. arthroplasty-derived synovium samples from people with OA (n=36) exhibiting a range of degrees of synovial inflammation; 3. from people with RA (n=14) were used. The same cases were used throughout the whole study for all different IHC protocols. Two control cases (PM) were subsequently removed as despite there being no reported clinical symptoms, the histological appearance of the synovitis scored 2 and 3 for these samples.

I applied principal component regression analysis to identify the principal components in the prediction of the dependent variable VEGF-A<sub>xxx</sub>b expression (fractional area).

The principal components (PC) were identified using the two highest eigenvalues, as parallel analysis (the default Graphpad Prism setting) yielded only one PC accounting for approximately 30% of the whole dataset variance. Two PCs were identified which accounted for ~40% of the total variance of the dataset.

Figure 22 shows the individual variable loadings (the correlation between the values for each column variable measured and the calculated values for the PCs) and the relationship between these and the two PCs. The key information shown in this type of plot are clusters of variables such as DYRK1a, pan-VEGF-A and pan-VEGF-A intensity and the direction of correlation between the variables and the PCs. The clustering of DYRK1a, pan-VEGF-A and pan-VEGF-A intensity indicates that these are providing similar information, and so in further studies measuring only one would probably give sufficient information. The direction of the line shows the variables that correlate with the PCs and their direction, for example age and VEGF-A<sub>xxx</sub>b intensity correlate with PC1 in the opposite direction to all the other variables as they are on different sides of x=0, but in opposite directions with PC2 as they are on different sides of y=0.

PCR with dependent value of VEGF-A<sub>xxx</sub>b

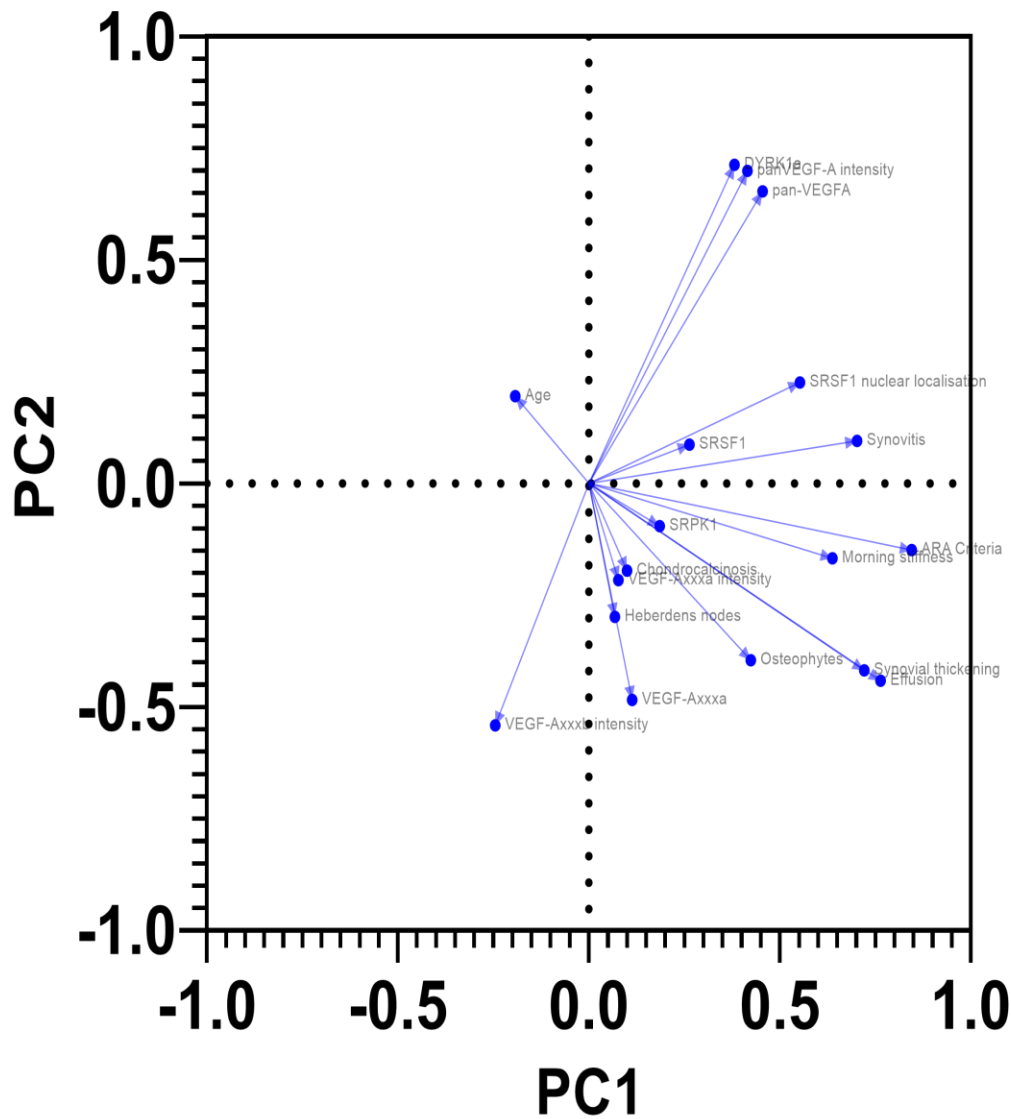


Figure 21 Loadings plot of the PCA analysis for the dataset of the VEGF-A splicing axis and indicators of OA and RA disease. The variable against which I determined dependencies was VEGF-A<sub>xxx</sub>b expression. Age, SRSF1, pan-VEGF-A, VEGF-A<sub>xxx</sub>a expression and intensity, DYRK1a expression, Heberden’s nodes, osteophytes, and chondrocalcinosis all contributed significantly to the linear regression model predicting VEGF-A<sub>xxx</sub>b expression. From the graph above I can identify the variables that have a positive relationship with both PC1 and PC2 (top right quadrant), a positive relationship with PC1 and negative relationship with PC2 (bottom right quadrant), etc. Clustering of variables such as DYRK1a expression, pan-VEGF-A expression and intensity indicates a close relationship between these variables, and possible redundancy in the model.

Principal component regression analysis was highly significant ( $F(DFn, DfD) = (2, 30) = 19.7$ ,  $p < 0.0001$ ) with the following variables contributing significantly to the regression model: age ( $p = 0.001$ ), degree of synovitis ( $p = 0.002$ ), presence of osteophytes ( $p = 0.002$ ) expression of SRSF1, activation of SRSF1 (nuclear localisation), pan-VEGF-A expression and intensity, VEGF-A<sub>xxx</sub>a expression and intensity, and DYRK1a expression, presence of Heberden's nodes and chondrocalcinosis (all  $p < 0.0001$ ).

The linear regression model generated was (only the values that showed significance are included):

$$\text{VEGF-A}_{xxx}b = 0.53 + 0.0005 * \text{Age} + 0.006 * \text{Synovitis} + 0.029 * \text{SRSF1 fraction area} + 0.0003 * \text{nuclear SRSF1} + 0.1198 * \text{pan-VEGF-A fractional area} - 0.16 * \text{VEGF-A}_{xxx}a \text{ fractional area} + 0.00002 * \text{pan-VEGF-A intensity} - 0.002 * \text{VEGF-A}_{xxx}b \text{ intensity} - 1.38 * \text{VEGF-A}_{xxx}a \text{ intensity} + 0.1439 * \text{DYRK1a fractional area} - 0.006 * \text{Heberden's nodes} - 0.016 * \text{osteophytes} - 0.016 \text{ chondrocalcinosis}.$$

The positive values in the regression equation indicate a positive relation between the variables and intercept (VEGF-A<sub>xxx</sub>b) while the negative values indicate a negative relationship. Age, synovitis, SRSF1 expression and localisation, pan-VEGF-A expression (as per fractional area or intensity) were all significantly and positively related to the VEGF-A<sub>xxx</sub>b isoform, while VEGF-A<sub>xxx</sub>a expression (as per fractional area or intensity), presence of Heberden's nodes, osteophytes and chondrocalcinosis were all significantly negatively related to the VEGF-A<sub>xxx</sub>b isoform.

To determine specific changes in splicing kinases and the VEGF-A splicing axis with synovial inflammation, knee synovium samples from 1. post-mortem knee synovium ( $n = 14$ ) from people with no history of arthritis or knee pain obtained at autopsy; 2. arthroplasty-derived synovium samples from people with OA ( $n = 35$ ) exhibiting a range of degrees of synovial inflammation; 3. from people with RA ( $n = 14$ ) were used. The same cases were used throughout the whole study for all different IHC protocols. Two control cases (PM) were subsequently removed as despite there being no reported clinical symptoms, the histological appearance of the synovitis scored 2 and 3 for these samples.

### **3.3.5 Expression of SRPK1 is increased in inflamed knee synovium from patients with RA or OA compared to controls, and expression is related to the severity of histological inflammation**

Two PM samples were lost during the experimental procedure, and two post-mortem samples had to be removed post-hoc, due to high levels of synovial inflammation, hence data derive from a final total sample size of 60; this included 11 post-mortem cases, 14 RA cases and 35 OA cases. Expression of SRPK1 was determined by fractional area of immunohistochemical staining, to determine whether there were increased numbers of cells expressing SRPK1. There were no significant differences in fractional area between the 3 groups (Figure 23A-D,  $p=0.3110$  and  $p=0.6317$  respectively). There was also no correlation between the expression measured by fractional area and the histological inflammation grade (Figure 23E,  $p=0.5374$ )

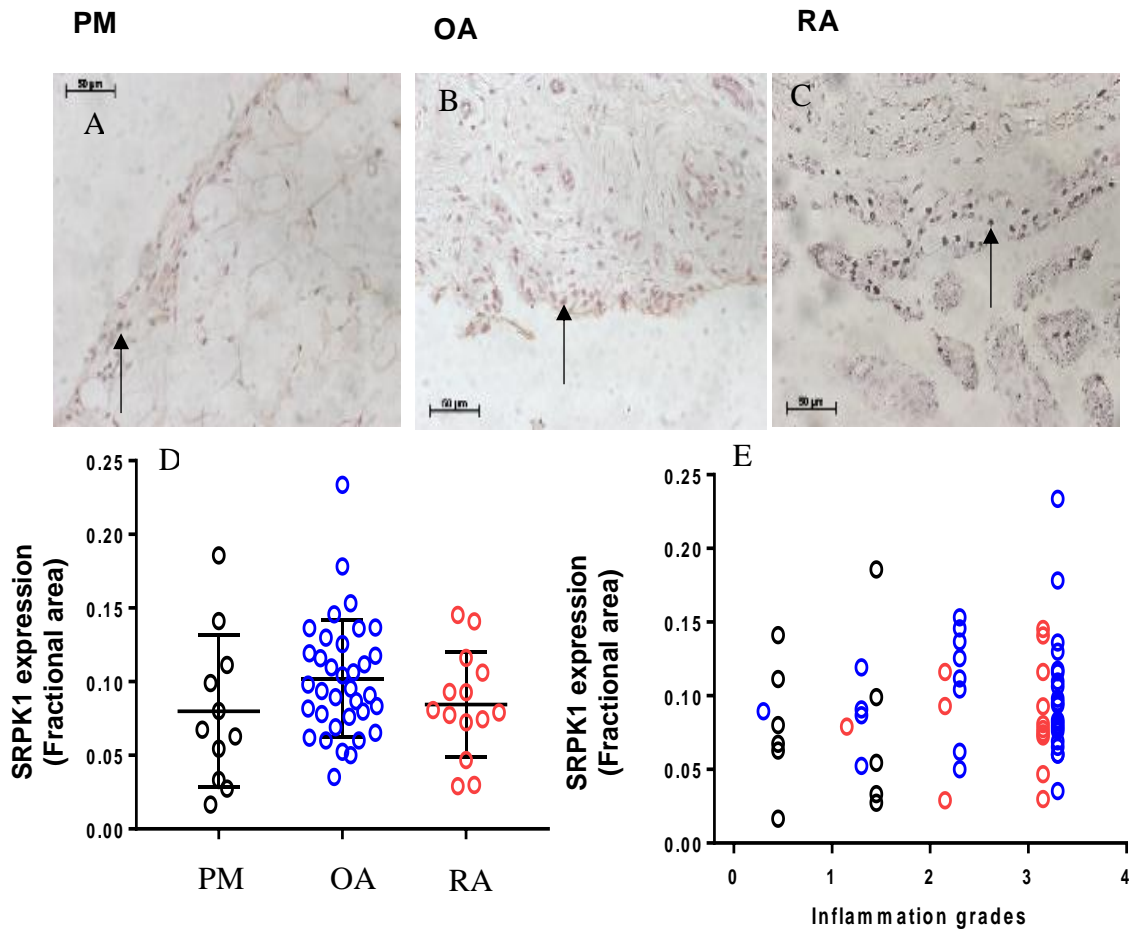
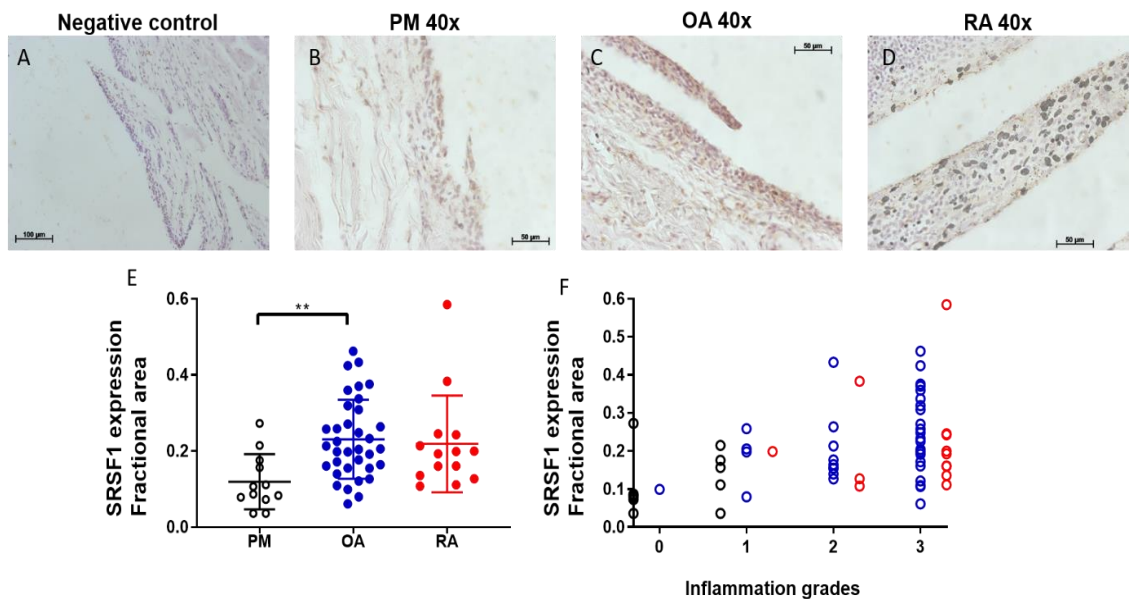


Figure 22 SRPK1 expression in synovium from human tissue. A-C typical images SRPK1 immunoreactivity. A-C Representative images of synovial lining from the 3 groups in the study. Black arrows show synovial fibroblasts with positive SRPK1 staining. A) representative image from the control/PM group with a thin synovial lining showing the low grade of inflammation (0-1) B) Average image of the tissue from the OA group showing higher cellularity compared to the PM group (inflammation grade 2-3). C) Representative image from the RA group with a distinct expression pattern shown by the black arrow D) No significance was documented in the difference between the fractional area of the in between groups comparisons ( $p > 0.3110$  and  $p > 0.6317$  respectively cf. PM). E) No significant relation between the expression of SRPK1 and the increase of inflammation grades ( $p < 0.5374$ ). Kruskal- Wallis test with Dunn's multiple comparisons test and Spearman's rank correlation

### 3.3.6 Expression of SRSF1 is increased in inflamed knee synovium from patients with RA or OA compared to controls and is related to severity of histological inflammation

Data derived from a total of 61 cases (RA=14, OA=35, PM=12) were analysed to identify the expression of SRSF1 was by fractional area of stain, to determine whether there were increased numbers of cells expressing the splicing factor. Similar to the previous studies, 2 PM samples were removed from the study since they scored highly in the inflammation scoring system (grade 2 and 3). During the experimental procedures tissue from samples was lost from the slides, leading to losing 1 PM sample. Expression of SRSF1 was significantly higher in osteoarthritic cases (Fig 24C) in comparison to the post- mortem controls (Fig 24B) controls and was positively correlated with the degree of inflammation ( $r= 0.52$   $**p<0.01$  c.f. control) (Figure 24).



**Figure 23 A-D) Representative images of the 3 groups that were used to quantify the fractional area (40x images from human synovium). SRSF1 is expressed in most cells in the human synovium E) The expression of SRSF1 as measured by fractional area. The total expression of SRSF1 is significantly higher in the osteoarthritic tissue compared to the post-mortem tissue ( $**p<0.01$  cf. control). The expression of SRSF1 is not greater when comparing the RA tissue to both the osteoarthritic and the control tissue ( $p>0.99$  cf. OA,  $p=0.057$  cf. controls, RA=14, OA=35, PM=12). F) SRSF1 expression is correlated with the inflammation scored (as calculated by the grading system set in Haywood et al., 2003). Correlation analysis showed a significant correlation between SRSF1 expression and inflammation score ( $r= 0.52$ ,  $***p= 0.0007$ ). Kruskal- Wallis test with Dunn's multiple comparisons test**

### **3.3.7 SRSF1 activation is increased in inflamed knee synovium from patients with RA or OA compared to controls and is related to severity of histological inflammation**

Visual inspection of the images showed distinct visualisation patterns of the localisation of SRSF1 in and around the cells in the synovial lining. As a splicing factor, SRSF1, can be localised either in the nucleus or the cytoplasm, denoting different functions. In figure 25, distinct nuclear staining can be observed in both the osteoarthritic and the RA samples (black arrows). After a qualitative analysis, the RA samples showcased a higher number of nuclear stained cells compared to either the osteoarthritic or the post-mortem samples. To quantify the nuclear localisation levels of SRSF1 cell counting was performed as described in Methods, using the same cases as in the previous study (ratio of nuclear stained cells to total number of positive cells. Cells were counted using a cell counter). In 3 out of the 12 PM samples cell counting was rendered impossible due to lacklustre quality of imaging when capturing using a 40x magnification lenses and with the removal of the two control cases, data derive from a total of 58 cases (RA=14, OA=35, PM=9).

A significant increase in the nuclear localisation of SRSF1 was observed in OA samples compared to PM controls (\*\* $p < 0.01$  cf. controls). Furthermore, the increase in SRSF1 nuclear localization was greater in RA samples compared to the other two groups (Figure 25). There was a significant positive correlation between the activated SRSF1 and inflammation score ( $r = 0.38$ , \*\* $p = 0.0027$ ).

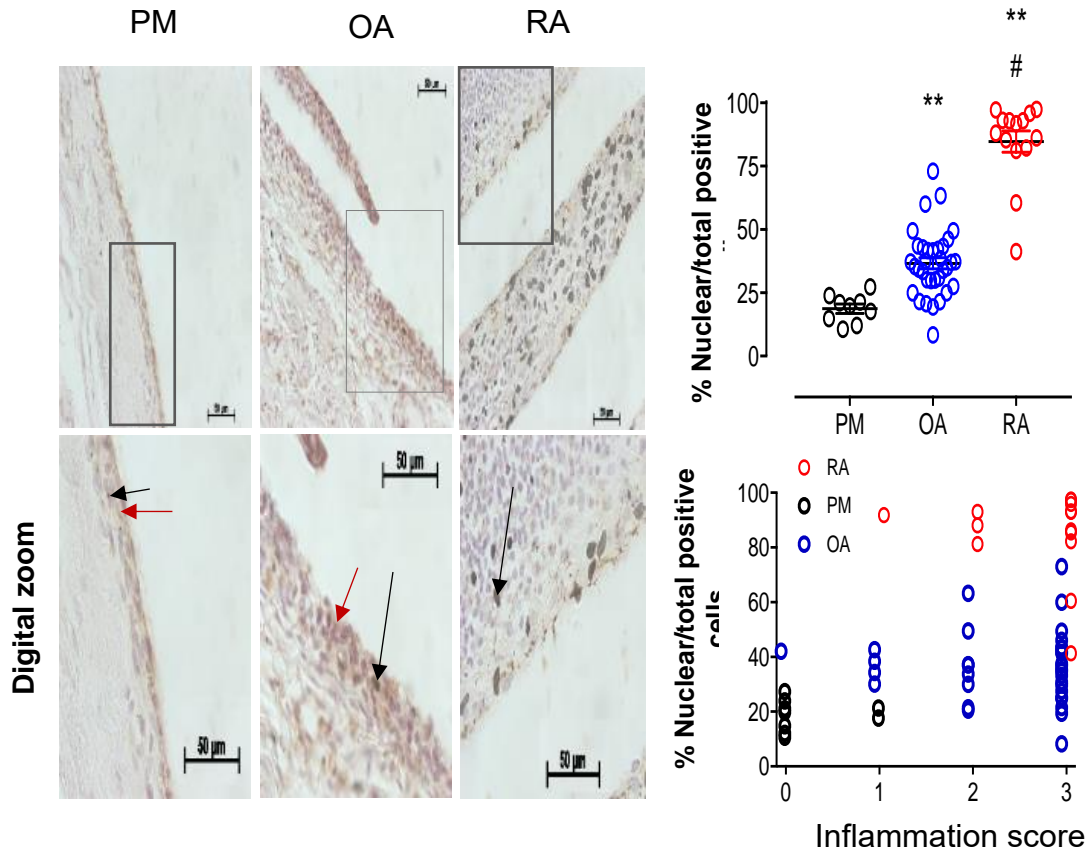


**Figure 24 SRSF1 is expressed in the cytosol in postmortem control and osteoarthritic synovium (red arrows) and in synoviocytes nuclei in both OA and RA synovium. There was a significant increase in the nuclear localisation (activation) of SRSF1 in OA samples compared to PM (\*\* $p < 0.01$  cf. controls, # cf. OA, RA=14, OA=35, PM=9). There is a significant correlation between the numbers of cells with activated SRSF1 and the inflammation scores ( $r = 0.38$ , \*\* $p = 0.0027$ ). Kruskal- Wallis test with Dunn's multiple comparisons test and Spearman's rank correlation**

### **3.3.8 Expression of total (pan)VEGF-A is increased during inflammation between patients with RA and OA compared to controls in knee synovial tissue and expression is positively related to the severity of histological inflammation**

The panVEGF-A antibody used is a mouse monoclonal IgG1 raised against the amino acids 1-140 of human VEGF and has the ability to detect all the splice variants of VEGF-A (Figure 5) from both families.

Similar to the previous studies, two PM samples were removed from the study since they scored highly in the inflammation scoring system (grade 2 and 3). During the experimental procedures tissue from samples was lost from the slides, leading to losing 2 PM samples, 1 RA sample and 1 OA samples; therefore, data presented from 57 cases. PanVEGF-A expression (fractional area) was present in PM, OA, and RA cases (Fig. 26). Expression of panVEGF-A measured by fractional area was significantly higher in samples from RA and OA cases in comparison to PM controls and was significantly higher in RA cases compared to OA ( $p=0.01$  RA cf OA,  $p<0.0001$  RA cf PM) (Fig 26E). Fractional area of panVEGF-A was positively correlated with the degree of inflammation ( $r=0.47$ ,  $p<0.001$ ) (Figure 26F).

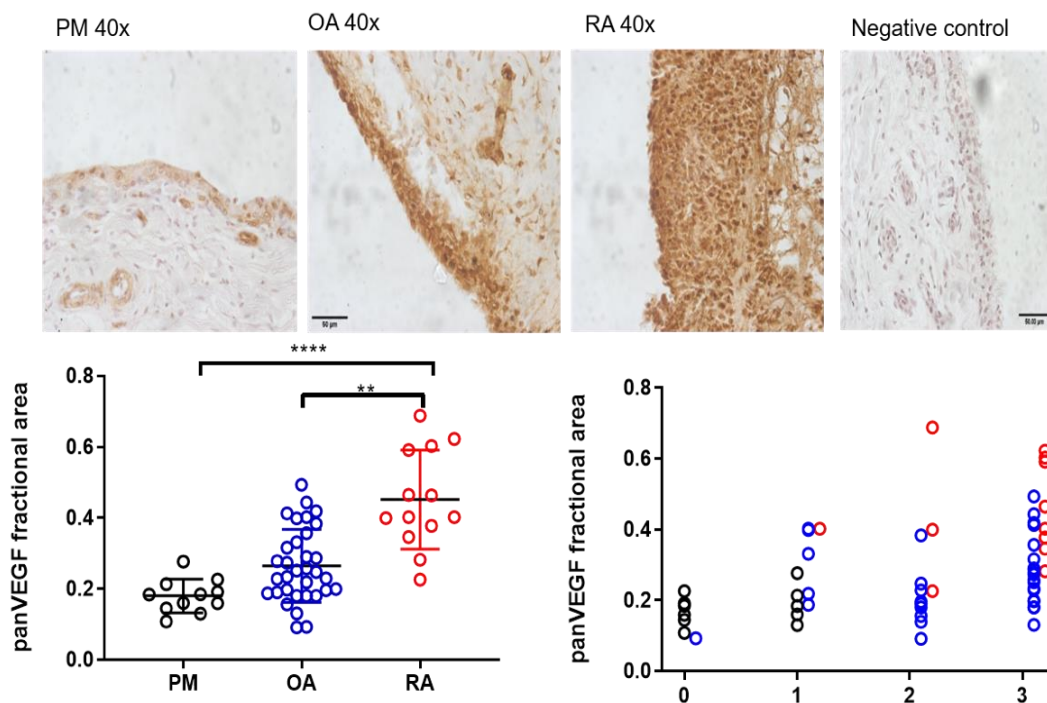


**Figure 25 Photomicrographs of representative samples of human synovium, showing the expression pattern of panVEGF-A in different groups. Fractional area of panVEGF-A immunoreactivity is significantly higher in both OA and RA groups cf. PM controls ( $p=0.01$  RA cf OA,  $p<0.0001$  RA cf. PM). Correlation showing a significant positive relationship between the expression of panVEGF-A and inflammation score ( $p<0.001$ ,  $r=0.47$ ). Kruskal- Wallis test with Dunn's multiple comparisons test and Spearman's rank correlation**

Visual inspection of the tissue showed differences in the intensity of the staining between the samples as can be seen in Figure 26, particularly between the post-mortem controls and the RA samples. RA samples show strong intensity regarding the immunoreactivity of panVEGF-A

close to the synovial lining, extending into deeper tissue, whereas both the control and the osteoarthritic samples have staining localised closer to the synovial lining, while producing moderately weaker signal. To investigate these changes the custom-made macro made by Dimitrios Amanitis (Appendix 1) in ImageJ was used, to quantify the intensity of the staining by measuring integrated density. Integrated density was measured as rho-r ( $\text{g}/\mu\text{m}^2$ ); in two - dimensions the density is calculated as mass per unit area.

Staining intensity of the growth factor was also significantly greater in RA and OA cases compared to PM cases (RA cf. PM  $p=0.006$ , OA cf. PM  $p=0.001$ ). A positive correlation between inflammation grade and panVEGF-A staining intensity was also evident ( $p=0.01$ ,  $r=0.32$ ) (Figure 27).

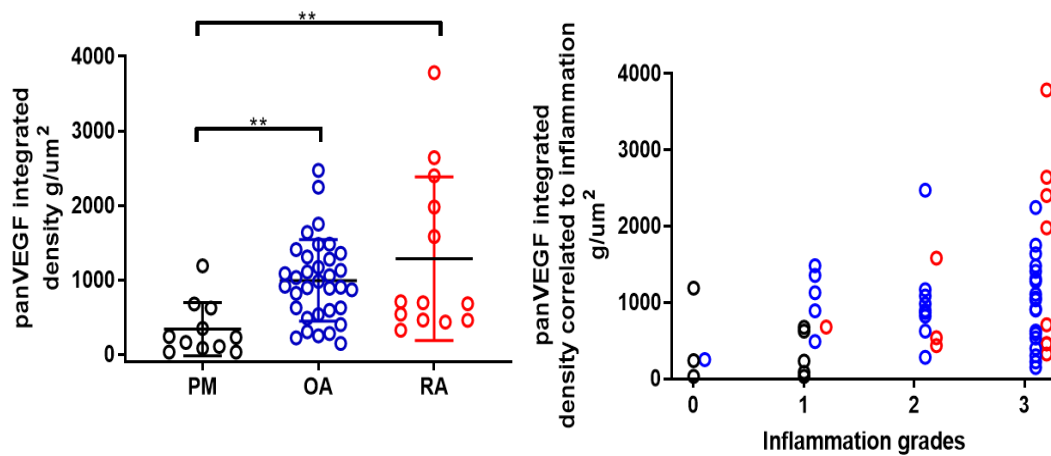


**Figure 26 panVEGF-A expression expressed as Integrated density. panVEGF-A immunoreactivity is significantly higher in both the disease groups compared to controls (RA cf. PM  $p=0.006$ , OA cf. PM  $p=0.001$ ). Correlation showcasing a significant positive relation between the intensity of panVEGF-A and inflammation grades ( $p=0.01$ ,  $r=0.32$ ). Kruskal-Wallis test with Dunn’s multiple comparisons test and Spearman’s rank correlation**

### **3.3.9 Expression of the VEGF-A<sub>xxx</sub>b isoforms is significantly decreased in inflamed knee synovium between patients with RA and OA compared to controls as well as having no relationship to the severity of inflammation**

The expression of panVEGF-A, as measured by fractional area and staining intensity was increased, but whether this is associated with an altered splice variant ratio is unknown. I therefore next investigated the expression of VEGF-A<sub>xxx</sub>a and VEGF-A<sub>xxx</sub>b isoforms with specific antibodies in the same cases, to identify whether the change in panVEGF-A expression results from changes in one or both of these isoforms. The three distinct groups with the same cases were included when monitoring the expression of the isoforms.

4 PM samples, 1 RA sample and 4 OA samples were lost during the experimental procedure lowering the total sample size to 53 cases, which however did not affect the calculated post-hoc power of the experiment.

VEGF-A<sub>xxx</sub>a expression was detected in all the groups (Figure 28 A-D). There were no significant changes in VEGF-A<sub>xxx</sub>a expression assessed by fractional area between the 3 groups (Figure 28A-D,  $p>0.05$ ). There was also no correlation between the expression measured by fractional area and the histological inflammation grade (Figure 28E,  $p>0.05$ )

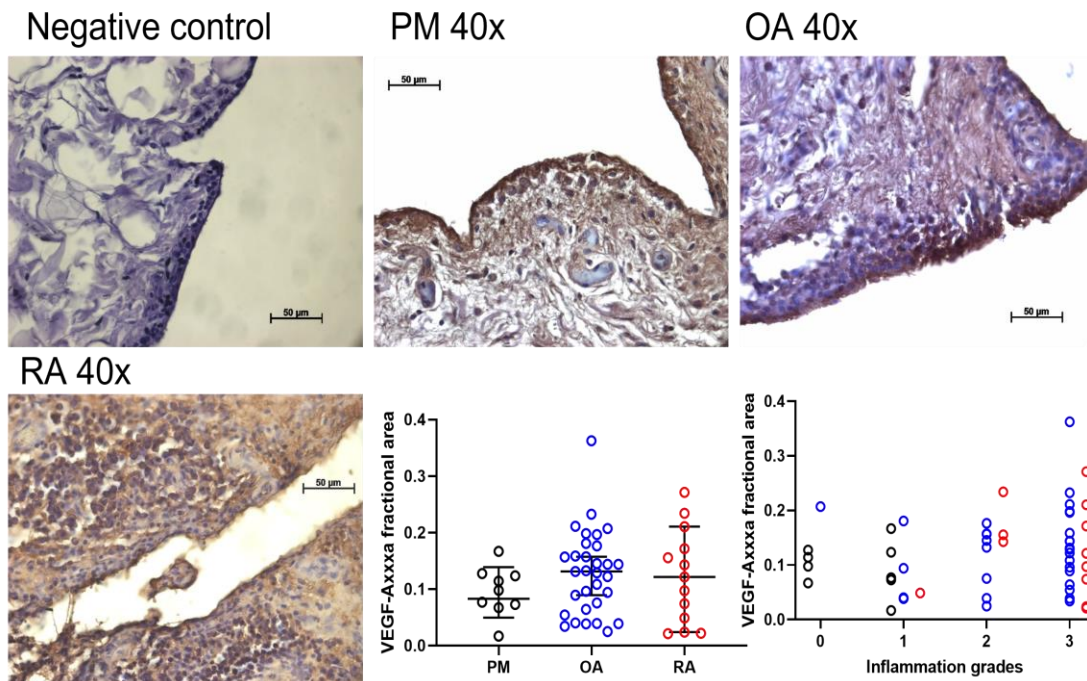


**Figure 27** Photomicrographs of representative samples from human knee synovium showing the expression pattern of VEGF-A<sub>xxx</sub> in the three different groups. Fractional area of the immunoreactivity of VEGF-A<sub>xxx</sub> with no change being recorded between the disease groups and the PM group ( $p > 0.05$ ). Correlation analysis shows no relationship between the expression of the isoform and the inflammation scores. Kruskal- Wallis test with Dunn's multiple comparisons test and Spearman's rank correlation

Similar to the panVEGF-A study, I investigated the intensity of the immunoreactivity (Fig 29), by analysing the integrated density ( $\text{g}/\mu\text{m}^2$ ) as described before. I did not identify any changes in the expression of the VEGF-A<sub>xxx</sub> isoform between groups, nor was there any correlation (either positive or negative) with the inflammation scores ( $p = 0.42$ ,  $r = 0.112$ ).

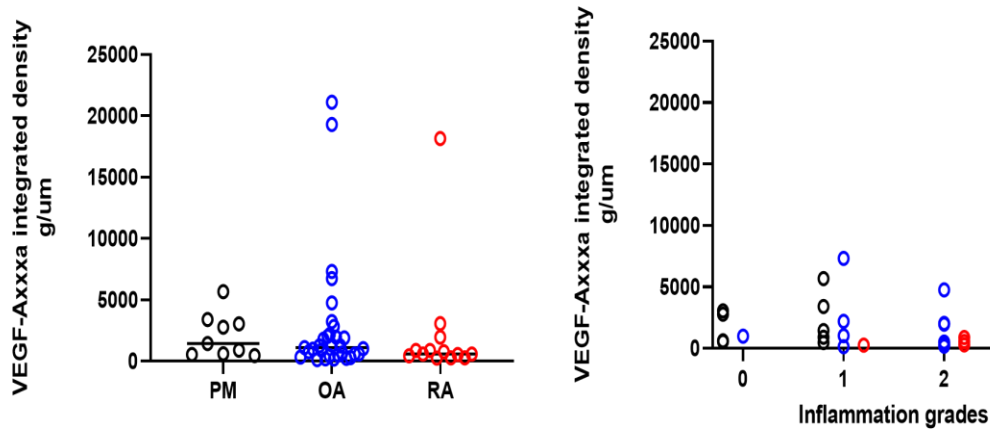


**Figure 28 VEGF-A<sub>xxx</sub>a expression as quantified by integrated density. A) The intensity of the immunoreactivity for the VEGF-A<sub>xxx</sub>a isoform was not different when assessed by the integrated density of the immunoreactivity in either of the groups. Kruskal- Wallis test with Dunn’s multiple comparisons test and Spearman’s rank correlation**

The expression of the anti-angiogenic / anti-nociceptive isoform VEGF-A<sub>xxx</sub>b was determined in the same cases. Like the previous analysis, the 3 groups RA, OA, and PMs were used with 2 PM samples being removed from the experiment due to high inflammation score as described previously and 2 more PM samples being lost during the experimental procedures resulting in a sample size of 61. VEGF-A<sub>xxx</sub>b expression was detected in cases from all groups (Figure 30A-D). There were no significant differences in VEGF-A<sub>xxx</sub>b fractional area between groups (Fig 30E), and VEGF-A<sub>xxx</sub>b expression did not correlate with inflammation score (Fig 30F).

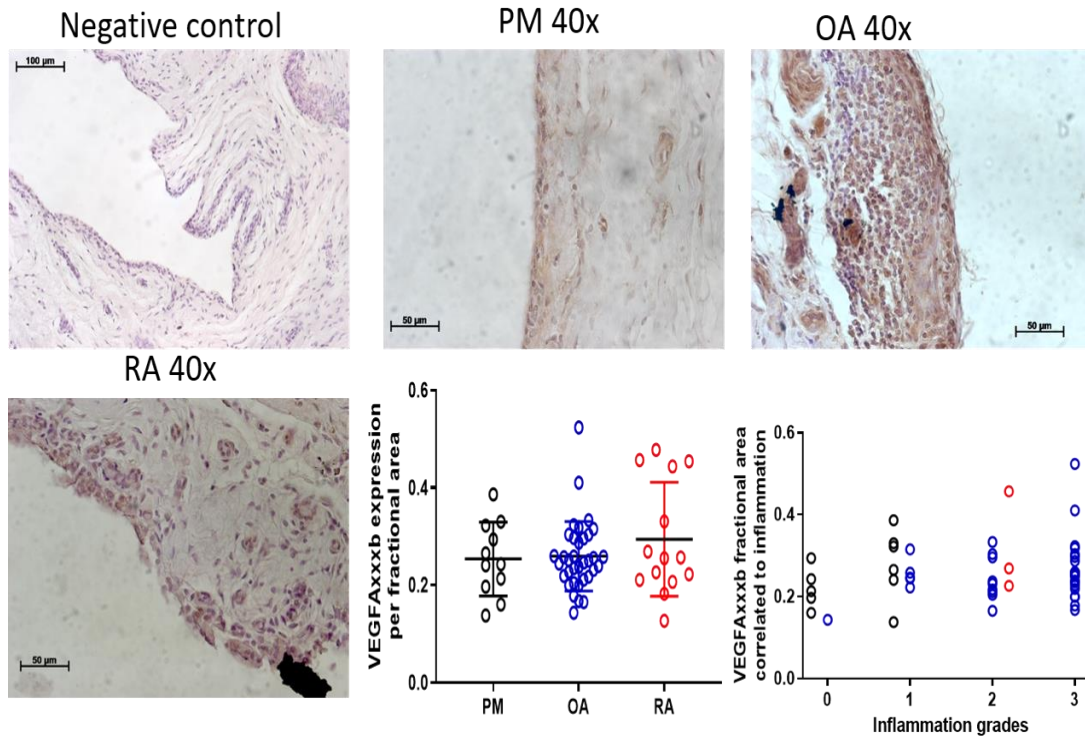


**Figure 29** Photomicrographs of representative samples from human knee synovium showing the expression pattern of VEGF-A<sub>xxx,b</sub> in the three different groups. Fractional area of the immunoreactivity of VEGF-A<sub>xxx,b</sub> with no change being recorded between the disease groups and the PM group ( $p>0.05$ ). Correlation showcasing no relationship between the expression of the isoform and the inflammation scores. Kruskal- Wallis test with Dunn's multiple comparisons test and Spearman's rank correlation

In contrast, the integrated density of VEGF-A<sub>xxx,b</sub> was significantly higher in the RA group compared to the control group (Fig 31) ( $*p=0.02$  cf. controls), and there was a significant positive correlation between integrated density of VEGF-A<sub>xxx,b</sub> and the inflammation score ( $r=0.34$ ,  $**p=0.007$ ).

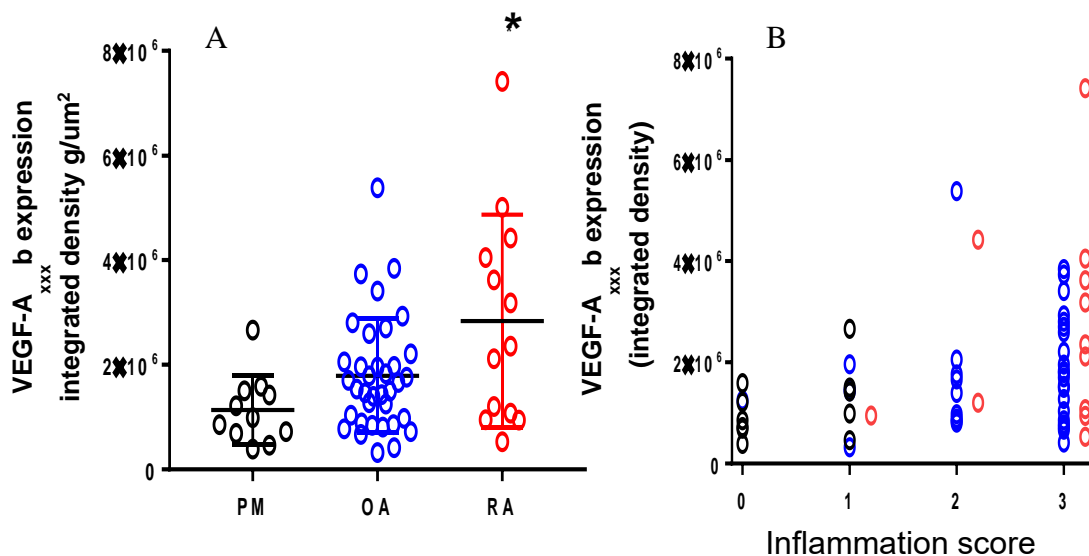


**Figure 30 VEGF-A<sub>xxx</sub>b expression (integrated density).** A) The intensity of the immunoreactivity for the b isoform was significantly increased in the RA group compared to PM (\* $p=0.02$  cf. controls, Kruskal- Wallis test with Dunn’s multiple comparisons test). B) A positive relationship between the intensity of the stain for VEGF-A<sub>xxx</sub>b and the inflammation scores was confirmed significant (Spearman’s  $r=0.34$ , \*\* $p=0.007$ ).

### 3.3.10 Ratios of VEGF-A<sub>xxx</sub>b / VEGF-A<sub>xxx</sub>a expression.

Following on the quantification of the VEGF isoform levels in the synovium tissue, I investigated whether the ratio of the two isoforms was significantly different between the disease groups and the control group (Figure 32). The ratios of the VEGF-A<sub>xxx</sub>b/VEGF-A<sub>xxx</sub>a isoform fractional area and integrated density were not significantly different between the groups (Figure 32  $p>0.05$ , one-way Anova, Kruskal-Wallis, Dunn’s multiple comparisons).

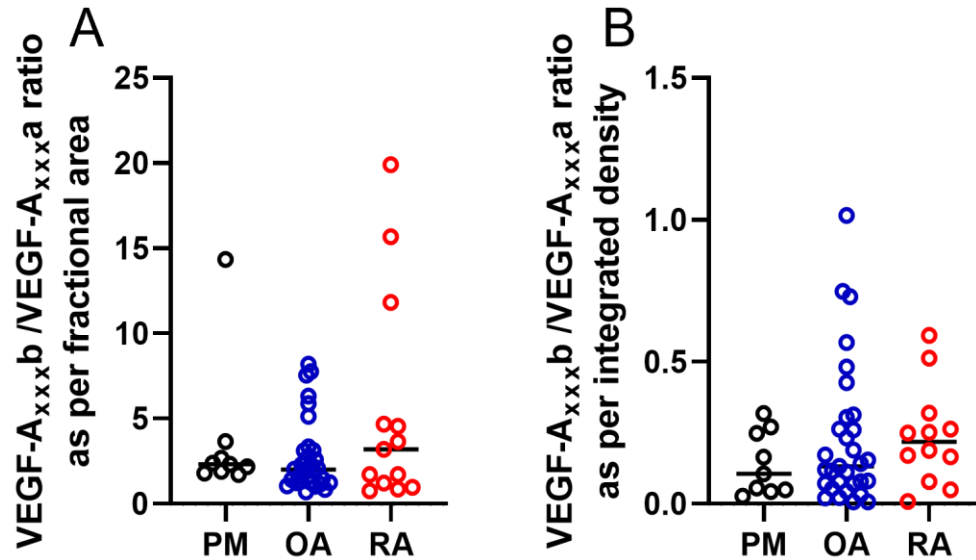
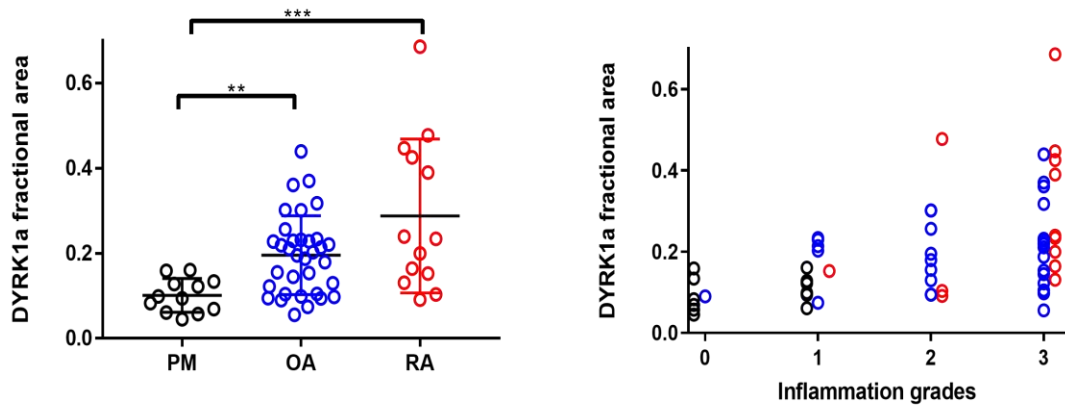
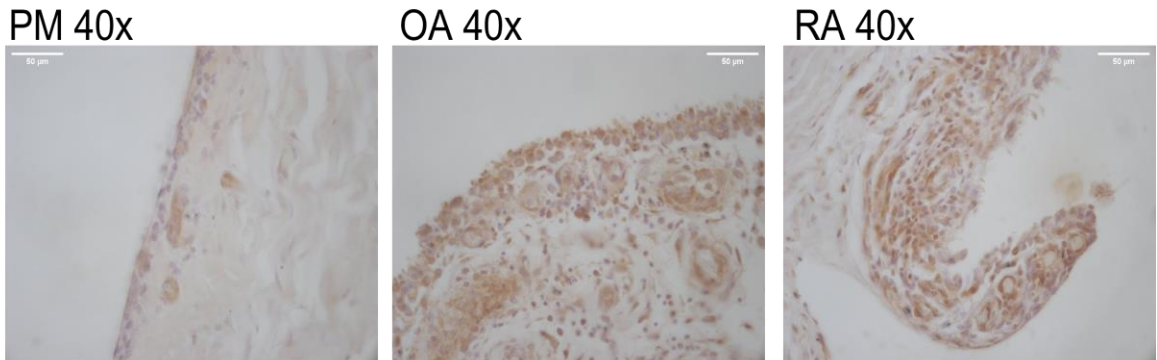


Figure 31 VEGF-A<sub>xxx</sub>b/ VEGF-A<sub>xxx</sub>a expression ratio for each individual group. The exact same matched samples were used as in the previous individual hypothesis. A) Ratio of VEGF-A<sub>xxx</sub>b/ VEGF-A<sub>xxx</sub>a as per fractional area, 9B) VEGF-A<sub>xxx</sub>b/ VEGF-A<sub>xxx</sub>a ratio as per integrated density. No significance difference is shown in between the groups, suggesting no alterations in the ratio of the two isoforms (p>0.05, One-way Anova, Kruskal-Wallis, Dunn's multiple comparisons)

### 3.3.11 Expression of the splicing kinase Dyrk1A is related to the severity of histological inflammation particularly in RA.

Data derived from a total of 60 cases (RA=13, OA=34, PM=13) were analysed to identify the expression of Dyrk1a by fractional area of stain and determine whether there were increased numbers of cells expressing the kinase. Expression of Dyrk1a was significantly higher in both OA and RA cases (Fig 33) in comparison to the post- mortem controls (Fig 33) controls and was positively correlated with the degree of inflammation (p=0.0002, r=0.46) (Figure 33)



**Figure 32** Photomicrographs of representative samples from human knee synovium showing the expression pattern of the splicing kinase DYRK1a in the three different groups. Fractional area of the immunoreactivity of DYRK1; RA cf. PM  $p=0.0006$ , OA cf. PM  $p=0.0056$ . Correlation showcasing a significant positive relation between the expression of DYRK1a and inflammation grades ( $p=0.0002$ ,  $r=0.46$ ) – Kruskal- Wallis test with Dunn’s multiple comparisons test and Spearman’s rank correlation

### 3.4 Summary of the Results

- PCA identified 2 principal components representing approximately 40% of the variability of the data. PCR analysis showed that the model all variables except for ARA criteria, effusion levels, synovial thickening, and morning stiffness significantly contributed to the linear regression model, and therefore VEGF-A<sub>xxx</sub>b expression.
- The expression of the splicing kinase SRPK1 showed no significant differences between the three groups, and was not related to the level of synovial inflammation
- SRSF1 expression and activation showed significant increase in expression in the OA group when compared to the control. Activation of SRSF1 as analysed by the degree of nuclear localisation of the splicing factor was significantly increased in both the RA and OA group in relation to the PM group.
- The levels of panVEGF-A were significantly increased in the disease groups compared to the controls, showcasing a positive relation to the inflammation.
- VEGF-A<sub>xxx</sub>b expression was higher in the RA group compared to controls and positively correlated with inflammation, while VEGF-A<sub>xxx</sub>a expression showed no significant change between groups or in relation to the inflammation levels.
- The splicing kinase DYRK1a showed a significant increase in expression in the disease groups when compared to controls and showed a significant positive relation to the inflammation scores.

### 3.5 Discussion

In these studies, I tested the hypotheses that the splicing axis SRPK1/SRSF1/VEGF-A is altered in OA and RA synovium and correlates with the degree of inflammation. VEGF-A is a major player in both especially RA and OA although with less information on the latter, however the contribution of the VEGF-A splicing axis has still to be investigated in the context of these diseases. Here I determined the differences between the different components of the VEGF-A splicing axis, their potential contribution in predicting VEGF-A<sub>xxx</sub>b expression, and the relationships with inflammation. It is important to understand the predictors of VEGF-A<sub>xxx</sub>b expression because not because of its predictive nature, but rather because VEGF-A<sub>xxx</sub>b is the one that is more beneficial to have.

A range of features in the synovium are associated with the inflammation in symptomatic OA and RA including but not limited to, synovitis and VEGF-A immunoreactivity, chondrocyte changes and severe cartilage integrity changes, when compared to control cases. Predominantly, when investigating synovium, high inflammation levels of synovitis and VEGF-A expression by the surrounding cells (e.g., fibroblast, macrophages etc) are key features of inflammation in the diseases.

#### 3.5.1 Principal component regression analysis - Predictors of VEGF-A<sub>xxx</sub>b expression in inflammation in OA and RA synovium

The aim of the PCR analyses was to investigate the relationships between variables and identify predictors of altered VEGF-A<sub>xxx</sub>b expression in synovium; identify what is driving the VEGF-A expression in late-stage disease.

All the measures of the VEGF-A splicing axis contributed significantly to the regression model, as did 3 of the 7 disease indicators, the presence of Heberden's nodes, presence of osteophytes and chondrocalcinosis. ARA criteria, effusion levels, synovial thickening, and morning stiffness did not contribute to the regression model. However, the variables cannot be effectively used to distinguish between the diseases (since they have not been looked individually in the model), thus giving no indication of what may happen in early disease stages. Fundamentally although, the indicators above can be considered major players in driving or reducing the VEGF-A<sub>xxx</sub>b expression from this analysis.

### 3.5.2 Changes in the VEGF-A splicing axis and relationship to inflammation in OA and RA synovium

Measure	OA	RA	Inflammation/synovitis (sig correlation)
SRPK1 expression	↔	↔	X
SRSF1 activation	↑↑	↑↑	✓ +ve
Pan VEGF expression	↑↑	↑↑	✓ +ve
VEGF-A <sub>xxx</sub> a isoforms			
FA	↔	↔	X
Integrated Density	↔	↔	X
VEGF-A <sub>xxx</sub> b isoforms			
FA	↔	↔	X
ID	↔	↑↑	✓ +ve
b/a ratio	↔	↔	X
Dyrk1a expression	↑↑	↑↑	✓ +ve

While SRPK1 expression did not change in any group, I identified increases in SRSF1 activation and an increase in panVEGF-A expression in both OA and RA, and a correlation with inflammation in synovium. However, in OA synovium, the levels of VEGF-A<sub>xxx</sub>b, VEGF-A<sub>xxx</sub>a and the ratio of VEGF-A<sub>xxx</sub>b/ VEGF-A<sub>xxx</sub>a did not change, nor did the ratio correlate with inflammation. This suggests an overall increase in panVEGF-A expression in late-stage OA which does not involve a change in VEGF-A splicing. In contrast, in late-stage RA synovium there was an increase in panVEGF-A and VEGF-A<sub>xxx</sub>b, implying that a change in VEGF-A<sub>xxx</sub>b isoforms contributed to the overall panVEGF-A increase.

### **3.5.3 The expression of the splicing kinase SRPK1 showed no significant differences between OA and RA and was not related to the level of synovitis.**

I investigated the expression of SRPK1 in arthritic tissue from RA and OA patients compared to PM control tissue. I hypothesised that given the level of inflammation in these cases, the expression of the kinase would also increase. SRPK1 expression, however, did not change in between groups or relative to the inflammation levels when comparing either RA or OA to our controls.

Previous evidence does suggest that SRPK1 may be upregulated in highly inflamed or proliferative tissue (Yao, Wang et al. 2021) or in situations where angiogenesis is important such as tumours (Amin, Oltean et al. 2011), findings that disagree with the results described in this study. However, as a kinase SRPK1 activity can be regulated by mechanisms other than its expression, increasing the activity of SRPK1.

As stated, TNF- $\alpha$  is a major contributors in both OA (Grunke and Schulze-Koops 2006) and RA (Farrugia and Baron 2016), contributing to disease pathogenesis, and SRPK1 is activated by TNF- $\alpha$  (Mavrou, Brakspear et al. 2015), as well as hypoxia (Jakubauskiene, Vilys et al. 2015). Therefore, it is likely that SRPK1 activity is controlled not by a change of expression levels of SRPK1, but rather a modification in the active state of the kinase. This can't be confirmed by immunohistochemistry experiments nor in post-mortem fixed tissue. Activity of SRPK1 can be measured indirectly by a downstream marker such as a change in an SRPK1 targets e.g., nuclear localisation of SRSF1 (Hulse, Beazley-Long et al. 2014) or a change in VEGF-A splicing (Stevens, Star et al. 2019). This was attempted in this chapter, when I performed the localisation analysis of SRSF1 in chapter 3.3.7, and these results will be discussed in the chapter 3.5.4. How SRPK1 kinase activity changes in synovitis could be understood by assessing it directly *in vitro* using fibroblast-like synoviocytes (FLS), measuring the kinase activity for example through a kinase reporter assay in primary human FLS. The work in the later chapter of this thesis aimed to identify these mechanisms however, due to time constraints as well as the COVID19 impact, the kinase assays were not completed. Other than my findings, there are no studies to date on serine-arginine proteins or SRPK1 in synovium or arthritis, and only three publications showing a direct involvement of SRPK1 in inflammation/neuroinflammation (Li, Li et al. 2020, Wei, Xu et al. 2021,

Yao, Wang et al. 2021). There is no published evidence showing the effect of splicing kinases in context of RA and OA regarding the inflammatory aspect of these diseases

### **3.5.4 Expression and activation of SRSF1 were significantly increased in both OA and RA, and activation correlated with the level of synovitis.**

The expression of SRSF1 was significantly increased in OA synovium and had a strong positive correlation with the degree of synovitis. Expression was increased in RA synovium, but not significantly. In the control of alternative splicing, the activation of SRSF1 denoted by nuclear localisation is key. Nuclear localisation of SRSF1 was significantly increased in OA, and at still higher levels in RA synovium and had a strong positive correlation with the degree of synovitis. The significant changes in the translocation of SRSF1 can be interpreted as an RPK1 activity, and an active change in downstream alternative splicing. The greater activation in RA compared to OA could be due to the more severe or different type of inflammation in RA, given the differences in the immune responses between the diseases (Berenbaum 2013).

As with SRPK1, there are very few published studies on SRSF1 and arthritis, and the few that are available are concentrated on splicing in activated T cells in systemic lupus erythematosus (SLE) (da Glória, Martins de Araújo et al. 2014, Kono, Kurita et al. 2018, Ramanujan, Cravens et al. 2021). SRSF1 is increased in T cells in SLE and related to the disease severity (Katsuyama, Li et al. 2019). In a mouse model of systemic lupus erythematosus (Katsuyama, Li et al. 2019), targeted deletion of SRSF1 in T-cells leads to a lethal systemic autoimmunity with peripheral organ inflammation, and T-cell hyperactivity (Katsuyama, Li et al. 2019). SRSF1 is hypothesised to be a key regulator in autoimmune disease due to these observations (Cassidy, Herbert et al. 2022). There is also a small amount of evidence showing SRSF1 involvement in other inflammation such as muscle damage (Xiong, Shaibani et al. 2006), and of course in tumours as discussed previously.

SRSF1 is of course the main splicing factor known to control the alternative splicing of VEGF-A in the production of the pro-angiogenic/pro-nociceptive VEGF-A<sub>xxx</sub>a variants (Nowak, Woolard et al. 2008, Nowak, Amin et al. 2010). An increase in SRSF1 activation would be hypothesised to favour the production of the VEGF-A<sub>xxx</sub>a isoforms in inflammatory arthritis, leading to the large upregulation in total (pan)VEGF-A reported in multiple studies (Walsh 1999, Paleolog 2002,

Haywood, McWilliams et al. 2003, Walsh and Stocks 2017) in a variety of tissues and cell types (Pan, Xu et al. 2021). Several genes other than VEGF-A have been identified as downstream targets for SRSF1-controlled alternative splicing including, CD44 (Cell-cell interaction, cell adhesion and migration) (Naor and Nedvetzki 2003, Zhang, Luo et al. 2013), MKNK2 (effector in MAP kinase signalling pathway) (Das and Krainer 2014), some of which have of course been implicated in arthritis and may also be controlled by activation of SRSF1.

Interpretation of these findings in fixed human tissues are limited by the inability to directly measure SRSF1 activation and link this to disease activity. However, it is now well described that SRSF1, when activated translocates to the nucleus (Hulse et al 2014) where it is held in nuclear speckles (Malhi, Allen et al. 2022) and released to activate transcriptional alternative splicing by CLKs as described in the introduction (Aubol, Plocinik et al. 2013, Aubol, Wu et al. 2016, Aubol Brandon, Wozniak Jacob et al. 2021). Fluorescence imaging in synovium would have provided higher quality images and analysis, however as mentioned in Chapter 3.2, due to the nature and the fixation of the tissue, it was not possible to optimise fluorescent protocols to produce consistent and robust data. Using an immunoprecipitation-western blotting to identify changes in phosphorylation of SRSF1, in cytoplasmic versus nuclear compartments could bolster our qualitative data regarding the expression, phosphorylation and activity of SRSF1 but would lose the cellular localisation of immunohistochemistry and may not be easily performed on post-TKR or post-mortem tissues. Immunofluorescent staining for SRSF1 in cultured primary human fibroblast-like synoviocytes together with nuclear stains such as DAPI could be used to identify location (Malhi et al., 2022) and control by SRPK1 or other kinases *in vitro* but would then not be related to articular disease.

I would hypothesise that increased SRSF1 activation would change alternative splicing of VEGF-A towards use of the proximal splice site, reducing levels of VEGF-A<sub>xxx</sub>b, since when the splicing factor is phosphorylated and translocates to the nucleus, the splicing of VEGF-A switches in favour of the pro-angiogenic isoform.

### **3.5.5 Expression of total VEGF-A by both fractional area and integrated density increased in OA, further increased in RA, and correlated with inflammation.**

However, when investigating the relationship of VEGF-A<sub>xxx</sub>b with VEGF-A<sub>xxx</sub>a I identified an opposite pattern from the one describing the correlation between VEGF-A<sub>xxx</sub>b and SRSF1. VEGF-A<sub>xxx</sub>b and VEGF-A<sub>xxx</sub>a were negatively correlated, pertaining that as the former increases the latter would decrease, findings that come in agreement with previous literature. Of course, this negative relationship between VEGF-A<sub>xxx</sub>b, the predictors of arthritis and VEGF-A<sub>xxx</sub>a can be analysed in a reverse manner as well. VEGF-A<sub>xxx</sub>a expression levels are increased when there is presence of Heberden's nodes for example. I could speculate that increased levels of VEGF-A<sub>xxx</sub>a would be a predictor against arthritic symptoms, provided of course that the levels of the pro-angiogenic isoform are upregulated before the presence of the Heberden's node rather than as a response to them

I investigated the expression of VEGF-A in synovial tissue of both RA and OA patients compared to controls. This was performed using an antibody that would identify all the splice variants of VEGF-A by targeting the N-terminus of the protein, since I was interested about the levels of VEGF-A in the synovium. Moreover, when I measured the intensity of the stain, I identified that VEGF-A levels were significantly higher in OA samples compared to controls even though most of the previously published studies focus mostly on RA samples. I also identified a positive correlation to the expression levels of VEGF-A with the inflammation grades in our tissue, indicating a pathogenic relationship between the two.

Our dataset is in accordance with previously published literature that has investigated the presence and the role of VEGF-A in the synovium of either OA or RA tissue (Giatromanolaki, Sivridis et al. 2003, Haywood, McWilliams et al. 2003). The increased need for angiogenesis during synovitis drives the upregulation of VEGF-A expression which in some circumstances, perpetuates the inflammation. I have identified increased levels of VEGF-A in the inflammatory groups compared to the controls, supporting the association between VEGF's angiogenic function and inflammation. In accordance with literature (Walsh 1999), VEGF-A play a major role in a chain of events starting with inflammation of the synovium due to exogenic factors, increase

need for vascularisation to the inflamed areas for transportation of inflammatory cells, upregulation of the growth factor facilitating angiogenesis, which in turn perpetuates the inflammation. Qualitative analysis of the samples indicated VEGF-A expression by a majority of cells in the synovium including macrophages and fibroblasts suggesting a molecular mechanism through which OA and RA are being mediated with VEGF-A playing a major role (Haywood, McWilliams et al. 2003).

Of course, there are some limitations to the study of VEGF-A expression levels. The study was performed in fixed tissue in vitro so there is a possibility of inconsistency when compared to clinical phenomenon of either OA or RA. Secondly, a functional study over the expression of VEGF-A using cell culture raised synovial fibroblast would provide a better understanding of the intricacies surrounding VEGF-A expression. Third, by using a general antibody against VEGF-A I identified the increase of the expression levels, however I could not identify if that increase were catholic of the VEGF-A population including all the isoforms, or specific to certain isoforms only.

### **3.5.6 Expression of anti-angiogenic VEGF-A<sub>xxx</sub>b by fractional area not changed in the OA and RA groups, and not correlated with inflammation, but integrated density was higher in RA and correlated with inflammation. VEGF-A<sub>xxx</sub>a not altered**

To identify if the increase in the VEGF-A levels was specific to certain isoforms or if it was widespread among the VEGF-A population, I also investigated the levels of VEGF-A<sub>xxx</sub>b and VEGF-A<sub>xxx</sub>a isoform using a specific antibody for these splice variants.

I documented that there is no significant difference in the expression of the isoform as expressed in fractional area. By comparing these findings with the findings from the fractional area of VEGF-A immunoreactivity study, I could speculate that the increase that I identify in VEGF-A levels is attributed to the VEGF-A<sub>xxx</sub>a isoform.

Moreover, I investigated the intensity of the VEGF-A<sub>xxx</sub>b staining normalised to the area of expression. Interestingly, the integrated density was significantly higher in the RA group when compared to the controls and was significantly related to the inflammation levels. When compared to the intensity of the immunoreactivity for the VEGF-A levels, I can identify a similar

pattern as previously. The levels of panVEGF-A in OA are increased significantly over the controls, whereas VEGF-A<sub>xxx</sub>b levels in OA do not differ significantly from the control levels.

In contrast to our initial hypothesis the VEGF-A<sub>xxx</sub>a isoform prominent for its pro-angiogenic, pro-inflammatory functions demonstrated no significant changes between the disease groups and the controls either when expressed as fractional area or when I analysed the intensity of the immunoreactivity.

Building on previously published literature, the increase in angiogenesis that is evident in both OA and RA would denote the increase of the pro-angiogenic, pro-inflammatory isoform VEGF-A<sub>xxx</sub>a, while the anti-angiogenic isoform would be reduced and/or not change in expression levels. However, I for the first time showed that only the VEGF<sub>xxx</sub>b isoform was increased in the RA group, results that do not reflect the alterations in panVEGF-A. Potentially VEGF-A<sub>xxx</sub>b, is acting as a balance to the increased angiogenesis encountered in the disease groups.

We know that the VEGF-A<sub>xxx</sub>b isoform is a partial agonist against VEGFR2, however there are no signalling molecules that are activated by VEGF-A<sub>xxx</sub>b isoforms that are not activated by VEGF-A<sub>xxx</sub>a isoforms. Noone has looked at downstream signalling by VEGF-A<sub>xxx</sub>b isoforms so I can't yet say that it just activates less or more during the disease progression and onset as we don't know if it also activates different pathways. Downstream signalling which appears to be important for the VEGF-A<sub>xxx</sub>a isoforms, may look less significant for the b family, but that might be because we are looking at the wrong signalling pathways. The reported cytoprotection effects of VEGF-A are not being reduced. It is unclear whether the profound difference in cellular behaviour induced by VEGF-A<sub>xxx</sub>b relative to VEGF-A<sub>xxx</sub>a is due to an alteration in signalling with different signalling molecules or an alteration in the downstream signalling is insufficient, or whether both mechanisms are functional.

Moreover, when I investigated the ratio between the VEGF-A<sub>xxx</sub>b/ VEGF-A<sub>xxx</sub>a isoforms from our samples, no significant differences were prominent, denoting that VEGF-A as a whole, is potentially increased without altering the relation between the two isoforms.

Finally, the difference noted in the expression of the two isoforms may be a by-product of the specificity of the antibodies used; specifically, the panVEGF antibody is specific against the 189, 165, 121 amino acid splice variants, the VEGF-A<sub>xxx</sub>b is specific against the 165 amino acid splice variants only, similar to the VEGF-A<sub>xxx</sub>a specific antibody.

### **3.5.7 Expression of the related splicing kinase Dyrk1A is related to the severity of histological inflammation particularly in RA.**

I investigated the expression the alternative splicing kinase DYRK1a in arthritic tissue from RA and OA patients against control tissue. I hypothesised that provided the increase of angiogenesis and inflammation the expression of the kinase would also increase to facilitate for these changes, the kinase has been previously reported to positively regulate VEGF-A dependant activation of T cells. The DYRK1a kinase, was positively upregulated in both the disease groups, an effect that was positively corelated with the synovitis present in the tissue. These findings come in accordance with previously published data suggesting the kinase is upregulated in RA synovial tissue (Guo, Zhang et al. 2018), while also confirming that even though the inflammatory profiles of RA and OA are different, DYRK1a plays a role in the inflammatory process of both diseases, a finding which is confirmed by another study investigating the effects of DYRK1a inhibition affecting the Wnt-pathway as a potential anti-inflammatory drug to improve structure and symptoms of knee OA (Deshmukh, O'Green et al. 2019).

DYRK1a plays a major role in T cell activation and differentiation, with immediate effects on inflammation. Earlier in the chapter I provided information on the upregulation of VEGF-A in OA and RA implying an increase in the angiogenesis and inflammation evident in the synovial tissue. One of the underlying mechanisms here is that VEGF-A by activating its receptors namely VEGFR1/2, creates a signalling cascade which includes the extra extracellular regulated kinase/mitogen-activated protein kinases (ERK/MAPKs), the phosphoinositide 3-kinase (PI3K)/AKT pathway, or the phospholipase C $\gamma$  (PLC $\gamma$ )/Ca $^{2+}$  pathway (Rozen, Roewenstrunk et al. 2018). Through the PLC $\gamma$  pathway the Ca $^{2+}$  channels in the endoplasmic reticulum open, leading to an influx of intracellular Ca $^{2+}$ ; this influx of Ca $^{2+}$  leads to dephosphorylation of the nuclear factor of activated T cells (NFAT), which translocate to the nucleus and regulate angiogenesis events (Müller and Rao 2010). DYRK1a, plays a major role in regulating this NFAT translation, and upregulation of the kinase in the highly vascular and inflammatory synovium tissue of RA and OA patients suggest a mechanism under which the increased angiogenesis is driven (Müller & Rao, 2010). Moreover, regarding the inflammatory response evident especially in RA in conjunction with T cell activation, DYRK1a is the key kinase regulating the splicing between the inflammatory driven TH17 driving a pro-inflammatory immune pathway and the T $_{reg}$  cells a subpopulation of T cells that act to suppress immune responses (Müller and Rao 2010). Inhibition

of DYRK1a seems to drive the differentiation of T cells towards the T<sub>reg</sub> cells. The increased levels of inflammation in RA and in the late-stage OA samples in our disposal could be the result of this unbalanced differentiation of T cells attributed to upregulated levels of DYRK1a.

With this in mind I did confirm that in the RA cases DYRK1a upregulation seems to play a key role in the development of inflammation as it had been discussed previously, however I also set the basis to study the mechanism behind the activities of DYRK1a in OA, in conjunction with the VEGF-A levels and its splicing axis.

The relationship between these four variables is negative, as it can be seen in figure 22 (chapter 3.3.3) with the values being graphed in the lower quadrant, denoting that presence of increased VEGF-A<sub>xxx</sub>b would be translated in reduced levels of these aforementioned predictors. I could speculate that by monitoring the levels of VEGF-A<sub>xxx</sub>b, I could potentially track the ongoing changes, and potentially use it as evidence of early predictors of OA and RA. Of course, that is dependent on the speed through which a decrease in VEGF-A<sub>xxx</sub>b would become evident in relation to the appearance of the traditional predictors of arthritis.

### **3.6 Optimisation and limitations**

Regarding the immunofluorescence experiments using alkaline phosphatase the rationale behind the experimental procedure was to provide with a more suitable technique that would allow for a precise localisation study following protocols that have been published before (Haywood et al 2003). However due to several issues including high levels of background staining and non-specific, non-consistent staining throughout the samples this procedure had to be reconsidered. Providing that the tissue was fixed and embedded in paraffin most of our images were inconsistent due to the nature of the tissue and the fixing procedure. That rendered analysis of the fluorescent images impossible. However, given the benefits of double labelling as well as the ease of analysis such a technique will bring, it will probably be revisited in the future. Such a technique would allow for better quality imaging, thus more robust results, and analysis. A potential change in the protocol as well as experimenting with several different antibodies would potentially yield the results that are desirable, however in the timeline of this project such try-outs would require more attention and focus that would have left other much more pressing questions unanswered.

There are some limitations to this study. OA and RA prevalence is strongly associated with living patterns and more importantly age. This as a result could raise doubts in studies as to the changes documented in the histopathology of the synovium are specifically associated with the diseases or if they are characteristics derived from ageing. To address this limiting factor, cases were carefully selected from a large repository and were age matched between OA, RA, and controls.

Our cohort for the study was dominated by Caucasian people, which would skewer the results towards that ethnic group, rather than providing a bigger “picture” analysis. It is important to note that the IHC experiments utilised here are an expression study, and even though they provide us with a good representation of what is happening in the OA and RA tissue, they are lacking the details of a mechanistic approach experiments. Moreover, there could be situations that the expression levels of the kinases or factors in question are not altered, but their activity is enhanced. Without specific assays (e.g., kinase assay) this information could not be obtained. Moving forward, the localisation analysis that was performed for SRSF1 was based on purely qualitative analysis of the immunoreactivities on the tissue. Successful fluorescence protocol and staining would provide a more robust results of the localisation of SRSF1, since I could double label the tissue in question with DAPI, SRSF1 and pSRSF1, to identify the translocation of the splicing factor. The specificity of antibodies could also be considered here; as mentioned above the panVEGF-A utilised has the ability to detect the 189, 165, 121 amino acid splice variants, the VEGF-A<sub>xxx</sub>b is specific against the 165 amino acid splice variants only, similar to the VEGF-A<sub>xxx</sub>a specific antibody. This could potentially skewer the results slightly, since for example VEGF-A has more variants based on the amino-acid length (121,145,165,183,189,206). Moreover, all the tissue considered here is from end-stage OA/RA, in which the mechanism and progression of the disease may vastly differentiate from early OA for example.

### **3.7 Concluding remarks**

VEGF-A is increased in relation to inflammation in both RA and OA cases when compared to control tissues, a change driven by the alterations in expression of the individual isoforms VEGF-A<sub>xxx</sub>a and VEGF-A<sub>xxx</sub>b. This implies a connection between the VEGF-A splicing axis, including SRSF1 and SRPK1 with the distinct inflammatory phenotypes evident in RA (autoimmune driven response) and OA (“normal” inflammatory response). The effect of altered splicing is also

supported by the significant alterations in SRSF1 expression patterns between the disease groups and the control, taken into consideration the clear translocation of SRSF1 in the nuclei of the cells, a prerequisite for the isoform to promote the expression of the pro-angiogenic isoform of VEGF-A. Finally, confirmation of DYRK1a involvement in both the RA and OA samples, prompts the need to understand the underlying pathways. DYRK1a through VEGF-A plays a key role in T-cell transcription and differentiation, denoting a complex mechanism to promote angiogenesis through VEGF-A outside of the scope of SRPK1 and CLK1. Of course, these three alternative splicing kinases probably work in conjunction to each other instigating a mechanism through which SRPK1 phosphorylates SRSF1 which leads to upregulation of VEGF-A and specifically VEGF-A<sub>xxx</sub>a, followed up by alterations in the T cell differentiation promoting inflammatory responses further.

## **4. VEGF-A splicing events and pain in knee joint synovium from people with OA.**

### **4.1 Introduction**

OA is a major source of pain and disability. With end stage OA, surgical arthroplasty might offer pain relief, however knee replacement surgery is not always possible nor suitable for all patients. Existing drugs offer little benefit or adverse effects, while disease modifying OA drugs (DMOADS) that could treat or prevent structural disease are still being researched (Walsh and Stocks 2017).

Radiographic changes, such as joint space narrowing, have been associated with painful phenotype in OA, however this association is weak. For example, knee joint space narrowing may be a result of articular cartilage thinning, or meniscal extrusion, and so does not necessarily directly indicate significant joint damage showing that even though radiographs may provide us with information about articular damage, the association of this to pain is not robust (Neogi and Zhang 2013, Kittelson, George et al. 2014).

Using magnetic resonance imaging (MRI), we have access to more detailed representation of the structural changes in OA, to better determine potential associations with pain. Articular cartilage, meniscal location and tears, synovitis, bone marrow lesions (BMLs) and alterations in the subchondral bone can all be evaluated through MRI. As an example, we can identify the cartilage depth and focal defects, or synovitis by the evident synovial hypertrophy or effusion. Synovitis as defined by ultrasound, with effusion, synovial hypertrophy, and increased blood flow demonstrated by power Doppler signal (Hall, Doherty et al. 2014) is particularly and significantly associated with OA pain.

Current treatments have a number of limitations driving the need for new drugs against OA pain. NSAIDs, including COX-2 inhibitors, can be helpful but increase risks of gastric bleeding, renal damage, and ischemic cardiovascular events (Osteoarthritis: Care and Management in Adults, NICE Clinical Guideline 177; National Institute for Health and Care Excellence: London, 2014); opiates show little sustained benefit for OA pain, while being associated with gastrointestinal and cognitive adverse effects, not to mention the risk for abuse potential. Intra-articular treatments e.g., corticosteroids, have limited duration of efficacy, raising logistic issues for repeated treatment.

Once pain is severe, in the UK scoring >8/10, arthroplasty is the treatment of choice, and still remains one of the most effective treatments, although expensive and achieving only an 80% success rate in relieving knee pain (Dakin, Gray et al. 2012).

Synovitis in OA is characterised by innate immune response with macrophage infiltration rather than the acquired immune response and lymphocyte infiltration which is observed in RA. However, certain characteristics in the inflammatory profile and the inflammatory mediators in play are similar for both of these diseases. OA and RA synovial fluids contain high concentrations of TNF- $\alpha$  and IL-1 $\beta$ , as well as NGF, TGF- $\beta$  and VEGF-A. Many cytokine and inflammatory mediators within the synovial fluid have been associated with OA pain, the most widely investigated being TNF- $\alpha$ , IL-1 $\beta$ , IL-6, IL-8, IL-10 and C reactive protein, but the correlations between mediators and pain are only moderate, and inconsistent (Dainese, Wyngaert et al. 2022).

As mentioned in chapter 1.5.5, vascular endothelial growth factor-A (VEGF-A) is a key regulator of vascular growth, permeability, and in the context of this work, neuronal function. VEGF-A is widely, and principally recognised for its vascular effects, and as a result has been extensively investigated due to its upregulation in OA, and the increased synovial angiogenesis and flares of inflammation associated with increased pain (Hall, Doherty et al. 2014).

During end stage OA increased levels of pan-VEGF-A have been identified in articular cartilage (Smith, Oreffo et al. 2003), synovium and synovial fluid (Sohn, Sokolove et al. 2012), and subchondral bone (Corrado, Neve et al. 2013) as well as in bone marrow lesions (Shabestari, Shabestari et al. 2020). In OA, pan-VEGF-A synovial fluid levels are significantly correlated with both pain and inflammation (Gaballah, Hussein et al. 2016).

Intra-articular injections of exogenous VEGF-A in the knee joint of mice induces OA-like changes, including proteoglycan loss, calcification and degradation of the articular cartilage, osteophyte formation, and synovial hyperplasia (Ludin, Sela et al. 2013). Intra-articular and systemic treatment with bevacizumab (also known as Avastin), an anti-pan-VEGF-A antibody approved for the treatment of colorectal carcinoma, results in reduced cartilage damage, osteophytes, synovitis and most importantly in the context of this study, intra-articular treatment reduced pain in OA induced rabbits (anterior cruciate ligament transection model) (Nagai, Sato et al. 2014).

To date many studies have shown that VEGF-A can affect nociceptive behaviour in different animal models, with varying results and conclusions, presenting a confused picture of the role of VEGF-A in pain.

VEGF-A is reportedly unregulated (Lin, Li et al. 2010, Kiguchi, Kobayashi et al. 2014, Murakami, Kuniyoshi et al. 2014, Hulse, Beazley-Long et al. 2015) in peripheral nerves in neuropathic animal models, but downregulated in human diabetic neuropathy (Gardiner and Freeman 2016). Exogenous peripheral VEGF-A results in acute nociceptive behaviour in normal mice and rats (Hulse et al 2014) and causes uterine hypersensitivity (Chiumia, Hankele et al. 2020), and bladder pain and hypersensitivity (Malykhina, Lei et al. 2012, Xie, Iguchi et al. 2022) which is blocked by systemic anti-VEGF-A antibodies (Lai, Shen et al. 2017). Conversely, intraneuronal VEGF-A<sub>xxx</sub>a production/retrograde transport in injured nerves *ameliorates* nerve injury and neuropathic pain (Murakami, Arai et al. 2006, Pawson, Duran-Jimenez et al. 2010, Lee, Lee et al. 2016). Anti-VEGF-A antibody treatment blocks pain in diabetic neuropathy (Lin, Li et al. 2010), but systemic and local anti-VEGFR2 antibody DC101 can also increase pain behaviours in animal models (Hulse et al 2014).

Intrathecal VEGF-A<sub>xxx</sub>a administration (VEGF-A<sub>165a</sub> in all studies identified to date) exacerbated (Benton and Whittemore 2003) or had no effect on spinal cord damage, increased (Nesic, Sundberg et al. 2010) or partially decreased (van Neerven, Joosten et al. 2010) pain in spinal contusion injury models, and exacerbated pain behaviour in normal (Hulse, Drake et al. 2016, Micheli, Parisio et al. 2021) and neuropathic animals, through VEGFR1 (Micheli, Parisio et al. 2021) or VEGFR2 (Hu, Yang et al. 2019) or both (Lee, Son et al. 2019). VEGFR1 knockout blocked cancer pain in mouse models (Lee, Lee et al. 2016), as did intrathecal anti-VEGF-A antibodies (N-terminal antibodies targeting all VEGF-A isoforms) and VEGFR2 blockers in bone cancer models (Hu, Yang et al. 2019, Fan, Kan et al. 2022), suggesting spinal VEGF-A promotes pain behaviours.

All these described studies either use VEGF-A<sub>165a</sub> or panVEGF-A or a general receptor blockade, and none of these approach enables an understanding of the potential physiological/pathological interplay of different forms of VEGF-A. It is important to note that while the VEGF-A<sub>xxx</sub>b isoforms were identified in 2002, they were not widely acknowledged for many years (Harris, Craze et al. 2012, Kim, Lee et al. 2016). Very few studies have therefore considered alternative splicing of VEGF-A as an explanation for the differing findings on pain, but the identification of the VEGF-A<sub>xxx</sub>b splice variants and their investigation may explain some of

the contradictory findings when using exogenous VEGF-A<sub>xxx</sub>a, anti-VEGF-A antibodies or VEGF receptor inhibitors/blockers to investigate pain (Di Cesare Mannelli, Tenci et al. 2018, Tooke, Girard et al. 2019).

In the context of arthritic pain, only panVEGF-A or VEGF-A<sub>xxx</sub>a isoforms have been systematically investigated. This presents the question of if and how the splicing isoforms are altered in symptomatic OA. While a strong relationship between VEGF-A and OA has been described, particularly in cartilage clefts where neurovascular bundles can be found in advanced OA (Walsh, McWilliams et al. 2010, Shabestari, Shabestari et al. 2020), in synovium and subchondral bone (Wyatt, Nwosu et al. 2019, Qian, Xu et al. 2021), there are no published data on the expression or actions of the functionally distinct VEGF-A splice variants in human OA. The goal of this study was therefore to define the patterns of, and relationships between, panVEGF-A, VEGF-A splice variants, SRPK1, and SRSF1 expression and activation, and pain in human OA synovium.

**Primary hypothesis:** the activation of the SRPK1/SRSF1/VEGF-A splicing axis is greater in synovium from people reporting pain from OA (symptomatic OA) than in synovium from chondropathy matched, pain-free (asymptomatic) people with OA.

**Specific hypotheses:**

1. Expression of SRPK1 is increased in the synovium from people with symptomatic (painful) OA/chondropathy compared to matched pain-free controls (with asymptomatic OA/chondropathy).
2. Expression and activation of SRSF1 is increased in the synovium from people with painful OA compared to matched pain-free controls
3. Expression of panVEGF-A is increased in the synovium from people with painful OA compared to matched pain-free controls
4. Expression of the pronociceptive VEGF-A<sub>xxx</sub>a isoforms in human knee synovium is significantly positively associated, and levels of the antinociceptive VEGF-A<sub>xxx</sub>b isoforms are negatively associated with painful OA and altered in comparison to non-painful controls.
5. Expression of the related splicing kinase Dyrk1A is related to the increased levels of pain encountered in symptomatic chondropathy cases compared to asymptomatic chondropathy

## 4.2 Materials and Methods

General methodology is given in chapter 2 (Methods). Tissue collection and sample processing are described in section 2.2 from the same repository as the samples selected in Chapter 3. Details for histological grading are given in section 2.7.

Tissues were selected from age- and sex-matched cases in the Pain Centre Versus Arthritis joint tissue repository. Synovial tissue samples were matched for macroscopic chondropathy scores in 2 groups (n=20 per group). The *Symptomatic Chondropathy* (SC) group comprised samples from people undergoing total knee replacement (TKR) for OA knee pain. The patients from this group had all at least grade 4 chondropathy and self-reported the pain in their affected joint as being 8 or higher on a 0-10 numerical rating scale. The *Asymptomatic Chondropathy* (AC) group comprised samples collected post-mortem from people who died of unrelated illnesses and were recorded as not known to have sought help for knee pain in the 12 months prior to their death while also having at least a chondropathy of grade 4. The samples included in the study were selected on a qualitative inspection of the haematoxylin and eosin-stained index slides from the repository of the Pain Centre Versus Arthritis, according to the criterion described in section 3.2 on the presence of synovial lining and underlying synovium.

The chondropathy scoring system applied on these samples is based on previous literature (Walsh et al 2009). It is a result of macroscopic inspection of the articular surfaces of medial and lateral tibial plateau. This is possible by photographing the femoral condyles as well as the tibial plateau at 23cm.

The key components of the grading include the extent, the severity, and the loss of articular cartilage. There are 4 grades of chondropathy based on the severity of the articular cartilage:

Grade 0 or normal -> smooth, homogeneous white to off-white colour.

Grade 1 -> swelling and softening a light brown colouration.

Grade 2 -> superficial fibrillation, lightly broken surface, white to light brown in colour.

Grade 3 -> deep fibrillation, broken cartilage surface, dark brown, or red in colour.

Grade 4 -> subchondral bone exposure, white and dark brown/red in colour.

The chondropathy grading was done by a single individual, in these cases Roger Hill in King's Mill Hospital, part of Sherwood Hospitals NHS Foundation Trust. The grading is proportional to the observed level and amount of chondropathy, for example 1 sample may have 30% grade 2 chondropathy and 70% grade 3 chondropathy. The overall score of the samples is then calculated based on the following equation:

$$\text{Chondropathy score} = (\text{Grade 1} \times 0.14) + (\text{Grade 2} \times 0.34) + (\text{Grade 3} \times 0.65) + \text{Grade 4}$$

### **Immunohistochemical analysis**

Sections were stained for SRSF1, SRPK1, total (pan)VEGF-A, the two families of VEGF-A splicing isoforms (a and b) and Dyrk1A. Expression was estimated as fractional area (numbers of cells expressing). SRSF1 activation was assessed by the degree of nuclear localisation. Some sections were lost during tissue processing; final n values are shown below and in Figure legends.

Slides were de-waxed and rehydrated in Xylene and decreasing ethanol concentrations (100%, 90%, 70%) for 5 minutes each, followed by a 10-minute wash in PBS. Antigen retrieval was then performed in Tris-EDTA-Tween-20 (USB Corporation USA, Sigma Life sciences UK, Sigma Aldrich UK) solution pH 9 for 30 minutes at 65°C. The buffer was first brought to boiling point using a microwave for approximately 3-5 minutes and then the slides were immersed in the buffer and placed in a closed box inside a water bath. Optimisation for the conditions is described in Chapter 3.3. After 20 minutes the slides were transferred into running tap water and left to cool in for 10 minutes. Tissue sections mounted on slides were then encircled with a PAP pen to create a hydrophobic barrier around the sections to minimize the necessary volume of reagents and prevent loss of antibody solutions and other reagents from the slide during incubations. Endogenous peroxidases were blocked with H<sub>2</sub>O<sub>2</sub> (Sigma Aldrich, UK) for 20 minutes at room temperature in a sealed container containing a reservoir of 1x PBS to create a humid environment to minimize evaporation of solutions. After draining the H<sub>2</sub>O<sub>2</sub> from the sections, slides were replaced in the humid container and incubated in 5% BSA in PBS for 1 hour (Sigma Aldrich UK) at room temperature to block non-specific binding of the antibodies. The blocking solution was then aspirated before incubation in primary antibody dilutes in the blocking solution (see Table 9 at chapter 2 for primary antibody concentrations) overnight at 4 °C in the humid box. The next day the slides were washed in PBS for 5 minutes to remove the primary antibody and the slides were then incubated in secondary antibodies 1x PBS at room temperature in a humid environment for 2 hours. After two 5-minute washes in PBS, the

secondary antibodies were localized using the ABC kit (Vector Laboratories Ltd UK) for signal amplification for 30 minutes and visualized using a DAB (diaminobenzidine) kit (Vector Laboratories Ltd UK) applied for 15 minutes (both incubations were performed in room temperature in a humid environment, in the dark) for optimal development according to the manufacturer's guidelines. The peroxidase-DAB precipitation reaction was stopped with a 5-minute wash in dH<sub>2</sub>O, followed by light haematoxylin staining for morphological features. Slides were dipped into haematoxylin solution (RAL- diagnostics, France) for 2-3 seconds and then washed in tap water, to prevent strong haematoxylin staining masking the DAB signal. The tissue was then dehydrated in ascending ethanols (70%, 90%, 100%) and finally xylene for 5 minutes each and then mounted with glass coverslips using DPX and left to dry overnight (Figure 34).

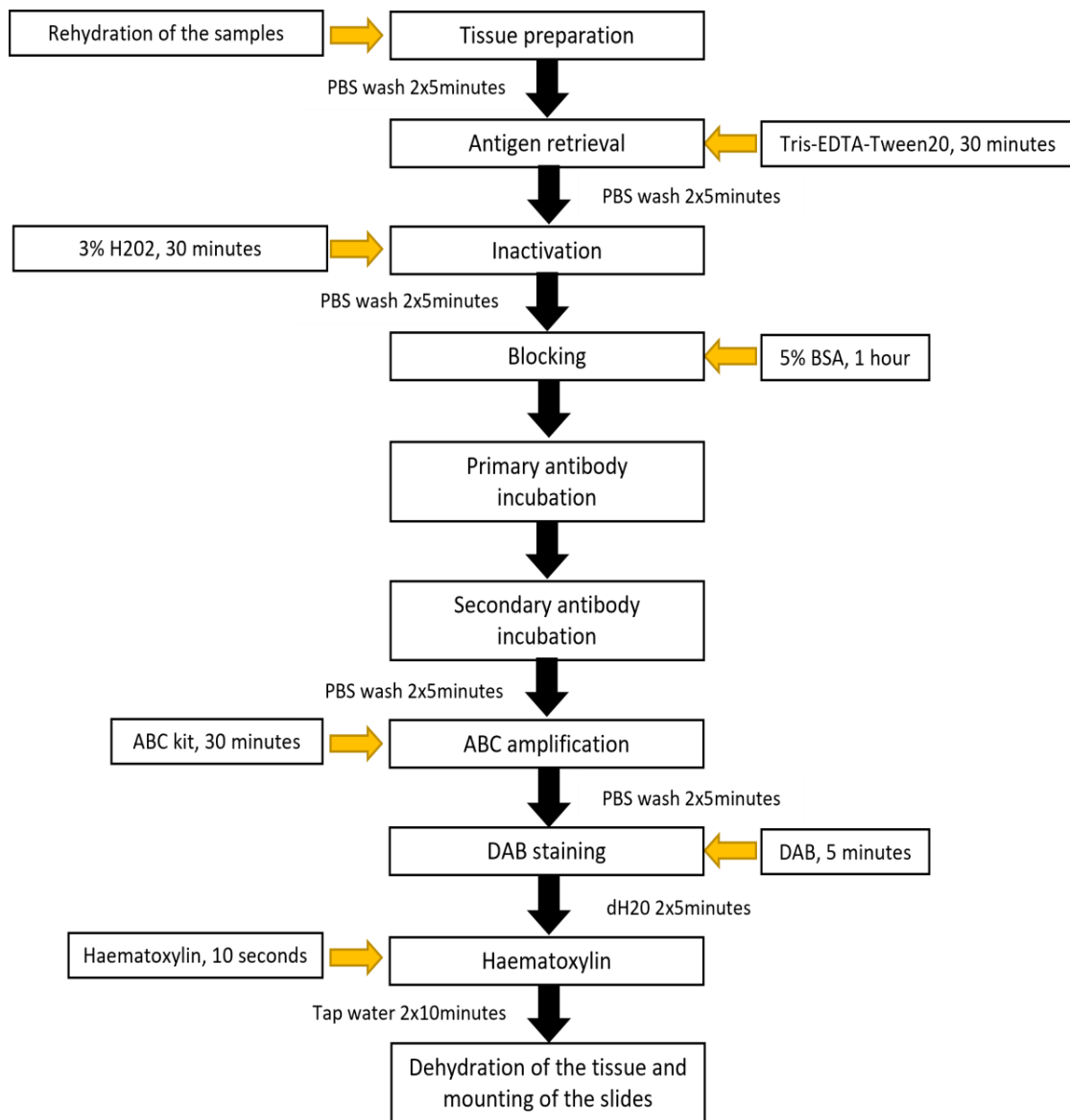


**Figure 33 Schematic representation of the IHC protocol used throughout the experimental work of the thesis. Antibody concentrations are shown in Table 9**

### **Image capture, data extraction and analysis**

All images and analysis were performed while blinded to the groups/samples to avoid any potential experimental bias. Histologic scoring and quantification were performed using a Zeiss Axioskop 50 microscope, by a single observer who was blinded to the details of the diagnostic group. I captured 3 fields per sample following the hot-spot technique, focussing on areas of the tissue that visually had more staining as described in the methods (Haywood et al 2003). Only

areas within 100µm of the synovial lining surface were captured and analysed. A custom-made macro allowed quantification of the DAB staining expressed as fractional area (Area of positive stain/Recorded area) per patient quantified by computer assisted image analysis by thresholding the output of the stain against the haematoxylin staining (Haywood et al 2003). Light images were captured using a 3-CCD camera and analysed using a KS300 image analysis system (Imaging Associates Ltd., UK) as well as Excel and GraphPad Prism (v8.4.2 for Windows GraphPad Software, San Diego, California USA, [www.graphpad.com](http://www.graphpad.com)). Specific methodology regarding the analysis procedures can be found in the method chapter.

### **Statistical analysis**

All statistical analyses were performed using GraphPad Prism software (v8.4.2 for Windows GraphPad Software, San Diego, California USA, [www.graphpad.com](http://www.graphpad.com)). Differences in fractional area of SRPK1 and SRSF1, panVEGF-A and VEGF-A splice variant expression were determined using Mann-Whitney's. Specific statistical analyses and outcomes are given in figure legends. PCR analysis was performed as explained in Methods chapter 2.4.7. Principal components in this study were selected based on the parallel analysis method, characterising a variance of ~40% of our dataset. Significance was denoted as *p* values of less than 0.05 as per convention.

## 4.3 Results

### 4.3.1 Case information – summary table and illustrations of the histology

Patient demographics for this chapter's samples are reported in table 13 and histopathological features based on which the chondropathy score were calculated are discussed previously in the Methods of this chapter. Provided that there were no data for effusion or the synovial thickening in the asymptomatic chondropathy group, I assumed that there was no presence of either in these patients.

**Table 11 Clinical details and pathological characteristics of study groups.**

Clinical or pathological characteristics	Features of symptomatic OA	
	Asymptomatic chondropathy (PM) (n=18)	Symptomatic chondropathy (TKR) (n=17)
<b>Race</b>	White 100%	
<b>Age in years, mean (SD)</b>	77.2±11.8*	66.2±8
<b>Median (range, n)</b>	80 (35, 18)	67 (28, 16)
<b>Male: female</b>	12:6	9:8
<b>Macroscopic Chondropathy score</b>	67±20 (18)	77±12 (11)
<b>**Left knee (mean ± SD (n))</b>		
<b>Effusion</b>	No data	11/16 (69%)
<b>Synovial Thickening</b>	No data	8/16 (50%)
<b>Heberden's nodes</b>	0/17	3/16 at grade >2 (19%)
<b>Osteophytes</b>	8/17 (47%)	15/15 (100%) †
<b>Synovitis (mean ± SD (n))</b>	2.38±0.697 (18)	2.33±0.685 (17)

Table 13. Tissues were obtained at the time of total knee replacement for OA or were obtained PM from cadaver donors. Some details and information were missing from some cases and so these samples were not included in calculating the values above. Where this occurs, group n values used for calculations are shown. \*p=0.003 (2-tailed t test), †p=0.001 Fisher's exact test). \*\*left knees were used for all cases.

### 4.3.2 Splicing axis changes in symptomatic painful chondropathy

Similar to the previous results chapter section 3.3.4 to determine changes in splicing kinases and the VEGF-A splicing axis between painful and pain-free samples I was interested in identifying the relationship between each of our variables and the general predictors of OA. The same cases were used throughout the whole study for all different IHC protocols. The principal components (PC) were identified using parallel analysis, which identified 1 PC accounting for ~47% of the total variance of the dataset.

Only one principal component was identified, and this shows the relationships between VEGF-A<sub>xxx</sub>b fractional area and the other variables (Figure 35). Figure 35 shows the individual variable loadings (the correlation between the values for each column variable measured and the calculated values for the PC) and the relationship between these and the PC. The key information shown in this loading plot are clusters of variables such as SRSF1 expression, SRSF1 nuclear localisation and pan-VEGF-A and the direction of correlation between the variables and the PC. The clustering of the above values for example indicates that these are providing similar information and so in further studies measurement of only one of this group of variables would likely give sufficient information. The direction of the line shows how the variables correlate with the PC and their direction, for example VEGF-A<sub>xxx</sub>b/VEGF-A<sub>xxx</sub>a ratio correlate with PC1 in the opposite direction to all the other variables as they are on different sides of  $x=0$  and  $y=0$ . For example, on the top left quadrant of Figure 35, I can see that VEGF-A<sub>xxx</sub>b and the VEGF-A<sub>xxx</sub>a/VEGF-A<sub>xxx</sub>b ratio are related in terms of relative change of their values. Increase in the value of the former would denote an increase in the levels of the ratio. The rest of the variables are in the lower left quadrant of the Cartesian system, denoting a negative relationship with VEGF-A<sub>xxx</sub>b, meaning that when the levels of the isoform are decreased/downregulated, these values will increase. It is important to note that the 0.0 (the intercept) in the Cartesian system of figure X represents the VEGF-A<sub>xxx</sub>b isoform dependant variable. The closer a variable is to the Y axis or the X axis, in other words the closer a variable is to 0 then the set of that parameter and VEGF-A<sub>xxx</sub>b, are considered orthogonal, denoting a non-relationship.

PCR with dependent value of VEGF-A<sub>xxx</sub>b

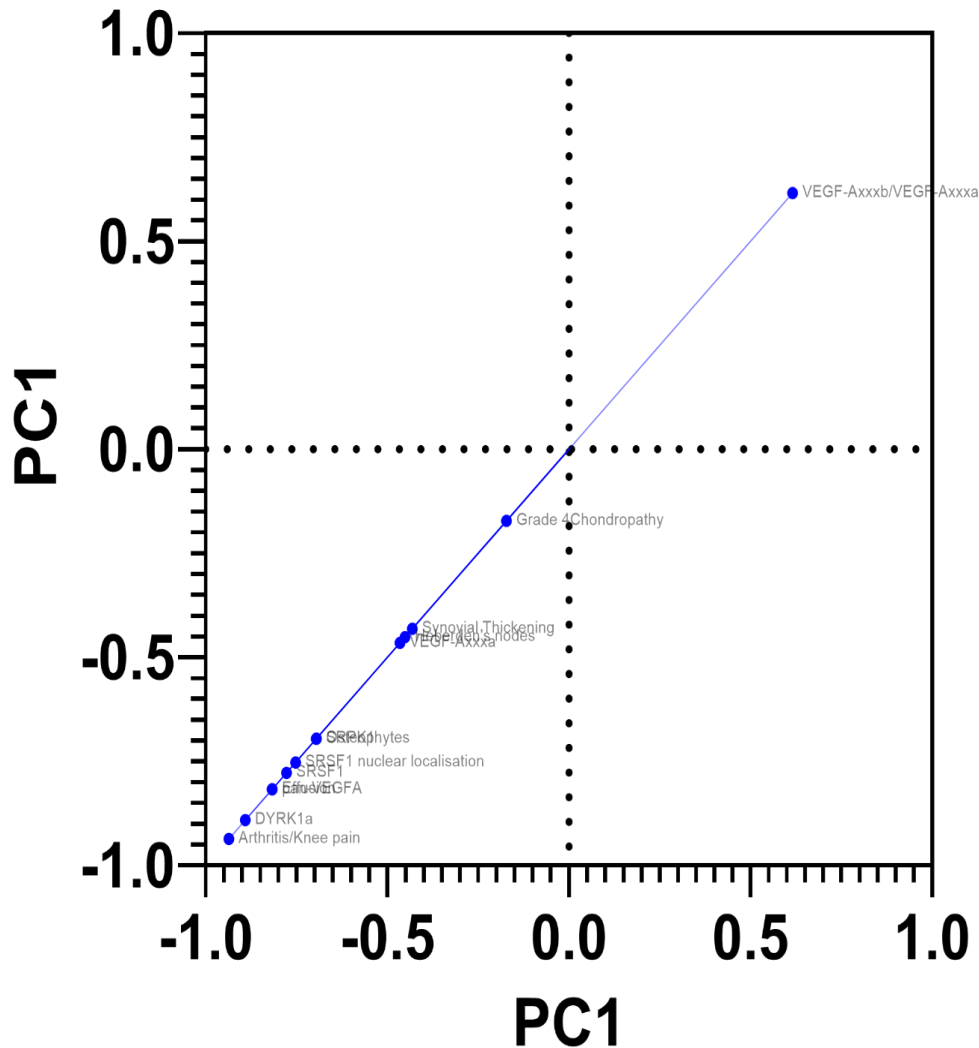


Figure 34 Loading plot of the PCA for the dataset of the VEGF-A splicing axis and indicators of OA disease. The variable against which I determined dependencies was the VEGF-A<sub>xxx</sub>b expression. Chondropathy score, SRPK1; SRSF1; SRSF1 localisation; pan-VEGF-A; VEGF-A<sub>xxx</sub>a; VEGF-A<sub>xxx</sub>b/VEGF-A<sub>xxx</sub>a ratio; DYRK1a, knee pain; effusion, synovial thickening; Heberden's nodes; osteophytes all contributed significantly to the linear regression model of predicting VEGF-A<sub>xxx</sub>b expression. From the graph above I can identify the variables that have a positive relationship with both PC1 and PC2 (top right quadrant), a positive relationship with PC1 and negative relationship with PC2 (bottom right quadrant), etc. Clustering of variables such as SRSF1 expression, pan-VEGF-A expression and SRSF1 localisation indicate a close relationship between these variables, and possible redundancy in the model. The variants situated in the bottom left quadrant; they have a negative relationship with VEGF-A<sub>xxx</sub>b. The VEGF-A<sub>xxx</sub>b/ VEGF-A<sub>xxx</sub>a ratio on the contrary has a positive relationship with VEGF-A<sub>xxx</sub>b based on the placement in the top right of the quadrant in the graph, denoting an increased VEGF-A<sub>xxx</sub>b will be increase the levels of the isoform ratio.

PCR was highly significant (F (DFn, DfD) =4.889 (1,15), p=0.043 for all measures; chondropathy score; SRPK1; SRSF1; SRSF1 localisation; pan-VEGF-A; VEGF-A<sub>xxx</sub>a; VEGF-A<sub>xxx</sub>b/VEGF-A<sub>xxx</sub>a ratio; DYRK1a, knee pain; effusion, synovial thickening; Heberden's nodes; osteophytes p=0,043.

The linear regression model generated was

$$\text{VEGF-A}_{xxx}b = 0.36 - 0.0001 * \text{Chondropathy score} - 0.15 * \text{SRPK1} - 0.12 * \text{SRSF1} - 0.0006 * \text{nuclear SRSF1} - 0.06 * \text{panVEGF-A} - 0.1 * \text{VEGF-A}_{xxx}a \text{ FA} + 0.006 * \text{VEGF-A}_{xxx}b / \text{VEGF-A}_{xxx}a \text{ ratio} - 0.09 * \text{DYRK1a} - 0.018 * \text{presence of knee pain} - 0.017 * \text{presence of effusion} - 0.013 * \text{presence of synovial thickening} - 0.006 * \text{presence of Heberden's nodes} - 0.015 * \text{presence of osteophytes}.$$

The positive values in the regression equation indicate a positive relation between the variables and the VEGF-A<sub>xxx</sub>b fractional area while the negative values indicate a negative relationship. The ratio of VEGF-A<sub>xxx</sub>b/VEGF-A<sub>xxx</sub>a was significantly and positively related to the levels of the VEGF-A<sub>xxx</sub>b isoform, whereas grade 4 chondropathy, SRPK1, SRSF1 (expression and localisation levels), pan-VEGF-A, VEGF-A<sub>xxx</sub>a, DYRK1a expression, effusion, synovial thickening, Heberden's nodes, osteophytes, and presence of pain were all significantly and negatively related to the VEGF-A<sub>xxx</sub>b isoform.

### **4.3.3 Alterations in the splicing axis SRPK1, SRSF1, panVEGF-A and VEGF-A<sub>xxx</sub>b in synovial tissue during synovitis**

Advanced OA cases, after qualitative assessment, displayed more severe synovial changes, with increased cellularity, inflammatory cell infiltration and lymphoid aggregates in most cases.

To test hypotheses 1- 4, the expression levels of the panVEGF-A splicing axis and activated (nuclear) SRSF1 were determined in the following knee synovium samples: 1. post-mortem knee synovium (n=20) from patients with no pain documented and known to not have sought help for knee pain prior to their death.; 2. group comprised of samples from people undergoing total knee replacement (TKR) for OA knee pain showcasing symptomatic chondropathy. The same samples were used throughout the studies to reduce the variance of the results.

### 4.3.4 Expression of SRPK1 is increased in the synovium from patients with painful symptomatic OA compared to controls showcasing asymptomatic chondropathy

Three samples per group were lost during the processing of the slides, due to poor adhesion of the tissue on the slides and the nature of the experiments. Data therefore derive from a total sample size of 34 (n=17 per group) (power calculations have not been affected due to lower N size as it has been confirmed post-hoc).

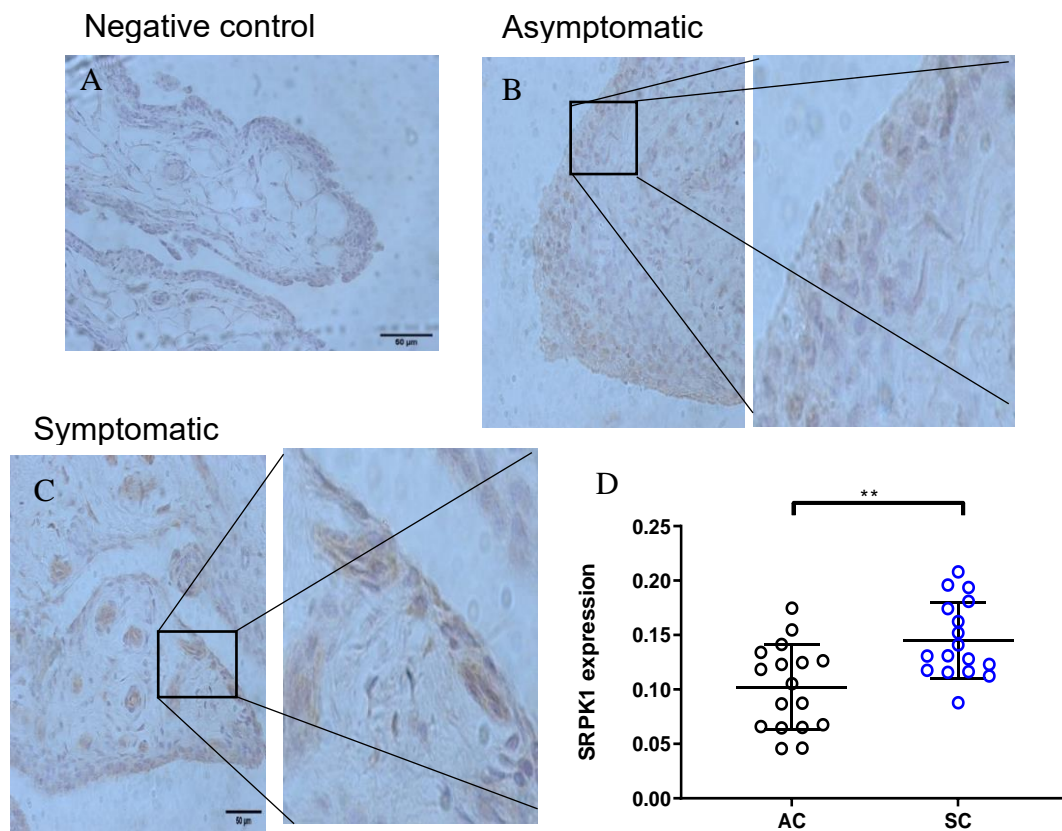


**Figure 35 SRPK1 expression in synovium from human tissue. A-C typical images SRPK1 immunoreactivity. A-C Representative images of synovial lining from the 2 groups in the study. A) representative image from the negative control, with no evident non-specific binding. B) Photomicrographs from the asymptomatic chondropathy group showcasing SRPK1 immunoreactivity with a thin synovial lining C) Representative image from the symptomatic chondropathy group with a distinct expression pattern around the vessels and endothelial cells D) Significant increase in the immunoreactivity of SRPK1 was reported as expressed by fractional area for the painful, symptomatic chondropathy group compared to the controls  $p=0.0063$  SC cf. AC.  $N=34$ . Mann-Whitney's non-parametric test.**

The immunoreactivity of SRPK1 as expressed per fractional area. The symptomatic chondropathy, painful group showed increased levels of expression of SRPK1, compared to the non-painful, non-symptomatic controls (Figure 36 A-D,  $p= 0.0068$ )

#### **4.3.5 Expression and activation of SRSF1 is increased in the synovium from patients with symptomatic painful OA compared to controls**

Samples used belonged to the same pool of samples as for the SRPK1 study. Similarly, to the previous study, samples were lost due to poor adhesion of the tissue on the microscopic slides lowering the final sample size to 16 for the symptomatic chondropathy group and 15 for the non-symptomatic. Expression of SRSF1 was determined by fractional area of the immunoreactivity, to determine whether there were increased numbers of cells expressing the splicing factor. Expression of SRSF1 was significantly higher in the painful symptomatic chondropathy group compared to the controls (\*\* $p=0.003$  Mann-Whitney, two-tailed t-test) Fig 37.

Visual inspection of images from SRSF1-stained tissues showed large numbers of cells in the synovium with nuclear SRSF1 staining. To quantify the localisation levels of SRSF1 cell counting was performed as described in Methods, using the same cases as in the previous study

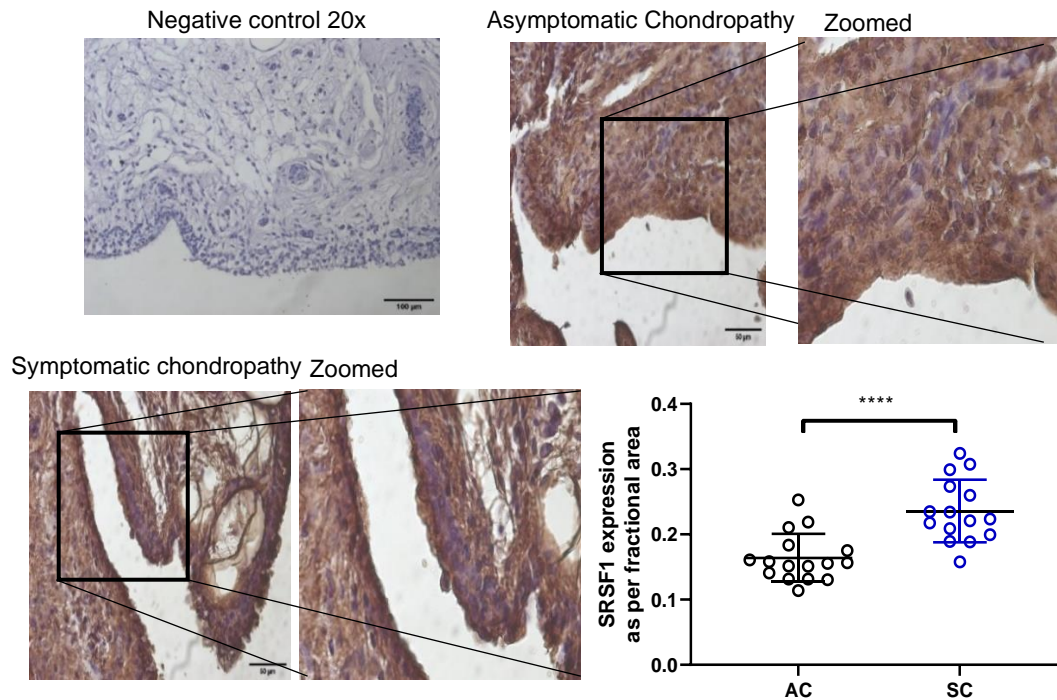


**Figure 36 SRSF1 expression in synovium from human tissue. A-C typical images SRSF1 immunoreactivity. A-C Representative images of synovial lining from the 2 groups in the study. Photomicrographs from the asymptomatic chondropathy group showcasing SRSF1 immunoreactivity with a thin synovial lining as well as in the inflamed synovium. Representative image from the symptomatic chondropathy group. Significant increase in the immunoreactivity of SRSF1 was reported as expressed by fractional area for the painful, symptomatic chondropathy group compared to the controls \*\*\*\* $p < 0.005$  SC cf. AC. Mann-Whitney's non-parametric test.**

The ratio of SRSF1 nuclear positive cells/ positive cells was calculated. A significant increase in the nuclear localisation translated as an increased ratio of nuclear to total positive cells from the TKR group to the control would suggest an increase in the translocation of SRSF1 in the nuclei of the cells, thus an increased activation rate of SRSF1 ( $p = 0.0005$ , AC  $n = 16$ , SC  $n = 15$ ) (Figure 38).

SRSF1 - SC

Zoomed

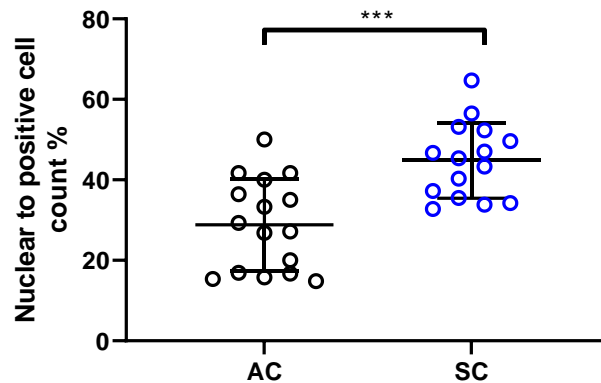
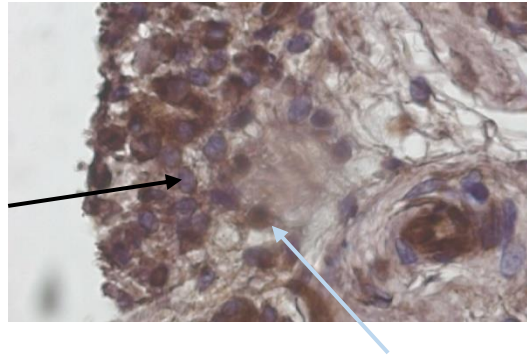
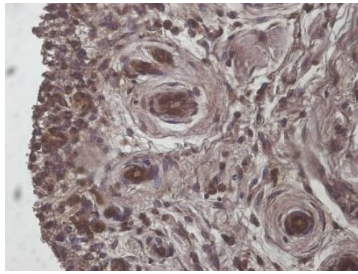


**Figure 37** SRSF1 is expressed in the cytosol in normal physiological conditions, and it is translocated in the nuclei during disorders such as OA. In blue arrows nuclear staining can be observed indicating SRSF1 presence in the nucleus. The black arrow showcases what a clean nucleus would look like with no nuclear staining present (except Haematoxylin). There was a significant increase in the nuclear localisation (activation) of SRSF1 in SC painful samples compared to AC ( $p=0.0005$ , AC  $n=16$ , SC  $n=15$ ). Mann-Whitney's non-parametric test.

#### **4.3.6 Expression of panVEGF-A is increased during painful OA compared to controls in knee synovial tissue**

The panVEGF-A antibody used is a mouse monoclonal IgG1 raised against the amino acids 1-140 of human VEGF, and with the ability to detect the 189, 165, 121 amino acid variants of VEGF-A. Similar to the previous studies, the same samples were discarded due to the tissue not adhering to the slides thus the final sample size was smaller (SC =15, AC=17). However, the power of the experiments was not affected by the lower  $n$  numbers. PanVEGF-A immunoreactivity as expressed per fractional area is significantly increased in symptomatic chondropathy cases compared to PM (\*\* $p<0.01$  cf control) (Fig 39).

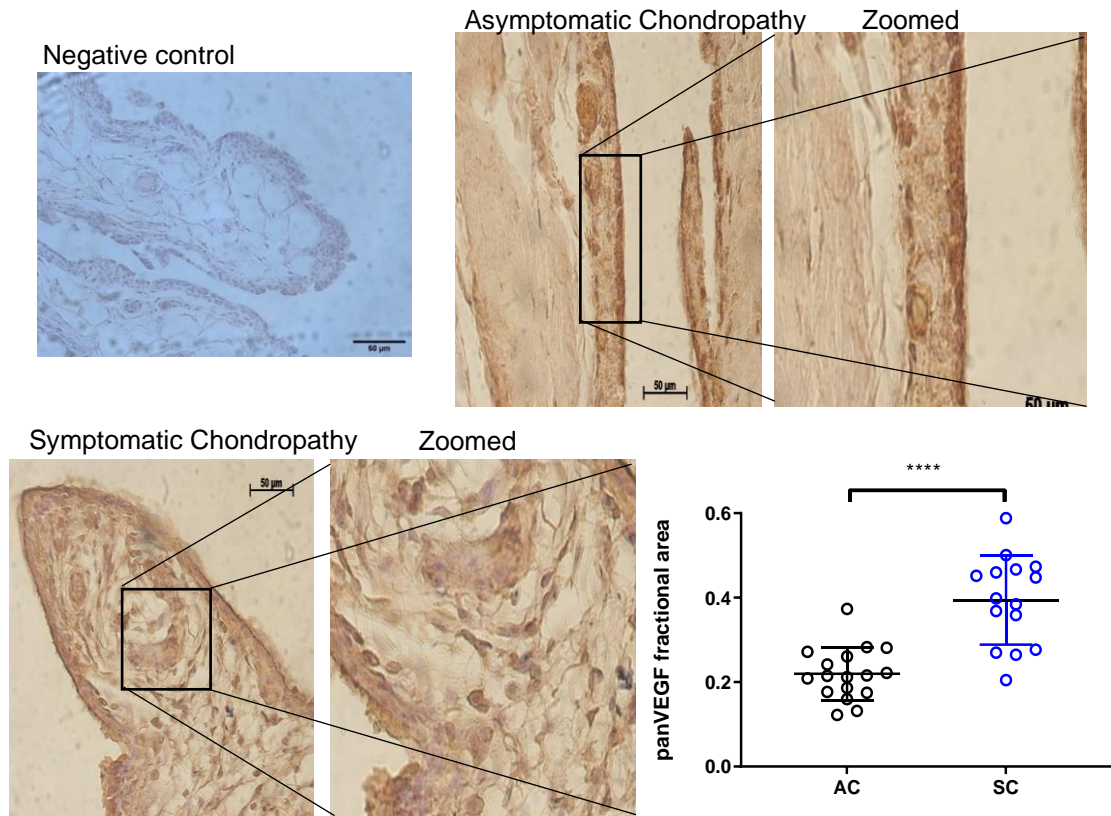


**Figure 38** Photomicrographs of representative samples of human synovium, showing the expression pattern of panVEGF-A in the two distinct groups. Fractional area of panVEGF-A immunoreactivity is significantly higher in the painful symptomatic group cf. controls (  $**p < 0.01$  cf control). Mann-Whitney's non-parametric test

The expression of panVEGF-A, as measured by fractional area and staining intensity, is increased, indicating that VEGF-A plays a role in painful OA, but whether this is associated with an altered splice variant ratio is unknown. As there are 2 families of isoforms for VEGF-A I investigated expression of both the VEGF-A<sub>xxx</sub>b and VEGF-A<sub>xxx</sub>a isoform to identify if the change in expression of panVEGF-A could be attributed to one or both isoforms.

#### **4.3.7 Expression of the VEGF-A<sub>xxx</sub>b and VEGF-A<sub>xxx</sub>a isoforms in human knee synovium is significantly associated to painful OA in comparison to non-painful controls.**

The expression of the anti-angiogenic and anti-nociceptive isoform VEGF-A<sub>xxx</sub>b was determined in the same cases. Two groups were used as before with some cases being lost due to tissue not adhering to the slides (Figure 40). VEGF-A<sub>xxx</sub>b expression was detected in cases from both groups

(Figure 41 A-D). VEGF-A<sub>xxx</sub>b was significantly decreased in the painful OA (SC) group (\*\*\*\*p<0.01 cf control n= 16 PM, n=13 OA), while VEGF-A<sub>xxx</sub>a was significantly increased in painful (SC, symptomatic chondropathy) cases compared to the non-painful cases with equivalent chondropathy and synovitis scores (\*p<0.01 cf control n= 15 AC, n= 15 SC).

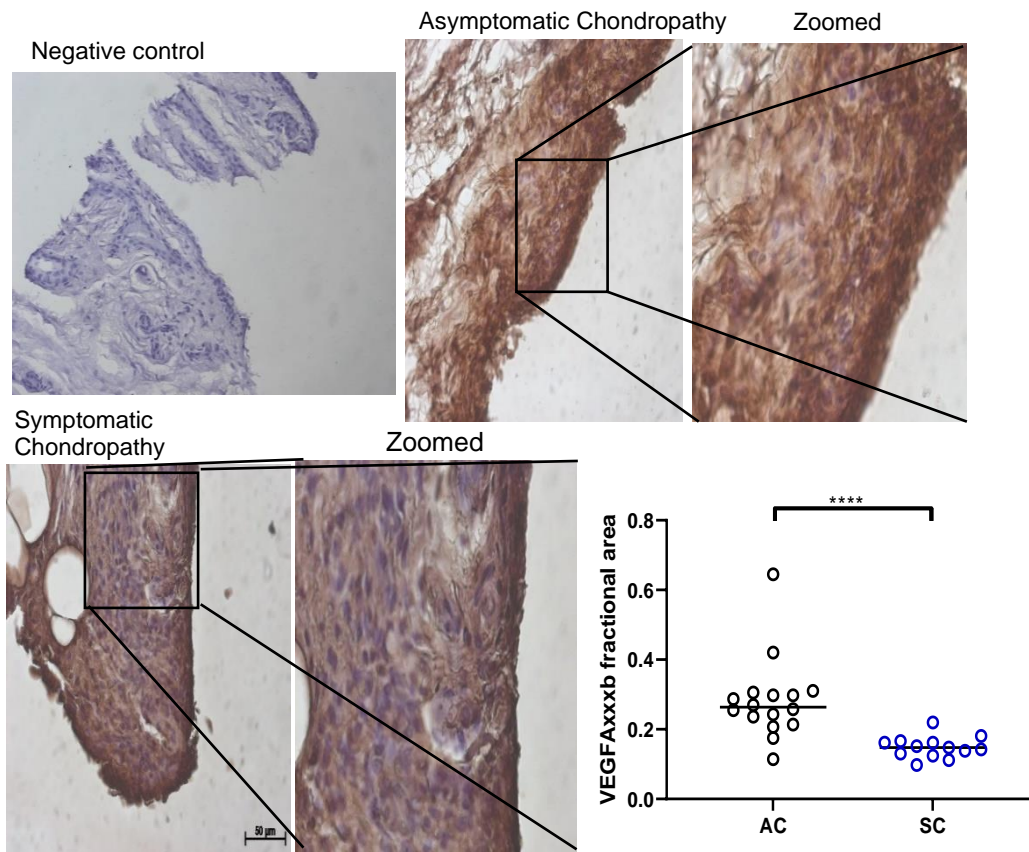


**Figure 39 Photomicrographs of representative samples from human knee synovium showing the expression pattern of VEGF-A<sub>xxx</sub>b between the symptomatic and non-symptomatic groups. Fractional area of the immunoreactivity of VEGF-A<sub>xxx</sub>b was calculated showcasing a decreased expression of the isoform in the symptomatic painful chondropathy compared to the non-painful group (\*\*\*\*p<0.01 cf control). Mann-Whitney's non-parametric test**

I then investigated the expression of the VEGF-A<sub>xxx</sub>a isoform using the same cases. As before there were 2 groups (painful symptomatic chondropathy and non-painful asymptomatic chondropathy) with 15 samples per group. The difference in numbers from the previous study was due to experimental conditions and loss of sections, which however did not affect the power of the experiment. VEGF-A<sub>xxx</sub>a expression was detected in both groups (Figure 41) and was found to be significantly increased in painful, symptomatic chondropathy TKR cases compared to the PM cases with no pain (\*p<0.01 cf control, n= 15 PM, n= 15 OA

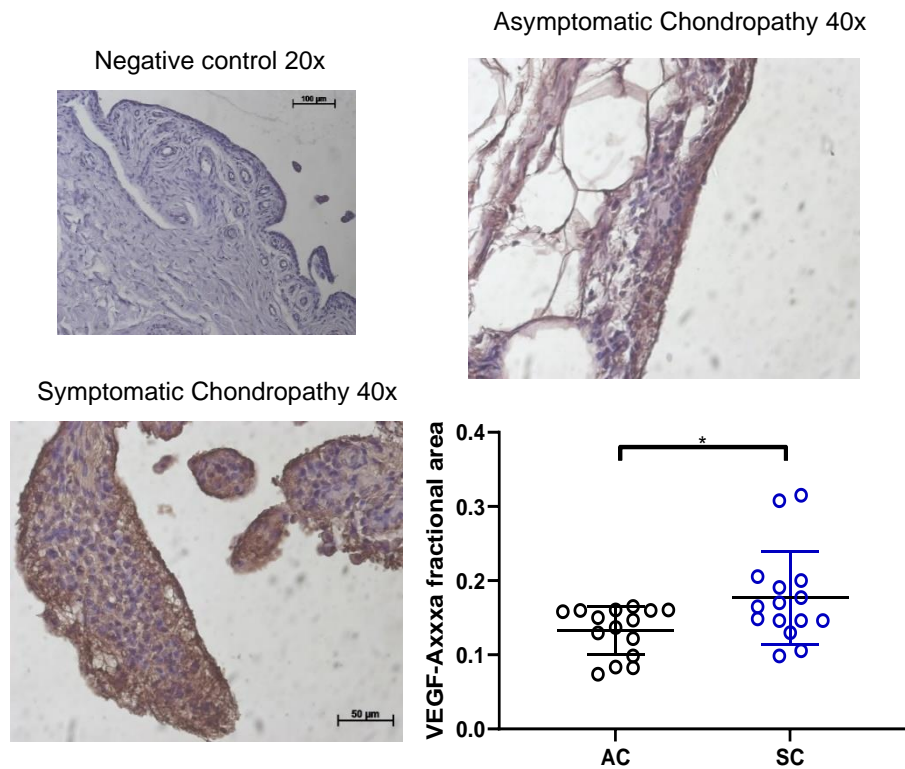


**Figure 40** Photomicrographs of representative samples from human knee synovium showing the expression pattern of VEGF-A<sub>xxx</sub>a in the two different groups. Fractional area of the immunoreactivity of VEGF-A<sub>xxx</sub>a significantly increased in symptomatic chondropathy cases with recorded pain compared to the asymptomatic cases with no pain scores (\* $p < 0.01$  cf control). N= 15 PM, n= 15 OA Mann-Whitney's non-parametric test

Finally, I investigated the relationship between the two isoform families expressed as a ratio of the VEGF-A<sub>xxx</sub>b isoform to VEGF-A<sub>xxx</sub>a isoform (Figure 42), to identify if there is relationship between VEGF-A splice variants and pain. The VEGF-A<sub>xxx</sub>b/VEGF-A<sub>xxx</sub>a isoform ratio was significantly higher for the AC group with pain-free asymptomatic chondropathy cases compared to the TKR cases with high pain scores (PM n= 12, OA n=13 \*\*\* $p < 0.01$  cf. controls)

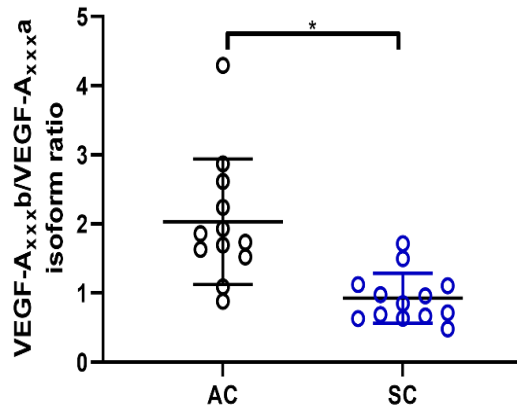


**Figure 41** VEGF-A<sub>xxx</sub>b/ VEGF-A<sub>xxx</sub>a expression ratio for the two groups. The exact same matched samples were used as in the previous individual hypothesis. Ratio of VEGF-A<sub>xxx</sub>b/ VEGF-A<sub>xxx</sub>a as per fractional area, the ratio is significantly increased in the asymptomatic chondropathy group denoting an increase either in the VEGF-A<sub>xxx</sub>b levels or a decrease in the VEGF-A<sub>xxx</sub>a levels when compared to the symptomatic chondropathy cases. P<0.01, Mann-Whitney's non-parametric test.

#### **4.3.8 Expression of the splicing kinase Dyrk1A is related to the increased levels of pain encountered in symptomatic chondropathy cases compared to asymptomatic chondropathy**

Samples used belonged to the same pool of samples as for the previous studies. Similarly, samples were lost due to poor adhesion of the tissue on the microscopic slides lowering the final sample size to 18 for the symptomatic chondropathy group and 15 for the non-symptomatic. Expression of DYRK1a was determined by fractional area of the immunoreactivity, to determine whether there were increased numbers of cells expressing the kinase. Expression of DYRK1a was significantly higher in the painful symptomatic chondropathy group compared to the controls Fig 43 (\*\*\*\*p=0.0001 Mann-Whitney, two-tailed t-test)

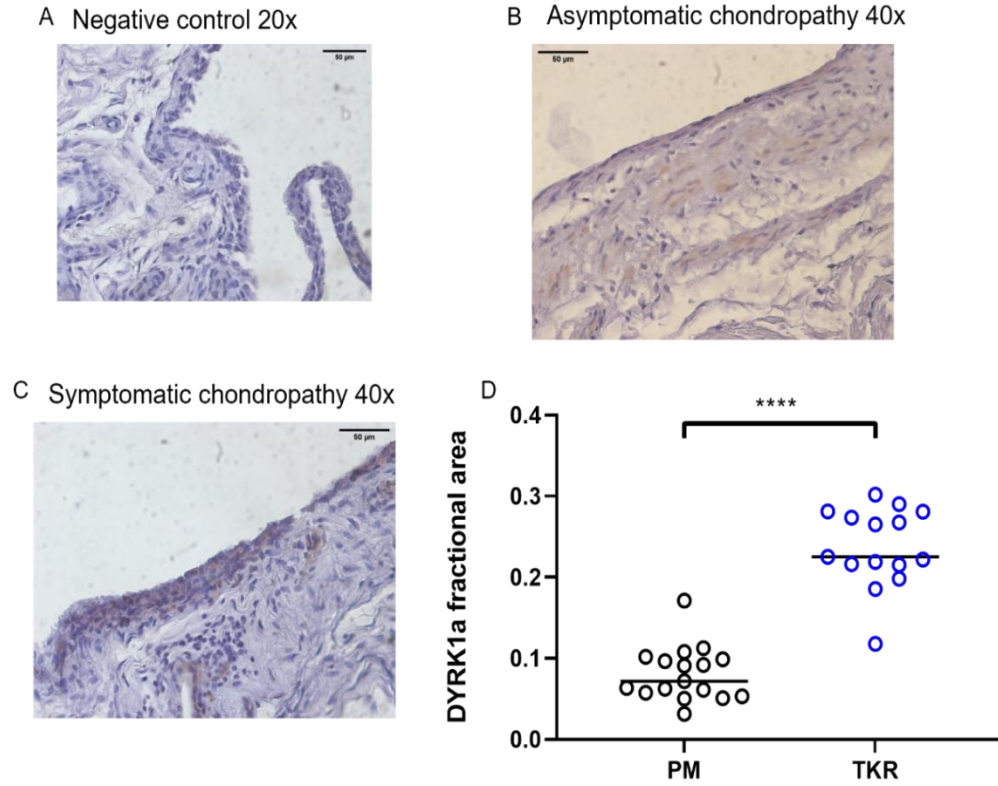


**Figure 42 A-C) Photomicrographs of representative samples from human knee synovium showing the expression pattern of the splicing kinase DYRK1a in the two distinct groups. D) Fractional area of the immunoreactivity of DYRK1; TKR cf PM  $p=0.0001$ ; Mann-Whitney's non-parametric test**

#### 4.4 Summary of the results

- There was increased expression of the splicing kinase SRPK1 in the symptomatic chondropathy (SC) group compared to the asymptomatic (AC) group
- There was increased expression of the splicing kinase SRSF1 in the symptomatic chondropathy (SC) group compared to the asymptomatic (AC) group. Activation of SRSF1 as analysed by the degree of nuclear localisation of the splicing factor was also significantly increased in the SC group compared to the controls.
- The expression of panVEGF-A and DYRK1a were significantly increased in the SC group compared to the controls.
- VEGF-A<sub>xxx</sub>b expression increased in the AC group compared to SC group, while VEGF-A<sub>xxx</sub>a expression was increased in the SC group compared to the control. The ratio of VEGF-A<sub>xxx</sub>b/VEGF-A<sub>xxx</sub>a was significantly increased in the AC group.

#### 4.5 Discussion

In these studies, I tested the hypotheses that the splicing axis SRPK1/SRSF1/VEGF-A was altered in painful symptomatic chondropathy cases (knees from patients who undergone TKR) when compared to non-painful asymptomatic chondropathy patients.

VEGF-A has recently become recognised as having a role in neuropathic pain development and maintenance, although there is less information on this in the context of arthritis. Although pan-VEGF-A has been extensively studied in both RA and OA, the VEGF-A splicing axis and splice variants had not been investigated in the context of these diseases. Here I studied the relationships between the expression of VEGF-A, the VEGF-A alternative splice variant families and constituents of the VEGF-A alternative splicing axis isoforms with pain.

A range of features in OA are associated with the presence of painful symptomatic OA (Takano, Uchida et al. 2018), including but not limited to bone and neurovascular invasion of articular cartilage, with VEGF evoking pain through VEGFR1 and VEGFR2, and inflammatory flares (Nagao, Hamilton et al. 2017). Inhibition of VEGF receptor signalling leads to reduced pain (Hamilton, Nagao et al. 2016) suggesting that targeting of VEGF ligands or receptors may potentially counteract arthritis and associated pain.

Structural changes such as subchondral bone alterations contribute to knee OA pain according to recent studies (Zhang, Nevitt et al. 2011), and by matching for chondropathy I could exclude

one confounding variable and focus on the symptomatic vs asymptomatic aspect of the OA disease to investigate.

As a result of this association between chondropathy and age, the specificity and association of disease with macroscopic changes in the joint can be questioned. To address this, cases were carefully selected from a large repository and were age and chondropathy matched cases with reported pain and controls with no reported pain.

#### **4.5.1 Expression of SRPK1 is increased in the synovium from patients with painful symptomatic OA compared to controls with asymptomatic chondropathy**

I investigated the expression of SRPK1 in arthritic synovium from symptomatic (painful) cases compared to tissue from non-painful cases. I hypothesised that increased SRPK1 immunoreactivity would be found in the painful cases, as increased kinase expression could also contribute to increased phosphorylation of SRSF1, and an increase of the pro-nociceptive isoform VEGF-A<sub>xxx</sub>a. SRPK1 expression significantly increased in the SC group, in line with our initial hypothesis, showing a relationship between OA and splicing mechanisms (Zhang, Qi et al. 2021), but in this case a different mechanism of back splicing in the formation of circular RNA formation.

An increase in the expression levels of SRPK1 potentially translates to an increase in the activation/phosphorylation and nuclear localization of its downstream splicing factor SRSF1 with an assumed alteration of VEGF-A splice variant isoforms. While SRPK1 has not been thoroughly researched in the context of arthritis pain, it is strongly implicated in neuropathic pain through control of VEGF-A (Hulse, Beazley-Long et al. 2014, Hulse, Drake et al. 2016, Bridgett, Dellett et al. 2017, Llorián-Salvador and González-Rodríguez 2018, Li, Li et al. 2020).

Currently, evidence suggests that inhibition of SRPK1 in neuropathic, chronic, or nociceptive pain may have a potential analgesic effect (Hulse 2017, Llorián-Salvador and González-Rodríguez 2018). However, in the context of arthritis we still do not understand how the downstream targets of SRPK1 affect pain, and whether potential analgesic effects evident in other disease models on selective inhibition of SRPK1 will also apply in other disease models, or in painful human diseases.

#### **4.5.2 Expression and activation of SRSF1 is increased in the synovium from patients with symptomatic painful OA compared to controls**

The downstream target of SRPK1, SRSF1, is phosphorylated by SRPK1 thereby altering the location and function of the splicing factor. Both the expression and activation of SRSF1 were significantly increased in the painful OA compared to non-painful OA, demonstrating a relationship between SRSF1 function and a painful OA phenotype. SRPK1-SRSF1 driven alternative pre-mRNA splicing of VEGF-A towards VEGF-A<sub>xxx</sub>a isoforms in the synovium could result in activation of synovial nociceptive neurons in OA, leading to pain. In asymptomatic chondropathy cases, reporting no pain, this SRSF1 activation was not seen, further supporting our hypothesis, and suggesting a contribution to the pain in symptomatic chondropathy.

In addition to the possibility that altered synovial VEGF-A splicing could exert the known direct actions of VEGF-A<sub>165a</sub> leading to the sensitisation of sensory neurons through actions on TRPV1 and TRPA1 channels (Beazley-Long, Hua et al. 2013, Hulse, Beazley-Long et al. 2014), SRSF1 may also act in sensory neurons to change their nociceptive functions. There is evidence of increased nuclear localisation of SRSF1 in injured neurons in rats with neuropathic pain, although the downstream targets of any effect on alternative splicing or pre-mRNA transport are unknown (Hulse, Drake et al. 2016). SRSF1 also contributes to nociceptive neuronal function through the control of neuronal TRPA1 channel alternative splicing.

These are the first data to show that expression and importantly activation of the splicing factor SRSF1 are associated with pain in OA. Although all the downstream actions of SRSF1 in OA synovium remain to be discovered, these data support the hypothesis the complex of SRPK1-SRSF1 plays a role in the development and maintenance of arthritic pain, possibly through alternative splicing of VEGF-A.

#### **4.5.3 Expression of panVEGF-A is increased during painful symptomatic chondropathy in OA compared to controls in knee synovial tissue**

The expression of panVEGF-A (i.e., all VEGF-A isoforms) was investigated in the painful SC group and compared to the AC group (controls) using an antibody that identifies all the VEGF-A

isoforms as it recognises the N terminus of the protein. All VEGF-A splice variants, in both families have a common N terminus (Figure 5 in intro), which is recognised by all available commercial anti-VEGF-A antibodies. VEGF-A has been widely studied and discussed with regard to its pro-inflammatory role in the pathogenesis in OA and RA as shown and discussed in Chapter 3.4, but in this study, I controlled for joint damage and inflammation to isolate the relationship between painful OA and VEGF-A expression and splicing. It is important to note however that the increased angiogenesis stimulated by increased VEGF-A, provided this was an increase in the pro-angiogenic VEGF-A<sub>xxx</sub>a isoforms, would also translate to increased macrophage migration and promote pain sensitization (Corliss, Azimi et al. 2016, Britto, Wyroba et al. 2018).

As previously reported VEGF-A was increased in OA synovium, but in our study only in the painful OA group. Only one study has reported a relationship between panVEGF-A expression and pain, where VEGF-A levels were higher in synovium from people with OA who reported high levels of pain (VAS score >6) compared to people with mild or moderate pain (VAS<6). The authors showed that VEGF-A could stimulate the production of apelin in synoviocytes, which is also a pro-nociceptive molecule (Takano, Uchida et al. 2018). Synovial VEGF-A expression could therefore evoke pain through either apelin, or through the direct effects of VEGF-A<sub>xxx</sub>a on nociceptive neurons (Hulse, Beazley-Long et al. 2014), provided that the increase in VEGF-A reflects a change in VEGF-A splice variants to increase expression of the pro-nociceptive VEGF-A<sub>xxx</sub>a. A potential mechanism through which VEGF-A may promote pain could be through direct effects on A $\delta$  fibres, which has been shown to be directly affected by increased levels of VEGF-A as well as by the complex of VEGF-A/VEGFR1 (Selvaraj, Gangadharan et al. 2015).

VEGF-A has been reported to alter nociception through both the VEGFR1 and VEGFR2 receptors (Beazley-Long, Moss et al. 2018), with inhibition of the receptors leading to reduction of pain sensitivity (Llorián-Salvador and González-Rodríguez 2018, Micheli, Parisio et al. 2021) . Targeting of VEGF receptors may not however be a useful analgesic strategy in OA pain, partly as both VEGFR1 and VEGFR2 have been implicated in nociception/pain, and partly as block of VEGF receptors results in changes in blood pressure (Cooper, Carter et al. 2019) that are unlikely to be well tolerated in the population with painful OA, that is a largely elderly population with comorbidities such as hypertension (Wong, Mak et al. 2022).

Increased VEGF-A levels identified in our study are also in accordance to previously published data (Hamilton, Nagao et al. 2016, Nagao, Hamilton et al. 2017, Qian, Xu et al. 2021). VEGF-A and nerve growth factor (NGF) are important growth factors in inflammatory arthritis, as both contribute to angiogenesis, and neuronal growth, survival, protection and axon/neurite outgrowth (Beazley-Long, Hua et al. 2013) and nociceptive neuronal sensitisation (McKelvey, Shorten et al. 2013, Hulse, Beazley-Long et al. 2014). Crosstalk between the two factors may therefore be an additional mechanism through which VEGF-A may acts on sensory neurons.

#### **4.5.4 The relative expression of the VEGF-A<sub>xxx</sub>b and VEGF-A<sub>xxx</sub>a splice isoforms in human knee synovium is significantly altered in painful OA.**

Even though VEGF-A has been intensively investigated for its contribution to arthritis and nociception, that cannot be said for the alternative splice variants VEGF-A<sub>xxx</sub>a and VEGF-A<sub>xxx</sub>b which have pro-nociceptive and anti-nociceptive functions respectively. The expression of the different splice variants *within* the VEGF-A family has been investigated; for example, VEGF-A<sub>189</sub>, VEGF-A<sub>165</sub> and VEGF-A<sub>121</sub> splice variants and VEGFR2 mRNA have been reported in OA (Pufe, Petersen et al. 2001, Petersen, Tsokos et al. 2002, Enomoto, Inoki et al. 2003, Fay, Varoga et al. 2006), and normal cartilage (Enomoto, Inoki et al. 2003), although there is disagreement as to which isoforms are expressed. VEGF-A<sub>165</sub> and VEGF-A<sub>121</sub> are reported in RA synovium (Pufe et al., 2001b). In respect to our results, an increase in VEGF-A in relation to pain would suggest that the pro-nociceptive isoform VEGF-A<sub>xxx</sub>a, would also increase, while VEGF-A<sub>xxx</sub>b would decrease or stay the same.

To identify whether the increase in pan-VEGF-A levels was specific to certain isoforms as hypothesised or if it represented an overall upregulation of all VEGF-A splice variants with no change in relative expression of the splice variant families. I investigated the expression of VEGF-A<sub>xxx</sub>b and VEGF-A<sub>xxx</sub>a isoforms using specific antibodies for these splice variants. The isoform specific anti-VEGF-A splice variant antibodies were developed by DO Bates; the anti-VEGF-A<sub>xxx</sub>b antibody is commercially available, but the anti-VEGF-A<sub>xxx</sub>a specific antibody was a gift from DO Bates. In accordance with the hypothesis, and the evidence for pro- and anti-nociceptive properties of the alternatively spliced isoform families, VEGF-A<sub>xxx</sub>b expression was significantly

higher in the pain-free OA group and VEGF-A<sub>xxx</sub>a expression was significantly higher in the painful OA group.

Previous literature has confirmed the pro-nociceptive actions of VEGF-A<sub>xxx</sub>a, both on nociceptive behaviour in rats and mice, and when administered directly to primary C-fibre nociceptive *afferents in vivo* (Hulse, Beazley-Long et al. 2014). VEGF-A<sub>xxx</sub>a activates (causes action potential firing) and sensitizes (lowers the threshold at which action potential firing occurs) C nociceptors through VEGFR2 and intracellular signalling that affects the transduction of stimuli by Transient Receptor Potential (TRP) channels, namely TRPV1 and TRPA1 (Hulse, Beazley-Long et al. 2014), (Llorián-Salvador and González-Rodríguez 2018)). VEGF-A<sub>xxx</sub>b exerts anti-nociceptive functions by competing with VEGF-A<sub>xxx</sub>a for VEGFR binding, and potentially through alternative intracellular signalling pathways, which are not yet understood. The synovial angiogenesis and cell proliferation evident during OA is driven by an upregulation of VEGF-A (section 4.3.6), and based on these results, that is also largely due to an upregulation of VEGF-A<sub>xxx</sub>a. This is the first report of a difference in VEGF-A alternative splice variant expression in synovium from painful OA knee joint.

With regard to the physiological or pathophysiological effects of VEGF-A, it is the balance of the different isoforms that dictates whether there is a pro-angiogenic, pro-nociceptive (VEGF-A<sub>xxx</sub>a > VEGF-A<sub>xxx</sub>b) or anti-angiogenic, anti-nociceptive (VEGF-A<sub>xxx</sub>a < VEGF-A<sub>xxx</sub>b) environment I therefore compared the ratio of the two isoforms in painful and non-painful OA. As hypothesised, VEGF-A<sub>xxx</sub>b: VEGF-A<sub>xxx</sub>a ratio was significantly greater in pain free OA than painful OA. As the pain-free group had evidence of both chondropathy and synovitis that was not significantly different from the painful OA group (Table 13), enabling me to control for these aspects of joint disease, and allowing the associations between presence of pain and VEGF-A splicing to be explored.

Inflammation was present in both groups (Table 13) but examination of Figure 42 shows that in the pain-free OA synovium, the VEGF-A<sub>xxx</sub>b: VEGF-A<sub>xxx</sub>a ratios are >1 in all bar one case. This indicates that despite the presence of inflammation, the majority of the cases were in an anti-angiogenic, and anti-nociceptive state, as non-reported pain. In contrast, 50% of the painful OA synovium cases were in a pro-angiogenic, but all cases reported pain. The reported pain cannot

therefore be entirely attributable to inflammation, and some is probably also attributable to other pro-nociceptive mediators, as well as VEGF-A. The ratio of VEGF-A<sub>xxx</sub>b to VEGF-A<sub>xxx</sub>a, as shown above, is lower in the painful symptomatic chondropathy samples, being explained by the relative increase of the pro-nociceptive isoform, an effect that has been described in investigations of chronic and or neuropathic pain in animal models (Richard P. Hulse, 2017; R. P. Hulse et al., 2014b; Llorián-Salvador & González-Rodríguez, 2018a).

Given the relationship between the isoforms ratios and pain, a case could also be made for the isoform ratio in synovium, or synovial fluid if the VEGF-A isoform ratios reflect those in synovium, as a biomarker for pain in OA. The VEGF-A<sub>xxx</sub>b: VEGF-A<sub>xxx</sub>a ratio might be predictive of potential response to interventions that alter VEGF-A isoform ratio or splicing such as treatment with VEGF-A isoform recombinant protein or inhibition of SRPK1 splicing. If someone with OA is experiencing pain, and there is evidence of a low VEGF-A<sub>xxx</sub>b: VEGF-A<sub>xxx</sub>a ratio, then such anti-VEGF-A<sub>xxx</sub>a therapy might be more effective whereas if the VEGF-A<sub>xxx</sub>b: VEGF-A<sub>xxx</sub>a is high then it may not be effective. For example, a similar response profile can be encountered in cancer treatment, when patients with low VEGF-A<sub>xxx</sub>b: VEGF-A<sub>xxx</sub>a ratios in metastatic colorectal cancer respond to bevacizumab, while those with high VEGF-A<sub>xxx</sub>b: VEGF-A<sub>xxx</sub>a ratios do not exhibit same responses (Bates, Catalano et al. 2012).

#### **4.5.5 Expression of the splicing kinase Dyrk1A is related to pain in symptomatic chondropathy OA cases compared to asymptomatic chondropathy**

I hypothesised that increased DYRK1a immunoreactivity would be prevalent in painful OA synovium. DYRK1a is also important in angiogenesis, where it regulates VEGF pro-angiogenic actions (Rozen, Roewenstrunk et al. 2018) and may therefore also interact with VEGF in other functions such as pain. Lorecivivint, a Wnt inhibitor that acts through inhibition of CLK2 and DYRK1a also reduces pain in OA models in rodents (Deshmukh, O'Green et al. 2019). DYRK1a homozygous and heterozygous knockout mice display increased nociceptive functions suggesting a role for DYRK1a in pain sensitivity (Brault, Nguyen et al. 2021). This supports our hypothesis and agrees with our findings of significantly increased DYRK1a expression in the SC group. DYRK1a knockout also affects the expression of six immediate-early genes (IEGs), specifically Nr4a1 (Nurr77), Arc (Arg3.1), Npas4, c-Fos,, Egr1 (Zif268) and Fos-b.(Brault, Nguyen et al. 2021). These immediate early genes are upregulated in neurons (i.e., glutamatergic

neurons) and implicated in neuronal plasticity (Brault, Nguyen et al. 2021) and are also associated with both pain and VEGF-A expression. For example, c-Fos, promotes the expression of dynorphin, involved in endogenous analgesia and modulating responses to several psychoactive substances, including cocaine, implicated in pain states., It is also involved in immune function being highly expressed in macrophages and however, it is quiescent in fibroblasts, but upregulated during monocytic differentiation (Ahmad and Ismail 2002). VEGF-A's pro-angiogenic properties, presumably derived from the VEGF-A<sub>xxx</sub>a isoform, are mediated through Nurr77 in HUVECs (Zeng, Qin et al. 2006). DYRK1a is a key player in inflammation and pain in OA, as shown by the actions of Lorecivint, a novel Wnt inhibitor acting through potent Clk-2 and DYRK1a inhibition which has the effect of reducing pain and inflammation in OA animal models (Deshmukh, O'Green et al. 2019) and recently in several clinical trials (Deshmukh, Ibanez et al. 2020, Yazici, McAlindon et al. 2020, Tambiah, Kennedy et al. 2021, Yazici, McAlindon et al. 2021). Nevertheless, the underlying mechanism through which DYRK1a alters pain, the mechanisms and functional interactions of VEGF-A and DYRK1a are unknown (Di Cesare Mannelli, Tenci et al. 2018).

#### **4.6 Concluding remarks and limitations**

These data show that the VEGF-A splicing cascade of SRPK1/SRSF1/VEGF splicing variants is altered in painful OA. Increases in the VEGF-A<sub>xxx</sub>a isoform expression are linked to, and potentially drive pain. I have shown that in OA the levels of VEGF-A<sub>xxx</sub>a isoform are increased and the VEGF-A<sub>xxx</sub>b levels reduced in painful symptomatic chondropathy cases compared to the control groups (asymptomatic chondropathy), however the overall level of the total VEGF-A is increased. Better understanding of the control and expression of the balance of VEGF-A isoforms could potentially open new options regarding pain management. Moreover, a case can be made regarding the VEGF-A<sub>xxx</sub>b/ VEGF-A<sub>xxx</sub>a ratio of isoforms to be potentially used as a predictor of OA pain, however we still do not yet understand how the isoform expression is altered from early to end stage OA. Finally, I have shown that DYRK1a is also upregulated in synovium from painful OA joints, and evidence suggest that although the principle functions of DYRK1a are in neurodegeneration, it may also interact with VEGF-A in pain states

This study has a number of a number of limitations in common with the inflammation study, including the tissue donors all being of Caucasian ethnic group, thus rendering it impossible to extrapolate the mechanisms proposed to different ethnic groups. The donor tissue derives from

people with a diagnosis of OA >5, years and may therefore represent mid-late-stage OA. Although cases are matched for chondropathy and synovitis, the durations of disease and pain symptoms are unknown. This approach can only give a snapshot of painful OA of duration >5 years, however it poses questions on how the expression of the VEGF-A splicing axis may be altered in early or mid-stage OA. Similar study of early or mid-stage OA would require invasive procedures that might not be justified.

Possibly the most important limitation is that specific pain scoring is not available for any of the cases. For asymptomatic PM cases, the information comes from questionnaires answered relatives and only confirms whether the donor had reported or been treated for knee pain in the year prior to death, and for the symptomatic cases the only pain information is that all donors had a reported pain score on VAS of >8. This limitation means that I cannot investigate the principle factors in the VEGF-A splicing factors important in the degree of pain experienced.

The selection of the samples was based on the presence of grade 4 chondropathy, which of course is a measurement an index of damage on the articular cartilage, however this approach was used to only match the samples and clearly state that I controlled for the chondropathy changes. In this case, the chondropathy score was measured macroscopically as described in (Walsh, Yousef et al. 2009), however other methods could be employed to have a more holistic approach to the levels of articular damage such as Mankin grades, Outterbridge system or the OARSI scores.

Moreover, the samples were tested for synovial inflammation and both the control, and the disease group had similar synovial inflammation scores. That means that the independent variable of the study was the pain differentiation between the samples. Of course, when it comes to the pain perception, to identify the levels of pain from the patients the VAS score system was employed. Even though this scale has been used in the past in publications (Aso et al., 2021), an argument could be made that it does not take in consideration enough variables used to describe pain, similar to what other pain scale systems do (e.g., WOMAC or KOOS).

Most of the donors, either with symptomatic or asymptomatic, were on different medications, in some cases multiple medications. These cannot be controlled or matched, and so their potential influence on the results and interpretation is not known. Finally, the experiments performed here only provide us with a single picture of the expression of different factors; Visualisation and expression patterns are extremely valuable in identifying protein expression in tissues for both understanding of the localisation and level of important factors in specific

processes, and for target validation in translation studies. Mechanistic studies can offer a more holistic view of the relations and functions of the components of the VEGF-A splicing axis in synovium and synoviocyte, but such approaches cannot replicate the length of disease duration, and the changes in VEGF-A splicing axis over the length of time of normal OA development.

## **5. The control of VEGF-A splicing in, and the effect of VEGF-A isoforms and splicing kinases on monocyte adherence to, human fibroblast like synoviocytes *in vitro*.**

### **5.1 Introduction**

The previous chapters dealt with how VEGF-A and its splicing axis affect and alter their expression either during inflammation or pain in human synovial tissue. However, even though the IHC experiments described can identify the alterations in VEGF-A splicing axis at a single time point, they do not provide adequate information about the mechanisms behind these changes, that would alter the activity of kinases for example by contributing to physiological effects such as inflammation, angiogenesis, and pain.

VEGF-A is expressed and may be altered in the majority of the cells present in human synovium (endothelial cells, macrophages, fibroblasts) (as can be seen in Chapter 3 and 4). I was interested in investigating the mechanisms leading to the changes in VEGF-A splicing I observed in human tissues through study of the expression and splicing of VEGF-A isoforms in human fibroblast-like synoviocytes (HFLS). VEGF-A and its upstream or downstream targets can be measured in isolated tissues or the whole organism, however, *in vitro* models promote the ability for isolated investigation and specific mechanistic analysis.

To model and investigate the effects of VEGF-A and splicing kinase inhibitors in inflammation, I used an *in vitro* inflammation assay developed in HFLS by Dr N Beazley-Long, which is based on previously published assays of monocyte adherence to brain microvascular endothelial cells and retinal pigmented epithelial cells (RPE) (Thichanpiang, Harper et al. 2014, Beazley-Long, Moss et al. 2018). Use of these *in vitro* models has shown the importance of VEGF-A and VEGFR2 in both the regulation of inflammatory adhesion molecules such as ICAM-1, and the adhesion of monocytes to cultured cells (Thichanpiang, Harper et al. 2014, Beazley-Long, Moss et al. 2018). Other *in vitro* inflammation model assays have been employed in the past, although no other assays monitor immune cell adherence to my knowledge. For example, Wilms and colleagues developed an *in vitro* model of the neuroinflammation found in multiple sclerosis using cultured primary microglia and astrocytes to measure levels of inflammatory mediators such as IL-1 $\beta$ , IL-6 and TNF- $\alpha$  in response to the inflammatory stimulator, lipopolysaccharide (Wilms, Sievers et

al. 2010). Haltmayer and colleagues established an *in vitro* inflammation model for OA, using horse osteochondral and synovium explants in co-culture, and showed that treatment with inflammatory mediators such as TNF- $\alpha$  and IL-1 $\beta$  elicits an response similar to naturally occurring OA in that synovial macrophages shift toward the pro-inflammatory M1 phenotype (Haltmayer, Ribitsch et al. 2019).

The monocyte adherence assay employed is based on ligands expressed in monocytes and their interaction with cell adhesion molecules on endothelial cells, or HFLS on exposure to cytokines such as TNF-alpha (Thichanpiang, Harper et al. 2014, Beazley-Long, Moss et al. 2018). Such cytokines activate and increase the binding of monocytes to, for example, the endothelium through adhesion molecules such as Intracellular Adhesion Molecule-1 (ICAM-1) (Lawson and Wolf 2009, Reglero-Real, Colom et al. 2016). TNF- $\alpha$  is an inflammatory cytokine that acts on the Tumour Necrosis Factor Receptor (TNFR) and is a major player in pain (Leung and Cahill 2010, Rustenhoven, Jansson et al. 2017, Ji, Nackley et al. 2018), as well as it promotes an inflammatory profile in HFLS inducing the release of further inflammatory molecules such as IL-6, IL-1 $\beta$  and VEGF-A (Lee, Lee et al. 2017, Zhang, Ding et al. 2019). ICAM-1, a member of the IgSF (immunoglobulin superfamily) group of cellular adhesion molecules, is expressed in endothelial cells and as preliminary data from our lab suggest, also in HFLS. Using this *in vitro* model, Dr Beazley-Long demonstrated that both panVEGF-A and ICAM-1 expression are dose-dependently increased by TNF- $\alpha$  in cultured primary HFLS, and TNF- $\alpha$  treatment results in THP monocyte adherence to HFLS monolayers (Figure 44). The mechanism through which this occurs is not known. The flowchart in Figure 44 is a visual representation of the hypotheses tested in these studies regarding VEGF-A contribution to synovial inflammation, modelled in cultured primary HFLS.

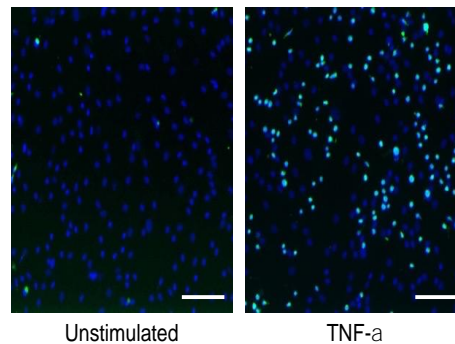
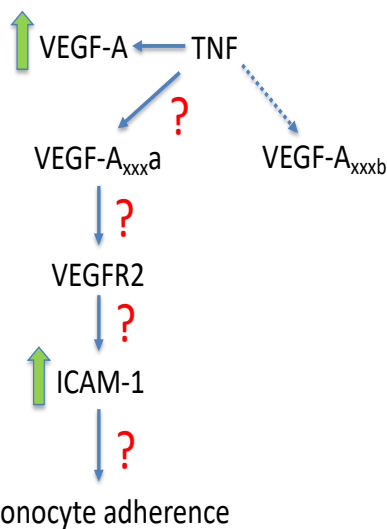
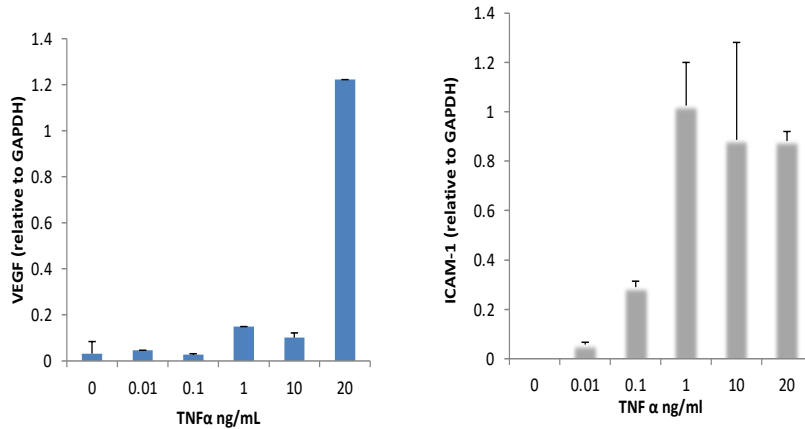


**Figure 43** PanVEGF-A and ICAM-1 are increased in a dose-dependent manner by TNF- $\alpha$  in cultured HFLS. The flow chart at the bottom left shows the hypothesised mechanism for how a hypothesised TNF- $\alpha$ -induced change in VEGF-A splicing might affect monocyte adherence in HFLS, based on the mechanism of monocyte adherence in RPE cells in the eye (Thichanpiang et al 2014). The question marks denote lack of evidence for that step in the proposed mechanism. Bottom right: Images of HFLS co-cultured with THP-monocytes labelled with CalceinAM with and without TNF- $\alpha$  treatment (data and figures supplied by Dr N Beazley-Long, n=3/group in the graphs). HFLS nuclei are labelled blue with DAPI. The small bright dots in the right-hand panel are fluorescent THP monocytes adhering to the HFLS monolayer. Scale bar 30  $\mu$ m. Data and Figure generated by Drs Nicholas Beazley-Long and Matthew Swift.

As we hypothesised that TNF- $\alpha$  would promote monocyte adherence through VEGF-A splicing in favour of the pro-angiogenic isoforms VEGF-A<sub>xxx a</sub>, VEGFR2 activation and ICAM-1 induction, we

wanted to test this through the control of VEGF-A splicing. Using inhibitors of splicing kinases, such as SRPK1, Clk1 and Dyrk1a inhibitors, particularly against those kinases responsible for the control of VEGF-A alternative splicing events provides a practical way to identify the effects downstream of their actions.

### **5.1.1 Development of small molecule splicing kinase inhibitors**

Multiple efforts have been made to develop novel SRPK1/2 and CLK inhibitors, SRPK1 inhibitors for use against HIV and HBV infections, since the kinases play a role in RNA viral replication (Fukuhara, Hosoya et al. 2006) and CLK inhibitors for use in cancer treatment. However, until 2017, specific, selective, and potent small molecule SRPK1 or CLK inhibitors were not available. Although relatively potent compounds such as TG003 (CLK1 inhibitor, Muraki et al 2004, Nishida et al 2011), T-025 (CLK inhibitor Iwai et al 2018), Harmine (Dyrk1A inhibitor, IC<sub>50</sub> 100nM, Bain et al 2007, Adayev et al 2011), SRPIN340 (SRPK1/2 inhibitor, Hagiwara) the majority of compounds have multiple off-target effects or lack of potency against targets of interest (Batson, Toop et al. 2017). In the work presented in this thesis I have analysed the effects of a number of different inhibitors of the splicing kinases SRPK1/2, Clk1/2, and DYRK1a, that is; SPHINX (SRPK1/2/3 inhibitor), SPHINX31 (SRPK1 potent and specific inhibitor), SRPINS1-6 (SRPK1/2 inhibitors built on the SPHINX31 chemical scaffold, Figure 45), SRPIN340 (SRPK1/2 inhibitor), Griffin 6 (Clk1/2 inhibitor) and T-025 (broad CLK inhibitor (Table 15)). The structures of these inhibitors can be found in Figure 45. The IC<sub>50</sub>s of the inhibitors are determined based on *in vitro* kinase assays (MRC PPU International Centre for Kinase Profiling) against a panel of 140 kinases. Specificity and potency are linked to their synthesis, resulting in binding to specific sites near the ATP site that then inhibit ATP binding through conformational change, rather than competing for the ATP binding site directly (Batson, Toop et al. 2017)

**Table 12 Relative potencies and selectivity for the most commonly used, selective small molecule SRPK, CLK and DYRK splicing kinase inhibitors. IC<sub>50</sub> / Kd values are also given in Table xx for T-025, SRPIN340, SPHINX and SPHINX31 for comparison to the unpublished SRPINs 1-6**

Small molecule inhibitor	Stated target (IC <sub>50</sub> )	Other targets (IC <sub>50</sub> /Kd, nM)
TG003 More potent at Dyrk1A than stated target	Clk1 inhibitor (20nM)	CLK2 (IC <sub>50</sub> 95nM) CLK4 (IC <sub>50</sub> 30nM) DYRK1A (IC <sub>50</sub> 12nM) Casein kinases delta and epsilon DYRK1B (Ohe and Hagiwara 2015)
T-025	Non-selective Clk inhibitor	Clk1 4.8nM Kd Clk2 0.096nM Clk3 6.5nM Clk4 0.61nM
SRPIN340	SRPK1 inhibitor (890nM)	SRPK2 (IC <sub>50</sub> , 100 mM range) (Gammons, Fedorov et al. 2013, Gammons, Dick et al. 2013)
SPHINX	SRPK1 inhibitor (580 nM)	Some inhibition of SRPK2 and SRPK3 (3%), (Gammons, Fedorov et al. 2013, Gammons, Dick et al. 2013)
SPHINX31	SRPK1 inhibitor (6nM)	No significant inhibition against a panel of ~140 kinases (Batson, Toop et al. 2017). See also Table

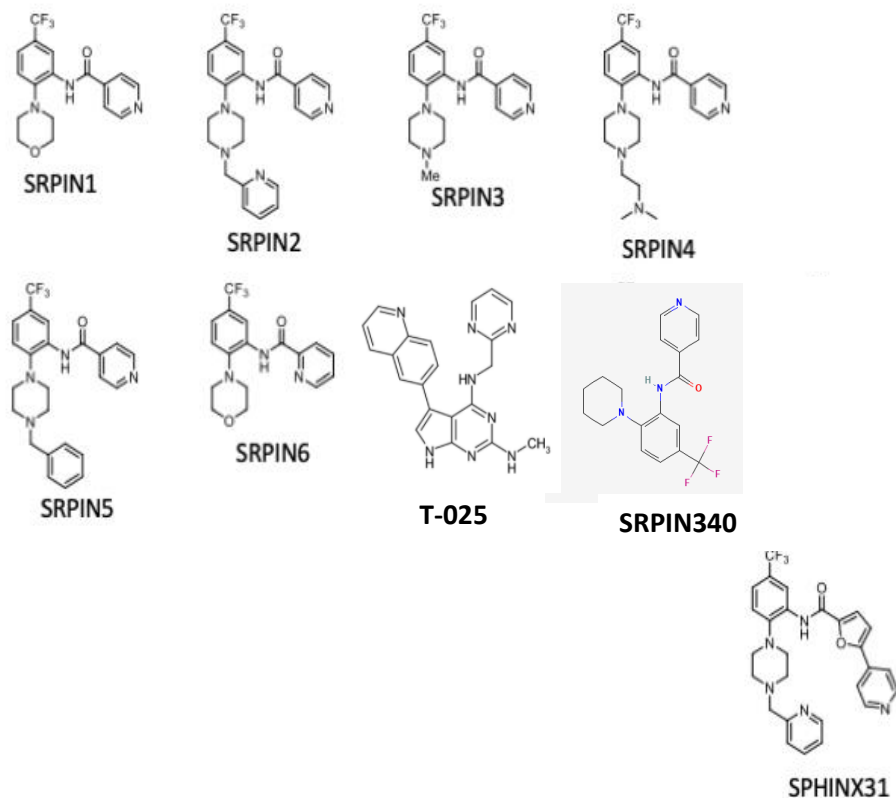


**Figure 44** Representations of the individual structures for the splicing kinase inhibitors used in this study. SPHINX31, and the SRPIN series were developed by Prof Jonathan Morris at Exonate Ltd (SPHINX31) or UNSW (SRPINs). Chemical structures were provided by Jonathan Morris or were downloaded from PubChem for SRPIN340 and T-025 (National Centre for Biotechnology Information (2022). [https://pubchem.ncbi.nlm.nih.gov/compound/\(SRPIN340](https://pubchem.ncbi.nlm.nih.gov/compound/(SRPIN340) or T-025 (Fukuhara et al 2006; Iwai et al 2018)))

PubChem Compound Summary for CID 2797577, SRPIN340. Retrieved April 25, 2022, (Iwai, Yaguchi et al. 2018).

### 5.1.2 SRPIN340

SRPIN340 was the first selective SRPK1/2 inhibitor synthesised by Fukuhara and colleagues in 2006 (Fukuhara, Hosoya et al. 2006) as a potential inhibitor of HIV. More than 100,000 chemicals were screened which identified SRPIN340 and TG-003 as SRPK1 and CLK1 inhibitors respectively (Fukuhara, Hosoya et al. 2006). SRPIN340 is an effective inhibitor against both SRPK1 and SRPK2 inhibiting more than 50% of the kinases' activity at 10nM, while not affecting CLK1 and CLK4 (Fukuhara, Hosoya et al. 2006).

SRPIN340 has been used as an SRPK1 inhibitor in cancer models such as leukemic cells in which it dose-dependently reduced cell death with IC<sub>50</sub> values of 50-100nM (Siqueira, Barbosa et al. 2015). In choroidal neovascularisation (CNV) models SRPIN340 reduced infiltration of macrophages *in vivo* and reduced the levels of the pro-angiogenic VEGF-A<sub>xxx</sub>a in RPE cells and melanoma cell lines (Gammons, Lucas et al. 2014). (Dong, Noda et al. 2013, Gammons, Dick et al. 2013). It also blocks pain behaviour and VEGF-A splicing changes in peripheral traumatic nerve injury, when given peripherally (Hulse, Beazley-Long et al. 2014) or centrally (Hulse, Drake et al. 2016), although it has not been used in the context of either OA or RA models. The SRPIN340 scaffold was used to synthesise related molecules, SRPINs 1-6, all SRPK1

### 5.1.3 SPHINX31

SPHINX31 (Exonate Ltd) was the first highly potent and selective SRPK1 inhibitor described (Batson et al 2017). It prevents TNF- $\alpha$  mediated activation of SRPK1, shown by reduced levels of phosphorylation of SRSF1 in PC-3 cells (Mavrou, Brakspear et al. 2015), and alters VEGF-A splicing in retinal pigmented epithelial cells, resulting in reduced choroidal re-vascularisation following retinal lesioning, a model of wet Age-related Macular Degeneration (Gammons, Lucas et al. 2014, Batson, Toop et al. 2017). SPINX31 also affects neuronal function, capsaicin-induced TRPV1 activation in primary sensory neurons (Hulse, Beazley-Long et al. 2014). SPHINX31 is a more successful SRPK1 inhibitor compared to previous molecules due to unique structural chemistry allowing it to target an associated site of the ATP binding site of SRPK1 rather than the binding site itself. The “hinge” region in SRPK1 is the binding site of the trifluoromethyl group in SPHINX31 (Figure 45) which forms a strong bond between kinase and inhibitor. Due to the hydrophobic nature of the hinge, once the kinase and the inhibitor bind, the presence of a pyridine group that attach to the sidechains of SPHINX31 increases the potency of the compound. Following this attachment, the “hinge” flips preventing any further ATP binding, thus preventing the kinase activity of SRPK1, and resulting in the specificity and potency of SPHINX31 as an SRPK1 inhibitor. SPHINX31 is a useful tool compound for investigations into alternative splicing and its downstream mechanisms (Batson, Toop et al. 2017). The SPINK31 cellular IC<sub>50</sub> is 320nM as the inhibitor needs to cross membranes and avoid efflux, compared to the *in vitro* IC<sub>50</sub> 6nM when determined against purified SRPK1.

#### 5.1.4 T-025

T-025 was reported as a potent pan-CLK inhibitor, with high potency against CLKs1-4, and the ability to inhibit tumour growth *in vitro* and *in vivo* (Iwai, Yaguchi et al. 2018). T-025 was initially developed against the CLK kinases however there is evidence that it also inhibits DYRK1A kinase. The inhibitor interacts with Glu244 and Leu246 in the CLK2 hinge region, resulting in higher selectivity for CLK2 over CLKs 1, 3 and 4 (Iwai, Yaguchi et al. 2018). However, there are still questions about its specificity since it has also been demonstrated to inhibit DYRK1A, DYRK2, HIPKs, IRAK4 and YSK4 with  $K_d < 100\text{nM}$  (Iwai, Yaguchi et al. 2018).

#### 5.1.5 SM04690 (Lorecivivint)

SM04690 (Lorecivivint, Biosplice Therapeutics) was initially reported as a Wnt (wingless-related integration site) inhibitor, with the potential to treat both OA joint disease and pain following a successful Phase 1 trial (Yazici, McAlindon et al. 2017). The mechanism of Wnt inhibition was subsequently reported to result from dual DYRK1A and CLK2 inhibition, although the paper reported that SM04690 also inhibited >90% of activity of seven kinases at  $0.5\mu\text{M}$ : CLK2, CLK3, DYRK1A, DYRK1B, GSK3B, HIPK1 and HIPK2 (Deshmukh, O'Green et al. 2019).

DYRK1A is a splicing kinase that has been implicated in the development of multiple disorders related to central nervous development, and in inflammatory processes. The kinase is suggested to be a potential cause of learning deficits in Down's syndrome, is associated with autism spectrum disorders (Tahtouh, Fedorov et al. 2012, Jarhad, Mashelkar et al. 2018) and Alzheimer's disease. CLK2 and DYRK1A inhibition by Lorecivivint reduced Wnt expression, leading to chondrogenesis, and inflammatory gene expression, reducing cytokine production by synoviocytes (Deshmukh, O'Green et al. 2019) and reduced pain behaviour in OA animal models. These findings suggest a role for both kinases in pain and disease modulation through mechanisms other than VEGF-A splicing and provides an encouraging rationale for examination of these 2 kinases in alternative models of inflammation.

#### 5.1.6 Griffin6

Griffin 6 is a novel unpublished selective inhibitor of CLKs 1 and 2 (kind gift of Prof J Morris, University of New South Wales, Australia). As explained previously, CLK1 works in conjunction with SRPK1 to control SRSF1 function through phosphorylation and activation. It is also strongly implicated altered alternative splicing in oncogenesis and neurodegeneration (Lee, Yun et al.

2019). Moreover, in liver CLK2 seems to play a role in gluconeogenesis (creation of glucose from non-carbohydrate sources (Tabata, Rodgers et al. 2014). More importantly, recently a novel inhibitor against CLK2 and DYRK1a has been introduced, namely Lorecivint, tying the kinase with pain and the inflammation present in OA. Lorecivint inhibits both pain and inflammation in OA, while altering the disease state of the joint (e.g., cartilage damage) (Deshmukh, O'Green et al. 2019).

### 5.1.7 Preliminary data

Treatment of human FLS with increasing concentrations of TNF- $\alpha$  resulted in increased VEGF-A and ICAM-1 expression (Fig 44), and adherence of fluorescently labelled THP-monocytes (Fig 44), suggesting the involvement of VEGF-A in monocyte adherence to HFLS, as previously shown in RPE and endothelial cells. This also shows that this *in vitro* model of monocyte adherence is suitable for use with HFLS. As a result, while acknowledging that TNF- $\alpha$  is a key factor in RA, rather than OA, experiments were designed to a) verify the expression of components of alternative splicing control (SRPK1, SRSF1) in HFLS in culture; b) investigate possible mechanisms of control of alternative VEGF-A splicing in synoviocytes, and c) to determine whether inhibition of SRPK1 could potentially affect the synovial inflammatory process using this *in vitro* model of synovial inflammation.

### Hypotheses

I tested the following specific hypotheses:

1. SRPK1, SRSF1 and VEGF-A are expressed in HFLS in culture. Expression of these mRNAs, and alternative splicing of VEGF-A is altered by TNF- $\alpha$ , and splicing kinase inhibition.

And based on further testing the hypothesised mechanisms underpinning TNF- $\alpha$ -stimulated monocyte adherence to HFLS *in vitro*,

2. THP-monocyte adherence to HFLS *in vitro* is mediated by VEGF-A induction of ICAM-1 expression.
3. THP-monocyte adherence to HFLS is mediated through an SRPK-1 /VEGF-A-dependent mechanism and is reduced by inhibition of SRPK1 and/or VEGF receptors *in vitro*.

## 5.2 Materials and Methods

General methodology is given in chapter 2 (Methods). Cell culture, and treatment of HFLS are described in chapter 2. Section 2.9.

As a result of the interruption of experiments by the Covid pandemic, I was supplied with the method and the unpublished raw data from the monocyte adherence experiments by Dr N Beazley-Long. I then conducted all the analyses on these data shown in this thesis.

### 5.2.1 Splicing kinase inhibitors

Splicing kinase inhibitors were obtained as a gift from Professor Jonathan Morris, University of New South Wales Australia, under a collaboration with Profs Lucy Donaldson and David Bates.

The IC<sub>50</sub>s for the compounds used are shown in Table 15.

**Table 13 IC<sub>50</sub>s of the different compounds used in this study**

<i>Compound</i>	IC <sub>50</sub> SRPK1 (nM)	<i>Compound</i>	IC <sub>50</sub> SRPK1 (nM)
<i>SRPIN340</i>	890	<i>SRPIN2</i>	2630
<i>SPHINX</i>	580	<i>SRPIN3</i>	7244
<i>SPHINX31</i>	5.9	<i>SRPIN4</i>	844
<i>Griffin 6</i>	199 ±36	<i>SRPIN5</i>	355
<i>T-025</i>	4.8 (Kd)	<i>SRPIN6</i>	~100
<i>SRPIN1</i>	8912		

## 5.2.2 Workflow for effects of HFLS treatment with SRPK1 and Clk1/2 inhibitors in culture

Primary HFLS cells obtained from healthy subjects (since cells from either OA or RA patients were not readily available for purchase), were grown to 80% confluence, trypsinised and plated in 24 well plates, with 25.000 cells per well resuspended in 250  $\mu$ l of media. The cells were treated with vehicle (1% DMSO) or 1nM of TNF- $\alpha$  to promote an inflammatory response. Cells were also treated overnight with specific splicing kinase inhibitors SPHINX31, a SRPK1 specific inhibitor (Batson, Toop et al. 2017) Griffin 6, a novel compound that inhibits CLK1 and CLK2 at concentrations >30fold lower than those required to inhibit other kinases (table 15), and T-025, an inhibitor with affinity for CLKs and DYRK1A, at the concentrations shown in Table 16. All splicing inhibitors as seen in Table 16, were used at 3 $\mu$ M, since the IC<sub>50</sub> values displayed in Table 15, were a result of assays where only the kinase of interest and the substrate was present. In vitro kinase assays yield lower IC<sub>50</sub>s values than cellular assays, as the former do not take into account factors that may affect the ability of the compounds access the kinases, such as whether they can cross the cell membrane. The chosen concentrations were selected based on previous use of these inhibitors in cell assays and *in vivo* models (Batson et al., 2017). For analysis, the

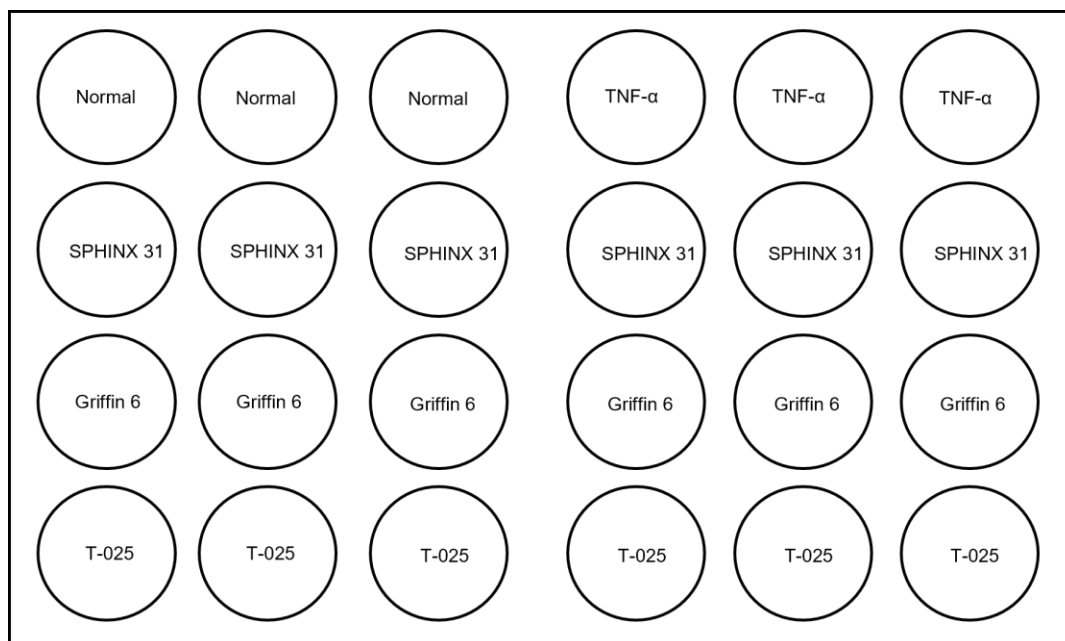


**Figure 45 Illustration of the structure of the 24 well plate and the treatments used for the RNA- extraction work**

plate was the experimental unit and each 24 well plate contained treatments in triplicate (Figure 46).

**Table 14 Compounds and concentrations used for the gene expression study**

Compound Name	Active concentration (diluted in DMEM)
DMSO	1%
TNF- $\alpha$	1ng/ml
SPHINX 31	3 $\mu$ M
Griffin 6	3 $\mu$ M
T-025	3 $\mu$ M

After treatment with splicing kinase inhibitors, total RNA was extracted from the cells (see section 2.12) and stored at -80°C. For total RNA quantification, absorbance ratios at 260/280nm (absorbance wavelength of RNA/ absorbance wavelength of DNA) and 260/230nm (absorbance wavelength of RNA/ absorbance wavelength of proteins and other contaminants that absorb at 230 e.g., EDTA or TRIzol) were determined for 1 $\mu$ l samples of each RNA sample. RNA concentration was then determined (ng/ml).

The values from these absorbances also indicate the purity of the RNA samples. Samples were only used if the 260/280 absorbance ratio was between 1.8-2.0. The 260/230 ratio, as a secondary measure of sample purity, was considered appropriate only if it was in the range of 2.0-2.2.

### **5.2.3 Expression of VEGF-A, SRPK1, SRSF1 and ICAM-1 in HFLS**

**RNA extraction.** To assess expression of the constituents of the VEGF-A splicing axis, specifically SRPK1, SRSF1, and the two VEGF-A isoform families, RNA was extracted as described previously (section 2.12).

Generation of cDNA using oligodT /random primers was as described in section 2.13.

A simple illustration of the protocol utilised for RNA extraction, PCR etc can be found in the figure bellow.

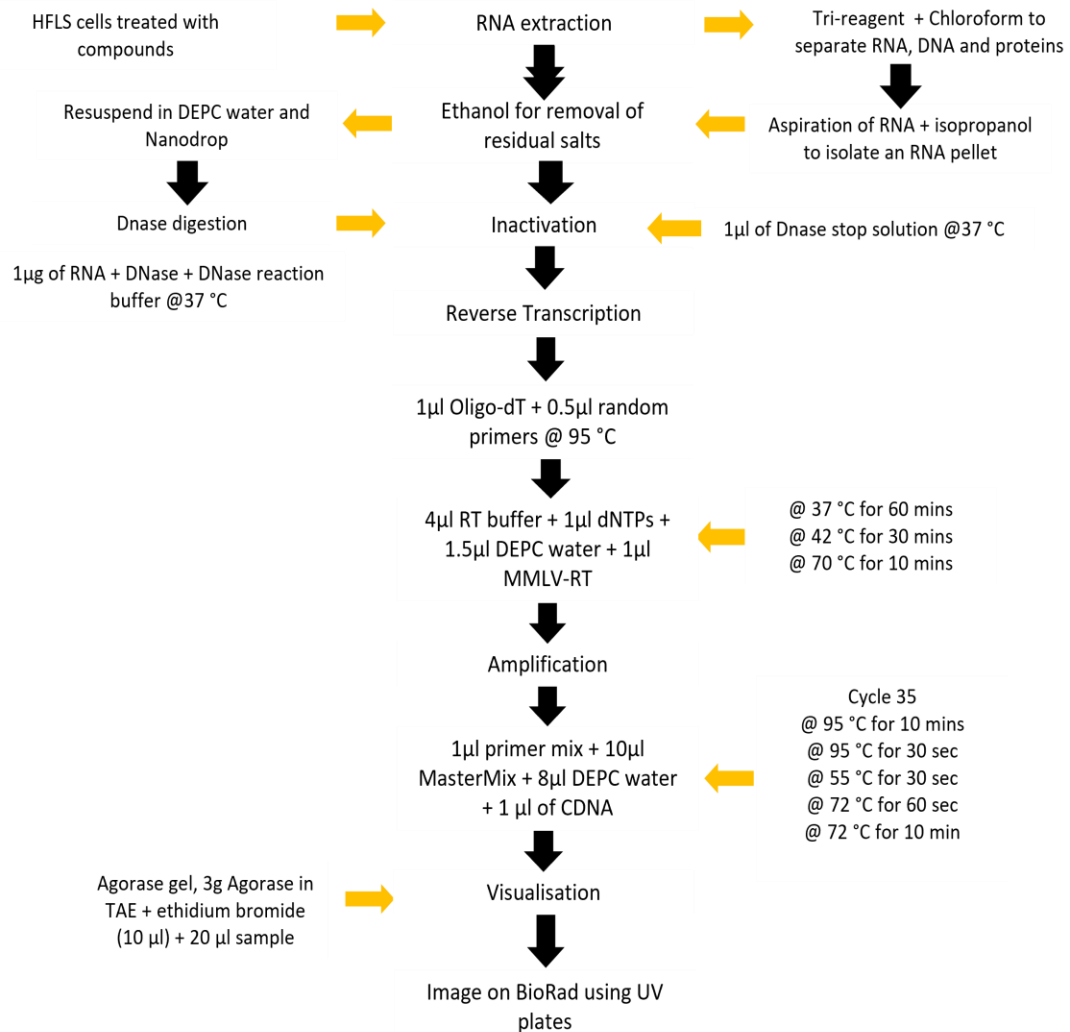


**Figure 46 Simple flow chart illustrating the experimental procedure from RNA extraction to visualisation of the PCR results**

**Reverse transcription.** In the usual protocol for PCR as detailed in chapter 2.13.2, 0.5µg (final concentration) of oligo-dT primer (Promega C110A) was used for reverse transcription from mRNA polyA tail. When using competitive VEGF-A primers to identify the two splice variant families, reverse transcription was done with the set 1 common downstream (exon 8) primer (0.5µg) and random primers (250ng) rather than oligo-dT primers. This was done as a result of

initial difficulty in identifying VEGF-A mRNA in the samples, so I decided to reverse transcribe only VEGF-A transcripts. Additionally, VEGF-A<sub>xxx</sub>b isoforms have extremely short polyA<sup>+</sup> tails, and as a result, oligo-dT reverse transcription often underrepresents these isoforms in cDNA libraries (personal communication with Dr Bates).

**Primer selection.** The primer sequences used for all targets are shown (5' to 3' sequence) in Table 11 section 2.13.2 as well as in Table 17 below, which also includes the expected amplicon sizes for each reaction.

In Figure 47 a representative simulation of the primer binding sites on the exons of VEGF-A sequencing can be seen.

Primers for SRSF1 (Zhou, Wang et al. 2019), SRPK1 (Wang, Zhou et al. 2020), ICAM-1 (Ashander, Appukuttan et al. 2016) and  $\beta$ -actin (Nowak, Amin et al. 2010) expression were identified from previously published studies, and specificity of the primers for the targets was checked using Ensembl and NCBI primer blast. The SRPK1 primer set should produce a product of 217bp, the SRSF1 set a product of 95bp, ICAM-1 at 217bp and  $\beta$ -actin at 150bp (table 16).

**Table 15 Primer sequences and expected amplicon size for the targets.**

<b>Primer Target</b>	<b>Forward Primer</b>	<b>Reverse Primer</b>	<b>Product Size(s) (bp)</b>
Human VEGF-A isoforms <b>set 1</b>	GTAAGCTTGTACAAGATCCGCAGACG	ATGGATCCGTATCAGTCTTTCT	130bp and 64bp
Human VEGF (Both A <sub>165a</sub> and VEGF- A <sub>165b</sub> ) <b>set 2</b>	GAGATGAGCTTCCTACAGCAC	TTAAGCTTTCAGTCTTTCCTGGTGAGAGATCTGCA	220bp
Human SRSF1	GCCGCATCTACGTGGGTAAC	GAGGTCGATGTCGCGGATAG	95
Human SRPK1	GTGTGCCAGTCTTCCTCAACTG	GGTCAGCAATCTTCACCTTGAG	217
Human ICAM	GGCCTCAGTCAGTGTGA	AACCCCATTCAGCGTCA	217
b-actin	AGCCATGTACGTAGCCATCC	CTCTCAGCTGTGGTGGTGAA	150

Two sets of previously optimised and published human VEGF-A primers were used; set 1 from (Nowak, Amin et al. 2010) and set 2 from (Woolard, Wang et al. 2004). Set 1 are competitive PCR primers hybridising in exon 7 and exon 8b in the VEGF-A gene (Table 11 section 2.13.1). These thus amplify both VEGF-A<sub>xxx</sub>a isoforms, with a product size of 199 bp as exon 8a is included in the transcript when the proximal splice site is used, and the VEGF-A<sub>xxx</sub>b isoforms, giving a 65bp product due to the use of the distal splice site and exclusion of exon 8a. Thus, when both transcripts are present, two amplicons will be detected. The second set of human primers (Table 11 section 2.13.1) amplify all VEGF-A isoforms as the upstream primer hybridises in the common sequence in exon 4/8b and the downstream primer hybridises in exon 8b, giving a product size of 220bp.

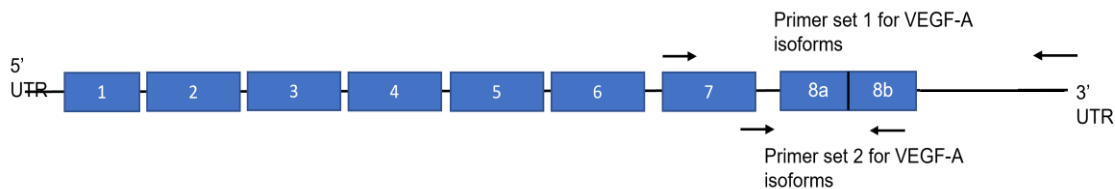


**Figure 47 Representative simulation of the primer binding sites on the exons of VEGF-A sequencing. Primer set 1 (as seen in Table 17) recognises the region from the 5' site of exon 7 to the 3' site of the untranslated regions. The primer set 2 recognises the 5 terminal nucleotides of exon 7 and in the 3' site it is complementary to the exon 9.**

**Optimisation of PCR reactions for different primer sets.** Before finalizing the above conditions, for both pairs different temperatures were tested regarding the PCR cycles to specifically find the optimal annealing temperature. Starting at 55°C, with increments of 3°C to the temperature of 67°C, multiple reactions were run to determine the optimal annealing temperature.

The optimised PCR conditions for VEGF-A (primer set 1) and SRSF1 PCR are shown in Table 18. VEGF-A PCRs using the set 2 primers were not successful providing no results or identification of any bands through the optimisation efforts thus they are not discussed further in this piece of work. Due to Covid impacts and time constraints, the SRPK1 PCR could not be fully optimised, and further study of these targets was therefore not possible.

Following PCR amplification, samples were stored at 4°C. PCR amplicons resolved on 3% agarose gels in 1x TAE buffer (Full methods in section 2.13) and visualised on a BioRad Gel Doc set to automatic exposure detection time.

**Table 16 Optimised PCR conditions for VEGF-A, SRSF1 and ICAM-1. ICAM-1 experiments were optimised and performed by Dr N Beazley-Long**

<b>Target</b>	<b>Denaturation temperature and time</b>	<b>Annealing temperature/time</b>	<b>Extension temperature and time</b>	<b>Cycle number</b>
VEGF-A	95°C 10 min 95°C, 30s	55°C, 30s	72°C, 30s, final 72°C, 10 min	35
SRSF1	95°C 10 min 95°C, 30s	55°C, 30s	72°C, 60s, final 72°C, 10 min	35
ICAM-1	95°C 2 min 95°C, 30s	55°C, 30s	72°C, 60s, final 72°C, 2 min	35

### **cDNA sequencing**

After identifying the PCR amplicons on the gel as described above, for VEGF-A primer set 1, amplicons with the greatest signal intensity were isolated using a UV transilluminator and stored in Eppendorf tubes at 4°C before isolation of DNA for sequencing. In removing the amplicons from the gel, a scalpel was used to minimize excess agarose in the samples collected. The isolated bands were then weighed to determine volume. Assuming the density of the sample/gel ration is 1 g/ml, a gel slice weight in grams is equal to the volume in millilitres.

DNA was extracted from the gel using QIAquick® Gel Extraction Kit (Qiagen, UK) and the manufacturer's protocol. Three volumes of buffer QG (QIAquick® Gel Extraction Kit) were added to 1 volume of gel and heated to 50 °C until the sample was completely dissolved and the colour of the mixture turned yellow. If the colour of the mixture was orange or violet, 10µl of 3M sodium acetate, pH 5.0, was added and mixed to reduce pH. A volume of isopropanol equal to the weight of each individual gel slice was then added and the samples loaded onto QIAquick spin columns. 500 µl buffer QG was then added to the QIAquick column, and the column centrifuged at 10000 x g for 1 minute. The column was washed with 750 µl of buffer PE and again centrifuged for 1

min. The DNA was eluted from the column into a clean tube with 50 µl of Buffer (10 mM Tris-Cl, pH 8.5), to avoid any salt contamination of the cDNA samples, centrifuged for 1 minute at 10000 x g. Samples were stored in 4 °C, before being sent for sequencing analysis to the DNA sequencing facility in the Medical School, University of Nottingham.

Sequences were identified by alignment using BLAST (Altschul, Gish et al. 1990)

#### **5.2.4 Monocyte adherence to fibroblast-like synoviocytes – *in vitro* inflammation assay.**

The human monocytic leukemia cell line (THP-1) derives from the peripheral blood of a man with acute monocytic leukemia (Bosshart and Heinzelmann 2016) and was obtained from the American Type Culture Collection (ATCC, Mantissa, VA). Cells were grown in RPMI-1640 medium with 10% fetal bovine serum (FBS), 1% penicillin, 100 µg/ml of streptomycin, and 2 mM L-glutamine. The THP-1 cells were grown to at least 80% confluence and were passaged, when necessary, as described for HFLS in section 2.9.

For use in the *in vitro* inflammation assay, THP-1 cells were grown in the same conditions to 80-100% confluence and then dissociated from the plates with trypsin as described for HFLS also as in section 2.11. THP-1 cells were suspended in RPMI-1640 medium and fluorescently labelled by incubation in Calcein AM (Sigma) at a final concentration of 2.5 µM in 5% CO<sub>2</sub>/95% O<sub>2</sub> at 37 °C for 1 h. Cells were concentrated by gentle centrifugation at 400 xg for 10 min, the supernatant discarded, the cell pellet washed twice with PBS and resuspended in RPMI-1640 with 10% FBS and 1% penicillin/streptomycin before use.

Synoviocytes from healthy and RA donors were plated in black sided 96 well plates (Corning) and grown to >80% confluence prior to overnight serum starvation, in DMEM +1%P/S (section 2.11). Synoviocytes monolayers were then treated with 20ng/mL TNF-α or DMSO vehicle (maximum 1% and equivalent in all treatments) plus SRPK1 inhibitor for 24h under serum free conditions. THP-1 cells were washed and fluorescently labelled with calceinAM as above (2.5mM, 1h), prior to adding them to the SRPK1-treated synoviocyte monolayers at 30,000 THP-1 cells per well and were co-incubated with the HFLS for 2h. Cells were then thoroughly washed twice in warm PBS (5 min, 70rpm in a gyro-rotator) to remove unattached monocytes. Cells were then fixed in paraformaldehyde (PFA in phosphate buffer) for 20 min, washed twice in PBS+ 0.05% Tween80 and placed in 100mL PBS. Calcein-labelled THP-1 fluorescence was measured (Victor X4, Perkin-

Elmer) in each well. Two assay negative control groups were included on every plate: 1) 100mL PBS and 2) monocytes alone (i.e., no HFLS to control for any adherence to the plate). Visual inspection of the plates was used to check whether washing was adequate. If the fluorescent signal from monocytes alone was greater than PBS, this indicated that monocytes had attached to the plate alone, and the plate was re-washed to remove any plate-adherent THP-1 monocytes until signal reduced and then all wells were re-read.

No information on the synoviocyte donors was available, other than the health or arthritis type.

#### **HFLS treatment with VEGF-A splice variants, VEGF receptor inhibitors and splicing kinase inhibitors on ICAM-1 expression and monocyte adherence.**

To determine the effect of VEGF-A splice variants, VEGF receptor blockers and splicing kinase inhibitors on ICAM-1 expression (VEGF-A splice variant effects) and THP-1 monocyte adherence to HFLS (VEGF-A<sub>165b</sub> and splicing kinase inhibitor effects), cells were treated with 20ng/ml of TNF- $\alpha$  to promote an inflammatory state for 24 hours either alone, or in combination with:

- VEGF-A splice variants - human recombinant VEGF-A<sub>165a</sub> and VEGF-A<sub>165b</sub> (0.001-400ng/ml);
- VEGF receptor blockers PTK787 (200nM; blocks VEGFR1 and 2, VEGFR2 selective at this concentration (Grosios, Wood et al. 2004) and ZM32881 (10nM; VEGFR2 specific blocker (Whittles, Pocock et al. 2002);
- novel splicing kinase inhibitors SPHINX (1 $\mu$ M), SPHINX31 (3 $\mu$ M) SRPIN340 (5mM; inhibits SRPK and SRPK2 at this concentration), novel SRPK1 inhibitors SRPINs 1-9 (5 $\mu$ M, concentration determined from enzyme inhibition screen and the response to 1 $\mu$ M inhibitor and chosen to ensure complete inhibition).

Due to the difficulty in obtaining human primary cells during the pandemic, and the need to reduce differences in passage number the experimental unit was the treatment/well. Each treatment was done in either duplicate or triplicate on the plate, and the data shown are the mean of those values for each treatment well.

### **5.2.5 Cell culture for protein quantification**

HFLS cells were grown to 80% confluence as described previously (chapter 2.9), before being trypsinised and centrifuged at 100xg for 5 minutes to form a cell pellet. The pellet was then resuspended in 1 mL of DMEM + 20%FBS + 2mM L-glutamine media. Cells were then counted

using a haematocytometer, before being seeded in 6 well plates at a density of 100 000 cells per well with 1 mL of media and incubated for 24 hours to attach to the wells. The amount of FBS was then gradually reduced from 20% FBS in three steps, reducing to 10% FBS for 24hours, to 5% FBS for 24hours and finally to only DMEM and 2mM L-glutamine, to inhibit continuous growth and maintain a standardised number of cells in between the wells. Once in serum-free conditions, the cells were treated with TNF- $\alpha$  (1ng.ml<sup>-1</sup> or 1% DMSO in DMEM) overnight to induce an inflammatory response,  $\pm$  VEGFR2 inhibitor ZM32881 (10nM in DMEM overnight) or vehicle (DMSO, 1%) in DMEM (Figure 48). After treatment, cells were lysed, and proteins isolated and quantified using the Bradford assay as described in section 2.10.

### 5.3.3 Western blot – optimization and analysis

General methodology on the western blot protocol, including gel running, blot transfer and antibody incubations is described in chapter 2.11.

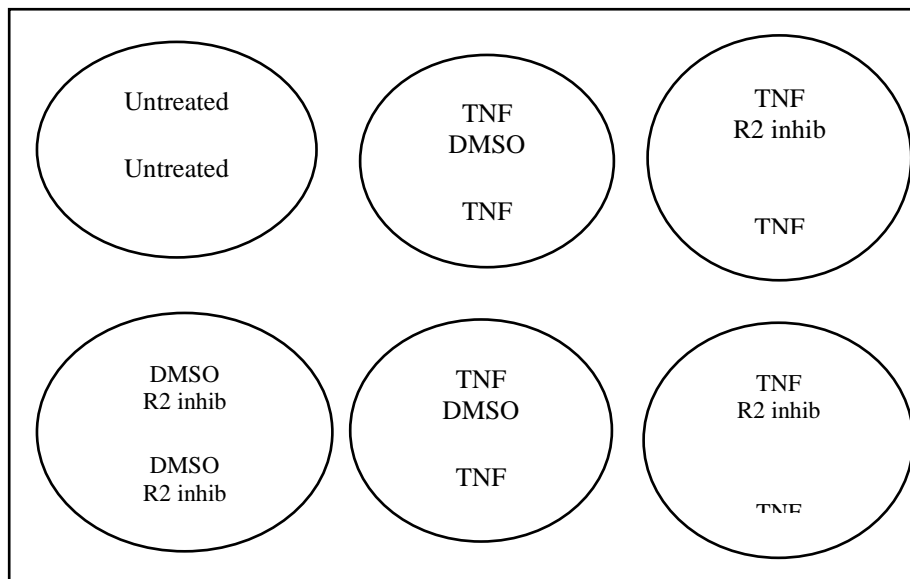


**Figure 48 Representative image of the standardised treatments used in order to identify differences in the protein expression of HFLS between normal, TNF- $\alpha$  treated and anti-VEGFR2 treated cells.**

Due to issues encountered with SDS-PAGE gels and Western blotting, the following changes were made to the protocol to optimise conditions. The effect of different amounts of protein per lane, ranging from 5ug to 50ug of protein was determined; and the optimal loading amount found to

be 20ug per lane. To prevent overheating of mini gels maximum voltage used was 120V and ice cold running buffer was used. The gel was equilibrated in transfer buffer after the completion of the electrophoresis, which provided a substantially cleaner and precise transfer from the gel to membrane during the wet electrophoretic transfer (the apparatus can be seen in chapter 2 section 2.11).

Two types of membrane are prevalent for use during for Western blotting, namely PVDF and nitrocellulose membranes. PVDF membranes have the benefit of increased binding protein capacity (up to 200  $\mu\text{g}/\text{cm}^2$ ), alongside being able to bind higher molecular weight proteins. PVDF can have higher levels of background and autofluorescence, however, as they are less fragile than nitrocellulose membranes, and so are preferred for experiments where re-probing of membranes is planned or necessary. In contrast, nitrocellulose membranes have lower protein binding capacity (up to 100  $\mu\text{g}/\text{cm}^2$ ), significantly lower background and are better suited for fluorescent visualisation. Despite the fragility disadvantage, for these reasons I used nitrocellulose membranes.

To optimise protein transfer and reduce potential for any degradation during transfer, I tested different transfer conditions including the voltage used for electrophoretic protein transfer (from 40V to 100V) and different times of transfer (1 - 4-hours). The transfer apparatus in the tank was also cooled with an ice pack to prevent temperature increases, with the optimal being transfer for 2 hours at 80V. The membrane was then removed and equilibrated in 0.01% TBS-Tween 20 wash buffer on a shaker for 10 minutes and blocked in 2% BSA in 0.01% TBS-Tween for 1 hour. I avoided using a higher concentration BSA for blocking non-specific binding as this can produce high levels of non-specific binding in fluorescent protocols. When fluorescent secondary antibodies were used the membranes were kept in the dark from the step including a fluorescent tag onwards, to avoid bleaching and autofluorescence.

The primary antibodies used were anti- ICAM-1 and anti-GAPDH as a housekeeping protein to correct for differences in sample loading. Membranes were rolled in 50 ml Falcon tubes with the side on which the proteins were transferred facing inwards, to minimise the amounts of reagents used. Primary antibody incubations were done overnight, at 4°C on a gel roller to maintain constant movement of primary antibody solution over the membrane and prevent drying of the membrane. After incubation with primary antibodies, the membranes were washed with 0.01% TBS-Tween 3 times, 10 minutes per wash in the Falcon tubes on the gel roller. Aggressive washing

resulted in loss of signal. The membranes were then probed with species-specific fluorescent secondary antibodies developed for the Licor imaging system for 1 hour at room temperature with constant agitation as for primary antibody probing, using donkey anti-rabbit IgG IRDye 680RD as a secondary for GAPDH (ab216779, Abcam) and a Goat anti-Mouse IgG H&L IRDye® 800CW as a secondary for ICAM. Longer incubation times with secondary antibodies resulted in higher non-specific background. Membranes were finally washed three times for 5-minutes in 0.01% TBS-Tween to remove any excess secondary fluorescent antibodies, before visualizing in the Licor Odyssey imaging system.

### **5.2.6 Data extraction and analysis**

To retrieve the raw data of the PCR results images of the gels were loaded to ImageJ, and a rectangular selection box was drawn over the first band visible in the gel. Using the “Analyse-Gel” functions from ImageJ all the bands were then selected, before selecting the function “plot lanes”, which produces a plot representing the relative density of each rectangle drawn, visualised as peaks in the graph. In order to measure the size of the peak, it needs to be isolated by “closing” it by drawing a straight line at the base of the peak. When all the peaks of interest have been “isolated”, through the function of ImageJ “Analyse-gels-Label peaks” the relative size will be calculated which can then be used for further analysis.

For ICAM-1 mRNA expression, HFLS from normal and RA joint donors were treated with the VEGF-A isoforms for 24 hours.  $\beta$ -actin was used as an internal loading control. ICAM-1 expression was corrected against  $\beta$ -actin expression, and then each independent value was normalized to the mean control value, i.e., the value from each experimental samples was divided by the mean of the DMSO control group. The DMSO controls were also normalised against the mean, hence the normalised mean of the control group = 1.

The experimental unit for synoviocyte ICAM1 expression and monocyte adherence was the treatment well. For PCR expression of SRPK1, SRSF1 and VEGF-A, the experiment was designed with the plate as experimental unit. Group numbers are shown on scatter graphs and in figure legends.



compared to TNF- $\alpha$  alone ( $p=0.33$  and  $p=0.9$  respectively), although Griffin 6 treatment did result in a non-significant increase in SRSF1 mRNA expression.

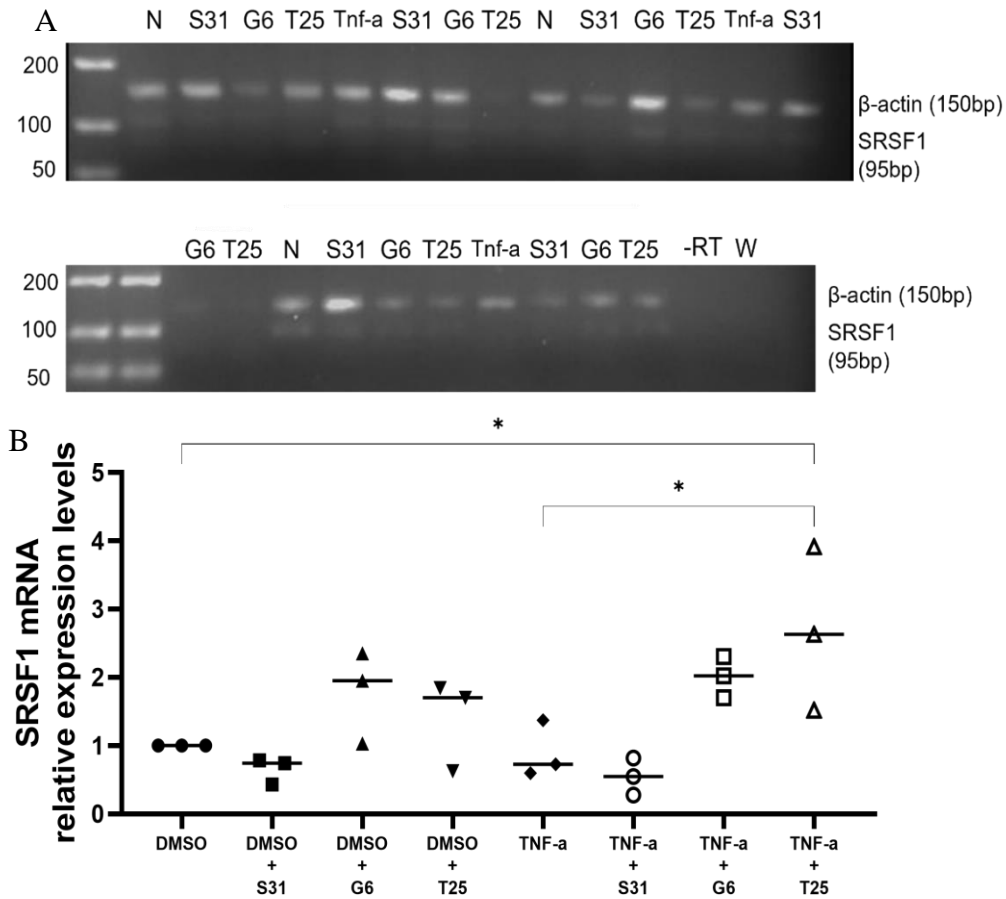


**Figure 50** Reverse transcription PCR for SRSF1 mRNA expression in Human fibroblast like synoviocytes (HFLS) after TNF- $\alpha$  and SPHINX31/Griffin 6/T-025 inhibitor treatment. Three separate biological replicas were used to identify the relationship of SRSF1 and the inflammatory phenotype of HFLS as well as the effect of splicing kinase inhibition. A) Images of the agarose gels, showing expression of SRSF1 mRNA in HFLS.  $\beta$ -actin and SRSF1 amplicons were amplified in separate PCR reactions, and an equal amount of each reaction loaded and run in the same wells to enable direct normalization of signal in relation to  $\beta$ -actin expression. B) SRSF1 band integrated density was normalized to  $\beta$ -actin from the same sample, and values compared to controls DMSO vehicle, and TNF- $\alpha$  treatments. Significant differences are indicated on the graph with median values (\* $p<0.05$ , one-way ANOVA + Tukey's multiple comparisons test).

The combined effect of TNF- $\alpha$  and T-025 on SRSF1 mRNA expression was greater and significantly different from the effect of TNF- $\alpha$  and DMSO alone ( $p < 0.02$ ,  $p = 0.04$ ,  $F = 4.8$ ,  $R^2 = 0.68$ , one way-ANOVA with Tukey's multiple comparison test).

### 5.3.1.3 Expression of VEGF-A mRNA in HFLS and effect of TNF- $\alpha$ and splicing kinase inhibitors.

**Total VEGF-A mRNA expression.** The VEGF-A reverse transcription PCR using primer set 2 amplifies total VEGF-A mRNA, from both splice variant families. Plasmids containing cDNA of each isoform were used as positive controls alongside the samples, validating that the PCR was working as intended, (Woolard et al., 2004), but no VEGF-A mRNA expression was detected (Figure 50). The VEGF-A<sub>165b</sub> plasmid was detected with a 220bp amplicon as previously shown (Woolard et al., 2004), while the VEGF-A<sub>165a</sub> plasmid was detected at ~150bp as expected (Woolard et al., 2004).

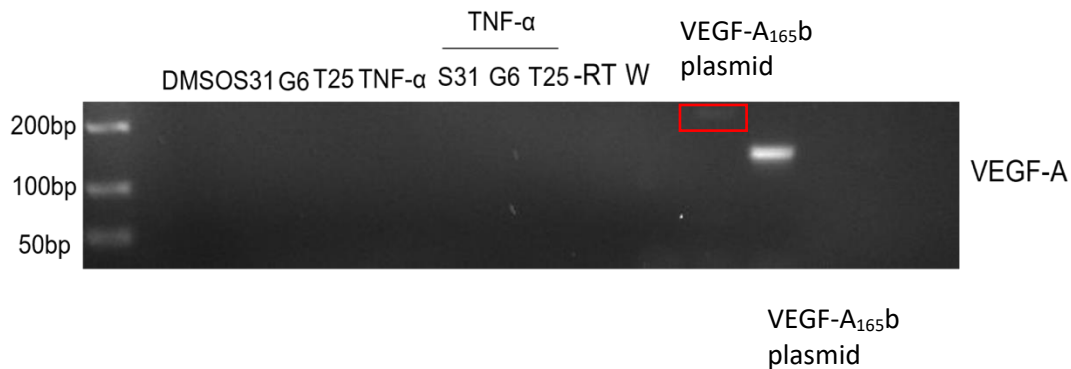


**Figure 51 PCR gel used to detect mRNA expression of VEGF-A in HFLS cells. VEGF-A was not detected in any of the treatments, however both of the positive controls used, namely the plasmids of both VEGF-A<sub>165a</sub> and VEGF-A<sub>165b</sub> were detected at their expected product sizes. Red box shows highlights the VEGF-A<sub>165b</sub> plasmid band.**

Competitive PCR with VEGF-A primer set 1 is predicted, and previously published, to result in two amplicons, 130bp representing VEGF-A<sub>165b</sub> with inclusion of exon 8a (see Figure 51), and 64bp representing VEGF-A<sub>165b</sub> without exon 8a. Two bands of ~65bp and 90bp in length were clearly detected at varying intensities in most treatments (Figure 51), but this was only the case in one of the three replicate plates. In the other two replicates, despite effective amplification

of  $\beta$ -actin and SRSF1 from the same samples (as shown above), I could not detect VEGF-A mRNA expression.

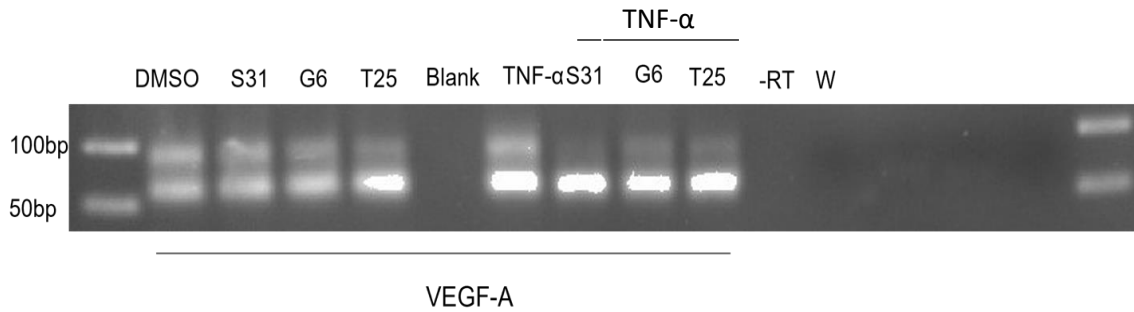


**Figure 52 Representative image of a PCR gel demonstrating the mRNA expression of VEGF-A in HFLS cells using the VEGF-A primer set 1. Two bands are clearly visible with the short one at ~64bp and the long one at ~90bp. N=1 denoting one plate with 3 wells per sample pooled for RNA extraction.**

As the longer amplicon was not the expected 130bp in length, the products were isolated and sequenced. Both bands were isolated separately and were re-amplified to ensure both sufficient DNA for sequencing, and to attempt to sequence each band separately (Figure 52). Further amplification of the short band yielded reasonably clean amplicons, but the re-amplification of the longer band again yielded two amplicons, suggesting contamination of the longer band with the shorter.

Those with the clearest and cleanest signal after re-amplification namely, the DMSO and TNF- $\alpha$  +T-025 long bands and the DMSO+S31 with the TNF- $\alpha$  short bands (figure 52) were gel purified and sequenced.

Sequencing results showed mixed sequences, probably due to the contamination of the two amplicons. However, VEGF-A cDNA sequences from the expected exons, albeit very short sequences, were identified in at least one of the samples. A sequence of 8 nucleotides derives from close to the splice site in exon 8 in the VEGF-A sequence, 33 nucleotides from the position of the downstream primer where expected.

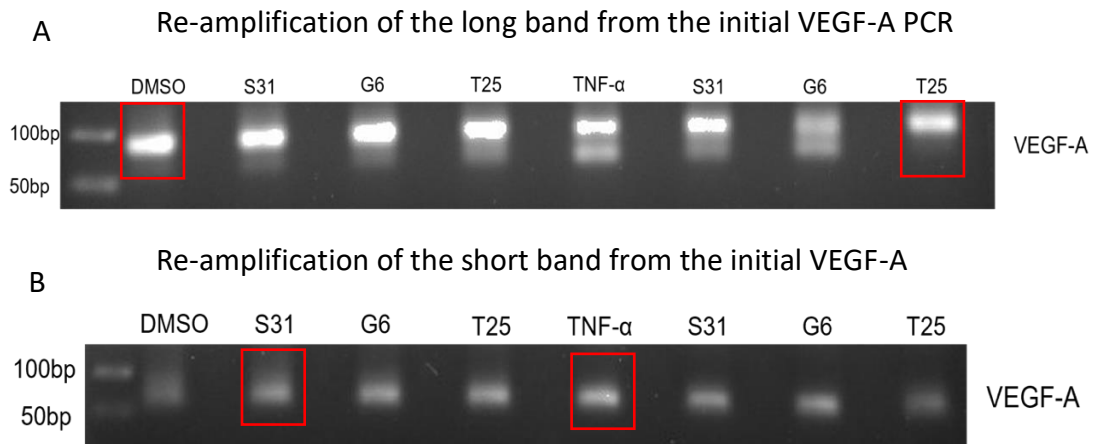


**Figure 53** Image of the PCR gel demonstrating the mRNA expression of VEGF-A after re-amplification, in order to sequence each band individually. A) The longer band was clearly detected in all the individual samples; however, two amplicons were detected in certain samples indicating potential contamination from the short band during isolation. B) Re-amplification of the short band demonstrating a clear signal on all the samples. The bands in the red frame were gel purified and sent for sequencing at DeepSeq University of Nottingham.

The probability of finding this 65bp sequence in an amplicon that did not derive VEGF-A is extremely low. This is not however conclusive evidence that the products derived from the VEGF-A cDNA.

As the VEGF-A PCR only yielded results on one of the four replicates, despite attempts at repetition, it was not possible to determine whether the splicing kinase inhibitors had any effect on VEGF-A splicing.

While I have not been able to show SRPK1 mRNA expression in these normal HFLS, they do express SRSF1 mRNA and the expression of this splice factor is altered, to some extent, by inhibition of splicing kinases. VEGF-A mRNA is also expressed, but due to lack of sufficient successful replicates, and impacts of the Covid pandemic on available laboratory time and reagents, I cannot make any conclusions on whether the splicing kinase inhibitors affect VEGF-A expression in these cells.

As I was not able to show that TNF- $\alpha$  altered VEGF-A splicing in HFLS using PCR, following discussion, I decided that it could be possible to use data from an *in vitro* functional assay of inflammation to investigate whether VEGF-A splice variants and inhibition of alternative splicing could affect VEGF-A control function. This *in vitro* model was developed, and the raw data were produced by Drs N Beazley-Long and M Swift, and I conducted the analyses presented here.

### **5.3.2 Mechanisms underpinning monocyte adhesion to human fibroblast-like synoviocytes *in vitro***

#### **5.3.2.1 VEGF-A splice variants alter ICAM-1 expression in human fibroblast-like synoviocytes.**

VEGF-A splice variants affected ICAM-1 mRNA expression differently in HFLS from normal or RA joints. VEGF-A<sub>165a</sub>, the pro-angiogenic, pro-nociceptive isoform dose-dependently increased ICAM-1 mRNA expression in HFLS from normal donor joints, while in RA derived HFLS, only the lowest concentration of VEGF-A<sub>165a</sub> (0.01 ng/ml) significantly increased the ICAM-1 mRNA expression (Fig 53A). The anti-angiogenic, anti-nociceptive isoform VEGF-A<sub>165b</sub> significantly increased ICAM-1 mRNA expression at the lowest concentration used (0.01ng/ml) in relation to DMSO controls and all other concentrations. At the higher concentrations VEGF-A<sub>165b</sub> resulted in a small but non-significant increase in ICAM-1 levels compared to control (Fig 54B). In HFLS from RA-affected joints, surprisingly, VEGF-A<sub>165a</sub> treatment resulted in a similar pattern of ICAM-1 mRNA expression to that caused by VEGF-A<sub>165b</sub> treatment of normal HFLS (Fig 53B). The lowest concentration altered ICAM-1 mRNA increasing it significantly compared to control, an effect that was lost when the cells were treated with 1 ng/ml of the VEGF-A<sub>165a</sub> isoform. VEGF-A<sub>165b</sub> evoked an effect on ICAM-1 mRNA expression that was not dose-dependent in RA HFLS.

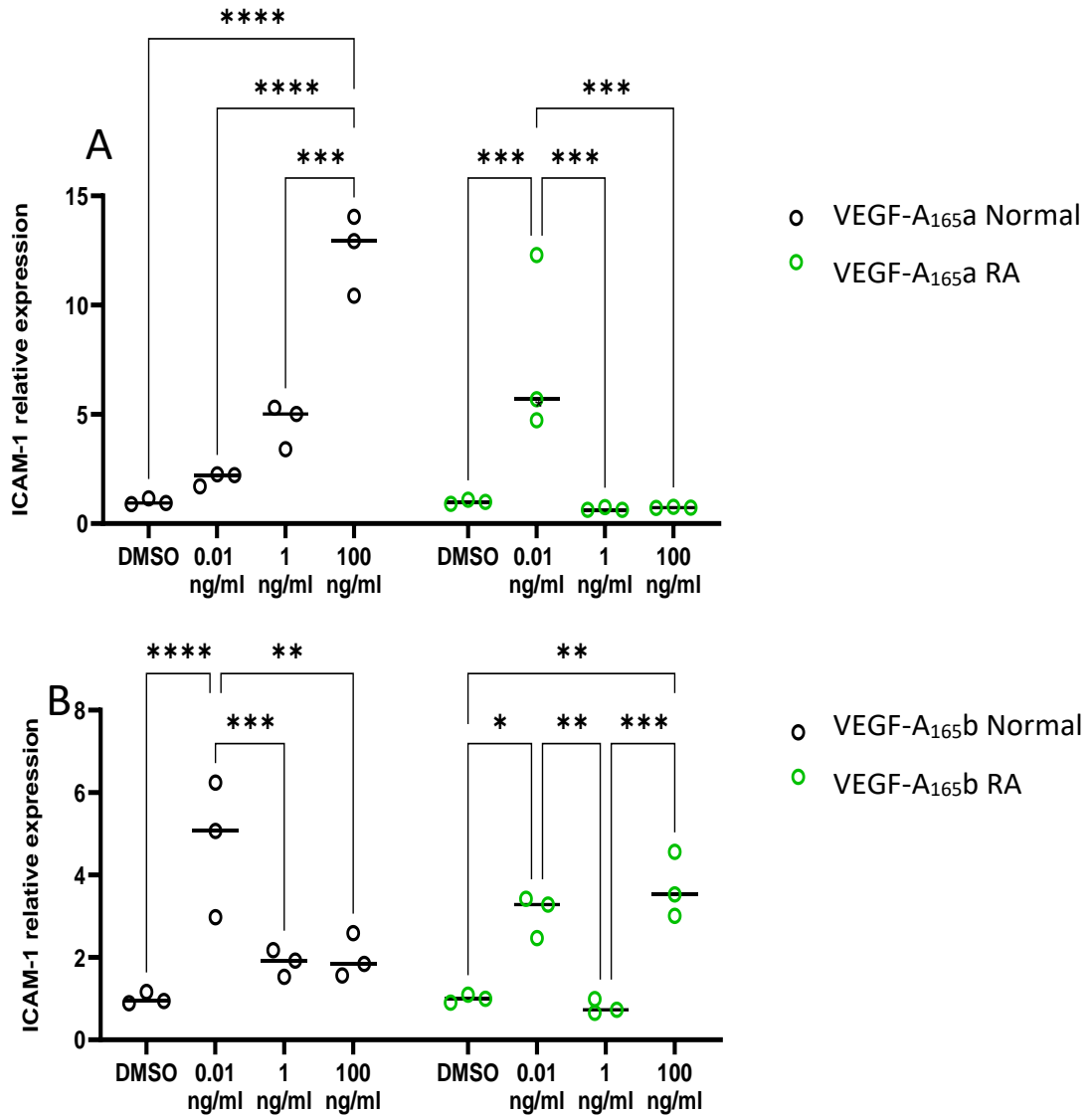


Figure 54 HFLS derived from both normal and RA joints were treated with ascending concentrations of VEGF-A<sub>165a</sub> or VEGF-A<sub>165b</sub>, to identify any potential alterations to the ICAM-1 gene expression levels. ICAM expression was quantified by qPCR and normalised to  $\beta$ -actin A) Effect of VEGF-A<sub>165a</sub> on ICAM-1 expression in normal HFLS is dose dependent, increasing ICAM-1 (DMSO cf 0.01ng/ml \*\*p=0.003; cf 1ng/ml \*\*\*\*p<0.0001; cf 100ng/ml \*\*\*\*p<0.0001). Similarly, ICAM-1 mRNA is increased in RA HFLS samples when treated with 0.01ng/ml of VEGF-A<sub>165a</sub> (\*\*\*\*p<0.0001 cf DMSO), while higher concentrations had no effect. B) Effect of VEGF-A<sub>165b</sub> on ICAM-1 expression had a similar pattern in normal and RA HFLS. In normal cells ICAM-1 mRNA levels were greatly increased when treated with 0.01ng/ml of VEGF-A<sub>165b</sub> (\*\*\*\*p<0.0001). In RA HFLS a similar pattern was observed with the 0.01 ng/ml treatment increasing the ICAM -1 mRNA expression compared to DMSO(\*p<0.005), an effect also observed in the group treated with 100ng/ml of VEGF-A<sub>165b</sub> (\*\*\*\*p<0.0001 cf DMSO). Two way-ANOVA with Tukey's multiple comparisons.

In order to directly compare the effects of each VEGF-A splice variant on normal and RA-derived HFLS, and to compare the effects of the two splice variants to each other, the data were replotted (Figure 55).

In normal HFLS the increase in ICAM-1 mRNA expression in response to VEGF-A<sub>165a</sub> was greater than that VEGF-A<sub>165b</sub> at **100ng/ml** (Fig. 55A, \*\*\*\*p=0.0001 VEGF-A<sub>165a</sub> cf. VEGF-A<sub>165b</sub>), an effect that was not observed at lower concentrations (1ng/ml p=0.06 VEGF-A<sub>165b</sub> cf. VEGF-A<sub>165a</sub>; 0.01ng/ml p=0.06 VEGF-A<sub>165b</sub> cf. VEGF-A<sub>165a</sub>). A similar but opposite effect was observed in the RA derived HFLS (Figure 54B), where at the lowest concentration VEGF-A<sub>165a</sub> increased the relative expression of ICAM-1 mRNA compared to the VEGF-A<sub>165b</sub> isoform (\*\*p=0.002), whereas at the highest concentration of 100ng/ml the mRNA expression of ICAM-1 was significantly increased when the cells were treated with VEGF-A<sub>165b</sub> (\*\*\*\*p<0.0001 VEGF-A<sub>165a</sub> cf. VEGF-A<sub>165b</sub>).

The effect of VEGF-A<sub>165a</sub> on ICAM-1 mRNA levels in normal compared to RA HFLS (Figure 55C) was similar to that of VEGF-A<sub>165a</sub> and VEGF-A<sub>165b</sub> in normal HFLS. Specifically, low concentration VEGF-A<sub>165a</sub> (0.01ng/ml) increased ICAM-1 mRNA to a greater extent in RA HFLS compared to normal (\*\*p<0.0001, normal HFLS cf. RA), an effect that was reversed at higher concentrations of the isoform (1ng/ml \*\*\*\*p<0.0001 RA cf. HFLS; 100ng/ml \*\*\*\*p<0.0001 RA cf. HFLS).

Regarding the effect of VEGF-A<sub>165b</sub> on ICAM-1 mRNA levels in between the HFLS and RA group (Figure 55D), no alterations were observed at the lowest concentration of treatment (0.01ng/ml p=0.3 normal cf. RA), ICAM-1 mRNA expression was lower but not significant in the RA HFLS at 1 ng/ml (p=0.7 normal cf. RA), and higher but again not significant in RA at 100ng/ml compared to normal HFLS (p<0.03 normal cf. RA)

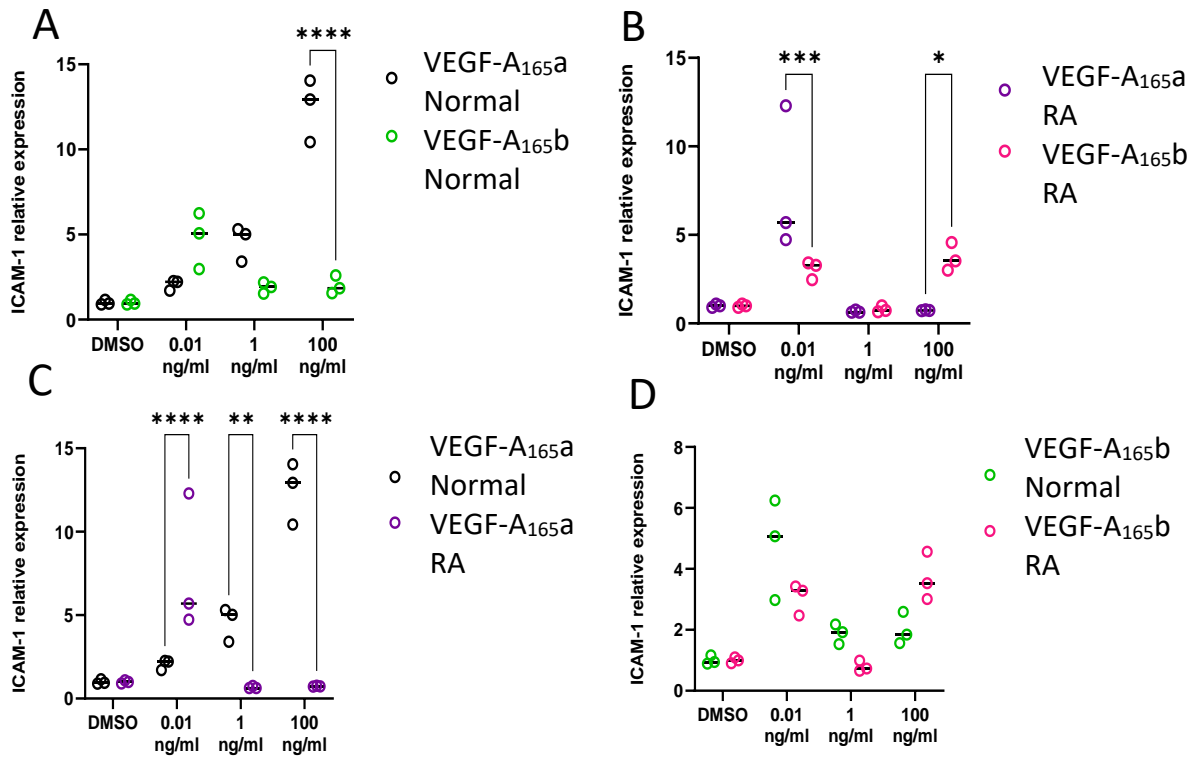
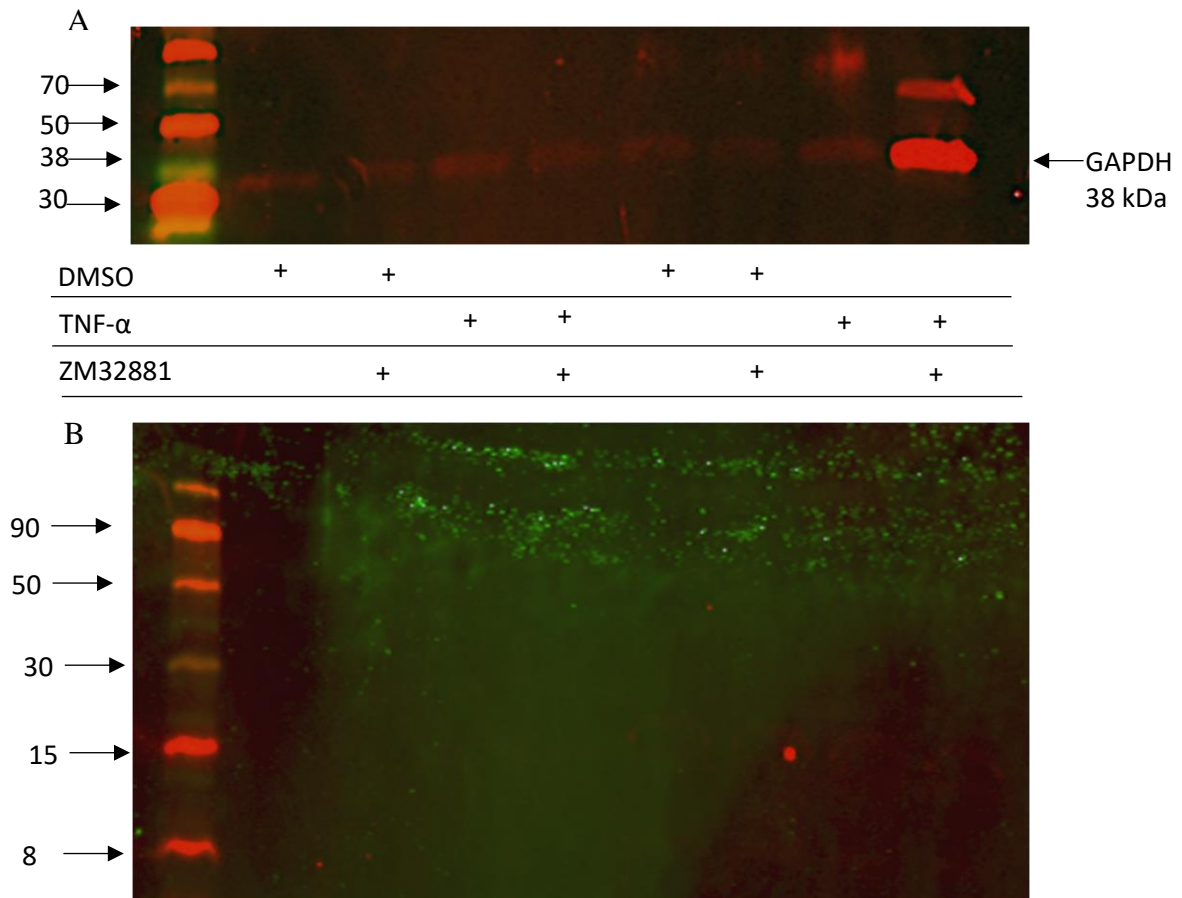


Figure 55 HFLS derived from both normal and RA joints were treated with ascending concentrations of VEGF-A<sub>165a</sub> or VEGF-A<sub>165b</sub>, to determine effect on ICAM-1 mRNA expression levels A) Increasing concentrations of VEGF-A<sub>165a</sub> have different effects on the levels of ICAM-1 mRNA expression in normal HFLS compared to VEGF-A<sub>165b</sub> treatment. At 0.01 ng/ml, and 1ng/ml treatments ICAM-1 is not significantly altered when treated with VEGF-A<sub>165a</sub> in comparison to VEGF-A<sub>165b</sub> ( $p>0.005$ ). At 100ng/ml treatments with VEGF-A<sub>165a</sub> promotes high levels of ICAM-1 mRNA expression levels (\*\*\*\* $p<0.0001$  1ng/ml, 100ng/ml VEGF-A<sub>165a</sub> cf VEGF-A<sub>165b</sub>. B) In RA cells a similar but opposite effect is observed with the 0.01ng/ml treatment of VEGF-A<sub>165b</sub> significantly decreasing the levels of ICAM-1 mRNA (\*\* $p=0.0002$  cf VEGF-A<sub>165a</sub>), while in the higher concentrations treatments ICAM-1 expression is favoured with the VEGF-A<sub>165b</sub> treatment (\*\*\*\* $P<0.00001$  cf VEGF-A<sub>165a</sub>). C) When comparing normal to RA HFLS per treatment, VEGF-A<sub>165a</sub> seems to further increase ICAM-1 levels in the RA samples in low concentration (0.01ng/ml \*\*\*\* $p<0.00001$  normal cf RA, an effect that is reversed in higher concentrations with the VEGF-A<sub>165a</sub> treated normal HFLS showcasing high levels of ICAM-1 mRNA (1ng/ml \*\* $p<0.0001$  normal cf RA; 100ng/ml \*\*\*\* $p<0.0001$  normal cf RA). D) Treating RA and normal HFLS with VEGF-A<sub>165b</sub> seem to not alter the levels of ICAM-1 significantly, when making in between group comparisons ( $p>0.005$ ). All data were analysed using two-way ANOVA with Tukeys multiple comparisons.

I then performed Western blots to attempt to confirm the presence and levels of ICAM-1 protein expression in TNF- $\alpha$  treated HFLS. I hypothesized that ICAM protein levels would increase in TNF- $\alpha$  treated HFLS as a result of the change in ICAM-1 mRNA expression (Figure 44). Cells were treated with TNF- $\alpha$  as for mRNA expression, and with a selective VEGFR2 inhibitor, ZM32881 to determine whether endogenous VEGF-A contributed to ICAM-1 expression (n=3). Figure 56 shows an example western blot with samples from two of the experimental repeats. Unfortunately, although GAPDH can be clearly seen on this blot, ICAM-1 protein was not successfully detected in any of the attempts. Despite changing experimental conditions, and due



**Figure 56** Western blot for ICAM-1 and GAPDH in human fibroblast like synoviocytes after TNF- $\alpha$  and anti-VEGFR2 treatment. A) Membrane was incubated with anti-GAPDH antibodies and fluorescently labelled secondary antibodies and imaged in a Licor Odyssey system. Clear signal of GAPDH can be seen in the sample treated with TNF- $\alpha$  and the ZM inhibitor, while also being detectable in the rest of the lanes. B) Membrane incubated with anti-ICAM-1 antibody and the appropriate secondary. No signal was detected issuing the need for further optimization. 50ug of protein was used per well. (GAPDH: Loading control, TNF- $\alpha$  1ng/ml; ZM32881 10nM; n=3 plates).

to time and COVID restraints I was unable to optimise the Western blot conditions; additionally, problems with equipment failure affected my ability to successfully detect ICAM-1 protein. I therefore decided to approach the same question using data generated using an indirect functional assay rather than direct measurement of ICAM-1 itself.

### **5.3.2.2 THP-monocyte adherence to HFLS is mediated through an ICAM-1/ VEGF-A/SRPK1-dependent mechanism and is reduced by inhibition of ICAM-1, SRPK1 and/or VEGF receptors *in vitro*.**

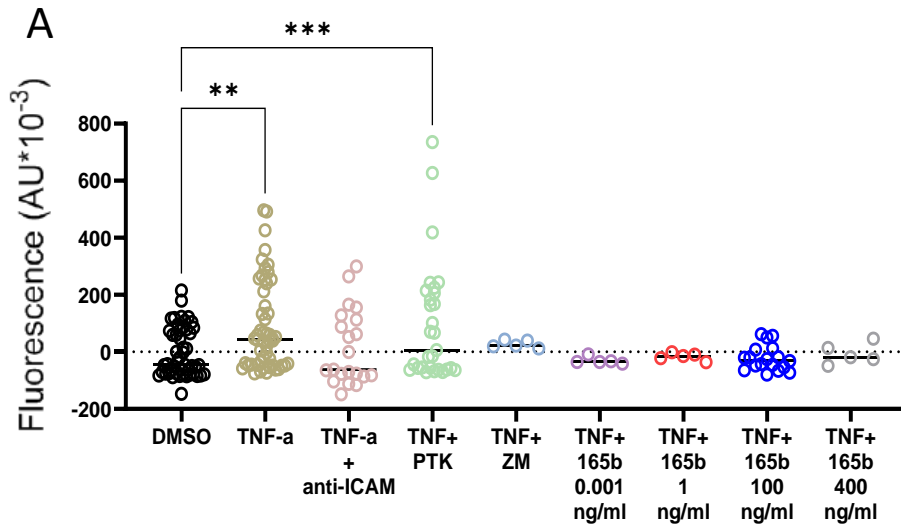
Human primary fibroblast-like synoviocytes derived from both normal and RA joints were cultured and stimulated with TNF- $\alpha$  to induce an inflammatory response, incubated with fluorescent THP-monocytes and anti-ICAM-1 neutralising antibody, as well as VEGF receptor blockers PTK787 and ZM323881 to determine whether the mechanism of monocyte attachment involved ICAM-1 and VEGF-A.

In both normal and RA HFLS TNF- $\alpha$  increased THP-monocyte adherence ( $p=0.002$ ,  $p=0.009$  respectively), which was reduced by treatment with the selective VEGFR inhibitor PTK787 in normal HFLS ( $p=0.0002$  cf. TNF- $\alpha$  treatment). In contrast, in the RA samples treated with PTK787 THP-monocyte adherence increased compared to the DMSO control ( $p=0.0007$  cf. DMSO, Figure 57A).

In normal HFLS, inhibition of VEGFR2 with the specific ZM323881 inhibitor significantly reduced the THP monocyte induced fluorescence ( $p=0.003$  cf. TNF- $\alpha$ ). A similar effect was also observed when the cells were treated with VEGF-A<sub>165b</sub>, with significant reductions at 0.001 ng/ml and 400ng/ml of ( $p=0.0007$  and  $p=0.008$  cf. TNF- $\alpha$  respectively, Figure 57B).

There was no obvious TNF- $\alpha$ -induced THP monocyte adherence in RA HFLS also treated with either ZM323881 or ascending concentrations of VEGF-A<sub>165b</sub>, however these were not significantly different from TNF- $\alpha$  stimulated HFLS alone. Even though these findings were not significant, these data still suggested that VEGF-A<sub>xxx</sub>b isoforms could inhibit THP monocyte adherence to human HFLS.

Monocyte attachment assay in RA human fibroblast like synoviocytes



Monocyte attachment assay in healthy human fibroblast like synoviocytes

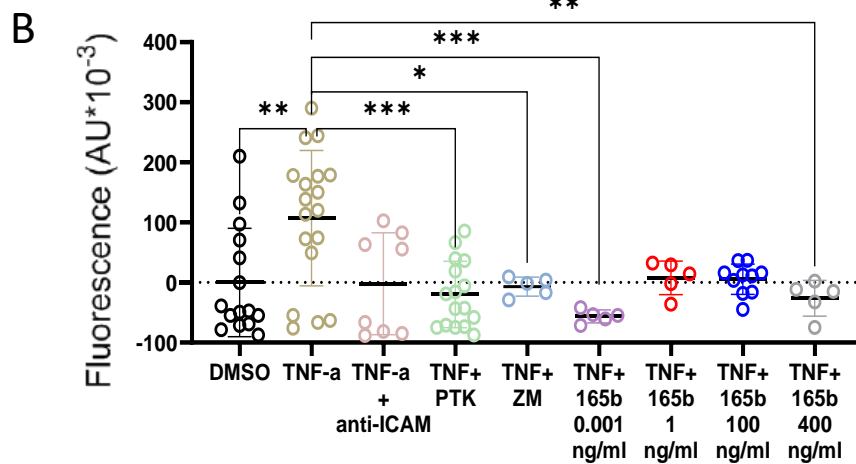


Figure 57 THP-1 cells were plated over HFLS to measure fluorescent levels of adherent monocytes. A) TNF- $\alpha$  treated RA HFLS promote the adherence of monocytes resulting in increased fluorescence levels when compared to the DMSO controls ( $p=0.009$  cf. DMSO), an effect that is also observed when RA HFLS are treated with the combination of TNF- $\alpha$  and PTK ( $p=0.0007$  cf. DMSO). The rest of the treatments with anti-ICAM or VEGF-A<sub>165b</sub> seem to influence the levels of fluorescence in comparison to TNF- $\alpha$  treatment however this effect is not significant. B) In healthy HFLS TNF- $\alpha$  increases the THP induced ICAM-1 fluorescence compared to DMSO ( $p=0.002$  cf DMSO), an event that is revoked when the cells are treated with PTK, ZM or VEGF-A<sub>165b</sub> ( $p=0.0002$  PTK cf TNF- $\alpha$ ;  $p=0.003$  ZM cf. TNF- $\alpha$ ;  $p=0.0007$  VEGF-A<sub>165b</sub> 0.001ng/ml cf. TNF- $\alpha$ ;  $p=0.008$  VEGF-A<sub>165b</sub> 400ng/ml cf TNF- $\alpha$ ). Two-way ANOVA with Tukey's multiple comparisons.

I therefore wanted to identify if the changes described above were due to TNF- $\alpha$  induced change in the VEGF-A splicing, as seen in other cells types, using SRPK1 inhibition in the THP monocyte adherence assay as an indirect measure of VEGF-A splicing. Validated SRPK1 inhibitors SPHINX and SPHINX31 were used in RA HFLS treated with DMSO or TNF- $\alpha$ , alongside treatment with VEGF-A<sub>165b</sub> (Figure 58A). Although TNF- $\alpha$  did not increase THP monocyte adherence in these experiments, SPHINX did significantly reduced THP monocyte adherence when compared to both the TNF- $\alpha$  ( $p=0.004$  cf. TNF- $\alpha$ ) and VEGF-A<sub>165b</sub> treated HFLS ( $p=0.003$  cf. VEGF-A<sub>165b</sub>). SPHINX31 slightly reduced monocyte attachment however the change was not significant.

Finally, given the effect of the known SRPK1 inhibitors on this *in vitro* assay of inflammation, I then used the assay to test the efficacy of novel SRPK1 compounds in a functional assay. These novel compounds were synthesised on the SRPIN340 structure and are known SRPK1 inhibitors (Table 15).

Of the SRPIN inhibitors, only SRPIN4 displayed a pattern of reducing monocyte attachment. Specifically, it significantly reduced THP monocyte adherence when compared to the TNF- $\alpha$  treated HFLS ( $p=0.001$ ). Moreover, it was a significantly more potent inhibitor compared to SRPIN2 and SRPIN3, an effect that was similar to the potency of SPHINX. SPINX31 and SRPIN340, both displayed a pattern of reducing monocyte attachment, however the change observed in this experiment was not significant.

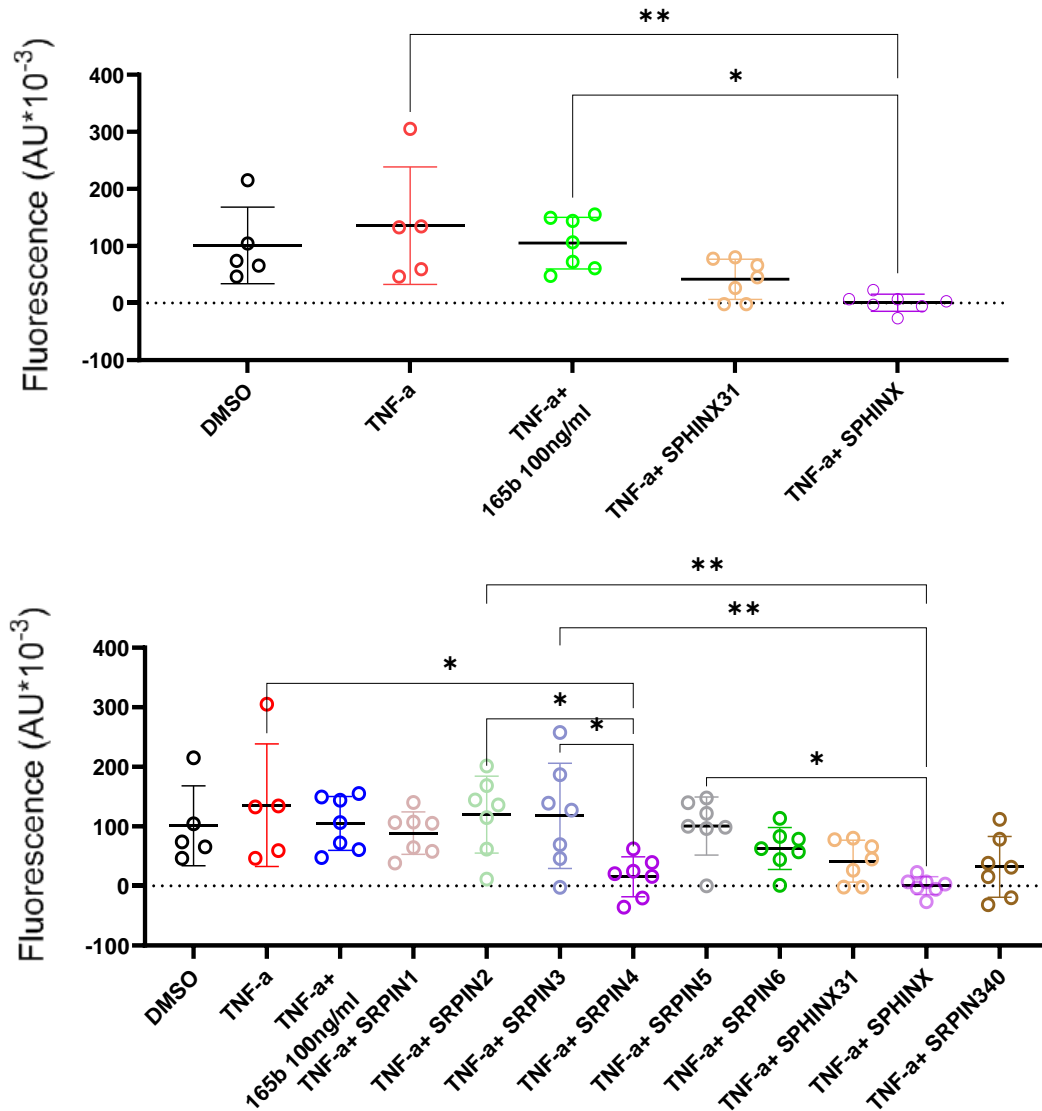


Figure 58 A) Treating RA HFLS with SPHINX after treatment with TNF- $\alpha$  reduces the overall levels of ICAM-1 fluorescence as induced by THP adherence ( $p=0.004$  SPHINX cf. TNF- $\alpha$ ;  $p=0.03$  SPHINX cf. VEGF-A<sub>165b</sub>). Similarly, to SPHINX, SPHINX31 showcases an overall reduction to the levels of ICAM fluorescence an effect that is not significant. B) Different SRPK1 inhibitors were tested in comparison to the effects of SPHINX on the RA HFLS, to identify how inhibition of SRPK1 affects THP monocyte adherence. Only SRPIN4 significantly reduced the fluorescence levels compared to the other inhibitors ( $p=0.01$  cf. TNF- $\alpha$ ;  $p=0.03$  cf. SRPIN2;  $p=0.03$  cf. SRPIN3). SPHINX was also more potent in comparison to the effects of SRPIN2 and SRPIN3 ( $p=0.006$  cf. SRPIN2;  $p=0.008$  cf. SRPIN3). SPHINX31 as well as SRPIN340, showcased a pattern of reducing the overall levels of fluorescence when compared to the TNF- $\alpha$  treated cells, however this was not a significant change. One-way Anova with Tukey's multiple comparisons.

## 5.4 Summary of results

- SRSF1 mRNA expression was increased in TNF- $\alpha$  stimulated HFLS by CLK inhibition by T-025, and partially by Griffin6, indicating that CLKs 1,2 and 4 are potentially involved in control of SRSF1 mRNA expression
- VEGF-A mRNA was expressed in HFLS, but the presence of splice variants could not be confirmed.
- Fluorescent THP-1 monocytes adhere to TNF- $\alpha$  stimulated HFLS, in part through an ICAM-1 mediated mechanism. THP-1 monocyte adherence to HFLS can be used as an *in vitro* model of synovial inflammation.
- THP-1 monocyte adherence to HFLS can be blocked by VEGF<sub>-165b</sub> and by both validated and novel SRPK1 inhibitors.

## 5.5 Discussion

### 5.5.1 SRPK1, and SRSF1 expression in HFLS in culture and alteration by TNF- $\alpha$ , and splicing kinase inhibition.

Our initial hypothesis was that blocking the kinases which play a role in the VEGF-A splicing axis would reduce the *activation* of SRSF1, but I also determined whether kinase inhibition affected mRNA expression of members of the splicing axis, as very little is known about this. On phosphorylation by SRPK1 in the cytoplasm SRSF1 translocates to the nuclear speckles of the cells (Aubol, Keshwani et al. 2018). After this change in the localization of SRSF1, CLK1 inside the nucleus is responsible for releasing the splicing factor from the speckles before SRSF1 can become functional. CLK1 acts to enable shuttling of mRNAs due to its RS Domain. The RS domain is one of the main building blocks of all SR proteins, with the general structural organization including the arginine/serine-rich domain (RS domain), an RNA recognition motif (RRM), RRM homology (RRMH) domain, and a Zinc knuckle (Zn) domain (Shepard and Hertel 2009). Of these domains, the RS, RRM and RRMH are the main structural features of the SR proteins and in the case of SRSF1, all three are present.

Previous literature suggests that SRSF1 has the ability to auto-regulate its own mRNA expression, results obtained from retroviral transduction of human, mouse, and rat cells (Sun, Zhang et al. 2010). This autoregulation effect works based on SRSF1 modulating its own alternative splicing either by decreasing the protein coding isoforms or increasing isoforms that are degraded by NMDs or retained in the nucleus. In principle, SRSF1 autoregulation seems to operate in an interplay between two modes; a “robust” mode where the concentration of the splicing factor is abundant in the cell, and thus no change in the expression pattern occurs, and an “adaptive” mode where the available SRSF1 is lower in the cell reducing feedback, and signalling the need to generate more SRSF1 protein (Ding, Su et al. 2020). Although SRPK1 inhibition had no effect on SRSF1 mRNA expression, we could speculate that the increase in SRSF1 mRNA expression on treatment with the pan-CLK inhibitor T-025 may be a result of an effect on the auto-regulatory functions of SRSF1. If the SRSF1 protein is not released from the speckles due to CLK1 inhibition, then feedback loops would signal that more ASF/SF2 protein is required for either the splicing in the nucleus of the cells, or the shuttling of mRNAs from the nucleus to the cytoplasm. As there was a smaller, similar but non-significant change in SRSF1 mRNA expression with CLK1&2

inhibition by Griffin6, and there were non-significant changes in the pattern of the SRSF1 expression. As G6 is a CLK1&2 inhibitor, and T-025 is pan-CLK + DYRK1A/B inhibitor that is more potent against CLK2, the results suggest that the extra targets inhibited by T-025 are enough to alter the mRNA expression of SRSF1. Specifically, we could hypothesise that the inhibition of CLK4 or DYRK1A would be enough to shift the result of SRSF1 expression. CLK4 has been implicated before in its ability to inactivate SRSF1, as well as its phosphorylation of the splicing factor SRP55, resulting in the distal splicing site selection and production of VEGF-A<sub>xxx</sub>b. DYRK1A inhibition from T-025 could also play a role in comparison to the G6 inhibitors. We already know that DYRK1a can phosphorylate SRSF1, as well as it can reduce pain and inflammation through the Wnt pathway. Perhaps the blocking of the kinase and thus its inability to phosphorylate SRSF1, feeds into an autoregulation of the splicing factor as discussed above, and eventually an increase in its mRNA expression. However, since no-one has looked before into these mechanisms and alteration, we could only hypothesise, even though it is clear that CLK2, as well as the inhibition of additional CLKs is important in the control of SRSF1 mRNA expression.

### **5.5.2 VEGF-A isoform and ICAM-1 expression in HFLS.**

Measurement of VEGF-A isoform mRNA expression is notoriously difficult, and I was unable to confirm either isoform expression or determine whether splicing was changed in the HFLS by kinase inhibition, despite using published primers and protocols (Nowak, Amin et al. 2010, Bates, Mavrou et al. 2013). Optimisation of the PCR proved difficult, and I could not isolate amplicons of the predicted sizes. Isolating the individual bands for sequencing was also difficult as there was contamination of the two bands, and while I did confirm VEGF-A sequence in at least one of the PCR products, I could not identify isoform specific sequences.

Difficulty in identification of VEGF-A isoforms by PCR can be due to many confounds. Recent findings (David Bates personal communication) show that VEGF-A<sub>xxx</sub>b isoforms do not have an extensive poly-A<sup>+</sup> tail, which can result in underrepresentation of VEGF-A<sub>xxx</sub>b isoforms in reverse transcription reactions using oligo-dT<sup>-</sup> primers. I therefore also used the downstream VEGF-A primer plus random hexamers for the reverse transcription reaction to isolate only VEGF-A cDNAs. Unfortunately, this still did not lead to clear isoform specific PCR products. In addition to a short polyA<sup>+</sup> tail, modelling of the secondary structure of the 3'UTR region of the VEGF-A<sub>xxx</sub>b

mRNA shows that it is different to that of VEGF-A<sub>xxx</sub>a (Qiu, Hoareau-Aveilla et al. 2009) which would lead to a potential difference in the efficiency of the RT reaction, resulting in much lower representation of VEGF-A<sub>xxx</sub>b transcripts. Problems can also arise through VEGF-A<sub>xxx</sub>a transcripts outcompeting VEGF-A<sub>xxx</sub>b transcripts in the PCR reaction particularly when VEGF-A<sub>xxx</sub>a transcripts are highly expressed such as in transformed cell lines/cancer cells where splicing is known to be switched in favour of VEGF-A<sub>xxx</sub>a (Shulzhenko et al., 2003, Bates et al., 2013, Harvey and Cheng, 2016). RT-PCR for VEGF-A isoforms with a competitive primer set as used here assumes that during the PCR reaction the two products amplify equally. In situations where VEGF-A<sub>xxx</sub>a may be expressed at higher levels, we would assume that the VEGF-A<sub>xxx</sub>b isoforms will also be amplified to some extent but could not confirm this by sequencing. Unfortunately, further optimisation and alteration of experimental conditions were not possible due to time constraints and the Covid pandemic.

ICAM-1 mRNA expression has recently been shown to be induced by VEGF-A/VEGFR2 activation in spinal cord endothelial cells in vivo (Beazley-Long et al 2018), and by VEGF-A<sub>xxx</sub>a isoforms in retinal pigmented epithelial (RPE) cells and retina resulting in increased retinal permeability (Ishida, Usui et al. 2003, Tang and Kern 2011, Thichanpiang, Harper et al. 2014). VEGF-A<sub>165</sub>b blocks the increased ICAM-1 expression in RPE cells and is therefore to be potentially anti-inflammatory (Ishida, Usui et al. 2003, Ved, Hulse et al. 2017). As TNF- $\alpha$  upregulates both ICAM-1 and VEGF-A mRNA in HFLS (Figure 44), I hypothesised that VEGF-A isoforms, specifically VEGF-A<sub>165</sub>a isoform would increase ICAM-1 expression in HFLS promoting an inflammatory response in HFLS. This was the case in normal HFLS, but surprisingly, in HFLS from a donor with RA, only the lowest concentration of VEGF-A<sub>165</sub>a significantly alter the ICAM levels compared to controls. In most normal tissues, VEGF-A<sub>xxx</sub>b is the predominant isoform and levels of VEGF-A<sub>xxx</sub>a are low (Pritchard-Jones, Dunn et al. 2007). When VEGF-A<sub>165</sub>b, a partial agonist at VEGFR2, is predominant it promotes a reduction of the number of available VEGFR2 on the cell surface (Ballmer-Hofer, Andersson et al. 2011). Increased exogenous VEGF-A<sub>165</sub>a, a full agonist of VEGF-A<sub>165</sub>b for the binding to the receptors, would promote HFLS synoviocyte VEGFR2 activation, recycling to the cell membrane and as I have shown, an increased pro-inflammatory phenotype with the induction of ICAM, and the production of other inflammatory molecules.

Activation of VEGF receptors stimulates angiogenesis, synoviocyte survival and hyperplasia, and synoviocyte-driven promotion of inflammatory responses through activation of macrophages

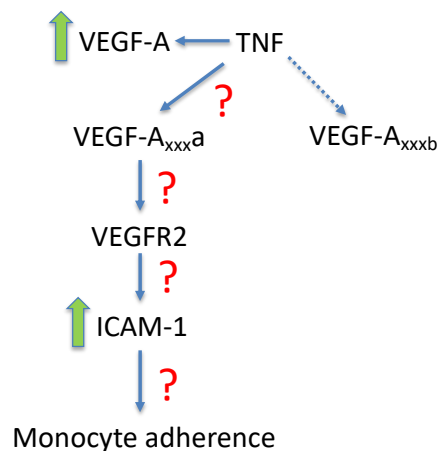
(Yoo, Kwok et al. 2008). In RA pan-VEGF-A is already upregulated, and in pro-inflammatory conditions, this upregulation is most likely to be due to an alteration in splicing events leading to increased VEGF-A<sub>165a</sub> production. We could therefore speculate that the difference in the effect of VEGF-A<sub>165a</sub> on RA HFLS, which would further increase in the proportion of VEGF-A<sub>165a</sub>, is incapable of producing further ICAM-1 mRNA changes, possibly as a result of any receptor response being already at maximum.

Surprisingly, when I investigated the effect of VEGF-A<sub>165b</sub> on ICAM-1 mRNA expression in normal HFLS, treatment with 0.01ng/ml of VEGF-A<sub>165b</sub> increased ICAM-1 mRNA compared to controls, an effect that was not seen at higher concentrations. This comes in disagreement with our initial hypothesis in which I predicted that as VEGF-A<sub>165b</sub> competes with VEGF-A<sub>xxx</sub>a at VEGFR2, it would exert opposite effects to VEGF-A<sub>165a</sub>, and therefore reduce ICAM-1 expression. In contrast VEGF-A<sub>165b</sub> resulted in a similar pattern of ICAM-1 expression in normal HFLS to that in RA HFLS treated with VEGF-A<sub>165a</sub>. As VEGF-A<sub>165b</sub> and VEGF-A<sub>165a</sub> are usually both present, and their expression can be related, considering the effects of each isoform alone on cultured cells may not reflect the situation in the joint. We know that in RA HFLS VEGF-A<sub>165a</sub> is highly likely to already be upregulated, so it is possible that introduction of VEGF-A<sub>165b</sub> may not be sufficient to alter the effect of any endogenous VEGF-A<sub>165a</sub> already present. As VEGF-A<sub>165b</sub> is a competitive antagonist for VEGF-A<sub>165a</sub> binding at VEGFR2, and blocks for example, the effects of VEGF-A<sub>165a</sub> in tumour growth (Hamdollah Zadeh, Amin et al. 2015) and sensory neuronal activation (Hulse, Beazley-Long et al. 2014), we would expect that it would have similar effects in RA HFLS, which was not the case. This may be that ICAM-1 levels were low in control RA HFLS, although such a floor effect is unlikely, as VEGF-A<sub>165b</sub> treatment increased ICAM-1 expression at some concentrations. It is not possible to reach a definitive conclusion on the detailed mechanisms of how the different VEGF-A isoforms might affect adhesion molecule expression from these experiments alone, although they seem to have distinct effects in normal and RA HFLS.

### **5.5.3 THP-monocyte adherence to HFLS *in vitro* is mediated by VEGF-A receptor 2 and ICAM-1.**

The THP-monocyte attachment assay was employed as an *in vitro* technique to model an inflammatory response in human fibroblast like synoviocytes treated with TNF- $\alpha$  as an indirect method to identify the effect of the VEGF-A<sub>165b</sub> isoform and SRPK1-mediated alternative splicing on HFLS, due to the difficulties encountered in detecting VEGF-A splicing changes through PCR.

The monocyte attachment assay has been demonstrated to be a useful tool in identifying specific binding mechanisms in epithelial and endothelial cells (Beazley-Long et al. 2018b; Thichanpiang et al. 2014). Preliminary work by Dr Nicholas Beazley-Long showed that VEGF-A<sub>xxx</sub>a directly induced THP-1 binding to HFLS. TNF- $\alpha$  upregulated pan-VEGF-A in RPE and podocytes (Nowak, Woolard et al. 2008), and further preliminary experiments also stimulated ICAM-1 mRNA expression, and increased levels of monocyte adherence in HFLS (Figure 44), leading to our



hypothesis that a similar mechanism of VEGF-A-mediated monocyte adherence might also occur in HFLS, promoting an inflammatory state. Additionally, the splicing kinase identified as key to the alternative splicing of VEGF-A isoforms, SRPK1, is also implicated in inflammatory processes (Patel, Sachidanandan et al. 2019).

The figure (left) shows the hypothesized mechanism of VEGF-A effects on monocyte

adherence in the *in vitro* model (also in Figure 44). The neutralizing anti-ICAM-1 antibody only partially reduced adherence, suggesting that other adhesion molecules may play a role in this monocyte binding, namely VCAM-1 and CD31/Platelet and Endothelial Cell Adhesion Molecule-1 (PECAM-1) (Wong and Dorovini-Zis 1995). While I was unable to demonstrate a change in VEGF-A splicing in TNF- $\alpha$  treated HFLS, I confirmed that VEGFR2 and not VEGFR1 is key to monocyte adherence, using the VEGFR2 selective and specific antagonists PTK787 and ZM32882. Moreover, when the cells were treated with VEGF-A<sub>165</sub>b, a competitive antagonist at VEGFR2, THP-1 monocyte adherence was reduced in both RA and normal HFLS. While the reduction in monocyte adherence was not statistically significant at some VEGF-A<sub>165</sub>b concentrations especially in RA HFLS, the lower monocyte adherence is very clear (Figure 57). These results replicate the previous findings in RPE cells (Thichanpiang, Harper et al. 2014), and are in accordance with our hypothesis that VEGFA<sub>xxx</sub>b would block VEGFA<sub>xxx</sub>a through inhibition of ICAM-1. Unfortunately, due to problems with Western blotting I was unable to directly confirm an effect on ICAM-1 protein expression. Although the pro-angiogenic and pro-inflammatory effect of VEGF-A on macrophages, (presumed to be VEGF-A<sub>xxx</sub>a with our now greater

understanding of the functions of the different splice variants) have obviously been recognized for some time (Yoo, Kwok et al. 2008), this is, to my knowledge, the first demonstration of a potential anti-inflammatory action of VEGF-A<sub>xxx</sub>b.

#### **5.5.4 THP-monocyte adherence to HFLS is mediated through an SRPK-1-dependent mechanism *in vitro*.**

SPHINX is a novel tool compound inhibitor of SRPK1 known to alter VEGF-A splicing also significantly reduced monocyte adherence fluorescence. The SPHINX chemical structure is the basis for SPHINX31 (Batson, Toop et al. 2017), whereas the SRPIN inhibitors are based on the SRPIN340 structure designed to have greater potency and selectivity for SRPK1 over SRPK2. SPHINX and SRPIN4 have similar IC<sub>50</sub> against SRPK1, significantly inhibit both SRPK1 activity *in vitro* (Batson et al), VEGF-A splicing (L Donaldson, personal communication) and reduced the binding of monocytes to TNF- $\alpha$  treated cells. This indicates that monocyte attachment is mediated by a mechanism that is disrupted by SRPK1 inhibition, with the hypothesised downstream target of increased splicing to VEGF-A<sub>xxx</sub>b). Inhibition of the splicing kinase SRPK1, through the inhibitors shifts the splicing from the pro-angiogenic isoform of VEGF-A (VEGF-A<sub>165a</sub>) to the anti-angiogenic one (VEGF-A<sub>165b</sub>) (Nowak, Amin et al. 2010, Amin, Oltean et al. 2011, Gammons, Fedorov et al. 2013). Co-treatment with an anti-VEGF-A<sub>xxx</sub>b neutralising antibody would confirm whether this splicing change does result in the inhibitory effect. There are currently no commercially available antibodies of this type, but while further work is needed to fully understand the mechanism of SRPK1 inhibition of monocyte adherence, these results support the current hypothesis. These data also show that, whatever the downstream target, SRPK1 inhibition also has potential anti-inflammatory action. Of the reported SRPK1 downstream splicing targets, the majority are implicated in cancer (Hulse, Beazley-Long et al. 2014), such as BCL-2 (Wang, Zhou et al. 2020), including of course VEGF-A, and VEGF receptors involved in angiogenesis (Jia, Jacquet et al. 2021), and many of these identified targets are also implicated in arthritis or inflammation. For example, the serine/threonine kinase MKNK2 regulates macrophage function (Su, Yu et al. 2015). While VEGF-A<sub>165b</sub> is an antagonist to VEGF-A<sub>165a</sub> for binding at VEGFR2, and does reducing monocyte adherence, the effect is small, and this may be because altering the VEGF-A<sub>165a</sub>/ VEGF-A<sub>165b</sub> ratio with exogenous protein is not effective

enough. Changing the isoform ratio by targeting VEGF-A splicing may therefore be a more effective mechanism to inhibit a pro-inflammatory state in HFLS.

The results using different inhibitors with different structures and  $IC_{50}$ s show that the monocyte adherence assay can detect differences between them. This indicates that this assay could potentially be used as a screening mechanism for novel anti-inflammatory compounds.

### 5.5.5 Splicing kinase inhibitors

There has been a considerable amount of work done on development of splicing kinase small molecule inhibitors, and this is increasing, due to their importance in cancers. Table 14 (introduction) compares some of the older compounds such as Harmine, and the more recent but non-specific compounds such as T-025. Due to the structural nature of kinases, it has been difficult to develop specific inhibitors until very recently. Some of the small molecules used here such as SPHINX and SPHINX31 are highly selective or specific for SRPK1 and are also very potent. These molecules were designed using structure activity relationships, and with modelling to test how and where the molecules bind to SRPK1 by Prof Jonathan Morris and his team at University of New South Wales, Australia, and this approach has contributed to the understanding of how to achieve greater selectivity.

As denoted by T-025, Harmine and the only kinase inhibitor in clinical trial for OA treatment, specific/selective drugs are difficult to design. Lorecivivint, a potential DMOAD and analgesic for OA, was published as a Wnt inhibitor, but acts through inhibition of CLKs and DYRKs, and also has effects at multiple targets (Deshmukh, O'Green et al. 2019). Specificity of new inhibitors is important to reduce off target effects, and in understanding of mechanism of action of new drugs.

New SRPK1 inhibitors are being more widely identified and developed. I tested several novel SRPK1 inhibitors to test the usefulness of the *in vitro* assay, namely the SRPINs 1-6 in comparison to the compound on which their design was based, SRPIN340. SRPIN340 has been used with success in the past, reducing the SRSF1 phosphorylation in tumour angiogenesis in metastatic melanoma (Gammons, Lucas et al. 2014), but was not very effective in this assay, with SPHINX and SRPIN4 having more potent inhibitory actions. The SRPINs exhibit different selectivities and potencies for the splicing kinase, but there seemed to be no relationship between effect in the

adherence assay and for example IC<sub>50</sub> value as SRPINs 5 and 6 have lower IC<sub>50</sub>s but SRPIN4 was the most effective inhibitor of monocyte adherence. Reduction of monocyte adherence by inhibition of SRPK1 using both SPHINX31 and SRPIN4 suggests that control of alternative RNA splicing of VEGF may also represent an anti-inflammatory strategy, but better understanding of the mechanisms involved in this assay, the targets of these inhibitors and the reasons why the inhibitor effectiveness is different in *in vitro* kinase and cellular assays.

## 5.6 Concluding remarks

To date, there is very little known about the control of SRSF1 mRNA expression in contrast to its activation (Aubol, Plocinik et al. 2013, Aubol, Wu et al. 2016, Aubol, Keshwani et al. 2018), although it is known to be upregulated by T cell activation (Moulton, Gillooly et al. 2014). To my knowledge, this is the first demonstration of a possible effect of CLKs on the control of SRSF1 mRNA expression.

I tested the hypothesis that TNF- $\alpha$  stimulation in HFLS altered VEGF-A in favour of VEGF-A<sub>165a</sub>, resulting in an increase in ICAM-1 expression through VEGFR2 activation, which mediates monocyte adherence to HFLS, promoting synovial inflammation. I was able to show that TNF- $\alpha$  stimulated adherence of THP-1 monocytes to HFLS, validating this *in vitro* model of synovial inflammation in this cell types. I also showed that monocyte adherence to HFLS could be blocked by an anti-ICAM-1 antibody (partial block), a VEGFR2 specific inhibitor and VEGF-A<sub>165b</sub>, supporting the hypothesis. There were some differences in the effect of VEGF-A<sub>165b</sub> on normal and RA-joint derived HFLS, suggesting that the stimulation of normal HFLS does not completely replicate the RA phenotype in HFLS.

Finally, inhibition of SRPK1 with previously published inhibitors (SPHINX31) also affected both ICAM-1 expression and monocyte adherence, not only also supporting the hypothesis, but also suggesting that SRPK1-splicing mechanisms affect monocytic inflammatory processes, and that this *in vitro* model could have both potential for use as a screening mechanism for more compounds.

## 6. Discussion

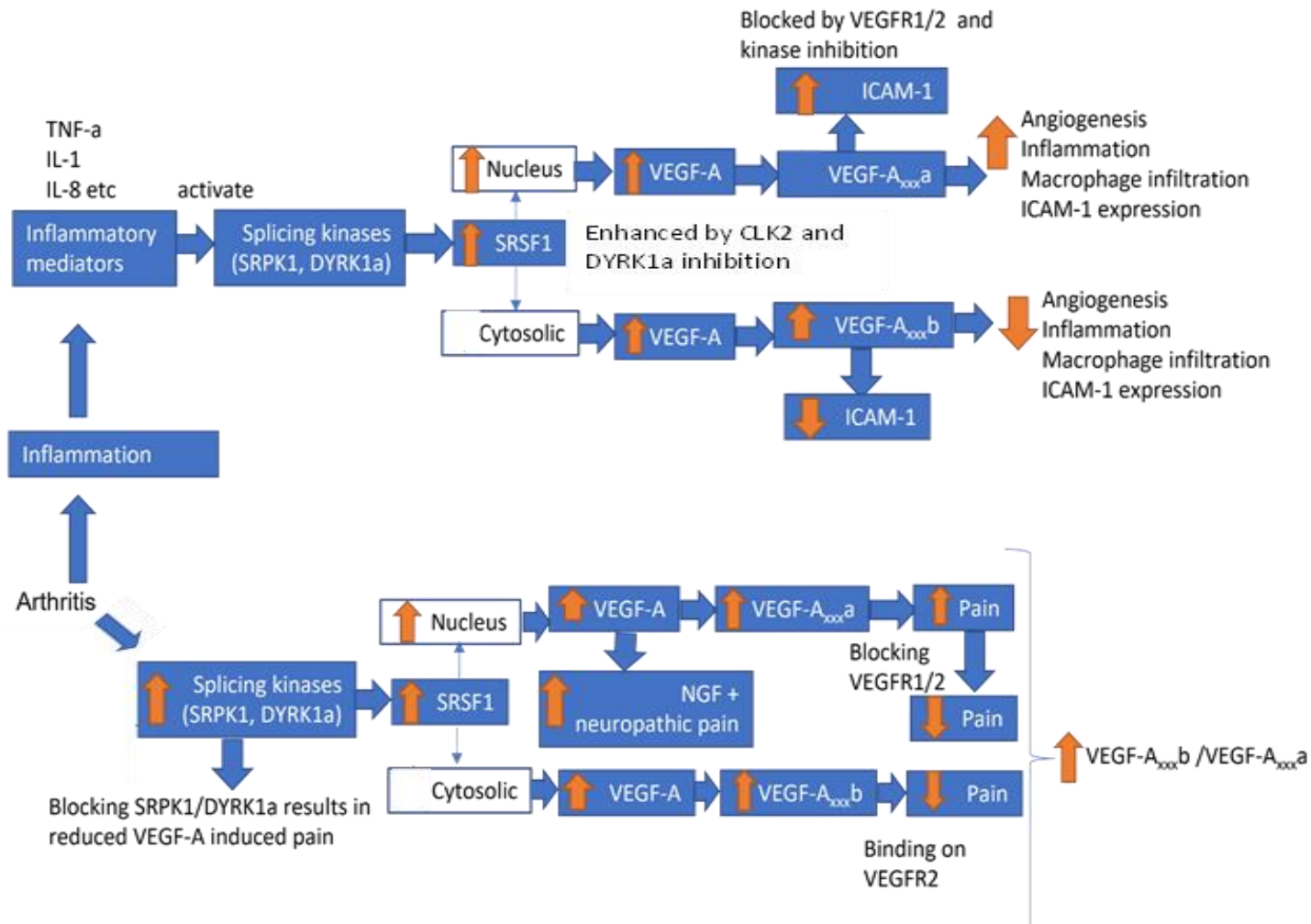


Figure 59 Summary of the hypotheses, findings, and their interpretation in the thesis. Upward arrow denotes an increase, downward arrow a decrease. VEGFR: VEGF receptor, NGF: nerve growth factor. A full explanation of the diagram is in the text.

Inflammation and pain are major characteristics of arthritic diseases, in middle aged and elderly population (Bitton 2009). OA of the knee is the most common type of arthritis, with the cartilage being considered the primary tissue through which the disease was being perpetuated. However, it is clear that all tissues in the synovial joint are affected by OA (Loeser, Goldring et al. 2012) Articular cartilage degradation, remodelling of the subchondral bone, synovial inflammation in both early and late-stage disease and meniscal changes are some of the pathophysiological features present in arthritis of the knee (Haywood, McWilliams et al. 2003, Benito, Veale et al. 2005, Ashraf, Mapp et al. 2011).

VEGF-A is strongly implicated in OA and RA, evident from the vascular invasion identified in late stage arthritis (Murata, Yudoh et al. 2008). VEGF-A levels in synovial fluid and serum correlate well with arthritic disease activity in both late-stage OA and RA and are strongly associated with the number of swollen joint (Sokolove and Lepus 2013). However, no splice variant studies with focus in arthritis have been performed before.

Pain in OA and RA is also often thought to be symptom derived from damage, particularly inflammatory process. However, in the context of this thesis I show evidence that the pain is potentially driven by the distinct splicing families of VEGF-A. There are already evidence in animals showing that the VEGF-A<sub>xxx</sub>a isoforms can cause pain, while the VEGF-A<sub>xxx</sub>b isoforms can block the pain.

In this thesis I presented evidence that symptomatic OA and RA are associated with alterations in the expression and splicing of VEGF-A and factors controlling expression. VEGF-A has been linked to both diseases although VEGF-A, its splicing and constituents of its splicing axis have not been previously shown to be related to OA and RA inflammation and pain. Figure 59 summarises the findings from the studies presented in the thesis.

Initially, during inflammation in arthritis (as seen in Figure 59 top line) we have an upregulation of inflammatory mediators including but not limited to TNF- $\alpha$ , IL-1 and IL-8, perpetuating pathogenesis, and the inflammatory profile evident in both OA and RA (Grunke and Schulze-Koops 2006, Farrugia and Baron 2016). Upregulation of these mediators has been proven to alter downstream splicing kinases including SRPK1, DYRK1a and CLK1/2. Alterations of these kinases induces a number of atypical splicing events; in breast, colon, lung, prostate, and pancreatic cancer elevated SRPK1 levels for example are directly associated with abnormal cell

proliferation, migration and trafficking as well as angiogenesis (Hatcher, Wu et al. 2018). In the context of this thesis SRPK1 expression is not altered in relation to the inflammation, while DYRK1a another kinase heavily associated with arthritis is significantly increased in OA or RA. This activation of the splicing kinases from the aforementioned inflammatory mediators drives the expression of SRSF1 upwards in the disease tissue compared to controls, by phosphorylating the latter and stimulating a translocation of the splicing factor in the nuclei of the cells an effect associated with splicing kinases of SRPK1 and CLK1/2. Our gene expression data derived from healthy HFLS cells treated with TNF- $\alpha$  to promote an inflammatory profile, suggest that SRSF1 increases its expression levels when the upstream kinases are inhibited with specific inhibitors, suggesting a mechanism of autoregulation of the splicing factor, to further facilitate the downstream alternative splicing events.

The increase in expression of SRSF1 as well as the increase in the nuclear localisation (as indicated by the upward arrow in Figure 59) was followed by an increase in the levels of VEGF-A for the two disease models over controls, with downstream alterations in the splicing events. This increase was evident either when the predominant expression of SRSF1 was in the nuclei of the cells in the synovium or when it's localisation was predominantly cytosolic. The OA and RA samples with the higher percentage of nucleic SRSF1 drove the levels of VEGF-A upwards suggesting that the angiogenesis and inflammation evident in arthritis is driven by this alternative splicing pathway. When translocated to the nuclei, SRSF1, according to literature that has been discussed previously, it increases the levels of VEGF-A<sub>xxx</sub>a isoform. In our samples however VEGF-A<sub>xxx</sub>a, was not significantly increased for the disease groups when compared to controls. Contrary to previous findings, VEGF-A<sub>xxx</sub>b was increased in the RA samples potentially acting as a balance to the increased angiogenesis in the disease group. Potentially VEGF-A<sub>xxx</sub>b is increased in the inflammatory tissue in an attempt to repair in long-term disease. Of course, this approach is further enhanced with our in vitro results showing that VEGF-A<sub>xxx</sub>b down-regulates ICAM-1 and monocyte adherence and therefore could have this effect. Of course, previous literature has established that in late-stage arthritis, angiogenesis is increased, an event that is not translated into the expected splicing shift that I encountered in my samples. I could speculate that since the overall levels of VEGF-A are rising in the disease state, the splicing events that take place result in a parallel increase of the pro-angiogenic and anti-angiogenic isoform rather than a complete shift towards one of the isoforms.

It is important to note here, that the IHC technique used to measure the expression and validate the localisation of SRSF1 in the cells of the synovium can be furthered optimised to provide a much cleaner and robust analysis. For example, by using IF protocols (as I attempted to do so, but the condition the tissue did not permit for consistent results chapter 3.3.2), double labelling of the tissue with a SRSF1 antibody + a pSRSF1 specific antibody and then analysis of the localisation of the two would provide a clearer response of the kinetics of SRSF1. Of course, more techniques could be employed to achieve robust results. Extraction of nuclei from the cells, and then imaging after treatment with SRSF1 antibodies could also provide strong results to identify both the expression and the localisation of SRSF1.

Nevertheless, through gene expression data that followed the IHC experiments I identified that ICAM-1 an inflammatory molecule playing a role in T-cell activation (van de Stolpe and van der Saag 1996) is upregulated in both healthy HFLS treated with TNF- $\alpha$  and RA derived HFLS, when treated with VEGF-A<sub>xxx</sub>a isoform. This increase was reverted when the cells were treated with either VEGFR1/2 inhibitors, or when I administered VEGF-A<sub>165</sub>b. These results lead us to conclude that in synoviocytes, VEGF-A<sub>xxx</sub>a, rather than panVEGF-A, leads to an increase in levels of angiogenesis, inflammation, macrophage infiltration and ICAM-1, effects that are blocked when the receptors of VEGF-A are inhibited. Similarly, I identified that if I block the splicing kinases responsible for the downstream activation of VEGF-A using specific SRPK1 inhibitors, we can reverse the ICAM-1 increased levels evident in TNF- $\alpha$  treated cells, suggesting that these inhibitors show potential as drugs by blocking the effects of VEGF-A<sub>xxx</sub>a by reducing the overall levels of the isoform.

Moving forward, I investigated how the splicing axis of VEGF-A potentially alters the pain state in OA as can be seen in Figure 59 bottom line. This was achieved through comparing symptomatic OA cases from people who underwent TKR against asymptomatic OA cases from post-mortem samples who had not reported any pain a separation that was based on differences in the chondropathy scores of the samples. Through the selection criteria I could isolate and control inflammation in the knee joint, focusing on alterations that would affect pain alone. Of course, the selection as mentioned previously was heavily skewed by the individual chondropathy scores of the patients with the TKR samples having grade 4 chondropathy and pain, while the PM samples had grade 4 chondropathy but no pain during the last 5 years of their lives + no medical evidence of doctor consultations for any knee pain. Initially I hypothesised that the splicing

kinases that drive the VEGF-A splicing axis would be increased in the painful subjects in conjunction to previous literature. I identified that two splicing kinases previously reported to be primary targets in reducing pain when inhibited, namely SRPK1 and DYRK1a (Hulse, Drake et al. 2016, Deshmukh, O'Green et al. 2019) where both increased in the painful subjects when compared to controls. This increase in the expression was followed by an increase in the SRSF1 levels of the painful samples compared to PMs. The localisation of SRSF1 in the nuclei of cells was increased in the symptomatic OA in relation to control tissue, an effect that was reflected in the panVEGF-A levels, which were also elevated in the painful subjects, an event that comes in agreement with the literature provided that VEGF-A is tightly related with NGF and the prevalence of neuropathic pain (McKelvey, Shorten et al. 2013). Moreover, NGF increases the levels of VEGF in normal neural cells (Campos, Muñoz et al. 2007), while vascular invasion into articular cartilage is associated with increased expression of nerve growth factor (NGF) within the vascular channels.

Following the localisation of SRSF1 and the overall increase of VEGF-A, I also detected an increase of the VEGF-A<sub>xxx</sub>a isoform in the painful group compared to controls, suggesting that pain is regulated by this isoform, while the VEGF-A<sub>xxx</sub>b was significantly expressed in the non-painful samples. This creates the basis of a VEGF-A<sub>xxx</sub>a induced pain response in knee OA, with literature suggesting that the VEGF-A induced pain can be reverted by inhibition of VEGFR1/2; an effect that we know already reduces the VEGF-A induced ICAM-1 expression in HFLS. However, such an approach is not therapeutically available, provided that the receptor blocking cannot happen locally, increasing the risk for detrimental cardiovascular events especially in the older population. A similar effect would be attainable with VEGF-A<sub>xxx</sub>b treatment since it acts as an antagonist for VEGF-A<sub>xxx</sub>a for binding on VEGFR2. Finally, by calculating the ratio of VEGF-A<sub>xxx</sub>b/VEGF-A<sub>xxx</sub>a which was increased in the non-painful group, I identified that that the ratio of the two isoforms could potentially be utilised as biomarkers to predict OA. Moreover, the ratio of the splicing isoforms could be used as a treatment indicator. For examples, if the joints of patients are painful, altering the splicing of VEGF-A could potentially be utilised as a specific treatment. Similarly, if a patient is experiencing pain, which would justify an invasive procedure, but no radiographic change then it could be an early diagnostic for OA. Providing also that circulating blood levels of VEGF-A are higher in OA and RA, we could identify the splicing ratio of the isoforms to identify if they could be used as predictive of early OA prior to symptoms.

It is important to note here that in our effort to characterise pain in between the two groups, I used chondropathy scores as a guidance. Of course, chondropathy score is a measure of severity of cartilage damage, and even though we used the Visual analogue scale (VAS) to characterise pain, the argument stands that the VAS score does not provide a thorough representation of the pain levels of the patients. It is acceptable to assume that patients that underwent TKR would have high pain scores, ranging from 8 – 10 in a 10 point scale (disregarding which pain score scale would be used to assess that), and the control samples that came from PM patients that had asymptomatic chondropathy would not have pain (provided that through the next of kin and their medical records, no visits to their doctors have been documented, or no complain have been made for pain in the knee joints), however the fact that I do not have specific pain scores represents a limitation to the study. In order to surpass such issues in following experiments, much more well-defined pain scores should be utilized such as WOMAC's or KOOS. This would give us a good understanding regarding the pain encountered by the TKR patients and create a solid base for consecutive experiments. Of course, it is important to understand that pain, as defined by IASP, is subjective, so even though pain scores such as WOMAC have a lot of items in the questionnaire to characterise pain as best as possible, any other pain questionnaire could have the same final result.

In conclusion, this is the first time the alternatively spliced VEGF-A isoforms have been closely related to the knee pathophysiology of OA or RA as well as the pain encountered in the diseases. Our results are indicative of the splicing mechanism partaking in pain and potentially inflammation mechanisms, denoting a potential mechanism that could be used to develop new drugs that would aim to reduce pain, or modify the inflammatory phenotype of the disease. The compounds used and the kinases they inhibit warrant future investigations into the mechanisms behind these inflammatory and anti-nociceptive effects. Back translating these results from human tissue to animals, while simultaneously translating from in vitro to in vivo experiments could bolster the arguments made by these investigations.

## 7. Proposed future work

- RNA sequencing investigations following splicing kinase inhibitor treatment of to identify alternative splicing targets in addition to VEGF-A splicing in fresh human synovium, and effects of kinase inhibition.
- Further exploration of the acute and chronic mechanisms in the control of VEGF-A alternative splicing in human synovium and other joint tissues where VEGF-A exerts effects, in normal and arthritic states.
- Back translate our IHC findings from the human studies to suitable OA and RA surgical or chemical animal models (Qian, Xu et al. 2021), together with behavioural nociceptive testing and treatment with kinase inhibitors, to confirm the presence of similar mechanisms in disease models, and determine the potential for kinase inhibitors to affect nociception and/or joint disease *in vivo*.
- Identify the potential of an altered VEGF-A<sub>xxx</sub>b/VEGF-A<sub>xxx</sub>a ratio as a biomarker or indication of treatment efficacy for painful OA, by examining quantitative sensory testing to assess somatosensory evoked responses to noxious or innocuous stimuli through controlled thermal electrical, mechanical, and/or chemical, test modalities, and synovial VEGF-A<sub>xxx</sub>b/VEGF-A<sub>xxx</sub>a ratio in people with early to mid to late-stage OA.

## 8. Appendix 1

Custom macro code made in Fiji to facilitate batch processing of images to quantify intensity of staining. In the macro a plugin from Fiji is being used, namely Read, and Write excel which transfers the data automatically to an excel file. The macro has been designed to open images automatically from the directory that is set by the user, split the images in 3 channels regarding on the needs of the researcher, thresholding the images at set values that need to be decided before hand, analyse particles and setting ROIs. Then, the ROIs are being imprinted on the channel of choice through a simple macro command and measurements are automatically collected from Fiji.

The macro code as it stands is:

```
dir = getDirectory( "Choose the Directory" );
list = getFileList( dir );
max = getNumber("How many images do you expect?", 3);
for ( i=0; i<list.length; i++ ) {
    open( dir + list[i] );
    title = getTitle()
        run("Colour Deconvolution", "vectors=[H DAB]");
        selectWindow(title + "-(Colour_2)" );
        run("Duplicate...", "ok");
        selectWindow(title + "-(Colour_2)-1" );
        run("Threshold...");
    setThreshold(0, 170);
    run("Analyze Particles...", "size=0-Infinity circularity=0-Infinity show=Nothing clear add ok");
        //waitForUser("string");
        close();
        selectWindow(title + "-(Colour_2)" );
        roiManager("show all");
        waitForUser("string");
        roiManager("measure");
        waitForUser("string");
        roiManager("Delete");
        close("*");
}
```

```
        run("Read and Write Excel");
        close("Results");
    }
    print("done")
```

## 9. References

- A, Y., H. R, W. D and W. DA (2008). "OC46 SFA(PATH); A MODIFICATION OF THE SFA GRADING SYSTEM OF CHONDROPATHY IN OSTEOARTHRITIS FOR USE WITH PATHOLOGICAL SAMPLES." Orthopaedic Proceedings **90-B(SUPP\_II)**: 369-369.
- Adams, R., C. Walsh, D. Veale, B. Bresnihan, O. FitzGerald and M. Barry (2010). "Understanding the relationship between the EQ-5D, SF-6D, HAQ and disease activity in inflammatory arthritis." Pharmacoeconomics **28**(6): 477-487.
- Ahmad, A. H. and Z. Ismail (2002). "c-fos and its Consequences in Pain." The Malaysian journal of medical sciences : MJMS **9**(1): 3-8.
- Aida, Y., M. Maeno, N. Suzuki, A. Namba, M. Motohashi, M. Matsumoto, M. Makimura and H. Matsumura (2006). "The effect of IL-1beta on the expression of inflammatory cytokines and their receptors in human chondrocytes." Life sciences **79**(8): 764-771.
- Aigner, T., E. Reichenberger, W. Bertling, T. Kirsch, H. Stöß and K. von der Mark (1993). "Type X collagen expression in osteoarthritic and rheumatoid articular cartilage." Virchows Archiv B **63**(1): 205.
- Akkiraju, H. and A. Nohe (2015). "Role of Chondrocytes in Cartilage Formation, Progression of Osteoarthritis and Cartilage Regeneration." Journal of developmental biology **3**(4): 177-192.
- Albert S. Baldwin, J. (1996). "THE NF- $\kappa$ B AND I $\kappa$ B PROTEINS: New Discoveries and Insights." Annual Review of Immunology **14**(1): 649-681.
- Albro, M. B., R. J. Nims, A. D. Cigan, K. J. Yeroushalmi, J. J. Shim, C. T. Hung and G. A. Ateshian (2013). "Dynamic mechanical compression of devitalized articular cartilage does not activate latent TGF- $\beta$ ." J Biomech **46**(8): 1433-1439.
- Altawil, R., S. Saevarsdottir, S. Wedrén, L. Alfredsson, L. Klareskog and J. Lampa (2016). "Remaining Pain in Early Rheumatoid Arthritis Patients Treated With Methotrexate." Arthritis Care Res (Hoboken) **68**(8): 1061-1068.
- Altman, R., E. Asch, D. Bloch, G. Bole, D. Borenstein, K. Brandt, W. Christy, T. D. Cooke, R. Greenwald, M. Hochberg and et al. (1986). "Development of criteria for the classification and reporting of osteoarthritis. Classification of osteoarthritis of the knee. Diagnostic and Therapeutic Criteria Committee of the American Rheumatism Association." Arthritis Rheum **29**(8): 1039-1049.
- Altschul, S. F., W. Gish, W. Miller, E. W. Myers and D. J. Lipman (1990). "Basic local alignment search tool." J Mol Biol **215**(3): 403-410.
- Amin, E. M., S. Oltean, J. Hua, M. V. Gammons, M. Hamdollah-Zadeh, G. I. Welsh, M. K. Cheung, L. Ni, S. Kase, E. S. Rennel, K. E. Symonds, D. G. Nowak, B. Royer-Pokora, M. A. Saleem, M. Hagiwara, V. A. Schumacher, S. J. Harper, D. R. Hinton, D. O. Bates and M. R. Lodomery (2011). "WT1 mutants reveal SRPK1 to be a downstream angiogenesis target by altering VEGF splicing." Cancer Cell **20**(6): 768-780.
- Amin, E. M., S. Oltean, J. Hua, M. V. R. Gammons, M. Hamdollah-Zadeh, G. I. Welsh, M.-K. Cheung, L. Ni, S. Kase, E. S. Rennel, K. E. Symonds, D. G. Nowak, B. Royer-Pokora, M. A. Saleem, M. Hagiwara, V. A. Schumacher, S. J. Harper, D. R. Hinton, D. O. Bates and M. R. Lodomery (2011). "WT1 mutants reveal SRPK1 to be a downstream angiogenesis target by altering VEGF splicing." Cancer cell **20**(6): 768-780.

Amin, S., A. Guermazi, M. P. Lavalley, J. Niu, M. Clancy, D. J. Hunter, M. Grigoryan and D. T. Felson (2008). "Complete anterior cruciate ligament tear and the risk for cartilage loss and progression of symptoms in men and women with knee osteoarthritis." Osteoarthritis Cartilage **16**(8): 897-902.

Ashander, L. M., B. Appukuttan, Y. Ma, D. Gardner-Stephen and J. R. Smith (2016). "Targeting Endothelial Adhesion Molecule Transcription for Treatment of Inflammatory Disease: A Proof-of-Concept Study." Mediators of inflammation **2016**: 7945848-7945848.

Ashraf, S., P. I. Mapp, J. Burston, A. J. Bennett, V. Chapman and D. A. Walsh (2014). "Augmented pain behavioural responses to intra-articular injection of nerve growth factor in two animal models of osteoarthritis." Annals of the rheumatic diseases **73**(9): 1710-1718.

Ashraf, S., P. I. Mapp and D. A. Walsh (2011). "Contributions of angiogenesis to inflammation, joint damage, and pain in a rat model of osteoarthritis." Arthritis & Rheumatism **63**(9): 2700-2710.

Ashraf, S., H. Wibberley, P. I. Mapp, R. Hill, D. Wilson and D. A. Walsh (2011). "Increased vascular penetration and nerve growth in the meniscus: a potential source of pain in osteoarthritis." Annals of the Rheumatic Diseases **70**(3): 523.

Aso, K., S. M. Shahtaheri, R. Hill, D. Wilson, D. F. McWilliams, L. N. Nwosu, V. Chapman and D. A. Walsh (2020). "Contribution of nerves within osteochondral channels to osteoarthritis knee pain in humans and rats." Osteoarthritis Cartilage **28**(9): 1245-1254.

Aspden, R. M. and F. R. Saunders (2019). "Osteoarthritis as an organ disease: from the cradle to the grave." Eur Cell Mater **37**: 74-87.

Aubol, B. E., M. M. Keshwani, L. Fattet and J. A. Adams (2018). "Mobilization of a splicing factor through a nuclear kinase-kinase complex." The Biochemical journal **475**(3): 677-690.

Aubol, B. E., R. M. Plocinik, J. C. Hagopian, C.-T. Ma, M. L. McGlone, R. Bandyopadhyay, X.-D. Fu and J. A. Adams (2013). "Partitioning RS Domain Phosphorylation in an SR Protein through the CLK and SRPK Protein Kinases." Journal of Molecular Biology **425**(16): 2894-2909.

Aubol, B. E., G. Wu, M. M. Keshwani, M. Movassat, L. Fattet, K. J. Hertel, X.-D. Fu and J. A. Adams (2016). "Release of SR Proteins from CLK1 by SRPK1: A Symbiotic Kinase System for Phosphorylation Control of Pre-mRNA Splicing." Molecular cell **63**(2): 218-228.

Aubol Brandon, E., M. Wozniak Jacob, L. Fattet, J. Gonzalez David and A. Adams Joseph (2021). "CLK1 reorganizes the splicing factor U1-70K for early spliceosomal protein assembly." Proceedings of the National Academy of Sciences **118**(14): e2018251118.

Baker, K., A. Grainger, J. Niu, M. Clancy, A. Guermazi, M. Crema, L. Hughes, J. Buckwalter, A. Wooley, M. Nevitt and D. T. Felson (2010). "Relation of synovitis to knee pain using contrast-enhanced MRIs." Annals of the rheumatic diseases **69**(10): 1779-1783.

Ballmer-Hofer, K., A. E. Andersson, L. E. Ratcliffe and P. Berger (2011). "Neuropilin-1 promotes VEGFR-2 trafficking through Rab11 vesicles thereby specifying signal output." Blood **118**(3): 816-826.

Barthel, C., N. Yeremenko, R. Jacobs, R. E. Schmidt, M. Bernateck, H. Zeidler, P.-P. Tak, D. Baeten and M. Rihl (2009). "Nerve growth factor and receptor expression in rheumatoid arthritis and spondyloarthritis." Arthritis Research & Therapy **11**(3): R82.

Barthel, C., N. Yeremenko, R. Jacobs, R. E. Schmidt, M. Bernateck, H. Zeidler, P. P. Tak, D. Baeten and M. Rihl (2009). "Nerve growth factor and receptor expression in rheumatoid arthritis and spondyloarthritis." Arthritis Res Ther **11**(3): R82.

Baschong, W., R. Suetterlin and R. H. Laeng (2001). "Control of Autofluorescence of Archival Formaldehyde-fixed, Paraffin-embedded Tissue in Confocal Laser Scanning Microscopy (CLSM)." Journal of Histochemistry & Cytochemistry **49**(12): 1565-1571.

Bates, D. O., P. J. Catalano, K. E. Symonds, A. H. R. Varey, P. Ramani, P. J. O'Dwyer, B. J. Giantonio, N. J. Meropol, A. B. Benson and S. J. Harper (2012). "Association between VEGF Splice Isoforms and Progression-Free Survival in Metastatic Colorectal Cancer Patients Treated with Bevacizumab." Clinical Cancer Research **18**(22): 6384-6391.

Bates, D. O., T.-G. Cui, J. M. Doughty, M. Winkler, M. Sugiono, J. D. Shields, D. Peat, D. Gillatt and S. J. Harper (2002). "VEGF<sub>165b</sub>, an Inhibitory Splice Variant of Vascular Endothelial Growth Factor, Is Down-Regulated in Renal Cell Carcinoma." Cancer Research **62**(14): 4123-4131.

Bates, D. O., A. Mavrou, Y. Qiu, J. G. Carter, M. Hamdollah-Zadeh, S. Barratt, M. V. Gammons, A. B. Millar, A. H. Salmon, S. Oltean and S. J. Harper (2013). "Detection of VEGF-A(XXX)b isoforms in human tissues." PLoS One **8**(7): e68399.

Batson, J., H. D. Toop, C. Redondo, R. Babaei-Jadidi, A. Chaikuad, S. F. Wearmouth, B. Gibbons, C. Allen, C. Tallant, J. Zhang, C. Du, J. C. Hancox, T. Hawtrey, J. Da Rocha, R. Griffith, S. Knapp, D. O. Bates and J. C. Morris (2017). "Development of Potent, Selective SRPK1 Inhibitors as Potential Topical Therapeutics for Neovascular Eye Disease." ACS Chem Biol **12**(3): 825-832.

Beazley-Long, N., J. Hua, T. Jehle, R. P. Hulse, R. Dersch, C. Lehrling, H. Bevan, Y. Qiu, W. A. Lagrèze, D. Wynick, A. J. Churchill, P. Kehoe, S. J. Harper, D. O. Bates and L. F. Donaldson (2013). "VEGF-A165b is an endogenous neuroprotective splice isoform of vascular endothelial growth factor A in vivo and in vitro." Am J Pathol **183**(3): 918-929.

Beazley-Long, N., C. E. Moss, W. R. Ashby, S. M. Bestall, F. Almahasneh, A. M. Durrant, A. V. Benest, Z. Blackley, K. Ballmer-Hofer, M. Hirashima, R. P. Hulse, D. O. Bates and L. F. Donaldson (2018). "VEGFR2 promotes central endothelial activation and the spread of pain in inflammatory arthritis." Brain, Behavior, and Immunity **74**: 49-67.

Beazley-Long, N., C. E. Moss, W. R. Ashby, S. M. Bestall, F. Almahasneh, A. M. Durrant, A. V. Benest, Z. Blackley, K. Ballmer-Hofer, M. Hirashima, R. P. Hulse, D. O. Bates and L. F. Donaldson (2018). "VEGFR2 promotes central endothelial activation and the spread of pain in inflammatory arthritis." Brain Behav Immun **74**: 49-67.

Benito, M. J., D. J. Veale, O. FitzGerald, W. B. van den Berg and B. Bresnihan (2005). "Synovial tissue inflammation in early and late osteoarthritis." Ann Rheum Dis **64**(9): 1263-1267.

Benton, R. L. and S. R. Whitemore (2003). "VEGF165 therapy exacerbates secondary damage following spinal cord injury." Neurochem Res **28**(11): 1693-1703.

Berberat, J. E., M. J. Nissi, J. S. Jurvelin and M. T. Nieminen (2009). "Assessment of interstitial water content of articular cartilage with T1 relaxation." Magn Reson Imaging **27**(5): 727-732.

Berenbaum, F. (2013). "Osteoarthritis as an inflammatory disease (osteoarthritis is not osteoarthrosis!)." Osteoarthritis Cartilage **21**(1): 16-21.

Binch, A. L. A., A. A. Cole, L. M. Breakwell, A. L. R. Michael, N. Chiverton, A. K. Cross and C. L. Le Maitre (2014). "Expression and regulation of neurotrophic and angiogenic factors during human intervertebral disc degeneration." Arthritis research & therapy **16**(5): 416-416.

Biselli-Chicote, P. M., J. M. Biselli, B. R. Cunha, R. Castro, J. V. Maniglia, D. S. Neto, E. H. Tajara, J. F. Góis Filho, E. E. Fukuyama, C. Pavarino É and E. M. Goloni-Bertollo (2017). "Overexpression of Antiangiogenic Vascular Endothelial Growth Factor Isoform and Splicing Regulatory Factors in Oral, Laryngeal and Pharyngeal Squamous Cell Carcinomas." Asian Pac J Cancer Prev **18**(8): 2171-2177.

Bitton, R. (2009). "The economic burden of osteoarthritis." Am J Manag Care **15**(8 Suppl): S230-235.

Blaney Davidson, E. N., D. F. Remst, E. L. Vitters, H. M. van Beuningen, A. B. Blom, M. J. Goumans, W. B. van den Berg and P. M. van der Kraan (2009). "Increase in ALK1/ALK5 ratio as a cause for elevated MMP-13 expression in osteoarthritis in humans and mice." J Immunol **182**(12): 7937-7945.

Blencowe, B. J. (2006). "Alternative splicing: new insights from global analyses." Cell **126**(1): 37-47.

Bondeson, J., S. D. Wainwright, S. Lauder, N. Amos and C. E. Hughes (2006). "The role of synovial macrophages and macrophage-produced cytokines in driving aggrecanases, matrix metalloproteinases, and other destructive and inflammatory responses in osteoarthritis." Arthritis Research & Therapy **8**(6): R187.

Bosshart, H. and M. Heinzemann (2016). "THP-1 cells as a model for human monocytes." Annals of translational medicine **4**(21): 438-438.

Boureau, F., H. Schneid, N. Zeghari, R. Wall and P. Bourgeois (2004). "The IPSO study: ibuprofen, paracetamol study in osteoarthritis. A randomised comparative clinical study comparing the efficacy and safety of ibuprofen and paracetamol analgesic treatment of osteoarthritis of the knee or hip." Annals of the Rheumatic Diseases **63**(9): 1028.

Brault, V., T. L. Nguyen, J. Flores-Gutiérrez, G. Iacono, M.-C. Birling, V. Lalanne, H. Meziane, A. Manousopoulou, G. Pavlovic, L. Lindner, M. Selloum, T. Sorg, E. Yu, S. D. Garbis and Y. Héroult (2021). "Dyrk1a gene dosage in glutamatergic neurons has key effects in cognitive deficits observed in mouse models of MRD7 and Down syndrome." PLOS Genetics **17**(9): e1009777.

Bridgett, S., M. Dellett and D. A. Simpson (2017). "RNA-Sequencing data supports the existence of novel VEGFA splicing events but not of VEGFAxxx isoforms." Scientific Reports **7**(1): 58.

Britto, D. D., B. Wyroba, W. Chen, R. A. Lockwood, K. B. Tran, P. R. Shepherd, C. J. Hall, K. E. Crosier, P. S. Crosier and J. W. Astin (2018). "Macrophages enhance Vegfa-driven angiogenesis in an embryonic zebrafish tumour xenograft model." Disease Models & Mechanisms **11**(12).

Bruno, M. A. and A. C. Cuello (2006). "Activity-dependent release of precursor nerve growth factor, conversion to mature nerve growth factor, and its degradation by a protease cascade." Proc Natl Acad Sci U S A **103**(17): 6735-6740.

Bucci, J., X. Chen, M. LaValley, M. Nevitt, J. Torner, C. E. Lewis and D. T. Felson (2022). "Progression of Knee Osteoarthritis With Use of Intraarticular Glucocorticoids Versus Hyaluronic Acid." Arthritis & Rheumatology **74**(2): 223-226.

Burr, D. B. and M. B. Schaffler (1997). "The involvement of subchondral mineralized tissues in osteoarthrosis: quantitative microscopic evidence." Microsc Res Tech **37**(4): 343-357.

Cai, A., C. Chatziantoniou and A. Calmont (2021). "Vascular Permeability: Regulation Pathways and Role in Kidney Diseases." Nephron **145**(3): 297-310.

Campos, X., Y. Muñoz, A. Selman, R. Yazigi, L. Moyano, C. Weinstein-Oppenheimer, H. E. Lara and C. Romero (2007). "Nerve growth factor and its high-affinity receptor trkA participate in the control of vascular endothelial growth factor expression in epithelial ovarian cancer." Gynecol Oncol **104**(1): 168-175.

Carmeliet, P., V. Ferreira, G. Breier, S. Pollefeyt, L. Kieckens, M. Gertsenstein, M. Fahrig, A. Vandenhoeck, K. Harpal, C. Eberhardt, C. Declercq, J. Pawling, L. Moons, D. Collen, W. Risau and A. Nagy (1996). "Abnormal blood vessel development and lethality in embryos lacking a single VEGF allele." Nature **380**(6573): 435-439.

Carter, J. G., J. Cherry, K. Williams, S. Turner, D. O. Bates and A. J. Churchill (2011). "Splicing factor polymorphisms, the control of VEGF isoforms and association with angiogenic eye disease." Curr Eye Res **36**(4): 328-335.

Cassidy, M. F., Z. T. Herbert and V. R. Moulton (2022). "Splicing factor SRSF1 controls distinct molecular programs in regulatory and effector T cells implicated in systemic autoimmune disease." Mol Immunol **141**: 94-103.

Charbonneau, M., R. R. Lavoie, A. Lauzier, K. Harper, P. P. McDonald and C. M. Dubois (2016). "Platelet-Derived Growth Factor Receptor Activation Promotes the Prodestructive Invadosome-Forming Phenotype of Synoviocytes from Patients with Rheumatoid Arthritis." Journal of immunology (Baltimore, Md. : 1950) **196**(8): 3264-3275.

Chen, M. and J. L. Manley (2009). "Mechanisms of alternative splicing regulation: insights from molecular and genomics approaches." Nature reviews. Molecular cell biology **10**(11): 741-754.

Chiumia, D., A.-K. Hankele, A. E. Groebner, K. Schulke, H.-D. Reichenbach, K. Giller, V. Zakhartchenko, S. Bauersachs and S. E. Ulbrich (2020). "Vascular Endothelial Growth Factor A and VEGFR-1 Change during Preimplantation in Heifers." International journal of molecular sciences **21**(2): 544.

Cho, E., Y. Feng, C. Rauskolb, S. Maitra, R. Fehon and K. D. Irvine (2006). "Delineation of a Fat tumor suppressor pathway." Nat Genet **38**(10): 1142-1150.

Cho, M.-L., Y. O. Jung, Y.-M. Moon, S.-Y. Min, C.-H. Yoon, S.-H. Lee, S.-H. Park, C.-S. Cho, D.-M. Jue and H.-Y. Kim (2006). "Interleukin-18 induces the production of vascular endothelial growth factor (VEGF) in rheumatoid arthritis synovial fibroblasts via AP-1-dependent pathways." Immunology letters **103**(2): 159-166.

Christensen, R., A. Astrup and H. Bliddal (2005). "Weight loss: the treatment of choice for knee osteoarthritis? A randomized trial." Osteoarthritis Cartilage **13**(1): 20-27.

Chung, A. S. and N. Ferrara (2011). "Developmental and pathological angiogenesis." Annu Rev Cell Dev Biol **27**: 563-584.

Claes, S., E. Vereecke, M. Maes, J. Victor, P. Verdonk and J. Bellemans (2013). "Anatomy of the anterolateral ligament of the knee." J Anat **223**(4): 321-328.

Clair, A. J., M. T. Kingery, U. Anil, L. Kenny, T. Kirsch and E. J. Strauss (2019). "Alterations in Synovial Fluid Biomarker Levels in Knees With Meniscal Injury as Compared With Asymptomatic Contralateral Knees." Am J Sports Med **47**(4): 847-856.

Clark, J. M. (1990). "The organisation of collagen fibrils in the superficial zones of articular cartilage." J Anat **171**: 117-130.

Coggeshall, R. E., K. A. Hong, L. A. Langford, H. G. Schaible and R. F. Schmidt (1983). "Discharge characteristics of fine medial articular afferents at rest and during passive movements of inflamed knee joints." Brain Res **272**(1): 185-188.

Cohen, S. P. and J. Mao (2014). "Neuropathic pain: mechanisms and their clinical implications." Bmj **348**: f7656.

Colebatch, A. N., C. J. Edwards, M. Østergaard, D. van der Heijde, P. V. Balint, M. A. D'Agostino, K. Forslind, W. Grassi, E. A. Haavardsholm, G. Haugeberg, A. G. Jurik, R. B. Landewé, E. Naredo, P. J. O'Connor, B. Ostendorf, K. Potocki, W. A. Schmidt, J. S. Smolen, S. Sokolovic, I. Watt and P. G. Conaghan (2013). "EULAR recommendations for the use of imaging of the joints in the clinical management of rheumatoid arthritis." Ann Rheum Dis **72**(6): 804-814.

Combe, B., R. Landewe, C. I. Daien, C. Hua, D. Aletaha, J. M. Álvaro-Gracia, M. Bakkers, N. Brodin, G. R. Burmester, C. Codreanu, R. Conway, M. Dougados, P. Emery, G. Ferraccioli, J. Fonseca, K. Raza, L. Silva-Fernández, J. S. Smolen, D. Skingle, Z. Szekanecz, T. K. Kvien, A. van der Helm-van Mil and R. van Vollenhoven (2017). "2016 update of the EULAR recommendations for the management of early arthritis." Ann Rheum Dis **76**(6): 948-959.

Cooper, S. L., J. J. Carter, J. March and J. Woolard (2019). "Long-term cardiovascular effects of vandetanib and pazopanib in normotensive rats." Pharmacol Res Perspect **7**(3): e00477.

Corliss, B. A., M. S. Azimi, J. M. Munson, S. M. Peirce and W. L. Murfee (2016). "Macrophages: An Inflammatory Link Between Angiogenesis and Lymphangiogenesis." Microcirculation **23**(2): 95-121.

Corrado, A., A. Neve and F. P. Cantatore (2013). "Expression of vascular endothelial growth factor in normal, osteoarthritic and osteoporotic osteoblasts." Clin Exp Med **13**(1): 81-84.

Cuellar, J. M., G. J. Scuderi, V. G. Cuellar, S. R. Golish and D. C. Yeomans (2009). "Diagnostic utility of cytokine biomarkers in the evaluation of acute knee pain." J Bone Joint Surg Am **91**(10): 2313-2320.

da Glória, V. G., M. Martins de Araújo, A. Mafalda Santos, R. Leal, S. F. de Almeida, A. M. Carmo and A. Moreira (2014). "T cell activation regulates CD6 alternative splicing by transcription dynamics and SRSF1." J Immunol **193**(1): 391-399.

Dainese, P., K. V. Wyngaert, S. De Mits, R. Wittoek, A. Van Ginckel and P. Calters (2022). "Association between knee inflammation and knee pain in patients with knee osteoarthritis: a systematic review." Osteoarthritis and Cartilage **30**(4): 516-534.

Dakin, H., A. Gray, R. Fitzpatrick, G. MacLennan and D. Murray (2012). "Rationing of total knee replacement: a cost-effectiveness analysis on a large trial data set." BMJ Open **2**(1): e000332.

Das, S. and A. R. Krainer (2014). "Emerging functions of SRSF1, splicing factor and oncoprotein, in RNA metabolism and cancer." Molecular cancer research : MCR **12**(9): 1195-1204.

Das, V., R. Kc, X. Li, O. S. I, A. J. van Wijnen, J. S. Kroin, B. Pytowski, D. T. Applegate, G. Votta-Velis, R. L. Ripper, T. J. Park and H. J. Im (2018). "Blockade of Vascular Endothelial Growth Factor Receptor-1 (Flt-1), Reveals a Novel Analgesic For Osteoarthritis-Induced Joint Pain." Gene Rep **11**: 94-100.

de Lange-Brokaar, B. J., A. Ioan-Facsinay, G. J. van Osch, A. M. Zuurmond, J. Schoones, R. E. Toes, T. W. Huizinga and M. Kloppenburg (2012). "Synovial inflammation, immune cells and their cytokines in osteoarthritis: a review." Osteoarthritis Cartilage **20**(12): 1484-1499.

Delcombel, R., L. Janssen, R. Vassy, M. Gammons, O. Haddad, B. Richard, D. Letourneur, D. Bates, C. Hendricks, J. Waltenberger, A. Starzec, N. E. Sounni, A. Noël, C. Deroanne, C. Lambert and A. Colige (2013). "New prospects in the roles of the C-terminal domains of VEGF-A and their cooperation for ligand binding, cellular signaling and vessels formation." Angiogenesis **16**(2): 353-371.

Delmas, P., J. Hao and L. Rodat-Despoix (2011). "Molecular mechanisms of mechanotransduction in mammalian sensory neurons." Nat Rev Neurosci **12**(3): 139-153.

den Broeder, A. A., N. van Herwaarden and B. J. F. van den Bemt (2018). "Therapeutic drug monitoring of biologicals in rheumatoid arthritis: a disconnect between beliefs and facts." Curr Opin Rheumatol **30**(3): 266-275.

Deshmukh, V., M. Ibanez, H. Hu, J. Cahiwat, Y. Wei, J. Stewart, J. Hood and Y. Yazici (2020). "A small-molecule inhibitor of the Wnt pathway, lorecivivint (SM04690), as a potential disease-modifying agent for the treatment of degenerative disc disease." Spine J **20**(9): 1492-1502.

Deshmukh, V., A. L. O'Green, C. Bossard, T. Seo, L. Lamangan, M. Ibanez, A. Ghias, C. Lai, L. Do, S. Cho, J. Cahiwat, K. Chiu, M. Pedraza, S. Anderson, R. Harris, L. Dellamary, S. Kc, C. Barroga, B. Melchior, B. Tam, S. Kennedy, J. Tambiah, J. Hood and Y. Yazici (2019). "Modulation of the Wnt pathway through inhibition of CLK2 and DYRK1A by lorecivivint as a novel, potentially disease-modifying approach for knee osteoarthritis treatment." Osteoarthritis Cartilage **27**(9): 1347-1360.

Di Cesare Mannelli, L., B. Tenci, L. Micheli, A. Vona, F. Corti, M. Zanardelli, A. Lapucci, A. M. Clemente, P. Failli and C. Ghelardini (2018). "Adipose-derived stem cells decrease pain in a rat model of oxaliplatin-induced neuropathy: Role of VEGF-A modulation." Neuropharmacology **131**: 166-175.

Dickenson, A. H. (2002). "Gate control theory of pain stands the test of time." Br J Anaesth **88**(6): 755-757.

Dickson, M. C., J. S. Martin, F. M. Cousins, A. B. Kulkarni, S. Karlsson and R. J. Akhurst (1995). "Defective haematopoiesis and vasculogenesis in transforming growth factor-beta 1 knock out mice." Development **121**(6): 1845-1854.

Ding, F., C. Su, K.-H. K. Chow and M. B. Elowitz (2020). "Dynamics and functional roles of splicing factor autoregulation." bioRxiv: 2020.2007.2022.216887.

Djoughri, L. and S. N. Lawson (2004). "Abeta-fiber nociceptive primary afferent neurons: a review of incidence and properties in relation to other afferent A-fiber neurons in mammals." Brain Res Brain Res Rev **46**(2): 131-145.

Donaldson, L. F. and N. Beazley-Long (2016). "Alternative RNA splicing: contribution to pain and potential therapeutic strategy." Drug Discov Today **21**(11): 1787-1798.

Donaldson, L. F. and N. Beazley-Long (2016). "Alternative RNA splicing: contribution to pain and potential therapeutic strategy." Drug discovery today **21**(11): 1787-1798.

Dong, Z., K. Noda, A. Kanda, J. Fukuhara, R. Ando, M. Murata, W. Saito, M. Hagiwara and S. Ishida (2013). "Specific inhibition of serine/arginine-rich protein kinase attenuates choroidal neovascularization." Molecular vision **19**: 536-543.

Dorn, T., H. G. Schaible and R. F. Schmidt (1991). "Response properties of thick myelinated group II afferents in the medial articular nerve of normal and inflamed knee joints of the cat." Somatosens Mot Res **8**(2): 127-136.

Downie, T. (1990). "Theory and Practice of Histological Techniques Edited by J.D. Bancroft & A. Stevens, Churchill Livingstone, Edinburgh, 740 pages, £55.00." Histopathology **17**(4): 386-386.

Duncan, H. (1983). "Cellular mechanisms of bone damage and repair in the arthritic joint." J Rheumatol Suppl **11**: 29-37.

Dvinge, H. (2018). "Regulation of alternative mRNA splicing: old players and new perspectives." FEBS Lett **592**(17): 2987-3006.

Dye, S. F., G. L. Vaupel and C. C. Dye (1998). "Conscious neurosensory mapping of the internal structures of the human knee without intraarticular anesthesia." Am J Sports Med **26**(6): 773-777.

Eblen, S. T. (2012). "Regulation of chemoresistance via alternative messenger RNA splicing." Biochem Pharmacol **83**(8): 1063-1072.

Eitner, A., G. O. Hofmann and H.-G. Schaible (2017). "Mechanisms of Osteoarthritic Pain. Studies in Humans and Experimental Models." Frontiers in Molecular Neuroscience **10**.

Enomoto, H., I. Inoki, K. Komiya, T. Shiomi, E. Ikeda, K. Obata, H. Matsumoto, Y. Toyama and Y. Okada (2003). "Vascular endothelial growth factor isoforms and their receptors are expressed in human osteoarthritic cartilage." Am J Pathol **162**(1): 171-181.

Fan, L. J., H. M. Kan, X. T. Chen, Y. Y. Sun, L. P. Chen and W. Shen (2022). "Vascular endothelial growth factor-A/vascular endothelial growth factor2 signaling in spinal neurons contributes to bone cancer pain." Mol Pain **18**: 17448069221075891.

Farrugia, M. and B. Baron (2016). "The role of TNF- $\alpha$  in rheumatoid arthritis: a focus on regulatory T cells." J Clin Transl Res **2**(3): 84-90.

Fay, J., D. Varoga, C. J. Wruck, B. Kurz, M. B. Goldring and T. Pufe (2006). "Reactive oxygen species induce expression of vascular endothelial growth factor in chondrocytes and human articular cartilage explants." Arthritis Res Ther **8**(6): R189.

Fehrenbacher, J. C., T. H. Burkey, G. D. Nicol and M. R. Vasko (2005). "Tumor necrosis factor alpha and interleukin-1beta stimulate the expression of cyclooxygenase II but do not alter prostaglandin E2 receptor mRNA levels in cultured dorsal root ganglia cells." Pain **113**(1-2): 113-122.

Felson, D. T. (2005). "The sources of pain in knee osteoarthritis." Curr Opin Rheumatol **17**(5): 624-628.

Felson, D. T., C. E. Chaisson, C. L. Hill, S. M. Totterman, M. E. Gale, K. M. Skinner, L. Kazis and D. R. Gale (2001). "The association of bone marrow lesions with pain in knee osteoarthritis." Ann Intern Med **134**(7): 541-549.

Fernandes, J. C., J. Martel-Pelletier and J. P. Pelletier (2002). "The role of cytokines in osteoarthritis pathophysiology." Biorheology **39**: 237-246.

Ferrara, N. (2005). "VEGF as a therapeutic target in cancer." Oncology **69 Suppl 3**: 11-16.

Ferrara, N., K. Carver-Moore, H. Chen, M. Dowd, L. Lu, K. S. O'Shea, L. Powell-Braxton, K. J. Hillan and M. W. Moore (1996). "Heterozygous embryonic lethality induced by targeted inactivation of the VEGF gene." Nature **380**(6573): 439-442.

Ferrara, N. and T. Davis-Smyth (1997). "The biology of vascular endothelial growth factor." Endocr Rev **18**(1): 4-25.

Ferrara, N., H. P. Gerber and J. LeCouter (2003). "The biology of VEGF and its receptors." Nat Med **9**(6): 669-676.

Ferrara, N. and W. J. Henzel (1989). "Pituitary follicular cells secrete a novel heparin-binding growth factor specific for vascular endothelial cells." Biochem Biophys Res Commun **161**(2): 851-858.

Finckh, A., M. H. Liang, C. M. van Herckenrode and P. de Pablo (2006). "Long-term impact of early treatment on radiographic progression in rheumatoid arthritis: A meta-analysis." Arthritis Rheum **55**(6): 864-872.

Finnson, K. W., W. L. Parker, Y. Chi, C. D. Hoemann, M. B. Goldring, J. Antoniou and A. Philip (2010). "Endoglin differentially regulates TGF- $\beta$ -induced Smad2/3 and Smad1/5 signalling and its expression correlates with extracellular matrix production and cellular differentiation state in human chondrocytes." Osteoarthritis Cartilage **18**(11): 1518-1527.

Florea, A., F. M. Mottaghy and M. Bauwens (2021). "Molecular Imaging of Angiogenesis in Oncology: Current Preclinical and Clinical Status." Int J Mol Sci **22**(11).

Franz, T., E. M. Hasler, R. Hagg, C. Weiler, R. P. Jakob and P. Mainil-Varlet (2001). "In situ compressive stiffness, biochemical composition, and structural integrity of articular cartilage of the human knee joint." Osteoarthritis and Cartilage **9**(6): 582-592.

Fu, B. M. and S. Shen (2004). "Acute VEGF effect on solute permeability of mammalian microvessels in vivo." Microvascular research **68**(1): 51-62.

Fu, X.-D. and M. Ares, Jr. (2014). "Context-dependent control of alternative splicing by RNA-binding proteins." Nature reviews. Genetics **15**(10): 689-701.

Fujioka, R., T. Aoyama and T. Takakuwa (2013). "The layered structure of the articular surface." Osteoarthritis and Cartilage **21**(8): 1092-1098.

Fukuhara, T., T. Hosoya, S. Shimizu, K. Sumi, T. Oshiro, Y. Yoshinaka, M. Suzuki, N. Yamamoto, L. A. Herzenberg, L. A. Herzenberg and M. Hagiwara (2006). "Utilization of host SR protein kinases and RNA-splicing machinery during viral replication." Proc Natl Acad Sci U S A **103**(30): 11329-11333.

Fukuhara, T., T. Hosoya, S. Shimizu, K. Sumi, T. Oshiro, Y. Yoshinaka, M. Suzuki, N. Yamamoto, L. A. Herzenberg, L. A. Herzenberg and M. Hagiwara (2006). "Utilization of host SR protein kinases and RNA-splicing machinery during viral replication." Proceedings of the National Academy of Sciences of the United States of America **103**(30): 11329-11333.

Gaballah, A., N. A. Hussein, M. Risk, N. Elsayy and S. Elabasiry (2016). "Correlation between synovial vascular endothelial growth factor, clinical, functional and radiological manifestations in knee osteoarthritis." The Egyptian Rheumatologist **38**(1): 29-34.

Gammons, M. V., O. Fedorov, D. Ivison, C. Du, T. Clark, C. Hopkins, M. Hagiwara, A. D. Dick, R. Cox, S. J. Harper, J. C. Hancox, S. Knapp and D. O. Bates (2013). "Topical Antiangiogenic SRPK1 Inhibitors Reduce Choroidal Neovascularization in Rodent Models of Exudative AMD." Investigative Ophthalmology & Visual Science **54**(9): 6052-6062.

Gammons, M. V., R. Lucas, R. Dean, S. E. Coupland, S. Oltean and D. O. Bates (2014). "Targeting SRPK1 to control VEGF-mediated tumour angiogenesis in metastatic melanoma." British journal of cancer **111**(3): 477-485.

Gammons, M. V. R., A. D. Dick, S. J. Harper and D. O. Bates (2013). "SRPK1 Inhibition Modulates VEGF Splicing to Reduce Pathological Neovascularization in a Rat Model of Retinopathy of Prematurity." Investigative Ophthalmology & Visual Science **54**(8): 5797-5806.

Garcia-Ramirez, D. L., N. T. Ha, S. Bibu, N. J. Stachowski and K. J. Dougherty (2021). "Spinal Cord Injury Alters Spinal Shox2 Interneurons by Enhancing Excitatory Synaptic Input and Serotonergic Modulation While Maintaining Intrinsic Properties in Mouse." The Journal of Neuroscience **41**(27): 5833.

Gardiner, N. J. and O. J. Freeman (2016). "Can Diabetic Neuropathy Be Modeled In Vitro?" Int Rev Neurobiol **127**: 53-87.

Gardner, E. (1948). "The innervation of the knee joint." The Anatomical Record **101**(1): 109-130.

Gavard, J. and J. S. Gutkind (2006). "VEGF controls endothelial-cell permeability by promoting the beta-arrestin-dependent endocytosis of VE-cadherin." Nat Cell Biol **8**(11): 1223-1234.

Gay, R. D., A. W. Clarke, Z. Elgundi, T. Domagala, R. J. Simpson, N. B. Le, A. G. Doyle and P. A. Jennings (2010). "Anti-TNF $\alpha$  domain antibody construct CEP-37247: Full antibody functionality at half the size." MAbs **2**(6): 625-638.

Gelber, A. C., M. C. Hochberg, L. A. Mead, N. Y. Wang, F. M. Wigley and M. J. Klag (2000). "Joint injury in young adults and risk for subsequent knee and hip osteoarthritis." Ann Intern Med **133**(5): 321-328.

Ghosh, G. and J. A. Adams (2011). "Phosphorylation mechanism and structure of serine-arginine protein kinases." Febs j **278**(4): 587-597.

Giatromanolaki, A., E. Sivridis, E. Maltezos, N. Athanassou, D. Papazoglou, K. C. Gatter, A. L. Harris and M. I. Koukourakis (2003). "Upregulated hypoxia inducible factor-1alpha and -2alpha pathway in rheumatoid arthritis and osteoarthritis." Arthritis research & therapy **5**(4): R193-R201.

Gigante, A., C. Bevilacqua, A. Pagnotta, S. Manzotti, A. Toesca and F. Greco (2003). "Expression of NGF, Trka and p75 in human cartilage." Eur J Histochem **47**(4): 339-344.

Giniatullin, R. (2020). "Ion Channels of Nociception." Int J Mol Sci **21**(10).

Goebel, A., D. Andersson, Z. Helyes, J. D. Clark, D. Dulake and C. Svensson (2022). "The autoimmune aetiology of unexplained chronic pain." Autoimmun Rev **21**(3): 103015.

Goel, H. L. and A. M. Mercurio (2013). "VEGF targets the tumour cell." Nature Reviews Cancer **13**: 871.

Goel, H. L. and A. M. Mercurio (2013). "VEGF targets the tumour cell." Nat Rev Cancer **13**(12): 871-882.

Golan-Gerstl, R., M. Cohen, A. Shilo, S. S. Suh, A. Bakàcs, L. Coppola and R. Karni (2011). "Splicing factor hnRNP A2/B1 regulates tumor suppressor gene splicing and is an oncogenic driver in glioblastoma." Cancer Res **71**(13): 4464-4472.

Goldring, M. B. and K. B. Marcu (2009). "Cartilage homeostasis in health and rheumatic diseases." Arthritis Res Ther **11**(3): 224.

Goldring, M. B. and M. Otero (2011). "Inflammation in osteoarthritis." Curr Opin Rheumatol **23**(5): 471-478.

Gonçalves, V., A. F. A. Henriques, J. F. S. Pereira, A. Neves Costa, M. P. Moyer, L. F. Moita, M. Gama-Carvalho, P. Matos and P. Jordan (2014). "Phosphorylation of SRSF1 by SRPK1 regulates alternative splicing of tumor-related Rac1b in colorectal cells." RNA (New York, N.Y.) **20**(4): 474-482.

Granno, S., J. Nixon-Abell, D. C. Berwick, J. Tosh, G. Heaton, S. Almodimeegh, Z. Nagda, J. C. Rain, M. Zanda, V. Plagnol, V. L. J. Tybulewicz, K. Cleverley, F. K. Wiseman, E. M. C. Fisher and K. Harvey (2019). "Downregulated Wnt/ $\beta$ -catenin signalling in the Down syndrome hippocampus." Sci Rep **9**(1): 7322.

Grisar, J., M. Munk, C. W. Steiner, L. Amoyo-Minar, M. Tohidast-Akrad, P. Zenz, G. Steiner and J. S. Smolen (2012). "Expression patterns of CD44 and CD44 splice variants in patients with rheumatoid arthritis." Clin Exp Rheumatol **30**(1): 64-72.

Grosios, K., J. Wood, R. Esser, A. Raychaudhuri and J. Dawson (2004). "Angiogenesis inhibition by the novel VEGF receptor tyrosine kinase inhibitor, PTK787/ZK222584, causes significant anti-arthritic effects in models of rheumatoid arthritis." Inflamm Res **53**(4): 133-142.

Grunke, M. and H. Schulze-Koops (2006). "Successful treatment of inflammatory knee osteoarthritis with tumour necrosis factor blockade." Annals of the Rheumatic Diseases **65**(4): 555.

Guimerà, J., C. Casas, C. Pucharcòs, A. Solans, A. Domènech, A. M. Planas, J. Ashley, M. Lovett, X. Estivill and M. A. Pritchard (1996). "A human homologue of Drosophila minibrain (MNB) is expressed in the neuronal regions affected in Down syndrome and maps to the critical region." Hum Mol Genet **5**(9): 1305-1310.

Guo, Q., Y. Wang, D. Xu, J. Nossent, N. J. Pavlos and J. Xu (2018). "Rheumatoid arthritis: pathological mechanisms and modern pharmacologic therapies." Bone research **6**: 15-15.

Guo, X., D. Zhang, X. Zhang, J. Jiang, P. Xue, C. Wu, J. Zhang, G. Jin, Z. Huang, J. Yang, X. Zhu, W. Liu, G. Xu, Z. Cui and G. Bao (2018). "Dyrk1A promotes the proliferation, migration and invasion of fibroblast-like synoviocytes in rheumatoid arthritis via down-regulating Spry2 and activating the ERK MAPK pathway." Tissue and Cell **55**: 63-70.

Guo, X., D. Zhang, X. Zhang, J. Jiang, P. Xue, C. Wu, J. Zhang, G. Jin, Z. Huang, J. Yang, X. Zhu, W. Liu, G. Xu, Z. Cui and G. Bao (2018). "Dyrk1A promotes the proliferation, migration and invasion of fibroblast-like synoviocytes in rheumatoid arthritis via down-regulating Spry2 and activating the ERK MAPK pathway." Tissue Cell **55**: 63-70.

Guyot, M. and G. Pagès (2015). "VEGF Splicing and the Role of VEGF Splice Variants: From Physiological-Pathological Conditions to Specific Pre-mRNA Splicing." Methods Mol Biol **1332**: 3-23.

Hall, M., S. Doherty, P. Courtney, K. Latief, W. Zhang and M. Doherty (2014). "Synovial pathology detected on ultrasound correlates with the severity of radiographic knee osteoarthritis more than with symptoms." Osteoarthritis and cartilage **22**(10): 1627-1633.

Halliday, D. A., C. Zettler, R. A. Rush, R. Scicchitano and J. D. McNeil (1998). "Elevated Nerve Growth Factor Levels in the Synovial Fluid of Patients with Inflammatory Joint Disease." Neurochemical Research **23**(6): 919-922.

Haltmayer, E., I. Ribitsch, S. Gabner, J. Rosser, S. Gueltekin, J. Peham, U. Giese, M. Dolezal, M. Egerbacher and F. Jenner (2019). "Co-culture of osteochondral explants and synovial membrane as in vitro model for osteoarthritis." PLOS ONE **14**(4): e0214709.

Hamdollah Zadeh, M. A., E. M. Amin, C. Hoareau-Aveilla, E. Domingo, K. E. Symonds, X. Ye, K. J. Heesom, A. Salmon, O. D'Silva, K. B. Betteridge, A. C. Williams, D. J. Kerr, A. H. Salmon, S. Oltean, R. S. Midgley, M. R. Lodomery, S. J. Harper, A. H. Varey and D. O. Bates (2015). "Alternative splicing of TIA-1 in human colon cancer regulates VEGF isoform expression, angiogenesis, tumour growth and bevacizumab resistance." Mol Oncol **9**(1): 167-178.

Hamilton, J. L., M. Nagao, B. R. Levine, D. Chen, B. R. Olsen and H. J. Im (2016). "Targeting VEGF and Its Receptors for the Treatment of Osteoarthritis and Associated Pain." J Bone Miner Res **31**(5): 911-924.

Haringman, J. J., D. M. Gerlag, T. J. Smeets, D. Baeten, F. van den Bosch, B. Bresnihan, F. C. Breedveld, H. J. Dinant, F. Legay, H. Gram, P. Loetscher, R. Schmouder, T. Woodworth and P. P. Tak (2006). "A randomized controlled trial with an anti-CCL2 (anti-monocyte chemotactic protein 1) monoclonal antibody in patients with rheumatoid arthritis." Arthritis Rheum **54**(8): 2387-2392.

Harirforoosh, S. and F. Jamali (2009). "Renal adverse effects of nonsteroidal anti-inflammatory drugs." Expert Opin Drug Saf **8**(6): 669-681.

Harper, S. J. and D. O. Bates (2008). "VEGF-A splicing: the key to anti-angiogenic therapeutics?" Nat Rev Cancer **8**(11): 880-887.

Harris, S., M. Craze, J. Newton, M. Fisher, D. T. Shima, G. M. Tozer and C. Kanthou (2012). "Do Anti-Angiogenic VEGF (VEGFxxx) Isoforms Exist? A Cautionary Tale." PLOS ONE **7**(5): e35231.

Hassan, H. and D. A. Walsh (2013). "Central pain processing in osteoarthritis: implications for treatment." Pain Management **4**(1): 45-56.

Hatcher, J. M., G. Wu, C. Zeng, J. Zhu, F. Meng, S. Patel, W. Wang, S. B. Ficarro, A. L. Leggett, C. E. Powell, J. A. Marto, K. Zhang, J. C. Ki Ngo, X.-D. Fu, T. Zhang and N. S. Gray (2018). "SRPKIN-1: A Covalent SRPK1/2 Inhibitor that Potently Converts VEGF from Pro-angiogenic to Anti-angiogenic Isoform." Cell Chemical Biology **25**(4): 460-470.e466.

Haywood, L., D. F. McWilliams, C. I. Pearson, S. E. Gill, A. Ganesan, D. Wilson and D. A. Walsh (2003). "Inflammation and angiogenesis in osteoarthritis." Arthritis Rheum **48**(8): 2173-2177.

Heidari, B. (2011). "Knee osteoarthritis prevalence, risk factors, pathogenesis and features: Part I." Caspian J Intern Med **2**(2): 205-212.

Heijink, A., A. H. Gomoll, H. Madry, M. Drobnič, G. Filardo, J. Espregueira-Mendes and C. N. Van Dijk (2012). "Biomechanical considerations in the pathogenesis of osteoarthritis of the knee." Knee Surg Sports Traumatol Arthrosc **20**(3): 423-435.

Hellgren, K., D. Di Giuseppe, K. E. Smedby, C. Sundström, J. Askling, E. Baecklund and f. t. A. s. group (2020). "Lymphoma risks in patients with rheumatoid arthritis treated with biological drugs—a Swedish cohort study of risks by time, drug and lymphoma subtype." Rheumatology **60**(2): 809-819.

Hellingman, C. A., E. N. Davidson, W. Koevoet, E. L. Vitters, W. B. van den Berg, G. J. van Osch and P. M. van der Kraan (2011). "Smad signaling determines chondrogenic differentiation of bone-marrow-derived mesenchymal stem cells: inhibition of Smad1/5/8P prevents terminal differentiation and calcification." Tissue Eng Part A **17**(7-8): 1157-1167.

Hill, C. L., D. G. Gale, C. E. Chaisson, K. Skinner, L. Kazis, M. E. Gale and D. T. Felson (2001). "Knee effusions, popliteal cysts, and synovial thickening: association with knee pain in osteoarthritis." J Rheumatol **28**(6): 1330-1337.

Hill, C. L., D. J. Hunter, J. Niu, M. Clancy, A. Guermazi, H. Genant, D. Gale, A. Grainger, P. Conaghan and D. T. Felson (2007). "Synovitis detected on magnetic resonance imaging and its relation to pain and cartilage loss in knee osteoarthritis." Ann Rheum Dis **66**(12): 1599-1603.

Hino, K., T. Maeda, K. Sekiguchi, K. Shiozawa, H. Hirano, E. Sakashita and S. Shiozawa (1996). "Adherence of synovial cells on EDA-containing fibronectin." Arthritis Rheum **39**(10): 1685-1692.

Hinz, B. (2009). "Tissue stiffness, latent TGF-beta1 activation, and mechanical signal transduction: implications for the pathogenesis and treatment of fibrosis." Curr Rheumatol Rep **11**(2): 120-126.

Hinz, B. (2015). "The extracellular matrix and transforming growth factor-β1: Tale of a strained relationship." Matrix Biol **47**: 54-65.

Hiratsuka, S., Y. Kataoka, K. Nakao, K. Nakamura, S. Morikawa, S. Tanaka, M. Katsuki, Y. Maru and M. Shibuya (2005). "Vascular endothelial growth factor A (VEGF-A) is involved in guidance of VEGF receptor-positive cells to the anterior portion of early embryos." Molecular and cellular biology **25**(1): 355-363.

Hochman, J. R., M. R. French, S. L. Bermingham and G. A. Hawker (2010). "The nerve of osteoarthritis pain." Arthritis Care Res (Hoboken) **62**(7): 1019-1023.

Honorati, M. C., M. Bovera, L. Cattini, A. Piacentini and A. Facchini (2002). "Contribution of interleukin 17 to human cartilage degradation and synovial inflammation in osteoarthritis." Osteoarthritis and Cartilage **10**(10): 799-807.

Honorati, M. C., L. Cattini and A. Facchini (2004). "IL-17, IL-1beta and TNF-alpha stimulate VEGF production by dedifferentiated chondrocytes." Osteoarthritis Cartilage **12**(9): 683-691.

Hoskins, A. A. and M. J. Moore (2012). "The spliceosome: a flexible, reversible macromolecular machine." Trends Biochem Sci **37**(5): 179-188.

Hu, P. F., J. L. Tang, W. P. Chen, J. P. Bao and L. D. Wu (2011). "Increased apelin serum levels and expression in human chondrocytes in osteoarthritic patients." Int Orthop **35**(9): 1421-1426.

Hu, X. M., W. Yang, L. X. Du, W. Q. Cui, W. L. Mi, Q. L. Mao-Ying, Y. X. Chu and Y. Q. Wang (2019). "Vascular Endothelial Growth Factor A Signaling Promotes Spinal

Central Sensitization and Pain-related Behaviors in Female Rats with Bone Cancer." *Anesthesiology* **131**(5): 1125-1147.

Hulejová, H., V. Barešová, Z. Klézl, M. Polanská, M. Adam and L. Šenolt (2007). "Increased level of cytokines and matrix metalloproteinases in osteoarthritic subchondral bone." *Cytokine* **38**(3): 151-156.

Hulse, R. P. (2017). "Role of VEGF-A in chronic pain." *Oncotarget* **8**(7): 10775-10776.

Hulse, R. P., N. Beazley-Long, J. Hua, H. Kennedy, J. Prager, H. Bevan, Y. Qiu, E. S. Fernandes, M. V. Gammons, K. Ballmer-Hofer, A. C. Gittenberger de Groot, A. J. Churchill, S. J. Harper, S. D. Brain, D. O. Bates and L. F. Donaldson (2014). "Regulation of alternative VEGF-A mRNA splicing is a therapeutic target for analgesia." *Neurobiology of disease* **71**: 245-259.

Hulse, R. P., N. Beazley-Long, N. Ved, S. M. Bestall, H. Riaz, P. Singhal, K. Ballmer Hofer, S. J. Harper, D. O. Bates and L. F. Donaldson (2015). "Vascular endothelial growth factor-A165b prevents diabetic neuropathic pain and sensory neuronal degeneration." *Clin Sci (Lond)* **129**(8): 741-756.

Hulse, R. P., R. A. Drake, D. O. Bates and L. F. Donaldson (2016). "The control of alternative splicing by SRSF1 in myelinated afferents contributes to the development of neuropathic pain." *Neurobiol Dis* **96**: 186-200.

Hulse, R. P., R. A. R. Drake, D. O. Bates and L. F. Donaldson (2016). "The control of alternative splicing by SRSF1 in myelinated afferents contributes to the development of neuropathic pain." *Neurobiology of Disease* **96**: 186-200.

Hunter, D. J., A. Guermazi, F. Roemer, Y. Zhang and T. Neogi (2013). "Structural correlates of pain in joints with osteoarthritis." *Osteoarthritis Cartilage* **21**(9): 1170-1178.

Ijichi, A., S. Sakuma and P. J. Tofilon (1995). "Hypoxia-induced vascular endothelial growth factor expression in normal rat astrocyte cultures." *Glia* **14**(2): 87-93.

Ishida, S., T. Usui, K. Yamashiro, Y. Kaji, E. Ahmed, K. G. Carrasquillo, S. Amano, T. Hida, Y. Oguchi and A. P. Adamis (2003). "VEGF164 is proinflammatory in the diabetic retina." *Invest Ophthalmol Vis Sci* **44**(5): 2155-2162.

Ishida, S., T. Usui, K. Yamashiro, Y. Kaji, S. Amano, Y. Ogura, T. Hida, Y. Oguchi, J. Ambati, J. W. Miller, E. S. Gragoudas, Y. S. Ng, P. A. D'Amore, D. T. Shima and A. P. Adamis (2003). "VEGF164-mediated inflammation is required for pathological, but not physiological, ischemia-induced retinal neovascularization." *J Exp Med* **198**(3): 483-489.

Ishijima, M., T. Nakamura, K. Shimizu, K. Hayashi, H. Kikuchi, S. Soen, G. Omori, T. Yamashita, Y. Uchio, J. Chiba, Y. Ideno, M. Kubota, H. Kurosawa and K. Kaneko (2014). "Intra-articular hyaluronic acid injection versus oral non-steroidal anti-inflammatory drug for the treatment of knee osteoarthritis: a multi-center, randomized, open-label, non-inferiority trial." *Arthritis Res Ther* **16**(1): R18.

Iwai, K., M. Yaguchi, K. Nishimura, Y. Yamamoto, T. Tamura, D. Nakata, R. Dairiki, Y. Kawakita, R. Mizojiri, Y. Ito, M. Asano, H. Maezaki, Y. Nakayama, M. Kaishima, K. Hayashi, M. Teratani, S. Miyakawa, M. Iwatani, M. Miyamoto, M. G. Klein, W. Lane, G. Snell, R. Tjhen, X. He, S. Pulukuri and T. Nomura (2018). "Anti-tumor efficacy of a novel CLK inhibitor via targeting RNA splicing and MYC-dependent vulnerability." *EMBO molecular medicine* **10**(6): e8289.

Iwai, K., M. Yaguchi, K. Nishimura, Y. Yamamoto, T. Tamura, D. Nakata, R. Dairiki, Y. Kawakita, R. Mizojiri, Y. Ito, M. Asano, H. Maezaki, Y. Nakayama, M. Kaishima, K. Hayashi, M. Teratani, S. Miyakawa, M. Iwatani, M. Miyamoto, M. G. Klein, W. Lane, G. Snell, R. Tjhen, X. He, S. Pulukuri and T. Nomura (2018). "Anti-tumor efficacy of a novel CLK inhibitor via targeting RNA splicing and MYC-dependent vulnerability." EMBO Mol Med **10**(6).

Iwanaga, T., M. Shikichi, H. Kitamura, H. Yanase and K. Nozawa-Inoue (2000). "Morphology and functional roles of synoviocytes in the joint." Arch Histol Cytol **63**(1): 17-31.

Jackson, J. R., J. A. Minton, M. L. Ho, N. Wei and J. D. Winkler (1997). "Expression of vascular endothelial growth factor in synovial fibroblasts is induced by hypoxia and interleukin 1beta." J Rheumatol **24**(7): 1253-1259.

Jakubauskiene, E., L. Vilyis, Y. Makino, L. Poellinger and A. Kanopka (2015). "Increased Serine-Arginine (SR) Protein Phosphorylation Changes Pre-mRNA Splicing in Hypoxia." J Biol Chem **290**(29): 18079-18089.

James, C. G., C. T. G. Appleton, V. Ulici, T. M. Underhill and F. Beier (2005). "Microarray Analyses of Gene Expression during Chondrocyte Differentiation Identifies Novel Regulators of Hypertrophy." Molecular Biology of the Cell **16**(11): 5316-5333.

Jarhad, D. B., K. K. Mashelkar, H. R. Kim, M. Noh and L. S. Jeong (2018). "Dual-Specificity Tyrosine Phosphorylation-Regulated Kinase 1A (DYRK1A) Inhibitors as Potential Therapeutics." J Med Chem **61**(22): 9791-9810.

Ji, R.-R., Z.-Z. Xu, X. Wang and E. H. Lo (2009). "Matrix metalloprotease regulation of neuropathic pain." Trends in pharmacological sciences **30**(7): 336-340.

Ji, R. R., A. Nackley, Y. Huh, N. Terrando and W. Maixner (2018). "Neuroinflammation and Central Sensitization in Chronic and Widespread Pain." Anesthesiology **129**(2): 343-366.

Jia, T., T. Jacquet, F. Dalonneau, P. Coudert, E. Vaganay, C. Exbrayat-Héritier, J. Vollaire, V. Jossierand, F. Ruggiero, J. L. Coll and B. Eymin (2021). "FGF-2 promotes angiogenesis through a SRSF1/SRSF3/SRPK1-dependent axis that controls VEGFR1 splicing in endothelial cells." BMC Biol **19**(1): 173.

Julius, D. and A. I. Basbaum (2001). "Molecular mechanisms of nociception." Nature **413**(6852): 203-210.

Kanyama, M., T. Kuboki, S. Kojima, T. Fujisawa, T. Hattori, M. Takigawa and A. Yamashita (2000). "Matrix metalloproteinases and tissue inhibitors of metalloproteinases in synovial fluids of patients with temporomandibular joint osteoarthritis." J Orofac Pain **14**(1): 20-30.

Kapoor, M., J. Martel-Pelletier, D. Lajeunesse, J.-P. Pelletier and H. Fahmi (2011). "Role of proinflammatory cytokines in the pathophysiology of osteoarthritis." Nature Reviews Rheumatology **7**(1): 33-42.

Kapoor, M., J. Martel-Pelletier, D. Lajeunesse, J. P. Pelletier and H. Fahmi (2011). "Role of proinflammatory cytokines in the pathophysiology of osteoarthritis." Nat Rev Rheumatol **7**(1): 33-42.

Karmakar, S., J. Kay and E. M. Gravallese (2010). "Bone damage in rheumatoid arthritis: mechanistic insights and approaches to prevention." Rheumatic diseases clinics of North America **36**(2): 385-404.

Katsuyama, T., H. Li, D. Comte, G. C. Tsokos and V. R. Moulton (2019). "Splicing factor SRSF1 controls T cell hyperactivity and systemic autoimmunity." J Clin Invest **129**(12): 5411-5423.

Kawamura, H., X. Li, S. J. Harper, D. O. Bates and L. Claesson-Welsh (2008). "Vascular endothelial growth factor (VEGF)-A165b is a weak in vitro agonist for VEGF receptor-2 due to lack of coreceptor binding and deficient regulation of kinase activity." Cancer Res **68**(12): 4683-4692.

Kay, J. and K. S. Upchurch (2012). "ACR/EULAR 2010 rheumatoid arthritis classification criteria." Rheumatology (Oxford) **51 Suppl 6**: vi5-9.

Kerbel, R. S. (2008). "Tumor angiogenesis." N Engl J Med **358**(19): 2039-2049.

Khan, A., S. Khan and Y. S. Kim (2019). "Insight into Pain Modulation: Nociceptors Sensitization and Therapeutic Targets." Curr Drug Targets **20**(7): 775-788.

Khor, B., J. D. Gagnon, G. Goel, M. I. Roche, K. L. Conway, K. Tran, L. N. Aldrich, T. B. Sundberg, A. M. Paterson, S. Mordecai, D. Dombkowski, M. Schirmer, P. H. Tan, A. K. Bhan, R. Roychoudhuri, N. P. Restifo, J. J. O'Shea, B. D. Medoff, A. F. Shamji, S. L. Schreiber, A. H. Sharpe, S. Y. Shaw and R. J. Xavier (2015). "The kinase DYRK1A reciprocally regulates the differentiation of Th17 and regulatory T cells." Elife **4**.

Kiguchi, N., Y. Kobayashi, Y. Kadowaki, Y. Fukazawa, F. Saika and S. Kishioka (2014). "Vascular endothelial growth factor signaling in injured nerves underlies peripheral sensitization in neuropathic pain." J Neurochem **129**(1): 169-178.

Kim, H.-R., K.-W. Kim, B.-M. Kim, M.-L. Cho and S.-H. Lee (2015). "The effect of vascular endothelial growth factor on osteoclastogenesis in rheumatoid arthritis." PLoS one **10**(4): e0124909-e0124909.

Kim, H. R., J. H. Lee, K. W. Kim, B. M. Kim and S. H. Lee (2016). "The relationship between synovial fluid VEGF and serum leptin with ultrasonographic findings in knee osteoarthritis." Int J Rheum Dis **19**(3): 233-240.

Kim, H. R., M. K. Park, M. L. Cho, C. H. Yoon, S. H. Lee, S. H. Park, L. Leng, R. Bucala, I. Kang, J. Choe and H. Y. Kim (2007). "Macrophage migration inhibitory factor upregulates angiogenic factors and correlates with clinical measures in rheumatoid arthritis." J Rheumatol **34**(5): 927-936.

King, D. F. and L. A. King (1986). "A brief historical note on staining by hematoxylin and eosin." Am J Dermatopathol **8**(2): 168.

Kittelson, A. J., S. Z. George, K. S. Maluf and J. E. Stevens-Lapsley (2014). "Future directions in painful knee osteoarthritis: harnessing complexity in a heterogeneous population." Physical therapy **94**(3): 422-432.

Kivelä, R., M. Bry, M. R. Robciuc, M. Räsänen, M. Taavitsainen, J. M. U. Silvola, A. Saraste, J. J. Hulmi, A. Anisimov, M. I. Mäyränpää, J. H. Lindeman, L. Eklund, S. Hellberg, R. Hlushchuk, Z. W. Zhuang, M. Simons, V. Djonov, J. Knuuti, E. Mervaala and K. Alitalo (2014). "VEGF-B-induced vascular growth leads to metabolic reprogramming and ischemia resistance in the heart." EMBO Molecular Medicine **6**(3): 307-321.

Kono, M., T. Kurita, S. Yasuda, M. Kono, Y. Fujieda, T. Bohgaki, T. Katsuyama, G. C. Tsokos, V. R. Moulton and T. Atsumi (2018). "Decreased Expression of Serine/Arginine-Rich Splicing Factor 1 in T Cells From Patients With Active Systemic Lupus Erythematosus Accounts for Reduced Expression of RasGRP1 and DNA Methyltransferase 1." Arthritis Rheumatol **70**(12): 2046-2056.

Kornaat, P. R., J. L. Bloem, R. Y. Ceulemans, N. Riyazi, F. R. Rosendaal, R. G. Nelissen, W. O. Carter, M. P. Hellio Le Graverand and M. Kloppenburg (2006). "Osteoarthritis of the knee: association between clinical features and MR imaging findings." Radiology **239**(3): 811-817.

Kras, J. V., C. L. Weisshaar, P. S. Pall and B. A. Winkelstein (2015). "Pain from intra-articular NGF or joint injury in the rat requires contributions from peptidergic joint afferents." Neurosci Lett **604**: 193-198.

Krenn, V., L. Morawietz, G. R. Burmester, R. W. Kinne, U. Mueller-Ladner, B. Muller and T. Häupl (2006). "Synovitis score: discrimination between chronic low-grade and high-grade synovitis." Histopathology **49**(4): 358-364.

Krenn, V., L. Morawietz, T. Häupl, J. Neidel, I. Petersen and A. König (2002). "Grading of chronic synovitis--a histopathological grading system for molecular and diagnostic pathology." Pathol Res Pract **198**(5): 317-325.

Ladomery, M. (2013). "Aberrant alternative splicing is another hallmark of cancer." Int J Cell Biol **2013**: 463786.

Ladomery, M. R., S. J. Harper and D. O. Bates (2007). "Alternative splicing in angiogenesis: the vascular endothelial growth factor paradigm." Cancer Lett **249**(2): 133-142.

Lafont, J. E. (2010). "Lack of oxygen in articular cartilage: consequences for chondrocyte biology." International journal of experimental pathology **91**(2): 99-106.

Lai, H. H., B. Shen, P. Vijairania, X. Zhang, S. K. Vogt and R. W. t. Gereau (2017). "Anti-vascular endothelial growth factor treatment decreases bladder pain in cyclophosphamide cystitis: a Multidisciplinary Approach to the Study of Chronic Pelvic Pain (MAPP) Research Network animal model study." BJU Int **120**(4): 576-583.

Lal, N., K. Puri and B. Rodrigues (2018). "Vascular Endothelial Growth Factor B and Its Signaling." Frontiers in Cardiovascular Medicine **5**.

Lane, N. E., T. J. Schnitzer, C. A. Birbara, M. Mokhtarani, D. L. Shelton, M. D. Smith and M. T. Brown (2010). "Tanezumab for the Treatment of Pain from Osteoarthritis of the Knee." New England Journal of Medicine **363**(16): 1521-1531.

Lawson, C. and S. Wolf (2009). "ICAM-1 signaling in endothelial cells." Pharmacol Rep **61**(1): 22-32.

Le, T. H. V. and S. M. Kwon (2021). "Vascular Endothelial Growth Factor Biology and Its Potential as a Therapeutic Target in Rheumatic Diseases." Int J Mol Sci **22**(10).

Lee, G. W., J. Y. Son, A. R. Lee, J. S. Ju, Y. C. Bae and D. K. Ahn (2019). "Central VEGF-A pathway plays a key role in the development of trigeminal neuropathic pain in rats." Mol Pain **15**: 1744806919872602.

Lee, H. L., H. Y. Lee, Y. Yun, J. Oh, L. Che, M. Lee and Y. Ha (2016). "Hypoxia-specific, VEGF-expressing neural stem cell therapy for safe and effective treatment of neuropathic pain." J Control Release **226**: 21-34.

Lee, J., S. Lee, H. Zhang, M. A. Hill, C. Zhang and Y. Park (2017). "Interaction of IL-6 and TNF- $\alpha$  contributes to endothelial dysfunction in type 2 diabetic mouse hearts." PLoS One **12**(11): e0187189.

Lee, J. Y., J.-S. Yun, W.-K. Kim, H.-S. Chun, H. Jin, S. Cho and J. H. Chang (2019). "Structural Basis for the Selective Inhibition of Cdc2-Like Kinases by CX-4945." BioMed Research International **2019**: 6125068.

Lee, Y. and D. C. Rio (2015). "Mechanisms and Regulation of Alternative Pre-mRNA Splicing." Annu Rev Biochem **84**: 291-323.

Lehner, B., F. X. Koeck, S. Capellino, T. E. Schubert, R. Hofbauer and R. H. Straub (2008). "Preponderance of sensory versus sympathetic nerve fibers and increased cellularity in the infrapatellar fat pad in anterior knee pain patients after primary arthroplasty." J Orthop Res **26**(3): 342-350.

Leung, L. and C. M. Cahill (2010). "TNF-alpha and neuropathic pain--a review." J Neuroinflammation **7**: 27.

Levi-Montalcini, R. (1987). "The nerve growth factor 35 years later." Science **237**(4819): 1154-1162.

Levy, A. P., N. S. Levy, S. Wegner and M. A. Goldberg (1995). "Transcriptional regulation of the rat vascular endothelial growth factor gene by hypoxia." J Biol Chem **270**(22): 13333-13340.

Li, Y., Y. Liem, E. Dall'Ara, N. Sullivan, H. Ahmed, A. Blom and M. Sharif (2021). "Subchondral bone microarchitecture and mineral density in human osteoarthritis and osteoporosis: A regional and compartmental analysis." J Orthop Res **39**(12): 2568-2580.

Li, Z., A. Li, L. Yan, T. Yang, W. Xu and P. Fan (2020). "Downregulation of long noncoding RNA DLEU1 attenuates hypersensitivity in chronic constriction injury-induced neuropathic pain in rats by targeting miR-133a-3p/SRPK1 axis." Mol Med **26**(1): 104.

Li, Z., A. Li, L. Yan, T. Yang, W. Xu and P. Fan (2020). "Downregulation of long noncoding RNA DLEU1 attenuates hypersensitivity in chronic constriction injury-induced neuropathic pain in rats by targeting miR-133a-3p/SRPK1 axis." Molecular Medicine **26**(1): 104.

Lichtman, J. W. and J. A. Conchello (2005). "Fluorescence microscopy." Nat Methods **2**(12): 910-919.

Lin, J., G. Li, X. Den, C. Xu, S. Liu, Y. Gao, H. Liu, J. Zhang, X. Li and S. Liang (2010). "VEGF and its receptor-2 involved in neuropathic pain transmission mediated by P2X<sub>2</sub>(/)<sub>3</sub> receptor of primary sensory neurons." Brain Res Bull **83**(5): 284-291.

Lin, J. C., Y. C. Lee, Y. C. Liang, Y. C. Fann, K. R. Johnson and Y. J. Lin (2017). "The impact of the RBM4-initiated splicing cascade on modulating the carcinogenic signature of colorectal cancer cells." Sci Rep **7**: 44204.

Lis, K., O. Kuzawińska and E. Bałkowiec-Iskra (2014). "Tumor necrosis factor inhibitors - state of knowledge." Arch Med Sci **10**(6): 1175-1185.

Liu, D., A. Ahmet, L. Ward, P. Krishnamoorthy, E. D. Mandelcorn, R. Leigh, J. P. Brown, A. Cohen and H. Kim (2013). "A practical guide to the monitoring and management of the complications of systemic corticosteroid therapy." Allergy Asthma Clin Immunol **9**(1): 30.

Liu, T., Y. Wang, J. Wang, C. Ren, H. Chen and J. Zhang (2022). "DYRK1A inhibitors for disease therapy: Current status and perspectives." Eur J Med Chem **229**: 114062.

Llorián-Salvador, M. and S. González-Rodríguez (2018). "Painful Understanding of VEGF." Frontiers in pharmacology **9**: 1267-1267.

Llorián-Salvador, M. and S. González-Rodríguez (2018). "Painful Understanding of VEGF." Frontiers in Pharmacology **9**.

Loeser, R. F., S. R. Goldring, C. R. Scanzello and M. B. Goldring (2012). "Osteoarthritis: a disease of the joint as an organ." Arthritis Rheum **64**(6): 1697-1707.

Lohela, M., M. Bry, T. Tammela and K. Alitalo (2009). "VEGFs and receptors involved in angiogenesis versus lymphangiogenesis." Curr Opin Cell Biol **21**(2): 154-165.

Lopez-Bellido, R., S. Puig, P. J. Huang, C.-R. Tsai, H. N. Turner, M. J. Galko and H. B. Gutstein (2019). "Growth Factor Signaling Regulates Mechanical Nociception in Flies and Vertebrates." The Journal of Neuroscience **39**(30): 6012.

Lopez-Bellido, R., S. Puig, P. J. Huang, C. R. Tsai, H. N. Turner, M. J. Galko and H. B. Gutstein (2019). "Growth Factor Signaling Regulates Mechanical Nociception in Flies and Vertebrates." J Neurosci **39**(30): 6012-6030.

Ludin, A., J. J. Sela, A. Schroeder, Y. Samuni, D. W. Nitzan and G. Amir (2013). "Injection of vascular endothelial growth factor into knee joints induces osteoarthritis in mice." Osteoarthritis Cartilage **21**(3): 491-497.

Ma, X. and S. Xu (2013). "TNF inhibitor therapy for rheumatoid arthritis." Biomed Rep **1**(2): 177-184.

Mabey, T., S. Honsawek, N. Saetan, Y. Poovorawan, A. Tanavalee and P. Yuktanandana (2014). "Angiogenic cytokine expression profiles in plasma and synovial fluid of primary knee osteoarthritis." Int Orthop **38**(9): 1885-1892.

Madry, H., C. N. van Dijk and M. Mueller-Gerbl (2010). "The basic science of the subchondral bone." Knee Surg Sports Traumatol Arthrosc **18**(4): 419-433.

Magnussen, A. L., E. S. Rennel, J. Hua, H. S. Bevan, N. Beazley Long, C. Lehrling, M. Gammons, J. Floege, S. J. Harper, H. T. Agostini, D. O. Bates and A. J. Churchill (2010). "VEGF-A165b is cytoprotective and antiangiogenic in the retina." Invest Ophthalmol Vis Sci **51**(8): 4273-4281.

Malfait, A. M. and T. J. Schnitzer (2013). "Towards a mechanism-based approach to pain management in osteoarthritis." Nat Rev Rheumatol **9**(11): 654-664.

Malhi, N. K., C. L. Allen, E. Stewart, K. L. Horton, F. Riu, J. Batson, W. Amoaku, J. C. Morris, K. P. Arkill and D. O. Bates (2022). "Serine/arginine rich protein kinase-1 (SRPK1) inhibition for the treatment of diabetic retinopathy." Am J Physiol Heart Circ Physiol.

Malykhina, A. P., Q. Lei, C. S. Erickson, M. L. Epstein, M. R. Saban, C. A. Davis and R. Saban (2012). "VEGF induces sensory and motor peripheral plasticity, alters bladder function, and promotes visceral sensitivity." BMC Physiol **12**: 15.

Mankin, H. J., H. Dorfman, L. Lippiello and A. Zarins (1971). "Biochemical and metabolic abnormalities in articular cartilage from osteo-arthritic human hips. II. Correlation of morphology with biochemical and metabolic data." J Bone Joint Surg Am **53**(3): 523-537.

Martel-Pelletier, J. and J. P. Pelletier (2010). "Is osteoarthritis a disease involving only cartilage or other articular tissues?" Eklem Hastalik Cerrahisi **21**(1): 2-14.

Mathiessen, A. and P. G. Conaghan (2017). "Synovitis in osteoarthritis: current understanding with therapeutic implications." Arthritis Research & Therapy **19**(1): 18.

Mavrou, A., K. Brakspear, M. Hamdollah-Zadeh, G. Damodaran, R. Babaei-Jadidi, J. Oxley, D. A. Gillatt, M. R. Lodomery, S. J. Harper, D. O. Bates and S. Oltean (2015). "Serine-arginine protein kinase 1 (SRPK1) inhibition as a potential novel targeted therapeutic strategy in prostate cancer." Oncogene **34**(33): 4311-4319.

McAlindon, T. E., R. R. Bannuru, M. C. Sullivan, N. K. Arden, F. Berenbaum, S. M. Bierma-Zeinstra, G. A. Hawker, Y. Henrotin, D. J. Hunter, H. Kawaguchi, K. Kwoh, S. Lohmander, F. Rannou, E. M. Roos and M. Underwood (2014). "OARSI guidelines for

the non-surgical management of knee osteoarthritis." Osteoarthritis Cartilage **22**(3): 363-388.

McDougall, J. J. (2006). "Arthritis and pain. Neurogenic origin of joint pain." Arthritis research & therapy **8**(6): 220-220.

McKelvey, L., G. D. Shorten and G. W. O'Keeffe (2013). "Nerve growth factor-mediated regulation of pain signalling and proposed new intervention strategies in clinical pain management." Journal of Neurochemistry **124**(3): 276-289.

McQuibban, G. A., G. S. Butler, J.-H. Gong, L. Bendall, C. Power, I. Clark-Lewis and C. M. Overall (2001). "Matrix Metalloproteinase Activity Inactivates the CXC Chemokine Stromal Cell-derived Factor-1 \*." Journal of Biological Chemistry **276**(47): 43503-43508.

McQuibban, G. A., J. H. Gong, J. P. Wong, J. L. Wallace, I. Clark-Lewis and C. M. Overall (2002). "Matrix metalloproteinase processing of monocyte chemoattractant proteins generates CC chemokine receptor antagonists with anti-inflammatory properties in vivo." Blood **100**(4): 1160-1167.

Meehan, R. T., E. A. Regan, E. D. Hoffman, M. L. Wolf, M. T. Gill, J. L. Crooks, P. J. Parmar, R. A. Scheuring, J. C. Hill, K. A. Pacheco and V. Knight (2021). "Synovial Fluid Cytokines, Chemokines and MMP Levels in Osteoarthritis Patients with Knee Pain Display a Profile Similar to Many Rheumatoid Arthritis Patients." J Clin Med **10**(21).

Messier, S. P., R. F. Loeser, G. D. Miller, T. M. Morgan, W. J. Rejeski, M. A. Sevick, W. H. Ettinger, Jr., M. Pahor and J. D. Williamson (2004). "Exercise and dietary weight loss in overweight and obese older adults with knee osteoarthritis: the Arthritis, Diet, and Activity Promotion Trial." Arthritis Rheum **50**(5): 1501-1510.

Micheli, L., C. Parisio, E. Lucarini, A. Vona, A. Toti, A. Pacini, T. Mello, S. Boccella, F. Ricciardi, S. Maione, G. Graziani, P. M. Lacal, P. Failli, C. Ghelardini and L. Di Cesare Mannelli (2021). "VEGF-A/VEGFR-1 signalling and chemotherapy-induced neuropathic pain: therapeutic potential of a novel anti-VEGFR-1 monoclonal antibody." J Exp Clin Cancer Res **40**(1): 320.

Milgram, J. W. (1983). "Morphologic alterations of the subchondral bone in advanced degenerative arthritis." Clin Orthop Relat Res(173): 293-312.

Miller Rachel, E., B. Tran Phuong, R. Das, N. Ghoreishi-Haack, D. Ren, J. Miller Richard and A.-M. Malfait (2012). "CCR2 chemokine receptor signaling mediates pain in experimental osteoarthritis." Proceedings of the National Academy of Sciences **109**(50): 20602-20607.

Miller, R. E., J. A. Block and A. M. Malfait (2017). "Nerve growth factor blockade for the management of osteoarthritis pain: what can we learn from clinical trials and preclinical models?" Curr Opin Rheumatol **29**(1): 110-118.

Milz, S. and R. Putz (1994). "Quantitative morphology of the subchondral plate of the tibial plateau." J Anat **185** ( Pt 1)(Pt 1): 103-110.

Moulton, V. R., A. R. Gillooly and G. C. Tsokos (2014). "Ubiquitination Regulates Expression of the Serine/Arginine-rich Splicing Factor 1 (SRSF1) in Normal and Systemic Lupus Erythematosus (SLE) T Cells \*." Journal of Biological Chemistry **289**(7): 4126-4134.

Müller-Ladner, U., C. Ospelt, S. Gay, O. Distler and T. Pap (2007). "Cells of the synovium in rheumatoid arthritis. Synovial fibroblasts." Arthritis Res Ther **9**(6): 223.

Müller-Ladner, U., C. Ospelt, S. Gay, O. Distler and T. Pap (2007). "Cells of the synovium in rheumatoid arthritis. Synovial fibroblasts." Arthritis Research & Therapy **9**(6): 223.

Müller, M. R. and A. Rao (2010). "NFAT, immunity and cancer: a transcription factor comes of age." Nat Rev Immunol **10**(9): 645-656.

Murakami, K., K. Kuniyoshi, N. Iwakura, Y. Matsuura, T. Suzuki, K. Takahashi and S. Ohtori (2014). "Vein Wrapping for Chronic Nerve Constriction Injury in a Rat Model: Study Showing Increases in VEGF and HGF Production and Prevention of Pain-Associated Behaviors and Nerve Damage." JBJS **96**(10): 859-867.

Murakami, T., M. Arai, Y. Sunada and A. Nakamura (2006). "VEGF 164 gene transfer by electroporation improves diabetic sensory neuropathy in mice." J Gene Med **8**(6): 773-781.

Murata, M., K. Yudoh and K. Masuko (2008). "The potential role of vascular endothelial growth factor (VEGF) in cartilage: How the angiogenic factor could be involved in the pathogenesis of osteoarthritis?" Osteoarthritis and Cartilage **16**(3): 279-286.

Murphy, G., V. Knäuper, S. Atkinson, G. Butler, W. English, M. Hutton, J. Stracke and I. Clark (2002). "Matrix metalloproteinases in arthritic disease." Arthritis Research & Therapy **4**(3): S39.

Myers, S. L., K. D. Brandt, J. W. Ehlich, E. M. Braunstein, K. D. Shelbourne, D. A. Heck and L. A. Kalasinski (1990). "Synovial inflammation in patients with early osteoarthritis of the knee." J Rheumatol **17**(12): 1662-1669.

Nagai, T., M. Sato, M. Kobayashi, M. Yokoyama, Y. Tani and J. Mochida (2014). "Bevacizumab, an anti-vascular endothelial growth factor antibody, inhibits osteoarthritis." Arthritis Res Ther **16**(5): 427.

Nagao, M., J. L. Hamilton, R. Kc, A. D. Berendsen, X. Duan, C. W. Cheong, X. Li, H.-J. Im and B. R. Olsen (2017). "Vascular Endothelial Growth Factor in Cartilage Development and Osteoarthritis." Scientific Reports **7**(1): 13027.

Nakahara, H., J. Song, M. Sugimoto, K. Hagihara, T. Kishimoto, K. Yoshizaki and N. Nishimoto (2003). "Anti-interleukin-6 receptor antibody therapy reduces vascular endothelial growth factor production in rheumatoid arthritis." Arthritis Rheum **48**(6): 1521-1529.

Naor, D. and S. Nedvetzki (2003). "CD44 in rheumatoid arthritis." Arthritis research & therapy **5**(3): 105-115.

Neogi, T., A. Guermazi, F. Roemer, M. C. Nevitt, J. Scholz, L. Arendt-Nielsen, C. Woolf, J. Niu, L. A. Bradley, E. Quinn and L. F. Law (2016). "Association of Joint Inflammation With Pain Sensitization in Knee Osteoarthritis: The Multicenter Osteoarthritis Study." Arthritis Rheumatol **68**(3): 654-661.

Neogi, T. and Y. Zhang (2013). "Epidemiology of osteoarthritis." Rheumatic diseases clinics of North America **39**(1): 1-19.

Nesic, O., L. M. Sundberg, J. J. Herrera, V. U. Mokkapati, J. Lee and P. A. Narayana (2010). "Vascular endothelial growth factor and spinal cord injury pain." J Neurotrauma **27**(10): 1793-1803.

Newfeld, S. J., R. G. Wisotzkey and S. Kumar (1999). "Molecular evolution of a developmental pathway: phylogenetic analyses of transforming growth factor-beta family ligands, receptors and Smad signal transducers." Genetics **152**(2): 783-795.

NHSDigital (Feb 2022). "<https://digital.nhs.uk/data-and-information/publications/statistical/patient-reported-outcome-measures-proms/finalised-hip--knee-replacements-april-2018--march-2019/patient-profile>."

Nowak, D. G., E. M. Amin, E. S. Rennel, C. Hoareau-Aveilla, M. Gammons, G. Damodoran, M. Hagiwara, S. J. Harper, J. Woolard, M. R. Ladomery and D. O. Bates (2010). "Regulation of vascular endothelial growth factor (VEGF) splicing from pro-angiogenic to anti-angiogenic isoforms: a novel therapeutic strategy for angiogenesis." *The Journal of biological chemistry* **285**(8): 5532-5540.

Nowak, D. G., J. Woolard, E. M. Amin, O. Konopatskaya, M. A. Saleem, A. J. Churchill, M. R. Ladomery, S. J. Harper and D. O. Bates (2008). "Expression of pro- and anti-angiogenic isoforms of VEGF is differentially regulated by splicing and growth factors." *Journal of cell science* **121**(Pt 20): 3487-3495.

Nummenmaa, E., M. Hämäläinen, T. Moilanen, K. Vuolteenaho and E. Moilanen (2015). "Effects of FGF-2 and FGF receptor antagonists on MMP enzymes, aggrecan, and type II collagen in primary human OA chondrocytes." *Scand J Rheumatol* **44**(4): 321-330.

Nwosu, L. N., P. I. Mapp, V. Chapman and D. A. Walsh (2016). "Blocking the tropomyosin receptor kinase A (TrkA) receptor inhibits pain behaviour in two rat models of osteoarthritis." *Ann Rheum Dis* **75**(6): 1246-1254.

Odell, I. D. and D. Cook (2013). "Immunofluorescence techniques." *The Journal of investigative dermatology* **133** 1: e4.

Ofman, J. J., C. H. MacLean, W. L. Straus, S. C. Morton, M. L. Berger, E. A. Roth and P. Shekelle (2002). "A metaanalysis of severe upper gastrointestinal complications of nonsteroidal antiinflammatory drugs." *J Rheumatol* **29**(4): 804-812.

Ohe, K. and M. Hagiwara (2015). "Modulation of alternative splicing with chemical compounds in new therapeutics for human diseases." *ACS Chem Biol* **10**(4): 914-924.

Okun, A., P. Liu, P. Davis, J. Ren, B. Remeniuk, T. Brion, M. H. Ossipov, J. Xie, G. O. Dussor, T. King and F. Porreca (2012). "Afferent drive elicits ongoing pain in a model of advanced osteoarthritis." *Pain* **153**(4): 924-933.

Ong, C. K., P. Lirk, C. H. Tan and R. A. Seymour (2007). "An evidence-based update on nonsteroidal anti-inflammatory drugs." *Clin Med Res* **5**(1): 19-34.

Orita, S., T. Koshi, T. Mitsuka, M. Miyagi, G. Inoue, G. Arai, T. Ishikawa, E. Hanaoka, K. Yamashita, M. Yamashita, Y. Eguchi, T. Toyone, K. Takahashi and S. Ohtori (2011). "Associations between proinflammatory cytokines in the synovial fluid and radiographic grading and pain-related scores in 47 consecutive patients with osteoarthritis of the knee." *BMC Musculoskeletal Disorders* **12**(1): 144.

Ossipov, M. H., K. Morimura and F. Porreca (2014). "Descending pain modulation and chronification of pain." *Current opinion in supportive and palliative care* **8**(2): 143-151.

Ourradi, K., T. Blythe, C. Jarrett, S. L. Barratt, G. I. Welsh and A. B. Millar (2017). "VEGF isoforms have differential effects on permeability of human pulmonary microvascular endothelial cells." *Respiratory Research* **18**(1): 116.

Paleolog, E. M. (2002). "Angiogenesis in rheumatoid arthritis." *Arthritis research* **4** **Suppl 3**(Suppl 3): S81-S90.

Pan, X.-w., D. Xu, W.-j. Chen, J.-x. Chen, W.-j. Chen, J.-q. Ye, S.-s. Gan, W. Zhou, X. Song, L. Shi and X.-g. Cui (2021). "USP39 promotes malignant proliferation and

angiogenesis of renal cell carcinoma by inhibiting VEGF-A165b alternative splicing via regulating SRSF1 and SRPK1." Cancer Cell International **21**(1): 486.

Pang, V., D. O. Bates and L. Leach (2017). "Competitive interplay between VEGF-A165a, VEGF-A165b, PLGF and VE-cadherin in the human fetoplacental endothelial barrier." Placenta **57**: 313.

Pang, V., David O. Bates and L. Leach (2017). "Regulation of human fetoplacental endothelial barrier integrity by vascular endothelial growth factors: competitive interplay between VEGF-A165a, VEGF-A165b, PIGF and VE-cadherin." Clinical Science **131**(23): 2763-2775.

Park, C.-H., M. J. Lee, J. Ahn, S. Kim, H. H. Kim, K. H. Kim, H. C. Eun and J. H. Chung (2004). "Heat Shock-Induced Matrix Metalloproteinase (MMP)-1 and MMP-3 Are Mediated through ERK and JNK Activation and via an Autocrine Interleukin-6 Loop." Journal of Investigative Dermatology **123**(6): 1012-1019.

Patel, M., M. Sachidanandan and M. Adnan (2019). "Serine arginine protein kinase 1 (SRPK1): a moonlighting protein with theranostic ability in cancer prevention." Mol Biol Rep **46**(1): 1487-1497.

Pawson, E. J., B. Duran-Jimenez, R. Surosky, H. E. Brooke, S. K. Spratt, D. R. Tomlinson and N. J. Gardiner (2010). "Engineered zinc finger protein-mediated VEGF-a activation restores deficient VEGF-a in sensory neurons in experimental diabetes." Diabetes **59**(2): 509-518.

Peach, C. J., L. E. Kilpatrick, R. Friedman-Ohana, K. Zimmerman, M. B. Robers, K. V. Wood, J. Woolard and S. J. Hill (2018). "Real-Time Ligand Binding of Fluorescent VEGF-A Isoforms that Discriminate between VEGFR2 and NRP1 in Living Cells." Cell Chem Biol **25**(10): 1208-1218.e1205.

Peach, C. J., L. E. Kilpatrick, J. Woolard and S. J. Hill (2019). "Comparison of the ligand-binding properties of fluorescent VEGF-A isoforms to VEGF receptor 2 in living cells and membrane preparations using NanoBRET." British Journal of Pharmacology **176**(17): 3220-3235.

Peach, C. J., V. W. Mignone, M. A. Arruda, D. C. Alcobia, S. J. Hill, L. E. Kilpatrick and J. Woolard (2018). "Molecular Pharmacology of VEGF-A Isoforms: Binding and Signalling at VEGFR2." Int J Mol Sci **19**(4).

Pearle, A. D., R. F. Warren and S. A. Rodeo (2005). "Basic science of articular cartilage and osteoarthritis." Clin Sports Med **24**(1): 1-12.

Pecchi, E., S. Priam, M. Gosset, A. Pigenet, L. Sudre, M. C. Liguillon, F. Berenbaum and X. Houard (2014). "Induction of nerve growth factor expression and release by mechanical and inflammatory stimuli in chondrocytes: possible involvement in osteoarthritis pain." Arthritis Res Ther **16**(1): R16.

Perpétuo, I. P., J. Caetano-Lopes, A. M. Rodrigues, R. Campanilho-Marques, C. Ponte, H. Canhão, M. Ainola and J. E. Fonseca (2017). "Effect of Tumor Necrosis Factor Inhibitor Therapy on Osteoclast Precursors in Rheumatoid Arthritis." Biomed Res Int **2017**: 2690402.

Pesesse, L., C. Sanchez and Y. Henrotin (2011). "Osteochondral plate angiogenesis: a new treatment target in osteoarthritis." Joint Bone Spine **78**(2): 144-149.

Petersen, W., M. Tsokos and T. Pufe (2002). "Expression of VEGF121 and VEGF165 in hypertrophic chondrocytes of the human growth plate and epiphyseal cartilage." J Anat **201**(2): 153-157.

Pincus, T. (2001). "Clinical evidence for osteoarthritis as an inflammatory disease." Current Rheumatology Reports **3**(6): 524-534.

Ploner, M., J. Gross, L. Timmermann and A. Schnitzler (2002). "Cortical representation of first and second pain sensation in humans." Proc Natl Acad Sci U S A **99**(19): 12444-12448.

Pritchard-Jones, R. O., D. B. A. Dunn, Y. Qiu, A. H. R. Varey, A. Orlando, H. Rigby, S. J. Harper and D. O. Bates (2007). "Expression of VEGF<sub>xxx</sub>b, the inhibitory isoforms of VEGF, in malignant melanoma." British Journal of Cancer **97**(2): 223-230.

Proetzel, G., S. A. Pawlowski, M. V. Wiles, M. Yin, G. P. Boivin, P. N. Howles, J. Ding, M. W. Ferguson and T. Doetschman (1995). "Transforming growth factor-beta 3 is required for secondary palate fusion." Nat Genet **11**(4): 409-414.

Pufe, T., W. Petersen, B. Tillmann and R. Mentlein (2001). "Splice variants VEGF121 and VEGF165 of the angiogenic peptide vascular endothelial cell growth factor are expressed in the synovial tissue of patients with rheumatoid arthritis." J Rheumatol **28**(7): 1482-1485.

Pufe, T., W. Petersen, B. Tillmann and R. Mentlein (2001). "The splice variants VEGF121 and VEGF189 of the angiogenic peptide vascular endothelial growth factor are expressed in osteoarthritic cartilage." Arthritis Rheum **44**(5): 1082-1088.

Qian, J.-J., Q. Xu, W.-M. Xu, R. Cai and G.-C. Huang (2021). "Expression of VEGF-A Signaling Pathway in Cartilage of ACLT-induced Osteoarthritis Mouse Model." Journal of orthopaedic surgery and research **16**(1): 379-379.

Qian, J.-j., Q. Xu, W.-m. Xu, R. Cai and G.-c. Huang (2021). "Expression of VEGF-A Signaling Pathway in Cartilage of ACLT-induced Osteoarthritis Mouse Model." Journal of Orthopaedic Surgery and Research **16**(1): 379.

Qian, J. J., Q. Xu, W. M. Xu, R. Cai and G. C. Huang (2021). "Expression of VEGF-A Signaling Pathway in Cartilage of ACLT-induced Osteoarthritis Mouse Model." J Orthop Surg Res **16**(1): 379.

Qin, Z., L. Qin, X. Feng, Z. Li and J. Bian (2021). "Development of Cdc2-like Kinase 2 Inhibitors: Achievements and Future Directions." J Med Chem **64**(18): 13191-13211.

Qiu, Y., C. Hoareau-Aveilla, S. Oltean, S. J. Harper and D. O. Bates (2009). "The anti-angiogenic isoforms of VEGF in health and disease." Biochem Soc Trans **37**(Pt 6): 1207-1213.

Radin, E. L. and R. M. Rose (1986). "Role of subchondral bone in the initiation and progression of cartilage damage." Clin Orthop Relat Res(213): 34-40.

Ralphs, J. R. and M. Benjamin (1994). "The joint capsule: structure, composition, ageing and disease." J Anat **184** ( Pt 3)(Pt 3): 503-509.

Ramanujan, S. A., E. N. Cravens, S. M. Krishfield, V. C. Kyttaris and V. R. Moulton (2021). "Estrogen-Induced hsa-miR-10b-5p Is Elevated in T Cells From Patients With Systemic Lupus Erythematosus and Down-Regulates Serine/Arginine-Rich Splicing Factor 1." Arthritis Rheumatol **73**(11): 2052-2058.

Rammohan, M., E. Harris, R. S. Bhansali, E. Zhao, L. S. Li and J. D. Crispino (2022). "The chromosome 21 kinase DYRK1A: emerging roles in cancer biology and potential as a therapeutic target." Oncogene **41**(14): 2003-2011.

Rang, H. P., S. Bevan and A. Dray (1991). "Chemical activation of nociceptive peripheral neurones." British Medical Bulletin **47**(3): 534-548.

Raychaudhuri, S. P., S. K. Raychaudhuri, K. R. Atkuri, L. A. Herzenberg and L. A. Herzenberg (2011). "Nerve growth factor: A key local regulator in the pathogenesis of inflammatory arthritis." Arthritis & Rheumatism **63**(11): 3243-3252.

Raynauld, J. P., C. Buckland-Wright, R. Ward, D. Choquette, B. Haraoui, J. Martel-Pelletier, I. Uthman, V. Khy, J. L. Tremblay, C. Bertrand and J. P. Pelletier (2003). "Safety and efficacy of long-term intraarticular steroid injections in osteoarthritis of the knee: a randomized, double-blind, placebo-controlled trial." Arthritis Rheum **48**(2): 370-377.

Rebhun, C. B., C. Moreira-Neto, S. Gune, L. Hill, J. S. Duker and N. K. Waheed (2020). "MACULAR ATROPHY IN NEOVASCULAR AGE-RELATED MACULAR DEGENERATION: A Pilot Post Hoc Analysis of Patients With Pigment Epithelial Detachments." RETINA **40**(2).

Reboul, P., J. P. Pelletier, G. Tardif, J. M. Cloutier and J. Martel-Pelletier (1996). "The new collagenase, collagenase-3, is expressed and synthesized by human chondrocytes but not by synoviocytes. A role in osteoarthritis." The Journal of Clinical Investigation **97**(9): 2011-2019.

Reglero-Real, N., B. Colom, J. V. Bodkin and S. Nourshargh (2016). "Endothelial Cell Junctional Adhesion Molecules: Role and Regulation of Expression in Inflammation." Arterioscler Thromb Vasc Biol **36**(10): 2048-2057.

Rein, P. and R. B. Mueller (2017). "Treatment with Biologicals in Rheumatoid Arthritis: An Overview." Rheumatol Ther **4**(2): 247-261.

Retting, K. N., B. Song, B. S. Yoon and K. M. Lyons (2009). "BMP canonical Smad signaling through Smad1 and Smad5 is required for endochondral bone formation." Development **136**(7): 1093-1104.

Richards, B. L., S. L. Whittle, D. M. van der Heijde and R. Buchbinder (2012). "The efficacy and safety of antidepressants in inflammatory arthritis: a Cochrane systematic review." J Rheumatol Suppl **90**: 21-27.

Robciuc, Marius R., R. Kivelä, Ian M. Williams, Jan F. de Boer, Theo H. van Dijk, H. Elamaa, F. Tigistu-Sahle, D. Molotkov, V.-M. Leppänen, R. Käkälä, L. Eklund, David H. Wasserman, Albert K. Groen and K. Alitalo (2016). "VEGFB/VEGFR1-Induced Expansion of Adipose Vasculature Counteracts Obesity and Related Metabolic Complications." Cell Metabolism **23**(4): 712-724.

Roman-Blas, J. A. and S. A. Jimenez (2006). "NF-kappaB as a potential therapeutic target in osteoarthritis and rheumatoid arthritis." Osteoarthritis Cartilage **14**(9): 839-848.

Rozen, E. J., J. Roewenstrunk, M. J. Barallobre, C. Di Vona, C. Jung, A. F. Figueiredo, J. Luna, C. Fillat, M. L. Arbonés, M. Graupera, M. A. Valverde and S. de la Luna (2018). "DYRK1A Kinase Positively Regulates Angiogenic Responses in Endothelial Cells." Cell Rep **23**(6): 1867-1878.

Rozen, E. J., J. Roewenstrunk, M. J. Barallobre, C. Di Vona, C. Jung, A. F. Figueiredo, J. Luna, C. Fillat, M. L. Arbonés, M. Graupera, M. A. Valverde and S. de la Luna (2018). "DYRK1A Kinase Positively Regulates Angiogenic Responses in Endothelial Cells." Cell Reports **23**(6): 1867-1878.

Rueden, C. T., J. Schindelin, M. C. Hiner, B. E. DeZonia, A. E. Walter, E. T. Arena and K. W. Eliceiri (2017). "ImageJ2: ImageJ for the next generation of scientific image data." BMC Bioinformatics **18**(1): 529.

Rustenhoven, J., D. Jansson, L. C. Smyth and M. Dragunow (2017). "Brain Pericytes As Mediators of Neuroinflammation." Trends Pharmacol Sci **38**(3): 291-304.

Ryu, S., J. H. Lee and S. I. Kim (2006). "IL-17 increased the production of vascular endothelial growth factor in rheumatoid arthritis synoviocytes." Clinical Rheumatology **25**(1): 16-20.

Sadda, S. R., R. Guymer, J. M. Monés, A. Tufail and G. J. Jaffe (2020). "Anti-VEGF; Vascular Endothelial Growth Factor Use and Atrophy in Neovascular Age-Related Macular Degeneration: Systematic Literature Review and Expert Opinion." Ophthalmology **127**(5): 648-659.

Saetan, N., S. Honsawek, A. Tanavalee, P. Yuktanandana, S. Meknavin, S. Ngarmukos, T. Tanpowpong and V. Parkpian (2014). "Relationship of plasma and synovial fluid vascular endothelial growth factor with radiographic severity in primary knee osteoarthritis." Int Orthop **38**(5): 1099-1104.

Salton, M. and T. Misteli (2016). "Small Molecule Modulators of Pre-mRNA Splicing in Cancer Therapy." Trends in Molecular Medicine **22**(1): 28-37.

Sandell, L. J. and T. Aigner (2001). "Articular cartilage and changes in arthritis. An introduction: cell biology of osteoarthritis." Arthritis Res **3**(2): 107-113.

Sanford, L. P., I. Ormsby, A. C. Gittenberger-de Groot, H. Sariola, R. Friedman, G. P. Boivin, E. L. Cardell and T. Doetschman (1997). "TGFbeta2 knockout mice have multiple developmental defects that are non-overlapping with other TGFbeta knockout phenotypes." Development **124**(13): 2659-2670.

Sanga, P., N. Katz, E. Polverejan, S. Wang, K. M. Kelly, J. Haeussler and J. Thippawong (2013). "Efficacy, safety, and tolerability of fulranumab, an anti-nerve growth factor antibody, in the treatment of patients with moderate to severe osteoarthritis pain." PAIN® **154**(10): 1910-1919.

Sawano, A., T. Takahashi, S. Yamaguchi, M. Aonuma and M. Shibuya (1996). "Flt-1 but not KDR/Flk-1 tyrosine kinase is a receptor for placenta growth factor, which is related to vascular endothelial growth factor." Cell Growth Differ **7**(2): 213-221.

Schaible, H. G. (2014). "Nociceptive neurons detect cytokines in arthritis." Arthritis Res Ther **16**(5): 470.

Schaible, H. G. and B. D. Grubb (1993). "Afferent and spinal mechanisms of joint pain." Pain **55**(1): 5-54.

Schaible, H. G. and R. F. Schmidt (1985). "Effects of an experimental arthritis on the sensory properties of fine articular afferent units." J Neurophysiol **54**(5): 1109-1122.

Schaible, H. G. and R. F. Schmidt (1988). "Time course of mechanosensitivity changes in articular afferents during a developing experimental arthritis." J Neurophysiol **60**(6): 2180-2195.

Scheiman, J. M. (2013). "The use of proton pump inhibitors in treating and preventing NSAID-induced mucosal damage." Arthritis Res Ther **15 Suppl 3**(Suppl 3): S5.

Sellam, J. and F. Berenbaum (2010). "The role of synovitis in pathophysiology and clinical symptoms of osteoarthritis." Nat Rev Rheumatol **6**(11): 625-635.

Selvaraj, D., V. Gangadharan, C. W. Michalski, M. Kurejova, S. Stösser, K. Srivastava, M. Schweizerhof, J. Waltenberger, N. Ferrara, P. Heppenstall, M. Shibuya, H. G. Augustin and R. Kuner (2015). "A Functional Role for VEGFR1 Expressed in Peripheral Sensory Neurons in Cancer Pain." Cancer Cell **27**(6): 780-796.

Senger, D. R. (2010). "Vascular endothelial growth factor: much more than an angiogenesis factor." Molecular biology of the cell **21**(3): 377-379.

Senger, D. R., S. J. Galli, A. M. Dvorak, C. A. Perruzzi, V. S. Harvey and H. F. Dvorak (1983). "Tumor cells secrete a vascular permeability factor that promotes accumulation of ascites fluid." Science **219**(4587): 983-985.

Shabestari, M., Y. R. Shabestari, M. A. Landin, M. Pepaj, T. P. Cleland, J. E. Reseland and E. F. Eriksen (2020). "Altered protein levels in bone marrow lesions of hip osteoarthritis: Analysis by proteomics and multiplex immunoassays." Int J Rheum Dis **23**(6): 788-799.

Shaik, F., G. A. Cuthbert, S. Homer-Vanniasinkam, S. P. Muench, S. Ponnambalam and M. A. Harrison (2020). "Structural Basis for Vascular Endothelial Growth Factor Receptor Activation and Implications for Disease Therapy." Biomolecules **10**(12).

Shen, H. and M. R. Green (2006). "RS domains contact splicing signals and promote splicing by a common mechanism in yeast through humans." Genes & development **20**(13): 1755-1765.

Shepard, P. J. and K. J. Hertel (2009). "The SR protein family." Genome biology **10**(10): 242-242.

Shi, J., T. Zhang, C. Zhou, M. O. Chohan, X. Gu, J. Wegiel, J. Zhou, Y. W. Hwang, K. Iqbal, I. Grundke-Iqbal, C. X. Gong and F. Liu (2008). "Increased dosage of Dyrk1A alters alternative splicing factor (ASF)-regulated alternative splicing of tau in Down syndrome." J Biol Chem **283**(42): 28660-28669.

Shibuya, M. (2001). "Structure and dual function of vascular endothelial growth factor receptor-1 (Flt-1)." Int J Biochem Cell Biol **33**(4): 409-420.

Shibuya, M. (2011). "Vascular Endothelial Growth Factor (VEGF) and Its Receptor (VEGFR) Signaling in Angiogenesis: A Crucial Target for Anti- and Pro-Angiogenic Therapies." Genes & Cancer **2**(12): 1097-1105.

Shibuya, M. (2013). "Vascular endothelial growth factor and its receptor system: physiological functions in angiogenesis and pathological roles in various diseases." J Biochem **153**(1): 13-19.

Shibuya, M. (2015). "VEGF-VEGFR System as a Target for Suppressing Inflammation and other Diseases." Endocr Metab Immune Disord Drug Targets **15**(2): 135-144.

Shiozawa, K., K. Hino and S. Shiozawa (2001). "Alternatively spliced EDA-containing fibronectin in synovial fluid as a predictor of rheumatoid joint destruction." Rheumatology (Oxford) **40**(7): 739-742.

Silva, J. C., H. A. Mariz, L. F. Rocha, Jr., P. S. Oliveira, A. T. Dantas, A. L. Duarte, R. Pitta, S. L. Galdino and M. G. Pitta (2013). "Hydroxychloroquine decreases Th17-related cytokines in systemic lupus erythematosus and rheumatoid arthritis patients." Clinics (Sao Paulo) **68**(6): 766-771.

Siqueira, R. P., É. d. A. A. Barbosa, M. D. Polêto, G. L. Righetto, T. V. Seraphim, R. L. Salgado, J. G. Ferreira, M. V. d. A. Barros, L. L. de Oliveira, A. B. A. Laranjeira, M. R. Almeida, A. S. Júnior, J. L. R. Fietto, J. Kobarg, E. B. de Oliveira, R. R. Teixeira, J. C. Borges, J. A. Yunes and G. C. Bressan (2015). "Potential Antileukemia Effect and Structural Analyses of SRPK Inhibition by N-(2-(Piperidin-1-yl)-5-(Trifluoromethyl)Phenyl)Isonicotinamide (SRPIN340)." PLOS ONE **10**(8): e0134882.

Smith, J. O., R. O. Oreffo, N. M. Clarke and H. I. Roach (2003). "Changes in the antiangiogenic properties of articular cartilage in osteoarthritis." J Orthop Sci **8**(6): 849-857.

Smith, M. D. (2011). "The normal synovium." Open Rheumatol J **5**: 100-106.

Smith, M. D., S. Triantafillou, A. Parker, P. P. Youssef and M. Coleman (1997). "Synovial membrane inflammation and cytokine production in patients with early osteoarthritis." J Rheumatol **24**(2): 365-371.

Sofat, N., V. Ejindu and P. Kiely (2011). "What makes osteoarthritis painful? The evidence for local and central pain processing." Rheumatology (Oxford) **50**(12): 2157-2165.

Sohn, D. H., J. Sokolove, O. Sharpe, J. C. Erhart, P. E. Chandra, L. J. Lahey, T. M. Lindstrom, I. Hwang, K. A. Boyer, T. P. Andriacchi and W. H. Robinson (2012). "Plasma proteins present in osteoarthritic synovial fluid can stimulate cytokine production via Toll-like receptor 4." Arthritis Res Ther **14**(1): R7.

Sokolove, J. and C. M. Lepus (2013). "Role of inflammation in the pathogenesis of osteoarthritis: latest findings and interpretations." Therapeutic advances in musculoskeletal disease **5**(2): 77-94.

Sondell, M., G. Lundborg and M. Kanje (1999). "Vascular endothelial growth factor has neurotrophic activity and stimulates axonal outgrowth, enhancing cell survival and Schwann cell proliferation in the peripheral nervous system." J Neurosci **19**(14): 5731-5740.

Sone, H., Y. Kawakami, M. Sakauchi, Y. Nakamura, A. Takahashi, H. Shimano, Y. Okuda, T. Segawa, H. Suzuki and N. Yamada (2001). "Neutralization of vascular endothelial growth factor prevents collagen-induced arthritis and ameliorates established disease in mice." Biochem Biophys Res Commun **281**(2): 562-568.

Soni, A., R. N. Batra, S. E. Gwilym, T. D. Spector, D. J. Hart, N. K. Arden, C. Cooper, I. Tracey and M. K. Javaid (2013). "Neuropathic features of joint pain: a community-based study." Arthritis Rheum **65**(7): 1942-1949.

Sophia Fox, A. J., A. Bedi and S. A. Rodeo (2009). "The basic science of articular cartilage: structure, composition, and function." Sports health **1**(6): 461-468.

Spector, D. L. and A. I. Lamond (2011). "Nuclear speckles." Cold Spring Harb Perspect Biol **3**(2).

Speel, E. J., B. Schutte, J. Wiegant, F. C. Ramaekers and A. H. Hopman (1992). "A novel fluorescence detection method for in situ hybridization, based on the alkaline phosphatase-fast red reaction." Journal of Histochemistry & Cytochemistry **40**(9): 1299-1308.

Stannus, O. P., G. Jones, L. Blizzard, F. M. Cicuttini and C. Ding (2013). "Associations between serum levels of inflammatory markers and change in knee pain over 5 years in older adults: a prospective cohort study." Annals of the Rheumatic Diseases **72**(4): 535.

Stevens, M., E. Star, M. Lee, E. Innes, L. Li, E. Bowler, S. Harper, D. O. Bates and S. Oltean (2019). "The VEGF-A exon 8 splicing-sensitive fluorescent reporter mouse is a novel tool to assess the effects of splicing regulatory compounds in vivo." RNA Biol **16**(12): 1672-1681.

Stoppiello, L. A., P. I. Mapp, D. Wilson, R. Hill, B. E. Scammell and D. A. Walsh (2014). "Structural associations of symptomatic knee osteoarthritis." Arthritis Rheumatol **66**(11): 3018-3027.

Su, X., Y. Yu, Y. Zhong, E. G. Giannopoulou, X. Hu, H. Liu, J. R. Cross, G. Rättsch, C. M. Rice and L. B. Ivashkiv (2015). "Interferon- $\gamma$  regulates cellular metabolism and mRNA translation to potentiate macrophage activation." Nat Immunol **16**(8): 838-849.

Sun, S., Z. Zhang, R. Sinha, R. Karni and A. R. Krainer (2010). "SF2/ASF autoregulation involves multiple layers of post-transcriptional and translational control." Nature Structural & Molecular Biology **17**(3): 306-312.

Suri, S., S. E. Gill, S. Massena de Camin, D. Wilson, D. F. McWilliams and D. A. Walsh (2007). "Neurovascular invasion at the osteochondral junction and in osteophytes in osteoarthritis." Annals of the rheumatic diseases **66**(11): 1423-1428.

Suri, S., S. E. Gill, S. Massena de Camin, D. Wilson, D. F. McWilliams and D. A. Walsh (2007). "Neurovascular invasion at the osteochondral junction and in osteophytes in osteoarthritis." Ann Rheum Dis **66**(11): 1423-1428.

Swales, C. and N. A. Athanasou (2010). "(i) The pathobiology of osteoarthritis." Orthopaedics and Trauma **24**(6): 399-404.

Swales, C., N. A. Athanasou and H. J. Knowles (2014). "Angiopoietin-like 4 is over-expressed in rheumatoid arthritis patients: association with pathological bone resorption." PloS one **9**(10): e109524-e109524.

Tabata, M., J. T. Rodgers, J. A. Hall, Y. Lee, M. P. Jedrychowski, S. P. Gygi and P. Puigserver (2014). "Cdc2-Like Kinase 2 Suppresses Hepatic Fatty Acid Oxidation and Ketogenesis Through Disruption of the PGC-1 $\alpha$  and MED1 Complex." Diabetes **63**(5): 1519-1532.

Tahtouh, T., O. Fedorov, O. Lozach, F. Carreaux, J. P. Bazureau, J. Meunier, T. Maurice, S. Knapp and L. Meijer (2012). "Leucettines, a family of pharmacological inhibitors of DYRKs & CLKs kinases derived from the marine sponge Leucettamine B." Planta Med **78**(11): PD1.

Takano, S., K. Uchida, G. Inoue, T. Matsumoto, J. Aikawa, D. Iwase, M. Mukai, M. Miyagi and M. Takaso (2018). "Vascular endothelial growth factor expression and their action in the synovial membranes of patients with painful knee osteoarthritis." BMC Musculoskelet Disord **19**(1): 204.

Takano, S., K. Uchida, M. Itakura, D. Iwase, J. Aikawa, G. Inoue, M. Mukai, M. Miyagi, K. Murata, H. Sekiguchi and M. Takaso (2019). "Transforming growth factor- $\beta$  stimulates nerve growth factor production in osteoarthritic synovium." BMC Musculoskelet Disord **20**(1): 204.

Tambiah, J. R. S., S. Kennedy, C. J. Swearingen, I. Simsek, Y. Yazici, J. Farr and P. G. Conaghan (2021). "Individual Participant Symptom Responses to Intra-Articular Lorecivint in Knee Osteoarthritis: Post Hoc Analysis of a Phase 2B Trial." Rheumatol Ther **8**(2): 973-985.

Tang, J. and T. S. Kern (2011). "Inflammation in diabetic retinopathy." Prog Retin Eye Res **30**(5): 343-358.

Thakur, M., A. H. Dickenson and R. Baron (2014). "Osteoarthritis pain: nociceptive or neuropathic?" Nat Rev Rheumatol **10**(6): 374-380.

Thichanpiang, P., S. J. Harper, K. Wongprasert and D. O. Bates (2014). "TNF- $\alpha$ -induced ICAM-1 expression and monocyte adhesion in human RPE cells is mediated in part through autocrine VEGF stimulation." Mol Vis **20**: 781-789.

Tian, H. and B. N. Cronstein (2007). "Understanding the mechanisms of action of methotrexate: implications for the treatment of rheumatoid arthritis." Bull NYU Hosp Jt Dis **65**(3): 168-173.

Tooke, K., B. Girard and M. A. Vizzard (2019). "Functional effects of blocking VEGF/VEGFR2 signaling in the rat urinary bladder in acute and chronic CYP-induced cystitis." Am J Physiol Renal Physiol **317**(7): F43-f51.

Tovey, M. G. and C. Lallemand (2011). "Immunogenicity and other problems associated with the use of biopharmaceuticals." Ther Adv Drug Saf **2**(3): 113-128.

Treede, R. D., T. S. Jensen, J. N. Campbell, G. Cruccu, J. O. Dostrovsky, J. W. Griffin, P. Hansson, R. Hughes, T. Nurmikko and J. Serra (2008). "Neuropathic pain: redefinition and a grading system for clinical and research purposes." Neurology **70**(18): 1630-1635.

Tsai, C.-H., S.-C. Liu, W.-H. Chung, S.-W. Wang, M.-H. Wu and C.-H. Tang (2020). "Visfatin Increases VEGF-dependent Angiogenesis of Endothelial Progenitor Cells during Osteoarthritis Progression." Cells **9**(5): 1315.

Tsuchida, A. I., M. Beekhuizen, M. C. t Hart, T. R. D. J. Radstake, W. J. A. Dhert, D. B. F. Saris, G. J. V. M. van Osch and L. B. Creemers (2014). "Cytokine profiles in the joint depend on pathology, but are different between synovial fluid, cartilage tissue and cultured chondrocytes." Arthritis Research & Therapy **16**(5): 441.

Tsunozaki, M. and D. M. Bautista (2009). "Mammalian somatosensory mechanotransduction." Curr Opin Neurobiol **19**(4): 362-369.

Uemura, A., M. Fruttiger, P. A. D'Amore, S. De Falco, A. M. Jousen, F. Sennlaub, L. R. Brunck, K. T. Johnson, G. N. Lambrou, K. D. Rittenhouse and T. Langmann (2021). "VEGFR1 signaling in retinal angiogenesis and microinflammation." Prog Retin Eye Res **84**: 100954.

Valdes, A. M., A. K. Suokas, S. A. Doherty, W. Jenkins and M. Doherty (2014). "History of knee surgery is associated with higher prevalence of neuropathic pain-like symptoms in patients with severe osteoarthritis of the knee." Seminars in Arthritis and Rheumatism **43**(5): 588-592.

van de Stolpe, A. and P. T. van der Saag (1996). "Intercellular adhesion molecule-1." J Mol Med (Berl) **74**(1): 13-33.

van der Kooij, S. M., S. le Cessie, Y. P. Goekoop-Ruiterman, J. K. de Vries-Bouwstra, D. van Zeben, P. J. Kerstens, J. M. Hazes, D. van Schaardenburg, F. C. Breedveld, B. A. Dijkmans and C. F. Allaart (2009). "Clinical and radiological efficacy of initial vs delayed treatment with infliximab plus methotrexate in patients with early rheumatoid arthritis." Ann Rheum Dis **68**(7): 1153-1158.

van Neerven, S., E. A. Joosten, G. A. Brook, C. A. Lambert, J. Mey, J. Weis, M. A. Marcus, H. W. Steinbusch, M. van Kleef, J. Patijn and R. Deumens (2010). "Repetitive intrathecal VEGF(165) treatment has limited therapeutic effects after spinal cord injury in the rat." J Neurotrauma **27**(10): 1781-1791.

Varey, A. H., E. S. Rennel, Y. Qiu, H. S. Bevan, R. M. Perrin, S. Raffy, A. R. Dixon, C. Paraskeva, O. Zaccheo, A. B. Hassan, S. J. Harper and D. O. Bates (2008). "VEGF 165 b, an antiangiogenic VEGF-A isoform, binds and inhibits bevacizumab treatment in experimental colorectal carcinoma: balance of pro- and antiangiogenic VEGF-A isoforms has implications for therapy." Br J Cancer **98**(8): 1366-1379.

Ved, N., R. P. Hulse, S. M. Bestall, L. F. Donaldson, J. W. Bainbridge and D. O. Bates (2017). "Vascular endothelial growth factor-A(165)b ameliorates outer-retinal barrier and vascular dysfunction in the diabetic retina." Clin Sci (Lond) **131**(12): 1225-1243.

Voscopoulos, C. and M. Lema (2010). "When does acute pain become chronic?" Br J Anaesth **105** Suppl 1: i69-85.

Walsh, D. A. (1999). "Angiogenesis and arthritis." Rheumatology **38**(2): 103-112.

Walsh, D. A. and L. Haywood (2001). "Angiogenesis: a therapeutic target in arthritis." Curr Opin Investig Drugs **2**(8): 1054-1063.

Walsh, D. A., D. F. McWilliams, M. J. Turley, M. R. Dixon, R. E. Fransès, P. I. Mapp and D. Wilson (2010). "Angiogenesis and nerve growth factor at the osteochondral junction in rheumatoid arthritis and osteoarthritis." Rheumatology (Oxford, England) **49**(10): 1852-1861.

Walsh, D. A., D. F. McWilliams, M. J. Turley, M. R. Dixon, R. E. Fransès, P. I. Mapp and D. Wilson (2010). "Angiogenesis and nerve growth factor at the osteochondral junction in rheumatoid arthritis and osteoarthritis." Rheumatology (Oxford) **49**(10): 1852-1861.

Walsh, D. A. and J. Stocks (2017). "New Therapeutic Targets for Osteoarthritis Pain." SLAS DISCOVERY: Advancing Life Sciences R&D **22**(8): 931-949.

Walsh, D. A., M. Wade, P. I. Mapp and D. R. Blake (1998). "Focally regulated endothelial proliferation and cell death in human synovium." The American journal of pathology **152**(3): 691-702.

Walsh, D. A., A. Yousef, D. F. McWilliams, R. Hill, E. Hargin and D. Wilson (2009). "Evaluation of a Photographic Chondropathy Score (PCS) for pathological samples in a study of inflammation in tibiofemoral osteoarthritis." Osteoarthritis and Cartilage **17**(3): 304-312.

Wang, C., Z. Zhou, C. S. Subhramanyam, Q. Cao, Z. S. L. Heng, W. Liu, X. Fu and Q. Hu (2020). "SRPK1 acetylation modulates alternative splicing to regulate cisplatin resistance in breast cancer cells." Communications Biology **3**(1): 268.

Wang, C., Z. Zhou, C. S. Subhramanyam, Q. Cao, Z. S. L. Heng, W. Liu, X. Fu and Q. Hu (2020). "SRPK1 acetylation modulates alternative splicing to regulate cisplatin resistance in breast cancer cells." Commun Biol **3**(1): 268.

Wang, Y.-H., S.-J. Kuo, S.-C. Liu, S.-W. Wang, C.-H. Tsai, Y.-C. Fong and C.-H. Tang (2020). "Apelin Affects the Progression of Osteoarthritis by Regulating VEGF-Dependent Angiogenesis and miR-150-5p Expression in Human Synovial Fibroblasts." Cells **9**(3): 594.

Wang, Y., J. Liu, B. O. Huang, Y. M. Xu, J. Li, L. F. Huang, J. Lin, J. Zhang, Q. H. Min, W. M. Yang and X. Z. Wang (2015). "Mechanism of alternative splicing and its regulation." Biomed Rep **3**(2): 152-158.

Wang, Z. and C. B. Burge (2008). "Splicing regulation: from a parts list of regulatory elements to an integrated splicing code." Rna **14**(5): 802-813.

Ward, A. J. and T. A. Cooper (2010). "The pathobiology of splicing." J Pathol **220**(2): 152-163.

Wei, X., S. Xu and L. Chen (2021). "LncRNA Neat1/miR-298-5p/Srpk1 Contributes to Sevoflurane-Induced Neurotoxicity." Neurochem Res **46**(12): 3356-3364.

Whittle, C., K. Gillespie, R. Harrison, P. W. Mathieson and S. J. Harper (1999). "Heterogeneous vascular endothelial growth factor (VEGF) isoform mRNA and

receptor mRNA expression in human glomeruli, and the identification of VEGF148 mRNA, a novel truncated splice variant." *Clinical Science* **97**(3): 303-312.

Whittle, S. L., A. N. Colebatch, R. Buchbinder, C. J. Edwards, K. Adams, M. Englbrecht, G. Hazlewood, J. L. Marks, H. Radner, S. Ramiro, B. L. Richards, I. H. Tarner, D. Aletaha, C. Bombardier, R. B. Landewé, U. Müller-Ladner, J. W. Bijlsma, J. C. Branco, V. P. Bykerk, G. da Rocha Castelar Pinheiro, A. I. Catrina, P. Hannonen, P. Kiely, B. Leeb, E. Lie, P. Martinez-Osuna, C. Montecucco, M. Ostergaard, R. Westhovens, J. Zochling and D. van der Heijde (2012). "Multinational evidence-based recommendations for pain management by pharmacotherapy in inflammatory arthritis: integrating systematic literature research and expert opinion of a broad panel of rheumatologists in the 3e Initiative." *Rheumatology (Oxford)* **51**(8): 1416-1425.

Whittles, C. E., T. M. Pocock, S. R. Wedge, J. Kendrew, L. F. Hennequin, S. J. Harper and D. O. Bates (2002). "ZM323881, a novel inhibitor of vascular endothelial growth factor-receptor-2 tyrosine kinase activity." *Microcirculation* **9**(6): 513-522.

Wibulswas, A., D. Croft, A. A. Pitsillides, I. Bacarese-Hamilton, P. McIntyre, E. Genot and I. M. Kramer (2002). "Influence of epitopes CD44v3 and CD44v6 in the invasive behavior of fibroblast-like synoviocytes derived from rheumatoid arthritic joints." *Arthritis Rheum* **46**(8): 2059-2064.

Wilkinson, M. E., C. Charenton and K. Nagai (2020). "RNA Splicing by the Spliceosome." *Annu Rev Biochem* **89**: 359-388.

Will, C. L. and R. Lührmann (2011). "Spliceosome structure and function." *Cold Spring Harb Perspect Biol* **3**(7).

Wilms, H., J. Sievers, U. Rickert, M. Rostami-Yazdi, U. Mrowietz and R. Lucius (2010). "Dimethylfumarate inhibits microglial and astrocytic inflammation by suppressing the synthesis of nitric oxide, IL-1 $\beta$ , TNF- $\alpha$  and IL-6 in an in-vitro model of brain inflammation." *Journal of Neuroinflammation* **7**(1): 30.

Witt, A., A. Salamon, D. Boy, D. Hansmann, A. Büttner, A. Wree, R. Bader and A. Jonitz-Heincke (2017). "Gene expression analysis of growth factor receptors in human chondrocytes in monolayer and 3D pellet cultures." *Int J Mol Med* **40**(1): 10-20.

Wojdasiewicz, P., A. Poniatowski Ł and D. Szukiewicz (2014). "The role of inflammatory and anti-inflammatory cytokines in the pathogenesis of osteoarthritis." *Mediators Inflamm* **2014**: 561459.

Wong, C. K., R. Y. Mak, T. S. Kwok, J. S. Tsang, M. Y. Leung, M. Funabashi, L. G. Macedo, L. Dennett and A. Y. Wong (2022). "Prevalence, Incidence, and Factors Associated With Non-Specific Chronic Low Back Pain in Community-Dwelling Older Adults Aged 60 Years and Older: A Systematic Review and Meta-Analysis." *J Pain* **23**(4): 509-534.

Wong, D. and K. Dorovini-Zis (1995). "Expression of vascular cell adhesion molecule-1 (VCAM-1) by human brain microvessel endothelial cells in primary culture." *Microvasc Res* **49**(3): 325-339.

Woolard, J., H. S. Bevan, S. J. Harper and D. O. Bates (2009). "Molecular diversity of VEGF-A as a regulator of its biological activity." *Microcirculation* **16**(7): 572-592.

Woolard, J., W. Y. Wang, H. S. Bevan, Y. Qiu, L. Morbidelli, R. O. Pritchard-Jones, T. G. Cui, M. Sugiono, E. Waive, R. Perrin, R. Foster, J. Digby-Bell, J. D. Shields, C. E. Whittles, R. E. Mushens, D. A. Gillatt, M. Ziche, S. J. Harper and D. O. Bates (2004). "VEGF165b, an inhibitory vascular endothelial growth factor splice variant: mechanism

of action, in vivo effect on angiogenesis and endogenous protein expression." Cancer Res **64**(21): 7822-7835.

Woolf, C. J., Q. P. Ma, A. Allchorne and S. Poole (1996). "Peripheral cell types contributing to the hyperalgesic action of nerve growth factor in inflammation." J Neurosci **16**(8): 2716-2723.

Wu, Q. and J. L. Henry (2010). "Changes in Abeta non-nociceptive primary sensory neurons in a rat model of osteoarthritis pain." Mol Pain **6**: 37.

Wyatt, L. A., L. N. Nwosu, D. Wilson, R. Hill, I. Spendlove, A. J. Bennett, B. E. Scammell and D. A. Walsh (2019). "Molecular expression patterns in the synovium and their association with advanced symptomatic knee osteoarthritis." Osteoarthritis and Cartilage **27**(4): 667-675.

Wylde, V., A. Beswick, J. Bruce, A. Blom, N. Howells and R. Gooberman-Hill (2018). "Chronic pain after total knee arthroplasty." EFORT open reviews **3**(8): 461-470.

Wylde, V., J. Rooker, L. Halliday and A. Blom (2011). "Acute postoperative pain at rest after hip and knee arthroplasty: severity, sensory qualities and impact on sleep." Orthop Traumatol Surg Res **97**(2): 139-144.

Xie, A. X., N. Iguchi, T. C. Clarkson and A. P. Malykhina (2022). "Pharmacogenetic inhibition of lumbosacral sensory neurons alleviates visceral hypersensitivity in a mouse model of chronic pelvic pain." PLoS One **17**(1): e0262769.

Xiong, Z., A. Shaibani, Y. P. Li, Y. Yan, S. Zhang, Y. Yang, F. Yang, H. Wang and X. F. Yang (2006). "Alternative splicing factor ASF/SF2 is down regulated in inflamed muscle." J Clin Pathol **59**(8): 855-861.

Yam, M. F., Y. C. Loh, C. S. Tan, S. Khadijah Adam, N. Abdul Manan and R. Basir (2018). "General Pathways of Pain Sensation and the Major Neurotransmitters Involved in Pain Regulation." International journal of molecular sciences **19**(8): 2164.

Yao, Y., H. Wang, X. Xi, W. Sun, J. Ge and P. Li (2021). "miR-150 and SRPK1 regulate AKT3 expression to participate in LPS-induced inflammatory response." Innate immunity **27**(4): 343-350.

Yazici, Y., T. E. McAlindon, R. Fleischmann, A. Gibofsky, N. E. Lane, A. J. Kivitz, N. Skrepnik, E. Armas, C. J. Swearingen, A. DiFrancesco, J. R. S. Tambiah, J. Hood and M. C. Hochberg (2017). "A novel Wnt pathway inhibitor, SM04690, for the treatment of moderate to severe osteoarthritis of the knee: results of a 24-week, randomized, controlled, phase 1 study." Osteoarthritis Cartilage **25**(10): 1598-1606.

Yazici, Y., T. E. McAlindon, A. Gibofsky, N. E. Lane, D. Clauw, M. Jones, J. Bergfeld, C. J. Swearingen, A. DiFrancesco, I. Simsek, J. Tambiah and M. C. Hochberg (2020). "Lorecivivint, a Novel Intraarticular CDC-like Kinase 2 and Dual-Specificity Tyrosine Phosphorylation-Regulated Kinase 1A Inhibitor and Wnt Pathway Modulator for the Treatment of Knee Osteoarthritis: A Phase II Randomized Trial." Arthritis Rheumatol **72**(10): 1694-1706.

Yazici, Y., T. E. McAlindon, A. Gibofsky, N. E. Lane, C. Lattermann, N. Skrepnik, C. J. Swearingen, I. Simsek, H. Ghandehari, A. DiFrancesco, J. Gibbs, J. R. S. Tambiah and M. C. Hochberg (2021). "A Phase 2b randomized trial of lorecivivint, a novel intra-articular CLK2/DYRK1A inhibitor and Wnt pathway modulator for knee osteoarthritis." Osteoarthritis Cartilage **29**(5): 654-666.

Yoo, S.-A., S.-K. Kwok and W.-U. Kim (2008). "Proinflammatory Role of Vascular Endothelial Growth Factor in the Pathogenesis of Rheumatoid Arthritis: Prospects for Therapeutic Intervention." Mediators of Inflammation **2008**: 129873.

Yoo, S. A., S. K. Kwok and W. U. Kim (2008). "Proinflammatory role of vascular endothelial growth factor in the pathogenesis of rheumatoid arthritis: prospects for therapeutic intervention." Mediators Inflamm **2008**: 129873.

Youssef, P. P., D. R. Haynes, S. Triantafillou, A. Parker, J. R. Gamble, P. J. Roberts-Thomson, M. J. Ahern and M. D. Smith (1997). "Effects of pulse methylprednisolone on inflammatory mediators in peripheral blood, synovial fluid, and synovial membrane in rheumatoid arthritis." Arthritis & Rheumatism **40**(8): 1400-1408.

Zarghi, A. and S. Arfaei (2011). "Selective COX-2 Inhibitors: A Review of Their Structure-Activity Relationships." Iran J Pharm Res **10**(4): 655-683.

Zeng, H., L. Qin, D. Zhao, X. Tan, E. J. Manseau, M. Van Hoang, D. R. Senger, L. F. Brown, J. A. Nagy and H. F. Dvorak (2006). "Orphan nuclear receptor TR3/Nur77 regulates VEGF-A-induced angiogenesis through its transcriptional activity." The Journal of experimental medicine **203**(3): 719-729.

Zentilin, L., U. Puligadda, V. Lionetti, S. Zacchigna, C. Collesi, L. Pattarini, G. Ruozi, S. Camporesi, G. Sinagra, M. Pepe, F. A. Recchia and M. Giacca (2010). "Cardiomyocyte VEGFR-1 activation by VEGF-B induces compensatory hypertrophy and preserves cardiac function after myocardial infarction." The FASEB Journal **24**(5): 1467-1478.

Zhang, F. J., W. Luo, S. G. Gao, D. Z. Su, Y. S. Li, C. Zeng and G. H. Lei (2013). "Expression of CD44 in articular cartilage is associated with disease severity in knee osteoarthritis." Mod Rheumatol **23**(6): 1186-1191.

Zhang, J.-M. and J. An (2007). "Cytokines, inflammation, and pain." International anesthesiology clinics **45**(2): 27-37.

Zhang, W., G. Nuki, R. W. Moskowitz, S. Abramson, R. D. Altman, N. K. Arden, S. Bierma-Zeinstra, K. D. Brandt, P. Croft, M. Doherty, M. Dougados, M. Hochberg, D. J. Hunter, K. Kwok, L. S. Lohmander and P. Tugwell (2010). "OARSI recommendations for the management of hip and knee osteoarthritis: part III: Changes in evidence following systematic cumulative update of research published through January 2009." Osteoarthritis Cartilage **18**(4): 476-499.

Zhang, W., L. Qi, R. Chen, J. He, Z. Liu, W. Wang, C. Tu and Z. Li (2021). "Circular RNAs in osteoarthritis: indispensable regulators and novel strategies in clinical implications." Arthritis Research & Therapy **23**(1): 23.

Zhang, X., R. Crawford and Y. Xiao (2016). "Inhibition of vascular endothelial growth factor with shRNA in chondrocytes ameliorates osteoarthritis." J Mol Med (Berl) **94**(7): 787-798.

Zhang, X., C. A. Tolzmann, M. Melcher, B. J. Haas, M. J. Gardner, J. D. Smith and J. E. Feagin (2011). "Branch point identification and sequence requirements for intron splicing in *Plasmodium falciparum*." Eukaryot Cell **10**(11): 1422-1428.

Zhang, Y., X. Ding, C. Miao and J. Chen (2019). "Propofol attenuated TNF- $\alpha$ -modulated occludin expression by inhibiting Hif-1 $\alpha$ / VEGF/ VEGFR-2/ ERK signaling pathway in hCMEC/D3 cells." BMC Anesthesiology **19**(1): 127.

Zhang, Y., M. Nevitt, J. Niu, C. Lewis, J. Torner, A. Guermazi, F. Roemer, C. McCulloch and D. T. Felson (2011). "Fluctuation of knee pain and changes in bone

marrow lesions, effusions, and synovitis on magnetic resonance imaging." Arthritis Rheum **63**(3): 691-699.

Zhang, Y., M. Nevitt, J. Niu, C. Lewis, J. Torner, A. Guermazi, F. Roemer, C. McCulloch and D. T. Felson (2011). "Fluctuation of knee pain and changes in bone marrow lesions, effusions, and synovitis on magnetic resonance imaging." Arthritis & Rheumatism **63**(3): 691-699.

Zhang, Y., J. Qian, C. Gu and Y. Yang (2021). "Alternative splicing and cancer: a systematic review." Signal Transduction and Targeted Therapy **6**(1): 78.

Zhou, X., R. Wang, X. Li, L. Yu, D. Hua, C. Sun, C. Shi, W. Luo, C. Rao, Z. Jiang, Y. Feng, Q. Wang and S. Yu (2019). "Splicing factor SRSF1 promotes gliomagenesis via oncogenic splice-switching of MYO1B." The Journal of Clinical Investigation **129**(2): 676-693.

Zhou, Z. and X. D. Fu (2013). "Regulation of splicing by SR proteins and SR protein-specific kinases." Chromosoma **122**(3): 191-207.

Zielinski, S., K. Bartels, K. Cebulski, C. Kühne and J. Kekow (2000). "Evidence of proteolytic activation of transforming growth factor beta in synovial fluid." Adv Exp Med Biol **477**: 477-481.

Zou, Y., Y. Li, L. Lu, Y. Lin, W. Liang, Z. Su, X. Wang, H. Yang, J. Wang, C. Yu, L. Huo and Y. Ye (2013). "Correlation of fractalkine concentrations in serum and synovial fluid with the radiographic severity of knee osteoarthritis." Annals of Clinical Biochemistry **50**(6): 571-575.